Submitted, accepted and published by:
Progress in Energy and Combustion Science 65 (2018) 6-66

Review and assessment of experimental results from Chemical Looping Combustion units burning solid fuels

J. Adánez*, A. Abad, T. Mendiara, P. Gayán, L.F. de Diego, F. García-Labiano

Department of Energy and Environment, Instituto de Carboquímica-ICB-CSIC

Miguel Luesma Castán 4, 50018, Zaragoza, Spain

* Corresponding author:

E-mail address: jadanez@icb.csic.es

Tel.: +34 976 733 977

Fax: +34 976 733 318

Abstract

Chemical Looping Combustion (CLC) has arisen during last years as a very promising combustion technology for power plants and industrial applications, with inherent CO_2 capture which avoids the energy penalty imposed on other competing technologies. The use of solid fuels in CLC has been highly developed in the last decade and currently stands at a technical readiness level (TRL) of 6. In this paper, experience gained during CLC operation in continuous units is reviewed and appraised, focusing mainly on technical and environmental issues relating to the use of solid fuels. Up to now, more than 2700 hours of operational experience has been reported in 19 pilot plants ranging from 0.5 kW_{th} to 4 MW_{th}. When designing a CLC unit, the preferred configuration for the scale-up of CLC of solid fuels is a two circulating fluidized beds (CFB) system. Coal has been the most commonly used solid fuel in CLC, but biomass has recently emerged as a very promising option to achieve negative emissions using bioenergy with carbon capture and storage (BECCS). Mostly low cost iron and manganese materials have been used as oxygen carriers in the so called in-situ gasification CLC (iG-CLC). The development of Chemical Looping with oxygen uncoupling (CLOU) makes a qualitative step forward in the solid fuel combustion, due to the use of materials able to release oxygen.

The performance and environmental issues of CLC of solid fuels is evaluated here. Regarding environmental aspects, the pollutant emissions (SO_2, NO_x, etc.) released into the atmosphere from the air reactor are no cause of concern for the environment. However, the presence of SO_2, NO_x and Hg at the exit of the fuel reactor affects CO_2 quality, which must be taken into account during the later compression and purification stages. The effect of the main variables affecting CLC performance is evaluated for fuel conversion, CO_2 capture rate, and combustion efficiency obtained in different CLC

units. Solid fuel conversion is normally not complete during operation, due to the undesired loss of char. A methodology is presented to extrapolate the current information to what could be expected in a larger CLC system. CO_2 capture near 100% has been reported using a highly efficient carbon stripper, highly reactive fuels (such as lignites and biomass, etc.) or by the CLOU process. Operational experience in *i*G-CLC has showed that it is not possible to reach complete fuel combustion, making an additional oxygen polishing step necessary. For the further scale-up, it is essential to reduce the unburnt compounds at the fuel reactor outlet. Proposals to achieve this reduction already exist and include both improvement to the gas-oxygen carrier contact, or new design concepts based on the current scheme for *i*G-CLC. In addition, CLOU based on copper materials has shown that complete fuel combustion could be achieved. Main challenges for the future development and scale-up of CLC technology have been also identified. A breakthrough in the future development of CLC technology for solid fuels will come from developing long-life materials for CLOU that are easy to recover from the ash purge stream.

Keywords: CO_2 capture, Chemical Looping Combustion (CLC), Chemical Looping with Oxygen Uncoupling (CLOU), Coal, Biomass, Oxygen carrier

61 **Index**

1. Introduction

The Paris Agreement, the new treaty of the United Nations Framework Convention on Climate Change (UNFCCC) that will substitute the Kyoto Protocol, urges decarbonization of the world energy systems in the near future in order to limit the average world temperature rising to 2 ºC above pre-industrial levels [1]. Chemical Looping Combustion (CLC) is recognized as a promising approach to CO_2 capture in processes requiring the combustion of a fuel for both heating and/or electricity generation [2]. Compared to other CO_2 capture technologies, CLC can gain dramatic energy savings through its inherent avoidance of any gas separation step [3]. The estimated costs per ton of CO_2 captured for a CLC plant burning solid fuels is around 20 USD/t CO_2 [4], significantly lower than those estimated for post-combustion technologies (36-53 USD/t CO_2), pre-combustion capture (28-41 USD/t CO_2) and oxycombustion (36-67 USD/t CO_2) [5, 6]. The basic principle behind this technology is preventing air and fuel mixing in the combustion chamber, as occurs in conventional combustion. In CLC, the oxygen needed for combustion is supplied through a redox cycle, where a solid oxygen carrier, normally a metal oxide, is reduced to supply the oxygen and then re-oxidized again by air.

CLC has been developed for combustion of gaseous, liquid and solid fuels, and is undergoing significant scale up at present [7-9]. In the early 2000s, the development of CLC technology gave a significant boost to combustion of gaseous fuels, mainly natural gas. Major advances were made in developing oxygen carrier materials [7, 10, 11] and demonstrating the CLC process in several units [7, 12, 13], with the 120 kW_{th} unit at Vienna University of Technology being the flagship of the CLC combustion with gaseous fuels [14]. Nowadays, the challenge in developing CLC technology with gaseous fuels is the scale-up both of the process, which is intended to be demonstrated

158 at the 10 MW_{th} scale [15], and the production of highly reactive and durable oxygen
159 carrier materials with no nickel in their composition [16-19]. Also, the combustion of
160 syngas or natural gas in a pressurized CLC system is being explored, which would
161 increase the net efficiency of the process for electricity generation by using gas and
162 steam turbines in a combined cycle [20, 21]. Most of the development with pressurized
163 CLC systems is based on a battery of fixed bed reactors with gas switching [22-24], but
164 also pressurized and interconnected reactors with an oxygen carrier circulating between
165 them are being assessed [25, 26]. Recently, combustion of liquid fuels has received
166 attention in order to use heavy fuels [27-29] or renewable fuels such as bio-ethanol [30].
167 To reach the goal set by the Paris Agreement, CO_2 emissions should start to decrease by
168 2020 and become negative by the end of the century [31, 32]. This fact combined with
169 the important role of coal combustion in the future energy mix [33, 34] have acted as
170 driving forces to boost the development of CLC technology with both coal and biomass
171 as fuels.
172 Significant developments have been made in the combustion of solid fuels using
173 Chemical Looping Combustion (CLC) during the last decade. Progress in this
174 technology up to mid-2011 was reviewed in a previous work [7], and later a brief
175 description of operational experience up to mid-2013 was done by Lyngfelt [35]. Thus,
176 operation of two 10 kW_{th} CLC units, located at Chalmers University of Technology
177 (Sweden) and Southeast University (China) [36-39], was described in that review. CLC
178 with solid fuels was first demonstrated with petcoke and bituminous coal at Chalmers
179 University of Technology in 2008 [36, 37]. Moreover, results obtained with various
180 oxygen carriers (ilmenite and iron ore) as well as solid fuels, including different coals
181 and biomass, proved the technology to be reliable [40]. In total, about 2700 hours of
182 operational experience was reported. These promising results encouraged the design and

183 construction of other units and important new knowledge has been gained in the last 5
184 years [41], including experience in a 1 MW_{th} unit at Darmstadt University of
185 Technology [42] and a 3 MW_{th} unit by Alstom USA [43, 44].
186 In this paper, the state of the art of the CLC operation with solid fuels in existing CLC
187 facilities is reviewed and updated. An overview of the more relevant results obtained in
188 these units is presented and results are appraised based on the design and operating
189 conditions used in each CLC unit. In order to compare results presented in different
190 research works, a methodology is given which enables the experimental results obtained
191 from the units to be analyzed in depth. In addition, future needs and research areas are
192 presented.

193 **2. Description of the CLC process with solid fuels**

194 The scheme of the CLC process with solid fuels is shown in Fig. 1. The solid fuel is fed
195 into the fuel reactor and mixed with the oxygen carrier particles. Then, devolatilization
196 takes place and char is generated. The interaction between char and oxygen carrier can
197 take place provided a close contact between solid particles is ensured [45, 46] as it is the
198 case of fixed/moving bed reactors. However, this interaction is not of relevance under
199 fluidized bed conditions [47] where the gas-solid contact is favored. Therefore, most of
200 the experimental units operate under the so-called *in situ* Gasification Chemical
201 Looping Combustion (*i*G-CLC) mode schematized in Fig. 2. Under this combustion
202 mode, the solid fuel gasification by steam and/or CO_2 takes place in the fuel reactor
203 following the scheme described by reactions (R1)-(R3). The process was designed to
204 use steam as a gasifying and fluidizing agent. However, recirculated streams, wet or
205 dry, including a mixture of H_2O+CO_2 can also be used (see Fig.1). The products
206 generated during coal devolatilization and gasification are oxidized by the oxygen
207 carrier particles following reaction (R4) to produce mainly CO_2 and H_2O. In addition,

the gas composition in the fuel reactor can be modified by the water-gas shift equilibrium; see reaction (R5).

$$\text{Coal} \rightarrow \text{volatile matter} + \text{Char} \quad \text{(R1)}$$

$$\text{Char (mainly C)} + H_2O \rightarrow H_2 + CO \quad \text{(R2)}$$

$$\text{Char (mainly C)} + CO_2 \rightarrow 2\,CO \quad \text{(R3)}$$

$$M_xO_y + H_2, CO, \text{volatile matter} \rightarrow M_xO_{y-1} + CO_2 + H_2O \quad \text{(R4)}$$

$$CO + H_2O \leftrightarrow CO_2 + H_2 \quad \text{(R5)}$$

Once steam is condensed, an almost pure CO_2 stream is obtained. Thus, the oxygen carrier is reduced in the fuel reactor, and then transferred to the air reactor, where it is re-oxidized using air; see reaction (R6).

$$M_xO_{y-1} + 1/2\,O_2 \rightarrow M_xO_y \quad \text{(R6)}$$

The ash generated in the combustion should be periodically purged to avoid accumulation in the CLC system, although this can lead to a certain loss of oxygen carrier. A makeup flow of oxygen carrier should also be added to correct the loss and that caused by particle attrition.

Following the scheme presented in Fig. 1, experimental units mostly based on two interconnected fluidized bed reactors have been built recently and operated to burn different types of coal with varying thermal power capacities. Gasification of char in the fuel reactor is the limiting step in coal conversion. If char is not fully converted in the fuel reactor, some of the char leaves the fuel reactor together with the oxygen carrier. Should the unconverted char reach the air reactor, it is burnt there producing CO_2 which cannot be captured, thus reducing the CO_2 capture efficiency of this technology. The use of a carbon stripper has been proposed to minimize the amount of char transferred to the air reactor by separating the unconverted char exiting the fuel reactor from the oxygen carrier, as shown in Fig. 1 [48-51]. Studies on the efficiency of the carbon

stripper have been carried out in order to evaluate the performance of *i*G-CLC on CO_2 capture [49] and to optimize the design and operation [50, 51].

In general, incomplete combustion of volatiles and char gasification products at the outlet of the fuel reactor has been observed. The presence of unburnt products could make an oxygen polishing step necessary, which would increase the cost of *i*G-CLC technology [4]. The oxygen polishing step is described as a process in which highly concentrated oxygen is used to complete the combustion of gaseous products from the fuel reactor; see Fig. 1. Some design suggestions have been proposed and analyzed in order to minimize the presence of unburnt compounds [52], and their implementation in *i*G-CLC units is still ongoing. The use of a moving bed as a fuel reactor has also shown high combustion efficiency [53]. Selection of the oxygen carrier may also improve CLC performance with solid fuels. Thus, a more reactive oxygen carrier has been shown to improve the combustion efficiency, with the resulting decrease in the oxygen required for oxygen polishing [54, 55].

Further improvement is achieved using materials with oxygen uncoupling capability [55-58]. In Chemical Looping with Oxygen Uncoupling schematized in Fig. 2 [59], the oxygen carrier is able to generate gaseous oxygen in the fuel reactor environment; see reaction (R7). Volatile matter and solid char are then burnt by oxygen as in conventional combustion, following reactions (R8) and (R9). As steam gasification is not needed in CLOU, recirculated CO_2 can be used as fluidizing agent.

$$2\ M_xO_y \rightarrow 2\ M_xO_{y-1} + O_2 \quad \text{(R7)}$$

$$\text{char (mainly C)} + O_2 \rightarrow CO_2 \quad \text{(R8)}$$

$$H_2, \text{CO, volatile matter} + O_2 \rightarrow CO_2 + H_2O \quad \text{(R9)}$$

Char and volatile matter conversion are better in CLOU than in *i*G-CLC. In fact, char gasification can limit the CO_2 capture, whereas the need to burn the volatiles and

gasification products with the oxygen carrier hinders complete combustion in *i*G-CLC. [56, 60, 61]. However, the combustion process with the gaseous O_2 released by the oxygen carrier in CLOU returns better results on efficiency.

The *in-situ* Gasification Chemical Looping Combustion process (*i*G-CLC) has drawn great interest due to the use of low cost oxygen carriers [7], although synthetic oxygen carriers are usually considered for CLOU [62-64]. Recently, great efforts have been made to develop suitable materials for use as oxygen carriers in CLOU, mainly focused on copper oxide [65-73] or combined oxides of Mn with other metals such as Ca, Mg, Cu, Fe or Si [74-88]. However, the combined oxides tested to date have not shown oxygen release capacities as high as copper oxide. When used in a continuous unit, they will act mainly as an *i*G-CLC oxygen carrier, but with the advantage of an additional gaseous oxygen contribution. This new concept was identified as Chemical Looping *assisted* by Oxygen Uncoupling (CL*a*OU) and it is in its early development stages [89]. Some studies have also centered on the use of natural ores or waste materials as an oxygen carrier for CLOU [90-94], which often requires a concentration stage of the active compound. However, experience in operating CLOU to burn solid fuels is still very limited. Table 1 and 2 summarize the chemical properties and chemical reactions taking place for the main redox pairs used in *i*G-CLC and CLOU combustion.

3. CLC units for solid fuel combustion

To date, there are eighteen CLC pilot plants worldwide burning solid fuels in the range 1 kW_{th} to 3 MW_{th} and a few new upcoming units. A brief summary including location, hours of operation and type of oxygen carriers tested is presented in Table 3. In addition, Fig. 3 shows an overview of the distribution of the operating CLC units for year of operation, thermal power and location. The CLC units included in Table 3 will be described in some detail in the following sections. To make their status clear, they

have been grouped into two categories: small or lab-scale units and semi-industrial scale units.

3.1. Small and lab-scale units

This section describes CLC units existing at lab-scale, as well as the main operating conditions including the oxygen carrier and solid fuels used. All these facilities are bound by the common feature of having air and fuel reactors, with the oxygen carrier circulating between both. Facilities operating with a thermal power of about 1-5 kW_{th} are deemed to be small units, while prototypes in the 10-100 kW_{th} range are defined as lab-scale units. However, several configurations can be found in the existing CLC units which would influence the performance of the system. Figs. 4-21 show the scheme of the different experimental units included here.

3.1.1. Chalmers University of Technology (CUT, Sweden)

The research group of Prof. Lyngfelt at Chalmers University of Technology has long experience in CLC of solid fuels and operated two units, 10 and 100 kW_{th}, with different types of solid fuels (bituminous coals, petcoke, woodchar).

The first operation of CLC with solid fuels in a 10 kW_{th} unit was presented in 2008 [36]. This unit consisted of two interconnected fluidized beds acting as fuel and air reactors, as shown in (Fig. 4A). The fuel reactor was divided into three chambers: a low velocity part (bubbling fluidized bed) where the fuel particles were devolatilized and gasified, a carbon stripper to separate unreacted coal particles from the oxygen carrier particles, and a high velocity part to help particle recirculation back to the fuel reactor via a small cyclone fitted at the entrance to the fuel reactor. The air reactor was a high velocity fluidized bed connected to a riser to bring the oxygen carrier particles back to the fuel reactor. Coal was fed into the upper part of the fuel reactor, in the low velocity part. This design caused most of the volatiles from coal to escape as unburnt products

from the fuel reactor. Later, the design was improved by extending the fuel feeding pipe so that the fuel discharged inside the bed [115]. Operation run extensively has used ilmenite [36, 37, 114, 115, 118, 119], manganese ore [54, 115, 116]or CaMn-based perovskites-type materials [57, 117] as an oxygen carrier. Improved results were found for CaMn-based perovskites as, in this case, a fraction of the transferred oxygen can be released as molecular oxygen [171]. Thus, a fraction of the fuel would be burnt via CLOU [172]. However, this material should be limited to non-sulfurous fuels, such as biomass, due to the deactivation problems encountered [117]. Bituminous coals have often been used in these works, but low-volatile fuels, such as petcoke or biochar, have been preferred in order to achieve high combustion efficiency in this unit [173].

In 2012, Lyngfelt et al. built a 100 kW_{th} CLC experimental unit for solid fuels [123, 174] consisting of two interconnected circulating fluidized beds with a carbon stripper between both reactors, as shown in Fig. 4B. The carbon stripper comprised four chambers to ensure high-efficiency separation of char particles. Before entering the carbon stripper, the solids were transferred from the bottom of the fuel reactor to the circulation riser. This allowed recirculation of the solids flow to be controlled by adjusting the flow fed to the circulation riser and also raising the solids to the carbon stripper level, for transport to the air reactor by gravity. By changing the fluidization velocity in the air reactor and the circulation riser, it should be possible to control the fuel reactor bed inventory and global solids circulation independently. Moreover, this unit was designed to have in-bed feeding of the fuel.

The scale-up of materials successfully tested in other units, e.g. 10 kW_{th} at CUT or 0.5 kW_{th} at ICB-CSIC, has been carried out in this 100 kW_{th} CLC unit, which has been operated with Fe-based oxygen carriers, such as ilmenite and iron ore, and different types of solid fuels: bituminous coal, petroleum coke and wood char [100, 121, 123,

124]. Also, adding manganese ore to the well-known ilmenite material returned satisfactory results [122]. The knowledge gained from the operation gave clear indications of the viability of the CLC process for solid fuels. For example, the carbon stripper was found to be highly efficient in separating unconverted char particles from the oxygen carrier [120], thus the CO_2 capture was close to 100%.

3.1.2. Southeast University (SU, China)

In the School of Energy and Environment at Southeast University in Nanjing two continuous CLC units were built and operated by the group headed by Prof. Shen. These units have a similar design, but the thermal power was different: 1 and 10 kW_{th} sketched in Fig. 5, respectively [38, 126]. In both cases, the air reactor is a fast fluidized bed and the fuel reactor is a spouted bed. This configuration was selected as there is an excellent mixing of solids in this type of reactor ensuring good mixing between the coal and oxygen carrier.

The first operation in these prototypes was performed using Ni-based oxygen carriers. Nevertheless, the use of nickel is not recommended for CLC of solid fuels, as these materials can contaminate the drained ashes and loose reactivity in presence of sulfur-containing fuels [125, 175, 176]. The presence of Ni in the ash may be unavoidable, thus generating a dangerous residue in the process. Later, limited operation was carried out using sintered iron oxide powders [39]. The 10 kW_{th} unit has been successfully tested in the combustion of coal and biomass with Ni- and Fe-based oxygen carriers. The fuel reactor has an inner seal to prevent unconverted char particles being present in the oxygen carrier stream to the air reactor. However, the inner seal could not prevent the char bypassing from the fuel reactor to the air reactor.

In the 1 kW_{th} CLC unit at Southeast University, char separation was improved by using an external loop-seal connecting the fuel reactor with the air reactor [126]. The fuel

conversion was also improved by introducing the fuel particles at the bottom of the spout-fluid bed, as seen in the scheme of the unit presented in Fig. 5. Exhaustive operations have been carried out in this unit, where iron ores based on hematite were used to burn different types of coal, biomass and in the co-combustion of coal and biomass [127-129, 133]. The iron ore was also modified with potassium with the aim of increasing the char gasification rate, and hence the CO_2 capture [130]. Recently, combustion experiments with sewage sludge have been performed, also using hematite as oxygen carrier [131, 132, 134]. In this case, the study focused on the fate of phosphorous compounds present in the fuel.

Also at Southeast University (China), the first CLC unit working under pressurized conditions (PCLC) was built and operated by Xiao et al. [135]. The fuel and air reactors were designed to be operated in fast and turbulent fluidization regimes, respectively; see Fig. 6. The fast fluidization regime in the fuel reactor can improve the gas-solid contact in addition to the contact between coal and oxygen carrier particles. Furthermore, this configuration together with the pressurized operation leads to a lower oxygen carrier inventory. Experiments were performed in the 1-5 atm range using a bituminous coal as fuel and an iron ore as oxygen carrier. A CO_2 concentration of 97.2% in the exhaust gas in the fuel reactor working at 5 atm absolute pressure was obtained.

3.1.3. Instituto de Carboquímica (ICB-CSIC, Spain)

The group headed by Prof. Adánez at ICB-CSIC has run two CLC units, including operation both in *i*G-CLC and CLOU modes burning coal and biomass. The experimental continuous unit of 0.5 kW_{th} [136], identified as ICB-CSIC-s1 (Fig. 7A), consisted of two fluidized bed reactors, connected by a U-shaped fluidized bed acting as a loop seal. In the ICB-CSIC-s1 unit, the fuel reactor was a bubbling fluidized bed where the coal was fed at the bottom and just above the fuel reactor distributor plate.

383 This configuration provided good contact between oxygen carrier particles and gases
384 from coal conversion, i.e. volatile matter and gasification products. The reduced oxygen
385 carrier was re-oxidized in the air reactor. The oxidized oxygen carrier was entrained
386 through a riser from the air reactor and returned to the fuel reactor. The solids flow
387 returning to the fuel reactor was regulated by a solids valve, and the value of this flow
388 could also be measured through a diverting solids valve. This feature enabled proper
389 evaluation of the effect of the solids circulation flow rate on the performance of the
390 process.
391 Note that this unit does not include a carbon stripper, so unconverted char escaping to
392 the air reactor was only affected by the residence time of solids in the fuel reactor. This
393 fact facilitates the evaluation of results obtained in the unit on char conversion and CO_2
394 capture. Thus, char conversion rates are often given from tests carried out with different
395 oxygen carriers and fuels such as bituminous coal, lignite, anthracite and biomass [101,
396 136-140]. This information can be used in theoretical models for design and
397 optimization purposes [177, 178].
398 Experiments in *i*G-CLC mode with different oxygen carrier materials based on iron,
399 such as natural ilmenite [136-138], iron ore [101, 139, 141], Fe-ESF which is a residue
400 from bauxite treatment [140], and a synthetic Fe-Mn-based material [79] have been
401 performed. Ilmenite, a mineral composed of $FeTiO_3$ and a highly reactive iron ore were
402 used in the combustion of coals from anthracite to lignite with high sulfur content [101,
403 137]. An increase in the CO_2 capture and combustion efficiencies with temperature was
404 observed. The CO_2 capture efficiency increased with decreasing coal rank, and higher
405 CO_2 capture values were obtained for lignite compared to anthracite. The use of Fe-
406 ESF, iron ore and Fe-Mn-based material improved the results obtained with ilmenite,
407 especially combustion efficiency [55, 79, 101, 140]. Biomass was also used as fuel,

obtaining promising results, with high CO_2 capture values even when CO_2 was utilized as a fluidizing agent in the fuel reactor [139, 141].

This ICB-CSIC-s1 unit was where the proof of concept for the CLOU process in burning coal was demonstrated for the first time using a bituminous coal and a Cu-based oxygen carrier consisting of 60% CuO supported on $MgAl_2O_4$ [142]. Complete combustion of coal was observed in all cases and CO_2 capture values close to 100% were obtained at 960 ºC in the fuel reactor. The CO_2 capture level depended on the coal rank and fuel reactor temperature, as assessed in experiments with the same oxygen carrier and coals from anthracite to lignite. The highest CO_2 capture efficiencies were reached with lignite and medium-volatile bituminous coals [58]. Using biomass as fuel improved CO_2 capture and 100% CO_2 capture was reached at 935 ºC [143]. Recently, a Cu-Mn mixed oxide was also tested as a CLOU oxygen carrier with a sub-bituminous coal, reaching complete combustion in all cases [88]. Coal combustion assisted by oxygen uncoupling (CLO*a*U mode) was also performed in this unit using a Fe-Mn-based material. The amount of oxygen released when using this oxygen carrier was significant when the solids circulation rate between fuel and air reactors was increased, as well as when optimizing the oxidation conditions in the air reactor [79].

Also at ICB-CSIC, an experimental unit of 50 kW_{th} for solid fuel combustion was recently built and operated [144]. The system included two interconnected circulating fluidized beds as fuel and air reactors (Fig. 7B). The fuel reactor is a circulating fluidized bed with a substantial dense phase at the bottom, which adds flexibility to the gas-solid contact. This unit also incorporated a carbon stripper between the fuel and air reactors. In addition, a double loop-seal below the fuel reactor cyclone allowed the solids circulation rate to be controlled independently from operating conditions in air or fuel reactors. Evaluation of the effect of operating conditions on the CO_2 capture and

combustion efficiencies was carried out with ilmenite as the oxygen carrier and a bituminous coal as fuel [145], so that optimum operating conditions could be determined. The effect of the carbon stripper efficiency on the CO_2 capture efficiency was also investigated, to determine optimum conditions in the unit. In order to improve combustion efficiency, the riser in the fuel reactor was modified by adding ring-type internals to boost gas-solid contact. The effect of the internals was also evaluated using ilmenite as oxygen carrier and bituminous coal. It was found that the presence of internals improved oxidation of volatile matter in the form of methane and led to the full conversion of hydrogen [146].

3.1.4. IFP Energies Nouvelles (IFPEN, France)

IFP Energies Nouvelles (IFPEN) headed by Prof. Gauthier et al., in an R&D project in collaboration with Total S.A., modified an existing 10 kW_{th} CLC unit for gaseous fuels to burn solid fuels [147]. This unit consists of three interconnected bubbling fluidized bed reactors (one fuel reactor and two air reactors, AR_1 and AR_2) and a carbon stripper (Fig. 8). The carbon stripper prevented unconverted char from entering the air reactor, but separated char was not recirculated to the fuel reactor. The solids circulation between reactors was controlled by pneumatic L-valves. Solids at the exit of the L-valve were transported through a vertical riser, followed by a horizontal conveying line. Solid-gas separation was then performed in a cyclone. Experiments were done in this unit using a bituminous coal and a natural ore (BMP) as oxygen carrier.

3.1.5. Hamburg University of Technology (TUHH, Germany)

At Hamburg University of Technology, a 25 kW_{th} CLC system of coupled fluidized beds for CLC was tested by the group headed by Prof. Werther [148]. The continuous CLC unit consisted of a circulating fluidized bed (air reactor) coupled with a two-stage bubbling fluidized bed (fuel reactor), as seen in Fig. 9. The two stages in the fuel reactor

were set one above the other. The solid fuel entered the lower bed where it was mostly converted and gasification took place. In the upper bed, the gases and particles leaving the lower bed can react with fresh oxygen carrier particles. The purpose of this two-stage fuel reactor is to enhance the conversion of combustible gases released in the lower fuel reactor stage by putting them in contact with freshly regenerated oxygen carrier particles in the upper stage. The lower bed also acts as carbon stripper when fine fuel was used. The first experiments conducted in this unit used Australian ilmenite as an oxygen carrier and lignite as fuel [148]. Good volatile matter conversion was observed due to the use of the upper fuel reactor, but there was also high CO and H_2 concentration in the flue gases. This fact was explained by char particles entering the upper fuel reactor, where they were entrained with the flue gases. Gasification of segregated char particles generates H_2 and CO which could not have the chance to react with the oxygen carrier particles. Some instability in the solids circulation was also reported. In experiments with a low solids inventory, most of the fluidization gas used in the fuel reactor and in the downcomer acting as a locking bed between fuel and air reactor was found in the air reactor [179]. A Computational Fluid Dynamic (CFD) model was developed to simulate this CLC unit and identify the origin of the instability. It was found that an increased pressure drop in the gas distributor in the upper stage of the fuel reactor caused a decrease in the level of solids in the right hand side of the downcomer, thereby facilitating the flow of the fluidizing gas in the fuel reactor to the air reactor. These types of simulations can be used in the future to draft guidelines for optimum operation of the unit. The last operations reported in this unit used an oxygen carrier based on CuO supported on γ-Al_2O_3 in the temperature range 800-900 ºC to burn two types of coal, i.e. lignite and bituminous coal [149]. These conditions allow work in *i*G-CLC mode, but with some gaseous oxygen release at the highest temperature.

Although it is not clearly stated, the experiments performed at 800-850 ºC are thought to be in *i*G-CLC mode, as the amount of oxygen released at those temperatures is almost negligible. Regardless of the coal used, almost complete conversion of the combustible gases was reached after the second stage of the fuel reactor. The composition of the gases leaving the first stage was also analyzed in the experiments performed. It was concluded that, with bituminous coal, the second stage could be eliminated, as the combustion efficiency was already high after the first bubbling bed. Therefore, the research group is currently working on a new design of the fuel reactor to allow coal feed into both stages [149].

3.1.6. Western Kentucky University (WKU, USA)

A 10 kW_{th} CLC unit was operated with solid fuels at the Institute for Combustion Science and Environmental Technology (ICSET) of Western Kentucky University (WKU) in 2012 by Cao et al.[150]. This unit consists of a bubbling fluidized bed fuel reactor and a circulating fluidized bed air reactor; see Fig. 10. A CuO/Al_2O_3 material was used as the oxygen carrier. The unit had previously been tested in successful operation with CH_4 and syngas since 2010. Later, biomass was used as fuel [180], but co-combustion of biomass with fuel gas, H_2 or CH_4, was required to maintain the system at high temperature. The presence of CuO could induce oxygen transference by oxygen uncoupling [59], but the presence of Al_2O_3 could hinder the oxygen uncoupling capability of the oxygen carrier material [67]. No details are given on operating the CLC unit with this oxygen carrier to indicate whether CLC or CLOU was the main process in the gaseous fuel combustion. Nevertheless, combustion of biomass was likely to take place via *i*G-CLCs due to the low temperature (about 800 ºC), which supresses oxygen uncoupling [143].

3.1.7. Ohio State University (OSU, USA)

As described above, the configuration where fuel and air reactors are both fluidized beds (bubbling or high velocity) is the commonest. However, the 2.5 kW_{th} bench scale unit and the 25 kW_{th} subpilot unit constructed and tested by the group headed by Prof. Fan at Ohio State University does not follow this scheme [9] (see Fig. 11). In this case, the fuel reactor (reducer) was designed to be a moving bed and the air reactor (combustor+riser) was an entrained bed. In the fuel reactor, the oxygen carrier particles descend by gravity and the gases produced ascend, counter-current to the solids. A non-mechanical L-valve connects the fuel reactor and air reactor to regulate the flow of solids between reactors, and the gas sealing between both reactors. Fuel is injected in the middle of the fuel reactor. The advantages of this configuration over a fluidized bed are the lower attrition of particles, better control of the fuel residence time and the high conversion of both the fuel and oxygen carrier. This results in almost full coal conversion with a high purity of CO_2, eliminating the need of down-stream polishing units. Intensive experimental work has been carried out in this experimental unit using solid fuels, such as lignite and sub-bituminous coal, and with synthetic particles based on iron oxide as oxygen carriers [53, 151-153].

The use of Fe-based oxygen carriers is preferred in this configuration. Thus, Fe_2O_3 can be reduced to FeO or even Fe, while full combustion of fuel to CO_2 and H_2O is still achieved [2]. Thus, the oxygen transport capacity is increased compared to the limited reduction of Fe_2O_3 to Fe_3O_4 in a circulating fluidized bed, due to the thermodynamic constraint in achieving complete combustion to CO_2 and H_2O when Fe_3O_4 is further reduced [181].

Nevertheless, scale-up of the process would involve overcoming several challenges. In order to maintain non-fluidized conditions in the moving-bed, the velocity in the reburn

zone of the fuel reactor should be kept below the minimum fluidization velocity. For a given fuel feed, this can be achieved by increasing the cross sectional area of the reburn zone or the oxygen carrier particle size [182]. The higher particle size of the oxygen carrier allows ash separation in the reducer reactor and ash entrainment through the reducer outlet, but a very large air excess is then needed in the air reactor to entrain solids and recirculate them to the fuel reactor. In order to keep the power demand for fluidization in the air reactor low, the solids inventory under fluidization should be decreased. Schwebel et al. [182] proposed staged oxidation in the air reactor, which would be divided into a bubbling bed feeding the riser and a subsequent moving bed. Another problem to be solved in the scale-up is the thermal gradients formed in wide moving bed reactors and the homogeneous distribution of coal throughout the cross sectional area of the reactor. Therefore, these authors proposed that the reactor was narrowed at the position where coal was fed, i.e. at the middle of the moving bed, with the purpose of further distribution of solids over the entire surface of the reactor as the solids moved down.

3.1.8. Guangzhou Institute of Energy Conversion (GIEC, China)

A 10 kW_{th} unit was erected by Zhao et al. at CAS Key Laboratory of Renewable Energy at Guangzhou Institute of Energy Conversion; see Fig. 12. The fuel reactor design followed a similar concept to that of the 10 kW_{th} unit at CUT. In this case, biomass (sawdust) gasification using a Fe_2O_3/Al_2O_3 oxygen carrier was performed in the CLC unit for syngas production instead of combustion [154, 155]. Later, a bi-metallic material based on Fe-Ni was tested in this unit in order to improve the H_2 yield [183]. More detailed information on the production of H_2 by chemical looping processes can be found elsewhere [7, 184].

3.1.9. Huazhong University of Science and Technology (HUST, China)

In the last few years, two units have been constructed by the group headed by Prof. Zhao at the State Key Laboratory of Coal Combustion at Huazhong University of Science and Technology in Wuhan, with a thermal power of 5 kW_{th} and 50 kW_{th}, respectively.

The scheme for the 5 kW_{th} unit is shown in Fig. 13A [156]. Preliminary results from the combustion of a bituminous coal with hematite as the oxygen carrier were recently published and optimization of the unit is under way.

Recently, the design and operation of a 50 kW_{th} CLC unit has been reported [157]; see Fig. 13B. The air reactor is a circulating fluidized bed in the turbulent regime in order to ensure a sufficiently high solids circulation rate. However, the fuel reactor is a bubbling fluidized bed to give a high residence time to the char particles to be gasified. A riser connected to the top of the fuel reactor transports the solids to a carbon stripper to separate char particles from the oxygen carrier before solids enter the air reactor. High CO_2 capture and combustion efficiencies have been obtained in preliminary results on coal combustion with an iron ore, where the solids inventory in the fuel reactor was as high as 2000 kg/MW_{th}.

3.1.10. VTT Technical Research Centre (VTT, Finland)

During 2015-2016, a new 10-50 kW_{th} scale dual fluidized bed chemical looping combustion unit was constructed by VTT Technical Research Centre [158]. This new unit was intended for the study of biomass combustion in CLC. The use of biomass as fuel gives rise to negative CO_2 emissions. This concept will be addressed in more detail in section 4.5.

The design of the VTT unit is shown in Fig. 14. The air reactor is a circulating fluidized bed and the fuel reactor is a bubbling fluidized bed. Entrained solids from the air reactor

583 are separated by a cyclone and the reactors are interconnected by loop seals. The unit
584 has no carbon stripper to minimize char transport from the fuel to the air reactor. A total
585 of 16 h continuous operation have been reported to date using ilmenite as oxygen carrier
586 and wood pellets as fuel [158].

587 **3.1.11. Upcoming CLC prototypes**

588 Some additional CLC units are planned to be built and operated with solid fuels in the
589 near future, and a brief description of these follows.

590 A dual fluidized bed system has been built at the Institute of Combustion and Power
591 Plant Technology (IFK) at University of Stuttgart to be operated in CLC mode [185-
592 187]. The unit consists of a bubbling fluidized bed fuel reactor, connected to a
593 circulating fluidized bed acting as air reactor. Preliminary results were obtained in semi-
594 batch mode using ilmenite to burn coal at the 10 kW_{th} scale [186]; see Fig. 15. Thus,
595 coal was continuously fed to the fuel reactor but ilmenite particles remained there
596 throughout the combustion period, i.e. there was no circulation of solids between air and
597 fuel reactors. Acceptable coal conversion was achieved, while ilmenite was able to
598 transfer oxygen. Results from continuous operation in this unit are expected to be in the
599 *i*G-CLC mode.

600 A three-tower CLC system is being developed by Japan Coal Energy Center (JCOAL)
601 [167]; see Fig. 16. The road map for the project includes building 100 kW_{th} and 1 MW_{th}
602 facilities by 2020, and the scale-up of the process to 10 MW and 40-70 MW by 2025
603 and 2030, respectively. The three-tower concept includes: i) a coal reactor (CR), where
604 coal is devolatilized and remaining char is gasified; ii) a volatile reactor (VR) above the
605 coal reactor, where volatile matter is converted; and iii) an air reactor to regenerate the
606 oxygen carrier. This concept is similar to that described by Proell and Hofbauer [188]
607 and used in the 25 kW_{th} CLC unit at TUHH [148]. A fluid dynamic study on the

608 suitability of stacking several fluidized beds for the fuel reactor has recently been
609 disseminated [189].
610 The University of Utah (UU) is erecting a 225 kW_{th} CLOU unit; see Fig. 17 [168, 169].
611 The design is based on dual circulating fluidized bed reactors and includes the
612 combustion of solid fuels such as coal or petcoke in CLOU mode. A suitable Cu-based
613 oxygen carrier has been developed in previous works for this purpose [69, 190]. This
614 unit includes a carbon stripper between fuel and air reactors.
615 Babcock & Wilcox (B&W), in collaboration with Ohio State University (OSU), has
616 designed a 250 kW_{th} CLC unit based on moving bed technology for the fuel reactor; see
617 Fig. 18 [170]. Several issues affecting the development of this technology will be
618 addressed, such as coal injection and distribution in the moving bed fuel reactor, the
619 separation of ash from oxygen carrier particles, as well as autothermal operation of the
620 system. The objective is to identify the development pathway for commercialization in
621 the year 2025 [191].

622 **3.2. Semi-industrial scale units**

623 In order to acquire experience on a semi-industrial scale, two CLC units on MW_{th} scale
624 have been designed, built and tested, with Alstom being the flagship of the technology
625 [44]. Thus, Darmstadt Technical University in collaboration with Alstom built a 1 MW_{th}
626 CLC pilot plant, while Alstom's research and development facility in Windsor
627 (Connecticut, USA) constructed a 3 MW_{th} facility following the Limestone-Based
628 Chemical Looping (LCL^{TM}) Process [192]. In addition, the 12 MW_{th} CFB boiler located
629 at Chalmers University of Technology in Sweden, was adapted to be used as CLC unit.
630 Thus, the 4 MW_{th} gasifier acted as the fuel reactor, while the boiler was the air reactor
631 [166].
632

3.2.1. 1 MW_{th} CLC unit at Darmstadt University of Technology (TUD, Germany)

The 1 MW_{th} CLC unit was designed to perform the combustion of coal via *i*G-CLC with naturally occurring Fe-based materials [42, 193, 194] using two interconnected circulating fluidized bed reactors. The initial design of this pilot unit incorporated a carbon separation system consisting of a cyclone system and a carbon stripper (see Fig. 19). In an early design, a low efficiency cyclone was used to recover mostly oxygen carrier particles which were sent to the carbon stripper. Light char particles escaping the low efficiency cyclone were recovered in a high efficiency cyclone and then recirculated to the fuel reactor. The carbon stripper was designed to separate char particles recovered by the low efficiency cyclone in the main oxygen carrier stream. The oxygen carrier circulation rate was controlled by using a screw conveyor attached to the loop seal [193]. In a second design, this conveyor has been replaced by an L-valve [42]. Operational results of the pilot plant have recently been reported using ilmenite as oxygen carrier and hard coal as fuel. Early results confirmed that coal combustion is possible in the 1 MW_{th} pilot plant, but autothermal operation has not been reached because of the low solids circulation rate used [42, 159]. Either partial combustion of coal by air in the fuel reactor or combustion of propane in the air reactor is required to maintain the operating temperature in the fuel reactor during these experimental campaigns. Autothermal operation has been obtained after some modifications to this unit. The temperature in the fuel reactor is 950 ºC. For this purpose, the carbon stripper has been removed from the CLC configuration [160]. Moreover, coarser coal particles are used compared to previous work in this unit which facilitates coal conversion by decreasing the amount of unconverted char particles escaping from the cyclones. However, the absence of the carbon stripper reduces the efficiency of CO_2 capture. Coal and partially-devolatilized biomass combustion has also been performed with an iron

ore as oxygen carrier at 900 ºC [161]. CO_2 capture and combustion efficiency with biomass is higher than with coal, but returns lower results than with ilmenite, which could be caused by lower temperature and/or differences in the solids circulation rate.

3.2.2. 3 MW_{th} CLC unit at Alstom Power (USA)

Alstom Power investigated CLC combustion of solid fuels based on the Limestone-Based Chemical Looping (LCL^{TM}) process [192]. In this process, $CaSO_4$ is the oxygen carrier but limestone ($CaCO_3$) is the calcium source. Limestone is fed together with coal as in the common coal combustion process in circulating fluidized beds with *in-situ* desulfurization [195]. After calcination of $CaCO_3$ in the fuel reactor, the CaO reacts with sulfur from coal to form CaS, which is oxidized to $CaSO_4$ in the air reactor. Therefore, sulfated limestone is used as oxygen carrier, which will be mixed together with unconverted CaO and ash from coal. The oxygen transport capacity depends on several factors, such as Ca/S ratio, sulfur retention or the sulfur and ash content of coal [164].

The 3 MW_{th} CLC unit consists of two interconnected circulating fluidized bed reactors; see Fig. 20. The fuel reactor (reducer) has an internal circulation loop. This reactor includes a so-called *cactus zone* where the solids returning from the two cyclones at the outlet of the fuel reactor and the solids returning from the air reactor (oxidizer) are mixed. The bottom area of the *cactus zone* is hydraulically connected to the air reactor and also acts as a carbon stripper. The slower solids moving in this area cause the solids to be densely packed.

The 3 MW_{th} CLC unit was first operated in 2011 [162]. Initially, the prototype was loaded with spent ash from a circulating fluidized bed, which would have a high $CaSO_4$ content. Next, coal was fed together with limestone. In order to achieve steady state, spent ash should be replaced by $CaSO_4$ being generated in-situ by the reaction of sulfur

683 with added limestone. Taking into account the design flow rates and solids inventory in
684 the system [164], full replacement could take about one day of operation. After
685 achieving full integration of the system, autothermal operation performed well at about
686 900-930 ºC [43], with the main observation being a carbon burnout of over 98%, low
687 unconverted char entering the air reactor, a combustion efficiency of about 80-85% and
688 low SO_2 emissions [163]. Sulfur emission was related to the $CaSO_4$ to fuel ratio. In
689 addition, the lower part of the cactus zone was highly effective in segregating
690 unconverted char particles, and therefore high CO_2 capture efficiency values were
691 obtained. More than 500 hours of operation in the prototype have been reported.
692 Recently, the 3 MW_{th} unit has been relocated to the Alstom Clean Energy Lab in
693 Bloomfield (Connecticut, USA) [44].

694 **3.2.3. 4 MW_{th} CLC boiler at Chalmers University of Technology (CUT, Sweden)**

695 Recently, operation in a circulating fluidized bed (CFB) boiler at CUT has been
696 reported; see Fig. 21 [166]. The CFB unit is a 12 MW_{th} boiler for biomass combustion,
697 in which a 2-4 MW_{th} gasifier was adapted in the return loop below the cyclone for
698 research purposes on dual fluidized bed gasification [165]. CLC operation was
699 performed using an oxygen carrier as bed material. Thus, the gasifier acted as the fuel
700 reactor, while the boiler was the air reactor. Experiments were carried out over 1000
701 hours using either ilmenite or manganese ore as an oxygen carrier. However, the
702 combustion efficiency achieved was about 60% due to segregation of char particles in
703 the bubbling fluidized bed. Thus, gasification products could not have the chance to
704 react with the oxygen carrier, as occurred with small coal particles in a smaller unit
705 [136]. Nevertheless, the solids mixing was improved by increasing the fluidization
706 velocity, thus increasing combustion efficiency. Optimization of operating conditions

and improvement of the fuel reactor design would result in higher conversion levels, which would enable the scale-up of CLC of biomass [166].

4. Experimental results obtained in CLC units for solid fuels

4.1. Parameters to evaluate the performance of a CLC unit

The operation of the CLC continuous units detailed in the above section has generated a significant amount of experimental data under different combustion conditions. Regardless of the type of configuration used in the CLC unit, one of the main problems encountered during operation was the existence of unconverted compounds at the outlet of the fuel reactor, which reduce the combustion efficiency, except for the case of the moving bed at OSU. As also shown in Fig. 1, these unburned compounds could be found in the form of both gaseous compounds (CO, H_2, CH_4, C_xH_y) and/or partially gasified char. Gaseous compounds come from volatile matter or gasification products. The char can either be elutriated with the gases leaving the fuel reactor or transferred together with the oxygen carrier particles to the air reactor where it is burnt, therefore decreasing the efficiency of the CO_2 capture.

In order to evaluate an *i*G-CLC system burning solid fuels, the amount of unburned compounds leaving the fuel reactor (both gases and partially gasified char) and the amount of carbon in the char transferred to the air reactor should be determined. This can be done through three performance parameters: solid fuel conversion, CO_2 capture and combustion efficiency [35, 145].

There are significant differences in the definitions used to estimate the solid fuel conversion, CO_2 capture efficiency and combustion efficiency. Some of the definitions of these and other parameters already calculated in literature are summarized below. Fig. 22 shows how the different parameters can be calculated based on the molar flows measured in a CLC unit.

Fuel conversion and CO_2 capture efficiency are based on a carbon balance (see Fig. 23), according to Eq. (1). In the following, carbon loss in the ash purge stream $F_{C,purge}$ has been considered negligible for the balance.

$$F_{C,sf} = F_{C,char} + F_{C,vol} = (F_{C,FR,out} - F_{CO_2,in}) + F_{C,AR,out} + F_{C,elut} + F_{C,purge} \quad (1)$$

In contrast, combustion efficiencies are based on oxygen balances (see Fig. 24). A table containing the main parameters and equations used to calculate the main parameters has been included in Figs. 23 and 24. Moreover, a column describing the parameter at boundary conditions has been added to provide a better understanding of the meaning of each parameter.

In addition, a standardized nomenclature has been used in this section to avoid misunderstandings. The corresponding name usually given in literature for some of these parameters has also been included.

4.1.1. Fuel conversion

The solid fuel converted in a CLC unit, both in fuel and air reactors, can be estimated through several carbon balances. In all cases, only carbon from fuel is considered and carbon in fluidizing CO_2 is not included. The following parameters are used to assess the fuel conversion.

- *Solid fuel conversion* (X_{sf}).

Solid fuel conversion, X_{sf}, is usually defined in the literature as η_{sf}. It is a measurement of the amount of solid fuel converted in the CLC unit, i.e. both in the fuel reactor and air reactor. Note that carbon not present in gaseous compounds corresponds to partially converted char lost by elutriation ($F_{C,elut}$) [136, 145, 196].

$$X_{sf} = \frac{\text{carbon in gases from FR and AR}}{\text{carbon in solid fuel}} \quad (2)$$

- *Char conversion in the CLC unit* (X_{char}).

Char conversion in the whole CLC unit, X_{char}, is usually defined in the literature as η_{char}. It specifies how much of the char ($F_{C,char}$) has been converted in the CLC unit, as it is realistic to assume that all the carbon contained in the volatiles is released into the fuel reactor gaseous stream and therefore contributes to the solid fuel conversion.

$$X_{char} = \frac{\text{fixed carbon converted in FR and AR}}{\text{fixed carbon in solid fuel}} = \frac{\text{fixed carbon in solid fuel - carbon in elutriated char}}{\text{fixed carbon in solid fuel}} \quad (3)$$

4.1.2. Carbon dioxide capture efficiency

Two different definitions can be found in literature to estimate the amount of carbon captured.

- CO_2 capture efficiency (η_{CC})

CO_2 capture efficiency specifies how much of the carbon introduced with the solid fuel is captured in gaseous form at the fuel reactor outlet

$$\eta_{CC} = \frac{\text{carbon in gases from FR}}{\text{carbon in gases from FR and AR}} \quad (4)$$

Carbon in gases exiting the fuel reactor comes from carbon contained in the volatiles (mostly methane) and the carbon in the gasified char. As a result, all this carbon will be converted to captured CO_2. Thus, the CO_2 capture efficiency calculated depends on the fraction of char that has been gasified [136, 140]. The amount of char being gasified in the fuel reactor ($X_{char,FR}$) can be calculated as:

$$X_{char,FR} = \frac{\text{fixed carbon gasified in FR}}{\text{fixed carbon in solid fuel - carbon in elutriated char}} \quad (5)$$

Note that the char conversion in the fuel reactor ($X_{char,FR}$) is not the same as char conversion previously defined for the whole CLC unit (X_{char}). Note as well that the

product $X_{char}{\cdot}X_{char,FR}$ is the carbon fraction in char being converted only in the fuel reactor, mainly by steam or CO_2 gasification in *i*G-CLC [47], and designated as $x_{char,FR}$:

$$x_{char,FR} = X_{char} X_{char,FR} = \frac{\text{fixed carbon gasified in FR}}{\text{fixed carbon in solid fuel}} \quad (6)$$

In some works, an easy extrapolation of the CO_2 capture efficiency to conditions where X_{sf} is close to 100% was done assuming that the char conversion rate does not depend on the degree of char conversion [101]. The estimated CO_2 capture efficiency was represented by η_{CC}^{*}. This parameter assumed that the char conversion would be the same with or without elutriation of unconverted char from the fuel reactor, as temperature is the most influential variable affecting char gasification rates [197]. Therefore, the value of the CO_2 capture can be estimated using the ultimate and proximate analysis of the coal and the char conversion obtained in the *i*G-CLC unit, according to the following expression.

$$\eta_{CC}^{*} = 1 - \frac{x_{fc}}{x_C} \cdot (1 - X_{char,FR}) \quad (7)$$

where x_{fc} is the fraction of fixed carbon in the solid fuel and x_C the fraction of carbon in the solid fuel.

- <u>Oxide oxygen fraction</u> (x_{oo})

Oxide oxygen fraction, χ_{oo}, is usually given in the literature as η_{OO}. This parameter is defined as the amount of oxygen used to oxidize the oxygen carrier in the air reactor divided by the sum of the oxygen used for oxidizing both the oxygen carrier and the char reaching the air reactor from the fuel reactor

$$\chi_{oo} = \frac{\text{oxygen reacted with the OC in AR}}{\text{total oxygen reacted in AR (OC+char)}} \quad (8)$$

The advantage of using this parameter is that only the O_2 and CO_2 concentration measured in the air reactor outlet is required to calculate it; see Eq. (9). However, the real CO_2 capture rate is not calculated.

$$\chi_{oo} = \frac{0.21 - y_{O_2,AR} - y_{CO_2,AR}}{0.21 - y_{O_2,AR} - 0.21 y_{CO_2,AR}} \quad (9)$$

Differences between η_{CC} and χ_{oo} will mainly depend on the oxygen taken to burn hydrogen in coal and the combustion efficiency in the CLC unit [36, 127].

4.1.3. Combustion efficiency

The combustion efficiency, which is also related to the purity of CO_2 at the fuel reactor outlet, is normally evaluated by oxygen demand.

- Total oxygen demand (Ω_T)

The total oxygen demand represents the amount of oxygen needed for complete combustion of unconverted products compared to the oxygen required to convert the fuel fed to CO_2 and H_2O.

$$\Omega_T = \frac{\text{oxygen needed to burn unconverted gases}}{\text{oxygen needed to burn solid fuel}} \quad (10)$$

Usually, only gaseous products exiting the fuel reactor are taken into account, because unconverted elutriated char would be separated from the gas stream and recirculated to the fuel reactor. This parameter gives a fast evaluation of the amount of oxygen required in a hypothetical oxygen polishing step after the fuel reactor; see Fig. 22. In CLC literature, this definition of oxygen demand is identified as total oxygen demand (Ω_T) [101, 138]. F_{CxHy} represents the gaseous hydrocarbons C2-C5 and tars.

- Combustion efficiency in fuel reactor ($\eta_{comb,FR}$)

The combustion efficiency in the fuel reactor ($\eta_{comb,FR}$) is a measure of the gas conversion in the fuel reactor. It is defined as the fraction of oxygen demanded by the

volatile matter and gasification products supplied by the oxygen carrier in the fuel reactor [136]

$$\eta_{comb,FR} = \frac{\text{oxygen transferred in FR}}{\text{oxygen demanded by solid fuel converted in FR}} \quad (11)$$

- Oxygen demand in FR (Ω_{FR})

Another definition of oxygen demand can be found in CLC literature for when the fuel fed is not totally converted in the fuel reactor, and it is usually designated by the symbol $\Omega_{OD.}$ In this paper, it is denoted as the oxygen demand in the fuel reactor (Ω_{FR}) and is related to the combustion efficiency in the fuel reactor ($\eta_{comb,FR}$). The oxygen demand in the fuel reactor (Ω_{FR}) is defined as the oxygen needed for complete combustion of unconverted gaseous products compared to the oxygen required to burn the fuel converted in the fuel reactor [36]:

$$\Omega_{FR} = 1-\eta_{comb,FR} = \frac{\text{oxygen needed to burn unconverted gases}}{\text{oxygen demanded by solid fuel converted in FR}} \quad (12)$$

The values of the two oxygen demand parameters are different, as Ω_{FR} is normally larger than Ω_T for similar experimental conditions. The oxygen demand in the fuel reactor (Ω_{FR}) is more affected by the degree of solid fuel conversion reached as the denominator takes as reference the effective fuel processed in the fuel reactor. The effective solid fuel may be less than the fuel fed, due to the losses from the unconverted char which may be elutriated ($F_{c,elut}$) or transferred to the air reactor, where it is burned to CO_2 ($F_{c,AR,out}$).The denominator in Ω_T does not depend on the fraction of char converted and, therefore, the total oxygen demand could be more intuitive, as it gives a more direct estimation of the amount of oxygen needed to reach complete combustion compared to the stoichiometric amount in an oxy-fuel combustion process. Thus, both

844 definitions of the oxygen demand are linked by the amount of carbon in the char that is
845 not converted in the fuel reactor (elutriated or transferred to the air reactor).

846 **4.2. Variables affecting the performance of the *i*G-CLC unit**

847 A comprehensive review was made to collect the parameters evaluating the combustion
848 performance in the CLC units presented in section 3. Table 4 gathers the main results
849 obtained for units operating under *i*G-CLC mode and Table 5 compiles results obtained
850 under CLOU conditions. Most of the results in Table 4 are based on Fe-based oxygen
851 carriers, as they are the most commonly chosen for *i*G-CLC [7]. In this selection,
852 particular attention was paid to the performance parameters previously mentioned, i.e.
853 solid fuel conversion, CO_2 capture efficiency and oxygen demand. If they have been
854 provided, Tables 4 and 5 incorporate their experimental values and the operating
855 conditions under which they were obtained.

856 As schematized in Fig. 25, the main operating conditions influencing CO_2 capture
857 efficiency and oxygen demand are the type of oxygen carrier chosen, the temperature in
858 the fuel reactor, the rate at which the oxygen carrier circulates between reactors and the
859 amount of solids present in the fuel reactor, the type of solid fuel used together with its
860 feeding rate, and the presence of a carbon stripper. In the following sections, the most
861 relevant information obtained in operating CLC units pertaining to the effect of these
862 variables on the solid fuel conversion, the CO_2 capture efficiency and oxygen demand
863 will be summarized.

864 **4.2.1. Relevance of the oxygen carrier**

865 The reactivity of the oxygen carrier both during reduction by the solid fuel and
866 oxidation in air is one of the most important aspects to be taken into account when
867 selecting a material for use in the *i*G-CLC process. The reactivity of the oxygen carrier
868 affects the oxygen demand and, to some extent, the CO_2 capture efficiency. Figs. 26A

and B plots most of the results summarized in Table 4 for oxygen carriers based on Ni, Fe and Cu, as well as for $CaSO_4$.

An oxygen carrier with high reactivity towards H_2, CO and CH_4 will reduce the amount of unburned gaseous products escaping from the fuel reactor and, therefore, the oxygen demand. Elemental studies based on density functional theory calculations (DFT) can be found in literature [203-207]). They analyze some aspects regarding the theoretical reactivity of oxygen carriers, such as the effect of metal oxide or the relevance of dopants addition.

Regarding CO_2 capture efficiency, there are other variables affecting the CO_2 capture reached besides the type of oxygen carrier. This fact makes it difficult to find clear trends based on the type of oxygen carrier used, see Fig. 26A. Nevertheless, the two properties of the oxygen carrier that can affect CO_2 capture efficiency are the reactivity [61] and capacity to transport oxygen. If the oxygen carrier presents high reactivity to H_2, the inhibiting effect of this gas on steam gasification of char would be reduced and the char gasification rate would be faster [208]. This would result in greater char conversion in the fuel reactor and, therefore, higher CO_2 capture efficiency. In addition, the oxygen transport capacity of the oxygen carrier, R_{OC}, can affect CO_2 capture, because the solids circulation rate required between fuel and air reactors depends on the R_{OC} value [209]. Thus, if an oxygen carrier with a high R_{OC} value is used, CO_2 capture would be increased by the reduced flow of circulating solids required between the fuel and air reactor [145].

The oxygen carriers used in *i*G-CLC are mainly based on oxides of Ni, Fe and Mn, although the use of $CaSO_4$ as an oxygen carrier has been also tested.

- Ni-based oxygen carriers

Ni-based oxygen carriers show high reactivity. Carbon capture efficiencies are high, as shown in Fig. 26A. In the figure, the yellow area covers all the cases in which high CO_2 capture efficiency was reached. Most of the experiments performed using NiO oxygen carriers fall into this area, except those using anthracite as fuel. However, there are some disadvantages in their use with solid fuels. First, they are easily poisoned by coals with high sulfur content [125, 175, 176]. Second, they are toxic and expensive compared to other metal oxides, and therefore the use of Ni is not advisable for solid fuels.

- Fe-based oxygen carriers

Most of the Fe-based oxygen carriers investigated until now are mainly minerals or industrial residues; as can also be seen in Fig. 26A, Fe-based materials have received most of the attention in the recent literature, especially ilmenite, a low-cost mineral ($FeTiO_3$). Ilmenite has excellent recyclability for the Fe_2TiO_5-$FeTiO_3$ redox pair and a relatively high oxygen transport capacity (R_{OC} = 5 wt.% for pure ilmenite) [210]. *A priori*, it presents good fluidization behavior and excellent physical stability. It shows a gain in the reactivity with the redox cycles until an activated state is reached [96, 136] and has demonstrated good reactivity to syngas components, i.e. H_2 and CO [211]. However, under some circumstances, e.g. high conversion during the reduction stage, Fe is found to migrate towards the outer surface of the particle, where a Fe-enriched shell is formed [96, 97]. Migrated Fe can be lost from the surface under the conditions existing in a circulating fluidized-bed [95]. This fact means that both the crushing strength of particles and the oxygen transport capacity decrease with operating time [97]. However, ilmenite's stability was maintained when variation in the conversion of

solids was limited to low values [136]. Typical reported values of total oxygen demand (Ω_T) operating with ilmenite and bituminous coal vary between 5-15% [120, 136, 145]. Some improvement in the performance of the *i*G-CLC was observed after adding $CaCO_3$ to ilmenite in a 10 kW_{th} CLC unit [114]. Thus, the oxygen demand decreased at 950 ºC due to the catalytic effect of lime on the water-gas shift reaction. This led to more highly reactive H_2 being produced to the detriment of the lower reactive CO with limestone addition. However, no effect was shown at 1000 ºC. In any case, the CO_2 capture was improved due to an increase in the char gasification rate.

In addition to ilmenite, iron ore has been widely used to burn coal [100, 101, 129, 133, 156, 161], biomass [127, 139, 141] or sewage sludge [132, 134] in several facilities ranging from 0.5 to 1000 kW_{th}. Moreover, it was used in the first *i*G-CLC operation under pressure [135]. As can be observed in Fig. 26B, lower values of Ω_T than those found for ilmenite have been reported using highly reactive Fe-based oxygen carriers, namely an iron ore and a bauxite waste [100, 101, 140]. These materials show higher reactivity to gasification products than ilmenite [98, 212], but the oxygen transport capacity is lower when Fe_2O_3 reduction is limited to Fe_3O_4 (R_{OC} = 3.3 wt% for pure hematite) due to thermodynamic restrictions enabling complete combustion of H_2 and CO in a fluidized bed reactor [181, 213]. In this case, faster solids circulation was required to increase the combustion efficiency, which decreased the CO_2 capture rate by 1-4 percentage points compared to the use of ilmenite [100] (see Fig. 26A). To maintain the CO_2 capture rate close to 100%, the design and operating conditions of the carbon separation system must be optimized.

With iron ore as an oxygen carrier, the combustion efficiency of biomass or sewage sludge was lower than that observed for coal when the fuel reactor was a fluidized bed [139], but the opposite was found with a spouted bed as the fuel reactor [132]. This fact

could be due to the different behavior of combustion of volatile matter and gasification products. From these results, it can be inferred that the combustion of volatile matter is improved when a spouted bed is used as the fuel reactor. In contrast, gasification products could be easily converted in a fluidized bed. Therefore, the final result obtained for each reactor type should be evaluated individually. An evaluation of the effect on CLC of the conversion of the volatile matter and gasification products will be shown in section 5.

In order to improve the performance of natural hematite, some studies have focused on modifying the original iron ore. Fundamental studies on the development of oxygen carriers based on Na-, K- or Ca-modified Fe-based materials showed that the presence of these compounds greatly boosted the oxygen carrier reactivity and char conversion rate [214-222]. Thus, the use of a K-modified iron ore improved the CO_2 capture and combustion efficiency burning coal in a 1 kW_{th} CLC unit [130]. The addition of K increased the reactivity of iron ore, and the catalytic effect of K on char conversion was suggested as a reason for the improved performance of this material in *i*G-CLC process. This effect can be also observed in Fig. 26A. The experiments performed with an iron ore and a high sodium coal as fuel lie under the yellow area, with similar CO_2 capture efficiencies to those obtained with NiO-based materials, due to the catalytic effect of Na on char gasification [133].

In contrast to the use of Fe-based materials in a fluidized bed reactor, almost full fuel combustion has been found when a Fe-based oxygen carrier was used in a counter-current moving bed reactor, even if Fe_2O_3 was reduced to metallic Fe [151-153]. In this case, thermodynamic restrictions to allow complete conversion of H_2 and CO to H_2O and CO_2 are overcome because Fe_2O_3 is put in contact with exiting gases in the counter-current mode [151]. However, higher particle size is required to prevent fluidization in

968 the moving bed reactor, which demands large quantities of air to transport particles in
969 the L-valve and air reactor riser [53].

970 • Mn-based oxygen carriers

971 Manganese ores are also low-cost materials being tested as oxygen carriers in *i*G-CLC
972 of solid fuels. Generally, the Mn_3O_4/MnO redox system is used in *i*G-CLC mode, which
973 possesses an oxygen transport capacity of R_{OC} = 7 wt.%. Experiments in a 10 kW_{th} unit
974 with low-volatile fuels, such as petcoke and wood char, showed that manganese ores
975 presented increased char gasification compared to ilmenite, which resulted in increased
976 CO_2 capture efficiency [54, 115]. Recently, mixtures of ilmenite and manganese
977 minerals were tested in the 100 kW_{th} unit at CUT [122] using two bituminous coals and
978 wood char. Results indicate that the addition of small amounts of manganese ore (up to
979 8%) to ilmenite could almost halve the amount of unconverted gas, while the fuel
980 conversion in the fuel reactor was barely affected. On one hand, the increase observed
981 in combustion efficiency was related to the higher reactivity of manganese ores with H_2
982 and CO, compared to ilmenite [93, 102]. On the other hand, the increase in the char
983 gasification rate was attributed not only to the higher reactivity of the manganese ore to
984 syngas, but also to the catalytic effect on char gasification of Na and K released by the
985 manganese ore and deposited on the char surface [105]. Nevertheless, Na and K is lost
986 during CLC operation, which means that eventually the gasification rate with
987 manganese ores would be similar to that observed with ilmenite after a few hours of
988 operation [103]. However, one manganese ore which maintains a relatively high char
989 conversion rate after several redox cycles has been identified [103]. No other reasons
990 have been found for the increase of the char conversion rate [223-225] and this effect
991 should be analyzed in more detail. The main problems of using manganese ores in CLC
992 units concerned the high fraction of fines generated, which caused operational problems

and decreased the life-time of the material [226]. Recently some attrition resistant manganese ores have been found [54, 102, 226] which encourages further research on the use of this kind of low cost material.

- $CaSO_4$ as oxygen carrier

The use of anhydrite ($CaSO_4$) as an oxygen carrier has received significant attention due to its high oxygen transport capacity (R_{OC} = 47 wt%) compared to Fe or Mn-based materials [7, 227, 228]. This property benefits the CO_2 capture rate, as slower solids circulation between fuel and air reactors would be required [145, 209]. However, several problems have been detected from lab-scale experiments, and operation in a CLC unit has not been carried out. These problems are related to the low reactivity of anhydrite ore [106, 109, 229] and the release of sulfur compounds during the redox process between $CaSO_4$ and CaS [107, 108, 110, 230]. Some solutions have been proposed to avoid sulfur release, including the following: (1) to have incomplete combustion in the CLC unit, which hinders sulfur release in the fuel reactor [231]; full combustion would be reached in another CLC unit downstream from the fuel reactor, based on a metal oxide material [232]; (2) suppression of side reactions involved in sulfur release by adding hematite to anhydrite [233-237]; (3) addition of Ca-based sorbents, i.e. CaO or $CaCO_3$, as desulfurization sorbents [238].

Despite anhydrite not having been tested in a CLC unit burning coal, the use of $CaSO_4$ as an oxygen carrier has been implemented via the Limestone-Based Chemical Looping (LCL^{TM}) process [192] at the 3 MW_{th} scale CLC unit [163]. In this case, the $CaSO_4$ oxygen carrier is generated in situ by the reaction of limestone with sulfur in coal; thus, in situ desulfurization is also carried out. In this way, problems associated with sulfur emission are avoided. In addition, $CaSO_4$ formed in the sulfation of limestone is more reactive than anhydrite ore and in the order of magnitude of Fe-based oxygen carriers

[111]. A similar performance would be expected in the LCL^{TM} process and *i*G-CLC with iron minerals.

- Synthetic oxygen carriers

Although low cost materials are normally preferred in solid fuel CLC, the use of synthetic materials may benefit some cases. The main reason for their development is their high reactivity together with other significant characteristics. In fact, promising results have been found for Fe-Mn [89] and Mn-Si-Ti [239] mixed oxides in the 0.5 kW and 10 kW CLC units at ICB-CSIC and CUT, respectively. Especially interesting are the magnetic properties shown by Fe-Mn materials, which could be used for magnetic separation from ash particles [240].

4.2.2. Relevance of the temperature in the fuel reactor

The effect of the fuel reactor temperature on the performance of the *i*G-CLC process has been intensively evaluated. As previously shown in Fig. 26, the fuel reactor temperature can affect both the final CO_2 capture efficiency and the oxygen demand. Regardless of the type of oxygen carrier used, it is clear from Fig. 26A that an increase in the fuel reactor temperature increases CO_2 capture and reduces oxygen demand as the fuel reactor temperature increases.

It must be remembered that high temperatures enhance char gasification in the fuel reactor, which is the limiting step in the *i*G-CLC process. Higher char gasification rates lead to greater char conversion in the fuel reactor and less char reaching the air reactor, therefore higher CO_2 capture efficiencies are obtained. Higher temperatures also favor the reactivity of the oxygen carrier to the gaseous fuels released in coal gasification, but the effect of temperature on the reactivity of the oxygen carrier is not as significant as the increase in the char gasification rate (Fig. 26B), even if highly reactive oxygen carriers are used. As an example, in the combustion of bituminous coal with ilmenite,

the activation energy for the reaction of ilmenite with H_2, CO and CH_4 in the temperature range appropriate for *i*G-CLC is between 65-135 kJ/mol [211], while the activation energy for steam gasification of bituminous char in the same temperature range is about 160 kJ/mol [177].

In order to reduce the amount of non-gasified char reaching the air reactor and increasing CO_2 capture efficiency, the experimental results obtained until now point to high temperatures around 1000 ºC in the fuel reactor for coal [118, 129, 136, 140, 145, 156]. This conclusion also applies to using a moving bed design as fuel reactor, where there is a temperature profile along the reactor. Due to the heat loss, the temperature at the bottom and top area is lower than in the middle section [241]. In the experiments performed with metallurgical coke as fuel and iron oxide as the oxygen carrier, it was observed that temperature was the most significant factor affecting carbon conversion. The conversion of the metallurgical coke increased faster in the middle section where the temperature was also the highest in the temperature profile. An increase in carbon conversion from 30% to 72% was observed when the temperature increased from 960 to 1010 ºC [241].

4.2.3. Relevance of the solids circulation rate

In a CLC system, the solids circulation rate between fuel and air reactors should be high enough to ensure that both the oxygen needed for combustion and the heat needed to maintain the heat balance are transferred between reactors [209]. The effect of the solids circulation rate on the CO_2 capture and combustion efficiency is usually evaluated through the oxygen carrier to fuel ratio, ϕ [242]. This parameter is defined as the molar ratio between the oxygen available in the circulating oxygen carrier and the stoichiometric oxygen required to burn the fuel. For correct calculation of the ϕ parameter, the oxygen carrier is assumed to be completely oxidized in the air reactor.

An oxygen carrier to fuel ratio value of $\phi = 1$ means that the stoichiometric oxygen can be supplied by the oxygen carrier, while if $\phi > 1$ an excess of oxygen would be transferred from the air to the fuel reactor. Note that the variation of solid conversion between the air and fuel reactor decreases as the ϕ parameter increases [243], which will be important for the following discussion. In Fig. 27A, it can be observed that in the units without a carbon stripper, an increase in the solids circulation rate leads to a decrease in the CO_2 capture efficiency [138, 140]. Faster solids circulation means shorter residence times in the fuel reactor and this directly affects char gasification. The shorter the residence time, the lower the char conversion and therefore, lower CO_2 capture efficiencies. In the CLC units with a carbon separation system (under the grey area in Fig. 27A), the CO_2 capture values were usually close to 100%. In this case, the solids circulation rate on the CO_2 capture was less effective because the presence of the carbon stripper increased the residence time of char particles in the fuel reactor. This effect has also been observed in the 10 kW_{th} CLC unit developed at IFPEN under experiments with a bituminous coal [147].

The 50 kW_{th} CLC unit at ICB-CSIC and the 100 kW_{th} CLC unit at CUT were designed to allow for independent control of the global solids circulation rate and solids inventory in the fuel reactor. In experiments using ilmenite and bituminous coals at CUT, an increase in the flow in the circulation riser led to a decrease in the residence time and a decrease in CO_2 capture was observed [123, 145]. Nevertheless, this effect was barely noticeable when the carbon separation system was highly efficient in separating char particles, thus avoiding unconverted char particles from entering the air reactor [120], and CO_2 capture rates were always close to 100%.

Fig. 27B plots the results for oxygen demand obtained in studies with different oxygen carriers when the value of the solids circulation rate was varied, while the fuel reactor

1093 temperature was maintained stable for each experimental series. The main effect is
1094 probably due to the variation of the average reactivity of solids in the fuel reactor, which
1095 depends on the variation of solids conversion [209].
1096 Some qualitative differences can be found in Fig. 27B in the results obtained from
1097 different CLC units, depending on the operating conditions. In some cases, the variation
1098 of the solids circulation rate barely affected the total oxygen demand [121, 123, 138,
1099 140]. In these cases, the variation of the solids conversion was low either because ϕ was
1100 high, e.g. $\phi > 2.5$ in the 100 kW_{th} at CUT [120] or the fuel conversion was not complete,
1101 e.g. in the 0.5 kW_{th} CLC at ICB-CSIC [138, 140]. Under such conditions, the variation
1102 of the average reactivity of solids in the fuel reactor is only slightly affected by the
1103 solids circulation rate [209], and it is logical to find that this parameter has little effect
1104 on the combustion efficiency [61]. In other cases, an increase in the solids circulation
1105 rate resulted in a significant decrease of the total oxygen demand in experiments
1106 performed in the 50 kW_{th} CLC unit at ICB-CSIC [145], when the ϕ ratio was
1107 maintained between 1 and 1.5, meaning that the variation in solids conversion was
1108 higher than in the other cases. These conditions increase the average reactivity [177],
1109 which eventually affects combustion efficiency.
1110 As a conclusion from the results obtained in different units, a ϕ value in the 2-4 interval
1111 is recommended in order to boost combustion efficiency, but without a detrimental
1112 effect on the CO_2 capture [244].

1113 **4.2.4. Relevance of the specific solids inventory in the fuel reactor**

1114 The solids inventory present in the fuel reactor is also an important variable to be
1115 considered in reaching low values of oxygen demand [61]. Fig. 28 shows the effect of
1116 the solids inventory on CO_2 capture efficiency and oxygen demand found in studies
1117 compiled in Table 4.

Experiments performed using ilmenite as an oxygen carrier and bituminous coal as fuel in the 50 kW_{th} unit at ICB-CSIC and 100 kW_{th} unit at CUT showed that the inventory in the fuel reactor has a relevant impact on the combustion efficiency or oxygen demand [121, 123, 145]. In general, the oxygen demand decreased as the solids inventory in the fuel reactor increased from 350 to 700 kg/MW_{th}. Theoretical results showed that a further increase would have a lower effect on the combustion efficiency, and a solids inventory higher than 1000 kg/MW_{th} would be not recommended, due to the resulting high pressure drop in the fuel reactor [244, 245]. However, the CO_2 capture efficiency in Fig. 28A was less dependent on the amount of oxygen carrier in the fuel reactor, since the char recirculated from the carbon stripper. Thus, the average residence time of solids in the fuel reactor was mainly affected by the presence of the carbon stripper rather than the amount of solids in the fuel reactor. This scenario is plausible when the carbon stripper is highly efficient [120], but CO_2 capture will increase with the solids inventory when the efficiency of the carbon stripper separating char particles is low, e.g. < 90% [61].

4.2.5. Effect of the H_2O/CO_2 ratio

The recirculation of part of the CO_2 from the flue gases to be used as a fluidizing/gasifying agent in the fuel reactor would be of interest to minimize steam generation and the energy costs associated with it; see Fig. 1. The effect of the composition of the gasifying agent on the performance of the *i*G-CLC process is summarized in Fig. 29. At ICB-CSIC, different H_2O/CO_2 ratios in the gasifying agent were fed into the fuel reactor in a 0.5 kW_{th} CLC unit [137]. In experiments with ilmenite and different types of coal, the CO_2 capture efficiency increased with a higher H_2O fraction in the feeding flow, because the gasification rate was higher using steam rather than CO_2 as a gasifying agent under similar experimental conditions, see Fig.

29A. This conclusion was also reached in experiments in the 10 kW_{th} CLC at IFPEN with a bituminous coal [147], where it was found that CO_2 was less effective than steam during char gasification.

Nevertheless, the extent of the difference in the char gasification rate when steam or CO_2 is used depends on the type of fuel [137]. Thus, for highly reactive coals such as lignite, the differences in CO_2 capture using either H_2O or CO_2 as a gasifying agent did not significantly affect the performance of the process and thus CO_2 could be used to replace steam, with the corresponding energy savings from stream production. Similar conclusions were reached in the two-stage bubbling fluidized bed fuel reactor at TUHH. In experiments using ilmenite and lignite, the results obtained from changing the fluidization medium from H_2O to CO_2 indicate that the gasification is not the conversion limiting step [148].

On the other hand, the oxygen demand in Fig. 29B seems to be hardly affected by the composition of the gasification agent [137]. When steam is used as a gasifying agent, H_2 and CO are produced as gasification products, while CO is the only product when CO_2 is used as gasifying agent. Even when ilmenite reacts faster with H_2 than with CO, the high solids inventory in the fuel reactor used in the experiments shown in Fig. 29B [137] meant that no significant changes in the oxygen demand were observed when the gasification products were enriched in H_2 or CO. Moreover, the reason for incomplete combustion of gaseous products in the 0.5 kW_{th} CLC unit used at ICB-CSIC was poor contact between the oxygen carrier and volatiles. Therefore, the composition of the gasification products (H_2 or CO-enriched) was not important for the final oxygen demand reached in this unit with a bubbling FR.

4.2.6. Effect of the coal used

The coal rank clearly influences CO_2 capture efficiency, as can be observed by comparing plots shown in Fig. 26A. Dedicated studies on the feasibility of using different types of coal in *i*G-CLC have been carried out in a 0.5 kW_{th} CLC unit at ICB-CSIC with ilmenite and iron ore as an oxygen carrier [101, 137] and anthracite, bituminous coals of varying volatile content, and lignite as fuels. They observed greater CO_2 capture efficiencies for the coals with a faster char gasification rate and higher volatile content, since the carbon from the volatiles is always captured in the fuel reactor. This effect was especially noticeable with lignite. In the case of coals with a slow gasification rate, such as anthracite, a highly efficient carbon stripper would be needed to separate unconverted char particles and send them back to the fuel reactor in order to obtain adequate CO_2 capture efficiencies.

In addition, lower values of oxygen demand were found for the coals with a faster char gasification rate and lower volatile content, since the oxygen demand in the 0.5 kW_{th} unit is limited by the low conversion of volatile matter [136]. When the combustion efficiency of the volatiles from the different types of coal was calculated, it was concluded that it depended on the composition of the released volatiles, the highest being obtained for those from bituminous coal (58-61% efficiency) and the lowest from anthracite (42%).

The effect of the coal rank on CO_2 capture efficiency and/or oxygen demand has been also noted in other studies at CUT [124]. Mexican petroleum coke and a bituminous coal were used in the 100 kW_{th} CLC unit with ilmenite as an oxygen carrier. Lower values of oxygen demand were found in experiments with petroleum coke with a lower volatile content.

Impurities present in the coal can also affect performance in an *i*G-CLC unit. Recently, Ge et al. [133] evaluated the CO_2 capture efficiency reached in experiments with hematite and four coals with different volatile content (three bituminous coals and one anthracite). One of the bituminous coals, known as ZD, contained very high sodium content (7.5%). The carbon capture efficiency values obtained followed the same order as the volatile content, except for ZD bituminous coal. Although the volatile content in ZD was lower than in the other bituminous coals, it returned the highest CO_2 capture efficiency, which was attributed to the catalytic effect of Na on char gasification (see results in Fig.26A).

Figs. 26A and B show the tendencies observed in the results gathered in Table 4. As can be seen, except for NiO-based oxygen carriers, or cases where a carbon stripper is included in the unit, the types of fuel under the yellow area in Fig. 26A are those with a higher content of volatiles, i.e. lignite, biomass and sewage sludge. The blue area in Fig. 26A shows the experiments with the lowest CO_2 capture efficiencies, most of which were performed with anthracite as fuel. The effect of the coal rank on the oxygen demand can also be corroborated from Fig. 26B. The lowest values in the figure were obtained in experiments with anthracite or petcoke.

The coal rank used was also taken into account when using a moving bed as fuel reactor. In coals with a high volatile content, a co-current flow pattern for gas and solids is preferred to counter-current, to facilitate the full conversion of coal through improved conversion of volatile matter [241].

4.2.7. Effect of pressure

There are few studies to date addressing the effect on CLC performance of operating at pressures higher than atmospheric. The most significant study was presented by Xiao et al. [135] from Southeast University. These authors performed a study in a CLC unit

consisting of two fluidized bed reactors operating in the fast/turbulent fluidization regime, which improved the gas-solid contact. They used bituminous coal as fuel and an iron ore as the oxygen carrier and the operating temperature in fuel and air reactors were set to 950 and 970 ºC, respectively. A decrease in the amount of unconverted gases (CO, H_2 and CH_4) was observed when the pressure was increased from 0.1 to 0.5 MPa. This fact was attributed to the enhancement of reduction reactions of the oxygen carrier with pressure, which was previously observed by the same authors in experiments in a batch fixed bed reactor [246, 247]. The combustion efficiency increased from 93.5% to 98% and the CO_2 capture efficiency rose from 82.9% to 86.8% when pressure was increased from 0.1 to 0.5 MPa [135]. The fact that less H_2 and CO were present in the fuel reactor atmosphere reduced char gasification inhibition and the char gasification rate increased, boosting CO_2 capture. No agglomeration or changes in the morphology or reactivity of the oxygen carrier were observed, although its specific surface area and the pore volume improved slightly. This experiment demonstrated the advantages that operation at high pressures could bring to the CLC process. The pressurized CLC unit operated for 19 hours with coal feeding and 13.5 hours at stable operation with a thermal power of 50 kW_{th}. Nevertheless, more work is needed to solve the challenges arising from operating at high pressures, before the process can be scaled up.

4.2.8. Effect of the carbon stripper

As mentioned before, high temperatures in the fuel reactor (1000 ºC) can increase the CO_2 capture efficiency obtained in the *i*G-CLC unit. In addition, the amount of non-gasified char reaching the air reactor and then decreasing the CO_2 capture efficiency can be further reduced by fitting a carbon stripper between the fuel and air reactors [48]. An efficient carbon stripper can separate almost all the ungasified char from the oxygen carrier before reaching the air reactor and send it back to the fuel reactor, thus obtaining

high CO_2 capture [60]. This effect is observed in Fig. 26A. The results obtained in CLC units with a carbon stripper fall under the yellow area covering the results with the highest CO_2 capture efficiencies. Several of the CLC units described in the previous sections of this paper incorporate a carbon stripper between the fuel and air reactors. Fig. 30 presents a summary of the different designs in operating CLC units. Nevertheless, only a few studies in the literature analyze the performance of the carbon stripper. It must be realized that the design and operating conditions of the carbon stripper heavily influence the efficiency of char separation, and hence the CO_2 capture achieved.

In the 10 kW_{th} unit at CUT, the carbon stripper was integrated into the fuel reactor (Fig. 30A) [36]. A similar design was used for the recently built 10 kW_{th} unit at GIEC [154, 155]. At the 1 MW_{th} unit at TUD, the carbon stripper consisted of a single chamber where char was separated from the oxygen carrier (Fig. 30B) [43]. Studies performed at TUHH [49] simulated the carbon stripping process using the carbon stripper as a fluidized bed. The influence of different operating parameters on the performance of char and oxygen carrier separation was analyzed. However, possible reactions taking place in the carbon stripper were not included in the simulation [120], but the velocity of the fluidizing gas in the carbon stripper was indicated as one of the main parameters influencing the carbon stripper operation and, therefore, the improvement in CO_2 capture efficiency. A two-chamber carbon stripper was tested at ICB-CSIC (Fig. 30C) [144]. Operating conditions in the carbon stripper were evaluated experimentally. The gas velocity was modified and maintained sufficiently low to avoid elutriation of oxygen carrier particles in experiments carried out in the 50 kW_{th} CLC unit at ICB-CSIC [145]. Clearly, CO_2 capture was improved by increasing the gas velocity due to more char being entrained from the bed. However, at the highest velocity (0.7 m/s), no

relevant improvement was observed compared to results obtained at 0.5 m/s. A two-chamber carbon stripper similar to that at ICB-CSIC was implemented at the newly designed 50 kW_{th} CLC unit at HUST [157].

A high efficiency carbon stripper was incorporated in the 100 kW_{th} unit at CUT (Fig. 30D) [123] . The design featured a four chambered bubbling fluidized bed, with the aim of forcing the solids to move upward and downward between chambers. Sufficient fluidization and flow of solids was observed in a cold flow model [248], a design that allows a very low fraction of unconverted char to reach the air reactor, thus achieving CO_2 capture values close to 100% with different fuels and oxygen carriers [100, 121-124]. From the experimental results obtained in the 100 kW_{th} unit, the efficiency of the carbon stripper was estimated using theoretical simulations [120]. An average value for the carbon stripper efficiency was estimated at 99.4% for the unit.

Moreover, the carbon stripper is an additional reactor in which char gasification can take place. The relevance of char gasification in the carbon stripper was evaluated in the 100 kW_{th} unit at CUT using ilmenite and a bituminous coal as fuel [123]. For this purpose, the steam supplied as the fluidizing agent in the carbon stripper was replaced with the same volumetric flow of nitrogen. Thus, the char separation efficiency of the carbon stripper would not be modified, but gasification of char particles cannot take place. According to the results reported, the CO_2 capture efficiency decreased from around 98.5 to 95.5%. Therefore, improvement in CO_2 capture efficiency due to char gasification in the carbon stripper was estimated to be 3 percentage points. By modeling the carbon stripper, it was found that the extent of char gasification in the carbon stripper was low, because the concentration of char in the reactor was low [244]. In fact, this is the purpose of the carbon stripper: to separate char from the oxygen carrier, so the solids will be oxygen carrier concentrated. A four-chambered carbon stripper was

also used at Tsinghua University (China) where a cold flow model of a 70 kW_{th} chemical looping combustor was used to analyze factors affecting the performance of the carbon stripper, such as gas velocity in the carbon stripper, the solids circulation rate and the inner structure of the carbon stripper [50]. The carbon stripper was designed as a turbulent fluidized bed in its lower part. The upper part was designed with the aim of increasing the gas velocity by a factor of 20 through a decrease in the sectional area. The experiments confirmed that the velocity of the gas used to fluidize the carbon stripper bed influenced the efficiency of carbon separation. Higher velocities improved the separation. The effect of decreasing the residence time of the solids in the fuel reactor by changing the solids circulation flow in the carbon stripper was also checked, and it was observed that lower residence times led to lower separation efficiency. It was suggested that the use of a carbon stripper is especially interesting for solid fuels with low reactivity.

The 3 MW_{th} CLC unit from Alstom also incorporates a carbon stripper, but in this case, the lower part of the cactus zone separated unconverted char particles (Fig. 30G) [43].

Finally, some new concepts for carbon stripper design have appeared recently at Tsinghua University (TU) (Fig. 30E and 30F): the annular carbon stripper [249] and the riser-based carbon stripper [51]. The typical range for gas velocities in the carbon stripper is 0.15-0.4 m/s [51]. Carbon strippers commonly operate in the bubbling or turbulent fluidization regime. Under these conditions, the separation of char from oxygen carrier particles takes place in the freeboard zone above the bed surface. Taking this into account and in order to maximize separation, a riser-based carbon stripper was proposed [51]. Using a cold flow model, it was observed that high separation efficiencies could be achieved when the gas velocity in the riser rose to an optimum value. A further rise in gas velocity did not lead to large increases in separation

efficiencies. Moreover, the separation efficiency decreased as the solids mixture feeding rate increased.

In any case, two strategies can be considered in order to separate unconverted char from oxygen carrier particles: a dedicated carbon stripper and in-built carbon-stripper. For either of these, the particle size of the oxygen carrier and coal must be carefully selected in order to show sufficiently different fluid dynamic properties for separation purposes. The particle size of the solid fuel should be large enough for efficient recovery by the cyclone system, and at the same time small enough to be successfully separated from oxygen carrier particles. Concerning char separation, the external carbon stripper enables specific control of the operating conditions without modifying the existing conditions in the fuel reactor. In this respect, the in-built carbon stripper in the fuel reactor would be less flexible, although it avoids adding another piece of equipment.

4.2.9. Effect of the fuel reactor design

Table 6 summarizes the characteristics of the main operating units. Some of the first CLC units designed to burn solid fuels used a bubbling fluidized bed or a spouted bed as fuel reactor. However, the latter design had no particular advantage, as although the spouted bed could minimize the losses of material due to elutriation, the gas-solid contact was inferior to a bubbling fluidized bed.

This was experimentally observed in the 1-10 kW_{th} CLC units at SU which used a spouted bed as fuel reactor [39, 126] .

In view of the configurations chosen in the *i*G-CLC units burning solid fuels currently under operation, the most common trend is to use two interconnected circulating fluidized beds as fuel and air reactors. The use of a circulating fluidized bed as fuel reactor makes operation of the unit more flexible than when a bubbling fluidized bed is used. The solids circulation rate and mass inventory in the fuel reactor can be more

easily regulated and this can result in better control of combustion conditions. This is shown when results obtained in the 0.5 kW_{th} (bubbling fuel reactor) and 50 kW_{th} (circulating fuel reactor) CLC units at ICB-CSIC are compared for the same oxygen carrier and coal [251]. Improved conversion of volatile matter was observed in the dilute region above the dense bed in the circulating fuel reactor of the 50 kW_{th} unit, which operated in the turbulent fluidization regime. [144].

At CUT, the overall performance in the 100 kW_{th} unit (high velocity fuel reactor) was higher than in the 10 kW_{th} unit (bubbling fuel reactor), as can be seen in Table 6. Both gas and solid fuel conversion were much higher in the larger unit. Using ilmenite and bituminous Colombian coal, CO_2 capture efficiencies above 99% and oxygen demands (Ω_{FR}) around 16% were reached in the 100 kW_{th} unit in the temperature range 940-980 ºC [123], while the values obtained and oxygen demand (Ω_{FR}) in the 10 kW_{th} unit were 82-96% and 20%, respectively, in experiments with South African bituminous coal [36]. The improvement in the CO_2 capture was due to the highly efficient carbon stripper included in the 100 kW_{th} unit. Fuel combustion was more efficient because of improved contact between gases from coal conversion and oxygen carrier particles, which was also promoted by a better mix between char and oxygen carrier particles.

In order to improve the gas-solids contact to further decrease the oxygen demand, a moving bed as fuel reactor is an interesting option. Table 6 shows results from the 25 kW_{th} CLC unit at OSU unit using Fe_2O_3 as oxygen carrier and solid fuels such as metallurgical coal, lignite and sub-bituminous coal. High solid fuel conversions (95-96%) and CO_2 purity of more than 99% at the outlet at the fuel reactor were reached [53, 152, 153, 241]. In tests with sub-bituminous coal, CO_2 capture efficiencies around 95% and oxygen demands (Ω_{FR}) as low as 0.14% were registered [153]. However, in order to consider the moving bed as an alternative to the circulating fluidized bed,

operational problems arising from the large particle size needed and the existence of temperature gradients in the fuel reactor should first be solved.

Following the comprehensive analysis above of the influence of different operating variables on CO_2 capture efficiency and oxygen demand in a CLC system, Figs. 31 and 32 are presented as a graphic summary. Both figures are based on results in CLC units at ICB-CSIC and CUT. Fig. 31 was obtained for the combustion of bituminous coals. Interesting general conclusions can be obtained from comparing these results using Fe-based oxygen carriers with different reactivity. First, the increase in both the residence time in the fuel reactor and the fuel reactor temperature led to an increase in CO_2 capture efficiency. Second, the presence of a carbon stripper enabled high CO_2 capture with short residence times (see results from the 50 kW_{th} unit in Fig. 31A). In Fig. 31B, where both CLC units incorporate a carbon stripper, high values of CO_2 capture were obtained regardless of the residence time.

A similar concluding analysis can be performed for the total oxygen demand in Fig. 32. From the figure, it is clear that both the oxygen carrier to fuel ratio and the specific solids inventory in the FR affect the value of the total oxygen demand. For the same type of solid fuel, high solids inventories decrease the total oxygen demand. However, the influence of the oxygen carrier to fuel ratio on the total oxygen demand is much less. In Fig. 32A, the total oxygen demand is also affected by the reactivity of the oxygen carrier. The higher the reactivity, the lower the oxygen demanded. In Fig. 32B, the effect of the type of solid fuel can be observed. Lower oxygen demand values are expected from petcoke in the 10 kW_{th} unit. The design also affected the final value of oxygen demand, as results for petcoke and bituminous coal in the 10 kW_{th} reactor show that lower oxygen demand values were obtained when the fuel was fed inside the fuel reactor bed.

4.3. Variables affecting the performance of the CLOU unit

The variables affecting the performance of the CLOU process are the same as those shown in Fig. 25 for *i*G-CLC. In this case, the temperature in both fuel and air reactors becomes even more important. Appropriate control and optimization are needed to obtain the amount of oxygen required in the fuel reactor, and complete regeneration of the oxygen carrier in the air reactor. The optimum temperature values for the specific oxygen carrier have been researched in different studies summarized in Table 5. In these studies, the influence on CO_2 capture and oxygen demand of different variables such as coal rank, coal feeding rate and solids inventory in the fuel reactor were also investigated. Results are summarized below.

The use of oxygen carriers with CLOU properties significantly improves the performance of CLC of solid fuels. Although there is an increasing number of studies on the development of this type of material [64, 67, 77, 78], only a few have been tested in a continuous CLC unit burning solid fuels. Fig. 33 shows the values of CO_2 capture efficiency for different fuel reactor temperatures and the oxygen carriers tested. At ICB-CSIC, two Cu-based oxygen carriers based on CuO (50-60%) and supported on $MgAl_2O_4$, i.e. Cu60MgAl and Cu50Fe10MgAl, were tested in the 0.5 kW_{th} continuous unit burning coals and biomass [142, 143, 199, 252]. The oxygen transport capacity, R_{OC}, of these oxygen carriers was 6 and 4.5 wt.%, respectively. The proof of the CLOU concept was carried out in the 0.5 kW_{th} CLC unit with Cu60MgAl material and a bituminous coal. At temperatures for coal combustion, both of the oxygen carriers showed complete combustion of volatile/gasification products, regardless the solid fuel used. A total of seventy five hours of continuous operation were run with these Cu-based materials. However, after this time, a decrease in the mechanical strength linked to an increase in the porosity of the materials was observed [143]. This same tendency

had been observed before in experiments in a batch fluidized bed reactor [68]. Thus, improvements in the lifetime of these materials should be incorporated in order to be considered for further scale-up.

On the other hand, a perovskite-type oxygen carrier ($CaMn_{0.9}Mg_{0.1}O_{3-\delta}$) with partial CLOU properties has been tested in the 10 kW_{th} unit at CUT using both petcoke and biochar with low sulfur content as fuels [57, 117]. The same material had previously been tested with gaseous fuels, when complete combustion of natural gas was reached [253]. In the experiments with solid fuels, this oxygen carrier showed better performance than other materials such as ilmenite, although the oxygen release rate was slower than for Cu-based oxygen carriers [81, 117]. Using petcoke as fuel, the combustion efficiency increased from 76.4 with ilmenite to 92.3% when the perovskite oxygen carrier was used. However, during the experiments with petcoke, sulfur accumulation in the oxygen carrier was observed, which affected its performance and made a regeneration step necessary.

4.3.1. Relevance of the temperature in the fuel reactor

The operating temperature in fuel and air reactors is a crucial parameter in the CLOU process because the oxygen concentration at the gas-solid equilibrium and the temperature are highly inter-dependent. Fig. 34 shows the oxygen equilibrium partial pressure with temperature for the main redox pairs in CLOU processes. Under CLOU mode, the temperatures in the reactors of a CLC unit should be optimized for each oxygen carrier. In order to maintain high efficiency in the CLOU process while complete combustion of the solid fuel is reached, the presence of oxygen at the outlet stream of the fuel reactor should be limited, so that the purity of the captured CO_2 is as high as possible. It is desirable to keep the outlet partial pressure of oxygen from the air reactor as low as possible. An oxygen concentration of 4% is a typical value. In the case

of Cu-based oxygen carriers, Abad et al. [142] found the temperature interval 900-950 ºC in the fuel reactor as adequate to avoid a large excess of oxygen in the outlet stream. They also observed an increase in the CO_2 capture efficiency as temperature increased. It should be remembered that both the oxygen partial pressure at equilibrium and the char combustion rate rise with the temperature, thus increasing CO_2 capture.

The combination of Cu and Mn oxides can shift the temperature interval for oxygen release to lower temperatures when compared to Cu and Mn oxides alone. In recent experiments by Adánez-Rubio et al. [88] with a Cu-Mn mixed oxide, lower temperatures could be reached in the fuel reactor (850 ºC) while allowing complete combustion of the fuel.

Other materials tested in CLC of solid fuels comprise the use of a perovskite-type oxygen carrier ($CaMn_{0.9}Mg_{0.1}O_{3-\delta}$) in the 10 kW_{th} CLC unit at CUT. It was found that a temperature range 950-1000 ºC in the fuel reactor was required to promote CLOU [57, 117]. Better CO_2 capture efficiencies and oxygen demand values were obtained compared to ilmenite.

4.3.2. Relevance of the solids circulation rate

There is also some information in the literature regarding the effect of the solids circulation rate on the performance of the combustion of a solid fuel under CLOU mode [254]. In experiments with Cu-based oxygen carriers in the 0.5 kW_{th} unit at ICB-CSIC, an increase in the solids circulation rate caused a reduction in the CO_2 capture efficiency [142]. This was attributed to a decrease in the char residence time in the fuel reactor as the solids circulation rate increased. However, no changes in the combustion efficiency were detected, although the solids conversion fell sharply from about 90% to 20%. In every case, the oxygen carrier released the oxygen needed to reach complete combustion of the fuel [142].

This was not so with Cu-Mn mixed oxide also tested in the same ICB-CSIC unit [88]. This time, the degree of conversion of the solids affected the amount of oxygen released and, therefore, the decrease in CO_2 capture efficiency was more noticeable as it was affected both by a reduction in the oxygen available and shorter residence time in the fuel reactor. The use of a carbon stripper would be recommended in this case to maintain an adequate value for CO_2 capture efficiency. Nevertheless, combustion efficiency was not significantly affected.

With the perovskite type $CaMn_{0.9}Mg_{0.1}O_{3-\delta}$ oxygen carrier tested at the 10 kW_{th} unit at CUT with solid fuels, a faster solids circulation rate due to an increase in the air reactor gas flow led to a decrease in both the CO_2 capture and the oxygen demand [57].

4.3.3. Relevance of the specific solids inventory in the fuel reactor

Regarding the effect of the solids inventory in the fuel reactor in CLC of coal under the CLOU mode, Abad et al. [142] performed experiments with a Cu-based oxygen carrier and a bituminous coal, varying the coal feeding rate and maintaining the fuel reactor temperature and solids circulation rate. In this way, the specific solids inventory per thermal power in the fuel reactor was decreased when the coal feeding rate increased. They observed complete combustion to H_2O and CO_2 in all the experiments. No relevant effect on the CO_2 capture efficiency was observed as there was excess oxygen in the fuel reactor in every case. Under these experimental conditions, the oxygen generated in the fuel reactor was not limited by the reactivity of the oxygen carrier [142], and its maximum oxygen release rate was determined in batch fluidized bed experiments; according to these, the solids inventory in the fuel reactor required to reach complete combustion of CO_2 and H_2O was estimated to be as low as 39 kg/MW_{th} at 930 ºC [254]. This value of the solids inventory in the fuel reactor was significantly lower than that needed for high combustion efficiencies in the *i*G-CLC process.

4.3.4. Effect of the H_2O/CO_2 ratio

In CLOU, oxygen in the oxygen carrier is mainly released as gaseous O_2 in the fuel reactor, which will react with the fuel the same as in common air combustion processes. Thus, char gasification is not required as an intermediate step in the solid fuel conversion, as occurs with *i*G-CLC. In order to test the influence of the presence of steam in the fluidizing agent, CO_2/H_2O mixtures were used in experiments carried out in the 0.5 kW_{th} CLC unit at ICB-CSIC, which showed that similar CO_2 capture or combustion efficiency was obtained in the presence of H_2O or CO_2 [199]. Therefore, recirculated CO_2 could be used as fluidizing medium instead of steam, which would lower costs.

4.3.5. Effect of the coal rank

The effect of the coal rank on the performance of CLOU was also evaluated at ICB-CSIC using a Cu-based oxygen carrier and four different coals (lignite, two bituminous and anthracite) [58]. Regardless of the coal rank tested, complete combustion to CO_2 and H_2O was obtained with an excess of oxygen at the fuel reactor outlet. As with *i*G-CLC, the CO_2 capture efficiencies were high for low-ranking coals. However, for less reactive coals, the use of a carbon stripper is also proposed in order to obtain high CO_2 capture efficiencies. The presence of a carbon stripper would also reduce the solids inventory needed. Moreover, the efficiency required for the carbon stripper in a CLOU operating unit is not as high as that needed for *i*G-CLC mode [55, 112].

4.3.6. Effect of the design

A comparison between different reactor designs for the CLOU process was recently published by Utah University [255]. Two configurations were analyzed. One used circulating fluidized beds for both the air and the fuel reactor, whereas the other used bubbling fluidized beds for both reactors. A computational fluid dynamic model was

developed and validated for each configuration, with several performance parameters of the CLOU unit being evaluated as a function of the total solids inventory and gas flows. The parameters evaluated were the solids circulation rate, the residence time, the pressure profiles in the reactors and loop seals and the velocity of the particles at different locations. As with *i*G-CLC, the dual CFB configuration proved more convenient for operation under CLOU mode, mainly due to the larger range of solids circulation rate that can be achieved. Nevertheless, if the solids circulation rate is not limited, high combustion efficiencies could be also obtained using a bubbling fluidized bed as fuel reactor. Solids inventories as low as 200 kg/MW_{th} could enable complete combustion of coal. A moving bed could also be an option for the CLOU process. However, special attention should be paid to the design in order to ensure contact between the volatiles released by the fuel and the oxygen released by the oxygen carrier.

4.3.7. *i*G-CLC materials assisted by oxygen uncoupling (CL*a*OU)

An alternative option to improve the reactivity of oxygen carriers is to develop CL*a*OU materials. These materials are able to release oxygen under optimized conditions, although it was mostly transferred via reduction with gaseous compounds, e.g. H_2, CO or CH_4, such as occurs in *i*G-CLC.

In the 0.5 kW_{th} unit at ICB-CSIC, Fe-Mn based oxides with oxygen transport capacities between 6.7-7.7 wt.% were tested as an oxygen carrier [79]. Some showed a certain oxygen uncoupling capacity (up to 12% of R_{OC}) due to the incorporation of TiO_2 into the mixed oxide structure [89]. These Fe-Mn-materials developed at ICB-CSIC reached combustion efficiencies of 99.5%, higher than those previously reported with other Fe-based oxygen carriers tested in the same unit [89].

For these Fe-Mn materials, Pérez-Vega et al. [89] proposed a fuel reactor temperature of 900 ºC and an air reactor temperature of 800 ºC, in order to reduce excess oxygen to

4% in the air reactor. The temperature difference between reactors could be further decreased if the excess air in the air reactor is increased with respect to the stoichiometric air. Together with the fuel and air reactor temperatures, control of the solids circulation rate was crucial in order to be able to regenerate the oxygen carrier in the air reactor sufficiently so that it could release oxygen in the fuel reactor to aid combustion via *i*G-CLC, which is the basis of the CL*a*OU process. As these results are promising, more research into the development of this type of oxygen carrier can be expected in the coming years.

4.3.8. Comparison of the *i*G-CLC and CLOU processes

For better clarity, Table 7 presents a summary of the above discussions on the influence of operating parameters on the performance of both *i*G-CLC and CLOU.

The presence of gaseous oxygen achieves combustion efficiencies of 100% in CLOU mode with a clearly lower solids inventory than in operation under *i*G-CLC mode. CO_2 capture values can be optimized by using a carbon stripper, whose efficiency need not necessarily be as high as in *i*G-CLC. The requirement to supply steam to the fuel reactor and carbon stripper is also avoided in CLOU, and recirculated CO_2 could be used instead. These facts make the CLOU process more advantageous when compared to *i*G-CLC. However, better control of the temperatures in the fuel and air reactors is required in CLOU, to optimize oxygen release and uptake. Another drawback is the short lifetime of the CLOU materials developed to date, which increases the need for a make-up flow. Moreover, the costs of the CLOU process would benefit from separating oxygen carrier particles from the ashes.

4.4. Combustion of biomass in *i*G-CLC and CLOU

Among the various options for achieving negative CO_2 emissions, most low-carbon scenarios rely on the use of BECCS (Bioenergy and Carbon Capture and Storage)

technologies [32]. Biomass is a CO_2-neutral fuel, i.e. the carbon dioxide released during biomass combustion has been previously removed from the atmosphere during biomass growth. If this CO_2 is captured, then negative CO_2 emissions are achieved [256-260]. Obviously, biomass-fueled CLC is taken as a BECCS technology [158]. Recently, research has been conducted to assess how the different properties of biomass compared to coal influence CLC performance [261]. The amount of volatiles released by biomass are larger than for coal, and biomass char is known to be more reactive than coal char, which would increase both the CO_2 capture efficiency and the oxygen demand for the process compared to the use of coal. Biomass ash components also differ from those in coal, and any interaction between oxygen carrier and biomass ashes should be assessed.

There are significant advantages to be gained from using biomass in CLC compared to conventional biomass combustion. In addition to a CO_2 negative balance, higher thermal efficiency, reduction in NOx formation, and lower corrosion in heat exchangers have also been reported. It must be remembered that heat in CLC systems is extracted in the air reactor where no alkaline components are present [261].

Most of the research on the use of biomass has been carried out under *i*G-CLC mode with Fe-based oxygen carriers [39, 56, 127, 139, 141, 158, 161]. One of the most relevant findings is that CO_2 can be used instead of H_2O as a fluidizing gas, with the corresponding energy saving associated with steam generation [39, 139, 141]. However, volatile matter is difficult to burn [141, 158], which explains the high oxygen demand often encountered. Following an analysis of the tar present in the combustion gases at the fuel reactor outlet, the content was observed to be relatively low [139]. Moreover, almost full conversion of biomass to gaseous species was achieved in a bench scale prototype using CO_2 as the gasification enhancer in the bottom part of a moving bed acting as fuel reactor [262].

Biomass combustion experiments in CLOU mode were conducted at ICB-CSIC [56, 143]. Important advantages compared to operating in *i*G-CLC mode were observed, such as the absence of unburnt/tar compounds at the fuel reactor outlet and the high CO_2 capture efficiencies reached, with solids inventories in the fuel reactor being much lower than in the *i*G-CLC process. However, there remains the need to find a durable and resistant oxygen carrier for CLOU.

A comparison between results obtained in *i*G-CLC and CLOU modes in the same unit has been performed using biomass as fuel [56]. Results shown in Fig. 35 highlight the differences found in CO_2 capture and combustion efficiency between both modes.

On a larger scale, more than 1000 hours of operational experience using biomass has recently been reported in the Chalmers boiler/gasifier loop (12 MW_{th}/ 2-4 MW_{th} respectively) using ilmenite and manganese ores as oxygen carriers and wood pellets as fuel [166]. For these tests, the 2-4 MW_{th} gasifier was used as the fuel reactor and the 12 MW_{th} boiler as the air reactor. The effect of different operating variables, such as fluidization velocity, fuel feeding rate, and solids circulation rate were analyzed. Although this plant is a non-optimized reactor design for CLC applications, relevant information for CLC combustion of biomass was obtained.

The same 12 MW_{th} circulating fluidizing bed boiler was also used for the Oxygen Carrier aided Combustion (OCAC) process using ilmenite or manganese ore as bed material and wood chips as fuel [263, 264]. OCAC refers to the process where an oxygen carrier instead of an inert solid is used as bed material in combustion in a fluidized bed boiler [265, 266]. In this process, the active oxygen carrier is reduced in fuel rich parts of the boiler and oxidized in oxygen rich locations. This technology has some interesting advantages over the use of silica sand in large CFB boilers, and is an excellent way of testing oxygen carriers before scaling up CLC units. In fact, promising

results were found during combustion of municipal solid waste in a 75 MW_{th} fluidized bed combustor using ilmenite as the oxygen carrier [267].

Relevant lessons can be learned for CLC development from OCAC. However, some aspects must be considered in order to extrapolate oxygen carrier behavior from OCAC to CLC. For example, interaction with ash and extent of the reaction of the oxygen carrier may be different, which would affect particle ageing [268].

In short, although recent advances predict a high potential for bio-CLC, there are still important challenges to overcome. Some of these concern the interaction among oxygen carriers and biomass ashes during long exposure. Although Na deposition on the iron ore based oxygen carrier particles does not seem to be a problem [269], the interaction of alkaline compounds with Mn-based oxygen carriers should be further investigated.

4.5. Evaluation of pollutant release in *i*G-CLC and CLOU processes

The performance of a CLC unit may be affected by pollutant formation during the combustion process. Pollutant formation in CLC could generate both environmental and operational problems, as shown in Fig. 36. Gaseous pollutants emitted in the air reactor will reach the atmosphere and, therefore, must comply with the current legislation for pollutant emission from power generation systems. On the other hand, gaseous pollutants present at the outlet stream from the fuel reactor affect the quality of the CO_2 captured and their presence should be taken into account in further conditioning of the CO_2 stream, in order for these to be stored safely [270].

Another aspect to be taken into account is the solid pollutants generated in a CLC unit. On one hand, solid fines from the oxygen carrier can be generated by attrition and lost by elutriation. This elutriated material should be recovered to avoid emission to the atmosphere and operational problems downstream. On the other hand, combustion of solid fuels generates ashes that should be drained from the CLC system to avoid

accumulation. During drainage, some oxygen carrier particles may be lost together with the ashes. These solid streams should be characterized and their disposal evaluated. In this respect, the literature reports that leaching tests have been used to analyze problems that might arise from disposing of these residues in a landfill [271].

Up to now, studies on pollutant formation in *i*G-CLC or CLOU have mainly focused on sulfur and nitrogen emissions [126, 129, 133, 153, 196, 199, 202, 252, 272, 273], but some studies on mercury emissions have also been presented recently [198, 199, 272]. Once coal is fed into the fuel reactor of the *i*G-CLC or CLOU system, a fraction of sulfur, nitrogen and mercury in the coal is released in the volatiles. The rest remains in the char. If this char reaches the air reactor, the nitrogen, sulfur and mercury in the char will be released in the air reactor during combustion of unconverted char. Sulfur can also accumulate in the oxygen carrier and may cause deactivation. A brief update on the formation of pollutants in *i*G-CLC or CLOU units is included here to outline the main results.

4.5.1. Fate of sulfur

- Sulfur emission in *i*G-CLC

Many of the studies performed with different fuels in CLC units ranging from 0.5 kW_{th} to 1 MW_{th} concluded that, under typical *i*G-CLC operating conditions, most of the sulfur in coal was released in the fuel reactor, mainly in the form of H_2S and SO_2 [126, 159, 272]. The H_2S/SO_2 molar ratio has been reported to be about 25/75 in studies using ilmenite at ICB-CSIC [272] or ilmenite/manganese ore at CUT [122]. A similar ratio (16/84) was reported using an iron ore based on hematite [100].

The H_2S/SO_2 molar ratio in the fuel reactor decreased when temperature in the fuel reactor increased as the oxidation reaction of H_2S to SO_2 was helped by the oxygen carrier. In the air reactor, sulfur was always found in SO_2 form due to sulfur present in

unconverted char. The amount of SO_2 decreased when the temperature in the fuel reactor increased as a lower char flow reached the air reactor [272].

The LCL^{TM} process by Alstom deserves special mention when assessing sulfur emissions. The system eliminates SO_2 emission by adding limestone together with the coal fed [192]. In fact, sulfated limestone has been found to be an efficient oxygen carrier, due to its oxygen transport capacity and reactivity [111]. Coal combustion with high sulfur retention and low SO_2 emissions has been reported in the 3 MW_{th} CLC unit [164], similar to the process taking place in circulating fluidized beds with in-situ desulfurization.

As mentioned before, the fate of sulfur compounds in a CLC unit is of interest not only for environmental or CO_2 quality, but also because sulfur compounds can poison the oxygen carrier used. Oxygen carrier interaction with gaseous sulfur compounds has been reported before with Ni-based oxygen carriers [175]. When coal was used with a Ni-based oxygen carriers, nickel sulfide/sulfate formation was observed, leading to a decrease in the oxygen carrier reactivity [125]. Nevertheless, note that the use of a Ni-based material with coal would not be advisable due to environmental issues.

For Fe-based materials, no dedicated studies have been done to evaluate the interaction with sulfur. Nevertheless, when reduced to Fe_3O_4, sulfur compounds would not be expected to form, according to thermodynamic calculations [181, 274]. In fact, an impregnated Fe-based oxygen carrier was successfully used recently in the combustion of sour and acid gases containing up to 20 vol% H_2S, and even solid elemental sulfur, without any sign of sulfide/sulfate formation or lower reactivity [275, 276]. It can be concluded therefore that Fe-based oxygen carriers are suitable for use with coals with high sulfur content.

- Sulfur emission in CLOU

The literature gives information on the emission of sulfur pollutants in CLOU combustion. In experiments carried out with a high-sulfur lignite and two different Cu-based oxygen carriers [199, 252] it was observed that most of the sulfur in coal was released as SO_2 in the fuel reactor. No H_2S was detected, as it was completely oxidized by the oxygen released by the oxygen carrier. The same occurred with *i*G-CLC, where the amount released also increased when the fuel reactor temperature increased. However, in this case, a partial reaction of SO_2 with CuO to form $(CuO)\cdot(CuSO_4)$ was detected. Formation of copper sulfate would decrease the oxygen transport capacity of the oxygen carrier although the reactivity would not be affected.

Other oxygen carriers with partial CLOU capabilities, such as those based on $CaMnO_3$, were also affected by the presence of sulfur compounds in the gases [57, 113, 117]. Formation of $CaSO_4$ has been found with this kind of material in the presence of sulfur [113]. It is worth mentioning that regeneration studies have been carried out both for Cu-based [277] and calcium manganate oxygen carriers [57, 117].

4.5.2. Fate of nitrogen

- Nitrogen emission in *i*G-CLC

One of the main advantages of CLC when compared to other combustion processes is that no thermal NO_x is generated because the temperatures reached in the air reactor where air is introduced are not high enough [278].

In *i*G-CLC, the only contribution to NO_x formation is the nitrogen contained in the fuel (fuel-N) [273]. NH_3, HCN and HNCO are the species normally released during coal devolatilization. Under reaction conditions in the fuel reactor, these nitrogen species can be oxidized to NO_x or converted to N_2. Although some authors reported the presence of significant amounts of NH_3 at the fuel reactor outlet [100], the majority of the studies

performed under *i*G-CLC conditions found that most of the nitrogen was released in the fuel reactor in the form of N_2, with minor amounts of NO [129, 202, 272]. In this respect, some authors found that the fraction of fuel-N converted to gaseous NO is higher with faster global solids circulation [121].

The nitrogen in the non-converted char reaching the air reactor is normally released as NO [159, 272, 273]. As mentioned before, temperatures in the air reactor are not high enough to cause thermal NO_x to form [278]. As with SO_2 emissions in the air reactor, NO emissions decreased with the increase in the fuel reactor temperature due to higher char conversion in the fuel reactor [272, 273]. In fact, no NO_x formation was observed in the air reactor with high fuel conversion in the fuel reactor, as occurred in the 25 kW_{th} CLC unit at OSU using a moving bed as fuel reactor [153]. The NO_x measurements made there indicated that around 10-15% of the fuel-N was converted to NO_x in the fuel reactor. No other nitrogen oxide species were detected in the fuel or air reactor.

- Nitrogen emission in CLOU

Some differences have been found in nitrogen pollutant formation in combustion in CLOU mode in comparison with *i*G-CLC combustion. In both processes, the only nitrogen compounds found were NO and N_2 in the fuel reactor and NO in the air reactor. However, in CLOU mode, about 20 wt.% of the nitrogen evolved in the fuel reactor was in the form of NO, while only 1% of the nitrogen was NO in the *i*G-CLC process [199, 272]. The differences can be attributed to the presence of gaseous oxygen in the fuel reactor in CLOU, which favored the conversion of nitrogen species to NO, while the reducing atmosphere in *i*G-CLC favored reduction to N_2.

4.5.3. Fate of mercury

Although mercury content in coal is very low, mercury emissions in coal combustion processes are deemed both an environmental and a health risk. Mercury is a highly volatile toxic element with a tendency to accumulate in both plant and animal tissues. Therefore, mercury emissions from coal should be kept to a minimum. In addition, operational problems could appear in the CO_2 conditioning step when CO_2 capture is considered. To date, few studies in the literature have analyzed the fate of mercury in *i*G-CLC or CLOU [198, 199, 272].

- Mercury emission in *i*G-CLC

At ICB-CSIC, dedicated experiments with Fe-based oxygen carriers and two types of coal (lignite and anthracite) were performed to evaluate the fate of Hg in *i*G-CLC [198]. It was found that the fraction of mercury released in the fuel reactor during coal gasification depended on both the fuel reactor temperature interval and the coal rank. An increase in temperature favored mercury release. However, the presence of significant pyrite content in the coal reduced the volatility of mercury. Once released, mercury was found in the fuel reactor atmosphere mostly as Hg^0, although the mercury in the char reaching the air reactor was mainly found as Hg^{2+} at the air reactor outlet stream. It should be noted that mercury speciation in the gaseous stream (Hg^0 or Hg^{2+}) determines the control measures to be applied to mercury, as Hg^{2+} is much more easily removed that Hg^0. The mercury content in the solid fines at the outlet of the air reactor, Hg(p), was negligible.

- Mercury emission in CLOU

At ICB-CSIC, studies on mercury emissions under CLOU conditions with a copper based oxygen carrier were performed [199]. The operational experience highlights the different mercury emissions registered under *i*G-CLC or CLOU operation. While the

ratio Hg^0 (g) /Hg^{total} (g) in fuel and air reactors was very similar for both processes, the amount of mercury in gaseous state released from both reactors was much lower in CLOU. In this process, a large amount of mercury was retained as particulate-bond mercury Hg(p) in the ashes elutriated from the system. The highly oxidizing atmosphere present in the CLOU process, together with the mercury oxidation caused by the presence of copper in the oxygen carrier meant that most of the mercury released during coal combustion was oxidized to Hg^{2+} making its retention in coal ashes easier.

4.5.4. Fate of tar

Tar formation is common in any gasification process. However, the presence of an oxygen carrier in CLC mode greatly reduces their content. [56, 136, 166]. The most common method for tar determination is the standarized tar protocol [279]. However, the literature reports other methods also used for improving tar collection, such as Solid Phase Adsorption (SPA) [280].

- Tar presence in *i*G-CLC

The type of fuel seems to have a decisive influence on the amount of tar in the CO_2 stream. In fact, no tars were detected during experiments at ICB-CSIC using coals of different rank and various oxygen carriers, such as ilmenite [136-138], bauxite waste material [140], or iron ore [101].

However, the use of other solid fuels with higher volatile matter, such as biomass, generates tar in the outlet stream of the fuel reactor, affecting the quality of the CO_2 stream. Tests carried out with several biomasses (pine sawdust, olive stone and almond shell) and Tierga Fe-ore as oxygen carrier in the 500 W_{th} CLC unit at ICB-CSIC showed tar contents of about 2.5-4.5 g/Nm^3 at temperatures 950-980 ºC. An increase in the operating temperature always led to a decrease in the amount of tar present in the fuel reactor outlet stream. Fig. 37 shows an example of the tar composition obtained at

980 ºC. Naphthalene was the major compound detected, followed by lower amounts of styrene, acenaphthylene and phenantrene [139, 281].

Data obtained in the 4 MW_{th} Chalmers gasifier during more than 1000 hours of operation using commercial wood pellets and different oxygen carriers, is of special importance [166] Yields of SPA-measurable tar, including BTX, of 21-22 g /kg daf fuel using ilmenite and a manganese ore as oxygen carriers were reported. The major compounds detected were benzene, toluene, naphthalene, styrene and indene, representing approximately 73-81% of the total mass of SPA species. The yield of hydrocarbons heavier than benzene was in the range of 10–11 g/Nm^3, which was 70% (w/w) lower than that obtained in a reference case with silica-sand as the bed material. These values were higher than those reported during tests at ICB-CSIC. Apart from the different methodology used in tar collection and analysis, the differences can be also attributed to the lower temperature (810-830 ºC) and a non-optimized contact between the oxygen carrier and the gasification products.

Reed et al. [282] limited the tar content valid for compressing and piping a biomass gasification gas any distance to the range of 0.05-0.5 g/Nm^3 Although the tar content values reported in literature for biomass fueled *i*G-CLC are higher than those limits, no fouling problems downstream from the fuel reactor due to the presence of tar are anticipated. In addition, it would be expected tar compounds will be burnt during the oxygen polishing step in an industrial CLC unit.

Calculations made by Mendiara et al. [281] showed that the total oxygen demand for tar would be about 1%, so that it should be taken into account in the oxygen polishing step. However, tar does not represent a problem in CLC, since the oxygen demanded by other unburned gaseous compounds (CO, H_2 and CH_4) is expected to be significantly higher.

- Tar presence in CLOU

Tests carried out at ICB-CSIC burning either coal or biomass under CLOU mode demonstrated the absence of tar at the fuel reactor outlet [56, 142, 143]. The presence of gaseous oxygen in the fuel reactor led to complete combustion of the tar compounds, even in those cases where a high volatile fuel is processed, such as biomass.

4.5.5. Overview on gaseous pollutant emission in CLC

The gaseous emissions in the CLC process originate in combustion of the unconverted char reaching the air reactor. It can be speculated that the presence of an efficient carbon stripper in the CLC unit [272] might help in controlling sulfur and nitrogen emissions from the air reactor in a CLC system. Should the emissions exceed those set by current legislation, control measures already in use in the current power plants could be applied. Regarding the quality of the CO_2 at the outlet of the fuel reactor, only recommendations concerning the presence of certain compounds have been given, including unburnt compounds (CO, CH_4, H_2) and O_2 [270]. For sulfur and nitrogen emissions, the recommendations only apply to the levels of H_2S, SO_2, N_2 and NO_x, but no recommendations for mercury have been specified [270], despite the operational problems that mercury can cause in the CO_2 conditioning equipment and transportation pipelines. Table 8 compares the values for SO_2 and NO_x obtained in recent studies in fuel and air reactors working in *i*G-CLC or CLOU modes [199, 272] with the values set as appropriate for CO_2 transport and storage (fuel reactor), and those set by legislation for emissions to the atmosphere (air reactor). The EU legal limit (Directive 2010/75/UE) [283] established for new built power plants up to 300 MW_{th} is 150 mg/Nm^3 (6% O_2), for SO_2 and NO_x emissions, respectively.

4.5.6. Residues

Solids residue generation in a CLC system is an important aspect to be considered due to the amount of waste that can be generated. However, no in-depth analysis of this aspect has been carried out by now.

In the combustion of a solid fuel, ashes are generated in the fuel reactor and they should be periodically removed from the system in order to avoid solid accumulation and the subsequent operational problems. One of the main concerns in solid-fueled CLC is the possible loss of oxygen carrier in the ash drainage process. In order to minimize these losses some solutions are being proposed. Recently, the use of a rotating fluidized bed was tested to improve the gas-solid and solid-solid separation process efficiency in comparison to conventional fluidized beds [284]. In addition, the use of oxygen carriers with magnetic properties could be also valid [240], especially for high-expensive CLOU materials.

Together with the ash drainage stream, the oxygen carrier fines lost by elutriation constitute the other source of solid residues in solid-fueled CLC. Depending on the nature of the oxygen carrier used and the solid fuel ashes, the presence of soluble toxic trace elements should be analyzed in order to assess whether to dispose of them in a landfill. In this respect, lixiviation studies of depleted oxygen carriers have been reported in literature for Fe-based materials, commonly used in the *i*G-CLC process [271] and in this case, the majority could be disposed in a landfill for nonreactive hazardous waste.

5. Evaluation and extrapolation of experimental results in *i*G-CLC units

The design of large CLC units should be based on the results obtained from currently operating CLC plants. As has been shown in previous sections, there are significant differences in the results available in the literature, which complicates the scale-up

process. The main concerns in the performance of the *i*G-CLC process in CLC units are the fact that the conversion of the solid fuel is not complete (X_{sf} < 1) due to partial recovery of char by the fuel reactor cyclone, as well as the presence of unconverted gases in the gas stream from the fuel reactor [42, 101, 123, 136, 145, 147, 148, 196]. In addition, unconverted char can pass to the air reactor, thus decreasing the real char fraction converted in the fuel reactor, and hence the CO_2 capture (η_{CC}<1). This presence of unconverted char in streams exiting the fuel reactor makes it difficult to extrapolate the current information to what could be expected in a larger *i*G-CLC system where both η_{CC} and X_{sf} should be as close to 100% as possible.

The extrapolation is not straightforward because it is not simple to calculate how much of the volatiles and gasification products evolved in the fuel reactor would be converted if X_{sf}= 1, as it depends, among other factors, on the solid fuel used and the type of reactor technology in the fuel reactor, e.g. bubbling fluidized bed (BFB), circulating fluidized bed (CFB) or spouted fluidized bed (SFB). Nevertheless, it would be very interesting to be able to predict results in an optimized unit from the results obtained in these smaller units, which are easier to operate and where the influence of different combustion parameters on the performance of the unit is more easily evaluated. Therefore, this section presents a novel methodology, based on current experimental results from CLC units, that helps to predict the expected values of oxygen demand when complete combustion of the solid fuel is reached ($\Omega_{T,full}$).

The oxygen required to burn the solid fuel, expressed as the kilograms of oxygen needed to burn one kilogram of solid fuel (Ω_{sf}), can be defined as the sum of the oxygen demanded by the volatiles released, (Ω_{vol}) and the oxygen demand of the char generated (Ω_{char}).

$$\Omega_{sf} = \Omega_{vol} + \Omega_{char} \quad (13)$$

To calculate Ω_{char} it can be assumed that the char is solely formed of carbon and ash. Some of the carbon in the char will be lost by elutriation, thus reducing the value of the solid fuel conversion (X_{sf}). Therefore, the values of the total oxygen demand (Ω_T) and the oxygen demand in the fuel reactor (Ω_{FR}) can be calculated, based on Eqs. (14) and (15) and equations in Fig. 22, as:

$$\Omega_T = \frac{(1-\eta_{comb,v})\cdot\Omega_{vol} + (1-\eta_{comb,g})\cdot\Omega_{char}\chi_{char,FR}}{\Omega_{sf}} \quad (14)$$

$$\Omega_{FR} = 1-\eta_{comb,FR} = \frac{(1-\eta_{comb,v})\cdot\Omega_{vol} + (1-\eta_{comb,g})\cdot\Omega_{char}\chi_{char,FR}}{\Omega_{sf} - \Omega_{char}(1-\chi_{char,FR})} \quad (15)$$

where $\eta_{comb,v}$ and $\eta_{comb,g}$ represent the combustion efficiency of the volatiles and char gasification products (mainly CO and H_2), i.e. how much of the volatiles and CO/H_2 from char gasification would be burned by the oxygen carrier particles to CO_2 and H_2O. Note that, as presented in section 4.1, the value of X_{char} is related to the value of the solid fuel conversion (X_{sf}) and $X_{char,FR}$ is linked to the value of CO_2 capture efficiency (η_{CC}). If the value of $x_{char,FR}$ is equal to one, complete gasification of the fixed carbon would be achieved and this would correspond to a CO_2 capture efficiency value of 100%. The idea behind the methodology presented in this paper is the following. Once a value of Ω_{FR} or Ω_T has been estimated for an experimental value of $x_{char,FR}$, it can be extrapolated to another $x_{char,FR}$ value, knowing the combustion efficiency of the volatiles released ($\eta_{comb,v}$) and the combustion efficiency of the gasification products ($\eta_{comb,g}$).

As mentioned before, the values of $\eta_{comb,v}$ and $\eta_{comb,g}$ in Eqs. (14) and (15) depend heavily on the solid fuel used and the configuration of the CLC unit where they were obtained. Depending on the values of $\eta_{comb,v}$ and $\eta_{comb,g}$, different behaviors of the

oxygen demand can be found. Figs. 38A to C show three typical examples. In all of these, the fuel used was the bituminous Colombian coal "El Cerrejón", as there is enough information on this fuel available in the literature. The oxygen demand for char (Ω_{char}) and volatile matter (Ω_{vol}) can be calculated from the analyses of coal and char. Table 9 presents the ultimate and proximate analysis of "El Cerrejón" Colombian coal and its corresponding char obtained by pyrolysis at 900 ºC in a nitrogen atmosphere at a heating rate of 20 ºC/min.

- Example 1

Fig. 38A represents the evolution of the oxygen demand parameters according to the definitions in Eqs. (14) and (15) as a function of the carbon fraction in char gasified in the fuel reactor. In this example, it is assumed that the gasification products are mostly converted to CO_2 and H_2O and volatiles are not. In this case, it is realistic to assume that $\eta_{comb,g} = 1$ and $\eta_{comb,v} = 0.6$. As can be observed in Fig. 38A, the value of Ω_{FR} is always larger than the value of Ω_T. The value of Ω_{FR} decreases only if there is complete conversion of the fuel fed, Ω_{FR} reaches the same value as Ω_T. In contrast, the total oxygen demand Ω_T remains unaffected and matches the value of the oxygen demand, assuming that there is complete combustion of the fuel ($\Omega_{T,full}$) in the full range of $x_{char,FR}$. Therefore, in this case, the total oxygen demand (Ω_T) provides a better representation of what would be expected at high solid fuel conversions.

- Example 2

A different situation arises when better volatile combustion is assumed. In order to show how $\eta_{comb,v}$ and $\eta_{comb,g}$ affect the relationship between Ω_{FR} and Ω_T, the exact opposite situation to example 1 is assumed and shown in Fig. 38C. Thus, $\eta_{comb,v} = 1$ and a value of $\eta_{comb,g} = 0.9$ is taken for the efficiency of the combustion of the volatiles and char gasification products, respectively. As can be seen, the oxygen demand in the fuel

reactor (Ω_{FR}) is again larger than the total oxygen demand (Ω_T), as both parameters increase when the carbon fraction in char being gasified in the fuel reactor increases, and both values converge when full carbon conversion of the fuel introduced is reached ($x_{char,FR} = 1$). According to Fig. 38C, the oxygen demand in the fuel reactor (Ω_{FR}) is closer to the real oxygen demand value if there is complete conversion of the fuel (indicated by dashed lines), especially when more than 70% of the char introduced has been converted in the fuel reactor.

- Example 3

Nevertheless, existing facilities had other configurations with intermediate behavior regarding $\eta_{comb,v}$ and $\eta_{comb,g}$. Fig. 38B shows the values for Ω_{OD} and Ω_T versus the carbon fraction in char being gasified in the fuel reactor for the case in which $\eta_{comb,v}$ = 0.8 and $\eta_{comb,g}$ = 0.9. Here, the oxygen demand in the fuel reactor (Ω_{FR}) and the total oxygen demand (Ω_T) show opposite trends. Neither of the oxygen demand values calculated would be representative of what could be expected in a larger CLC system. The values of Ω_{FR} decrease with the increase in $x_{char,FR}$ and they are always higher than the real value expected in optimized systems. In contrast, the values of Ω_T increase with $x_{char,FR}$, but they always underpredict the value expected with full conversion of the fuel. However, again this final value is the same for both definitions of the oxygen demand when $x_{char,FR}$ is equal to unity.

From the analysis in Fig. 38, several conclusions can be drawn:

i) The total oxygen demand (Ω_T) is always lower than the optimum or equal values when $x_{char,FR} < 1$. In addition, the total oxygen demand always has a linear dependency with $x_{char,FR}$, which makes it easier to extrapolate $x_{char,FR}$ to a value equal to 1 from experimental results.

ii) If $x_{char,FR} < 1$, an increase or decrease of Ω_{FR} can be expected, depending on the $\eta_{comb,v}$ and $\eta_{comb,g}$ values. Only when $\eta_{comb,v}$ and $\eta_{comb,g}$ are equal, would the oxygen demand value in the fuel reactor, Ω_{FR} be the same as the oxygen demand with complete conversion of the fuel. Thus, it seems that the total oxygen demand (Ω_T) is a friendlier parameter to show the performance of the CLC process in order to compare it with model predictions and the performance of other combustion processes, such as oxyfuel combustion. Thus, the use of the total oxygen demand concept to represent the performance of CLC is highly recommended.

iii) The values of the combustion efficiency of the volatiles released ($\eta_{comb,v}$) and the combustion efficiency of the gasification products ($\eta_{comb,g}$) vary notably depending on the combustion conditions and configuration of the CLC unit and, therefore, they should be determined specifically for each unit. The procedure to determine $\eta_{comb,v}$ and $\eta_{comb,g}$ is shown in the following section.

5.1. Determination of the combustion efficiency of volatiles and char gasification products ($\eta_{comb,v}$ and $\eta_{comb,g}$) from experimental results

According to Eq. (14) and (15), the value of the oxygen demand with complete conversion of the fuel can be estimated once the value of the combustion efficiency of the volatiles released ($\eta_{comb,v}$) and char gasification products ($\eta_{comb,g}$) are known. Some attempts to estimate the contribution to the oxygen demand of unconverted volatiles released by coal and char gasification products have already been reported in the literature [121, 136]

One of the possible ways to estimate both contributions to the oxygen demand is to perform experiments under similar conditions with a coal and its corresponding char produced separately [136]. The difference between this oxygen demand (Ω_{char}) and the value obtained in the combustion of the coal (Ω_T) is then attributed to the oxygen

demand associated with the combustion of the volatiles (Ω_{vol}). Once these two contributions have been estimated, the values of $\eta_{comb,v}$ and $\eta_{comb,g}$ can be calculated. This type of experiment was performed by Cuadrat et al. [136] in the 0.5 kW_{th} unit at ICB-CSIC using ilmenite as the oxygen carrier and "El Cerrejón" bituminous Colombian coal as fuel. In this case, the fuel reactor was a bubbling fluidized bed. These authors concluded that, by using ilmenite, all the gasification products were fully oxidized ($\eta_{comb,g} \approx 1$) and calculated the corresponding value for $\eta_{comb,v}$ = 0.61. Nevertheless, some concerns about the accuracy of this methodology may arise from the fact that the nature of the char fed is not the same as the char produced *in situ* in the fuel reactor and, therefore, the reactivity of the char could be different.

To avoid these possible discrepancies, other attempts included stopping the coal feed at a certain time and then evaluating the oxygen demand under the same experimental conditions. This oxygen demand would only be attributed to that of the char gasification products (Ω_{char}) being released by the char remaining in the CLC unit. This type of experiment was performed by Linderholm et al. [121] in the 100 kW_{th} unit at CUT using ilmenite as an oxygen carrier and "El Cerrejón" bituminous Colombian coal as fuel. In this case, the fuel reactor was a circulating fluidized bed. According to these authors, about one half of the oxygen demand could be attributed to unconverted volatile matter.

In this paper, the calculation of the combustion efficiency of the volatiles released ($\eta_{comb,v}$) and char gasification products ($\eta_{comb,g}$) is based on the experimental results already reported in the literature for the various types of CLC units burning solid fuels. In addition, both oxygen demand values Ω_{OD} and Ω_T have been taken from the literature when available. When one of the oxygen demands was not available, it was calculated from data given, following the methodology previously described by Gayán et al. [52].

2014 $\eta_{comb,v}$ and $\eta_{comb,g}$ are determined based on Eqs. (14) and (15). The following expression
2015 can be deduced:

2016 $$\frac{1}{\Omega_T} - \frac{1}{\Omega_{FR}} = \frac{\Omega_{char}(1 - x_{char,FR})}{(1-\eta_{comb,v}) \cdot \Omega_{vol} + (1-\eta_{comb,g}) \cdot \Omega_{char} \cdot x_{char,FR}} \quad (16)$$

2017 The linearization of this expression as shown in Eq. (17) enables determination of the
2018 combustion efficiency of the volatiles released ($\eta_{comb,v}$) and char gasification products
2019 ($\eta_{comb,g}$) from the ordinate at the origin and the slope of the line, respectively, for
2020 different values of the variable $x_{char,FR}$, assuming that the values of $\eta_{comb,v}$ and $\eta_{comb,g}$
2021 remain constant, regardless of the degree of char conversion in the fuel reactor:

2022 $$A = (1 - \eta_{comb,v}) + (1 - \eta_{comb,g}) \cdot B \quad (17)$$

2023 $$A = \frac{\Omega_{char}(1 - x_{char,FR})}{\Omega_{vol}\left[\frac{1}{\Omega_T} - \frac{1}{\Omega_{FR}}\right]}$$

2024 $$B = \frac{\Omega_{char}}{\Omega_{vol}} x_{char,FR}$$

2025 Among experimental data gathered in Table 4, only those publications providing
2026 enough information on the solid fuel conversion, CO_2 capture efficiency and oxygen
2027 demand were considered, i.e. mainly publications from ICB-CSIC [101, 136-141, 144,
2028 145, 198, 272] and CUT [36, 37, 100, 114-116, 118-124]. In both cases, the CLC
2029 configurations used were bubbling or circulating fluidized beds. Moreover, most of the
2030 results were obtained using ilmenite as the oxygen carrier and bituminous coals or
2031 petcoke as fuel. Where only one of the values of oxygen demand was provided, Eq. (18)
2032 correlates both values of oxygen demand, i.e. Ω_{FR} or Ω_T, so that one can be calculated
2033 using the other, provided the value of CO_2 capture efficiency and the ultimate and
2034 proximate analysis of the coal are available.

$$\Omega_{FR} = \Omega_T \frac{\Omega_{sf}}{\Omega_{sf} - (1 - X_{sf}) \cdot x_{fc} \frac{M_{O_2}}{M_C} - (1 - \eta_{CC}) x_C \frac{M_{O_2}}{M_C}} \quad (18)$$

The value of $x_{char,FR}$ can be also calculated from the values of solid fuel conversion and CO_2 capture efficiency as follows:

$$x_{char,FR} = 1 - (1 - \eta_{CC} X_{sf}) \left(\frac{x_C}{x_{fc}} \right) \quad (19)$$

Fig. 39A shows the results obtained in experiments on coal combustion in the 0.5 kW_{th} unit at ICB-CSIC with a bubbling bed fuel reactor and using either ilmenite or bauxite waste as oxygen carriers and a Colombian bituminous coal as fuel [136, 140]. Temperature in the fuel reactor was held constant at 890 ºC for experiments with ilmenite [136], and 905 ºC for those with bauxite waste [140], while the solids circulation rate was varied between 2 and 20 kg/h. In this way, the char converted in the fuel reactor was varied by modifying the residence time of solids in the fuel reactor. As shown in Fig. 39A, the values for $\eta_{comb,v}$ and $\eta_{comb,g}$ can be calculated from the fitted line. Table 10 summarizes the results obtained.

As was previously observed by Cuadrat et al. [136] the combustion efficiency of char gasification products in this CLC unit is very high.

In the 10 kW_{th} unit at CUT, the fuel reactor was also a bubbling fluidized bed. Fig. 39C shows the results for experiments in the unit using ilmenite as the oxygen carrier and petcoke and bituminous coal as fuel [115, 119]. During these experiments, the solids circulation and coal feed rates were varied, while temperature was fixed in the interval 950-970 ºC. Results were obtained with two different configurations of the fuel feeding chute: first with solid fuel feed above-bed and later the feed was modified to have in-bed feed of the solid fuel. The combustion efficiency values calculated are shown in Table 10. The initial configuration of this CLC unit enabled high conversion of volatiles

2058 to be reached only if solid fuels with low volatiles were used. This was due to the fact
2059 that the above-bed feeding system helped to prevent most of the volatiles from having
2060 the chance to contact the oxygen carrier particles when released. After the modification,
2061 the solids entered the fuel reactor bed and the combustion efficiency of volatiles
2062 increased. Thus, the conversion of volatile matter was higher than that found in the 0.5
2063 kW_{th} CLC unit at ICB-CSIC. However, the conversion of gasification products was
2064 lower in the 10 kW_{th} CLC unit at CUT. The reason for this could be gasification of char
2065 particles above the bed, due to the presence of a carbon stripper in the fuel reactor [36].
2066 In other experiments in the 0.5 kW_{th} CLC unit, the temperature in the fuel reactor was
2067 varied in the range 870-950 ºC and different coal sizes were used. Fitting curves are
2068 shown in Fig. 40. As can be observed, under these conditions it was not possible to
2069 obtain the values for $\eta_{comb,v}$ and $\eta_{comb,g}$ because a negative slope was obtained, which
2070 means $\eta_{comb,g} > 1$; see Eq. (16). The change in the fuel reactor temperature affected both
2071 the char gasification rate and the reactivity of the oxygen carrier and thus the values of
2072 $\eta_{comb,v}$ and $\eta_{comb,g}$ cannot be considered constant. Therefore, the experimental data used
2073 to evaluate Eq. (16) should always be obtained under similar conditions (mainly fuel
2074 reactor temperature, solids circulation rate and coal feed). Results taken from studies in
2075 other units also shown in Fig. 39 led to the same conclusion [122, 129, 148].
2076 Fig. 39B shows the analysis of experimental data obtained in the 50 kW_{th} unit at ICB-
2077 CSIC where the fuel reactor is a circulating fluidized bed [251, 285]. Ilmenite was used
2078 as the oxygen carrier. The fuel reactor temperature was in the short range of 970-990
2079 ºC, the fuel used was a bituminous coal (Taldinsky coal), and the solids circulation rate
2080 was around 120 kg/h. The values determined for $\eta_{comb,v}$ and $\eta_{comb,g}$ were 0.72 and 0.86,
2081 respectively. Compared to the previous results obtained with ilmenite in the 0.50 kW_{th}
2082 unit, the combustion efficiency of the volatiles was similar, although a lower specific

solids inventory was used in the experiments in the 50 kW_{th} unit. However, the combustion efficiency of gasification products in the 50 kW_{th} unit was slightly lower because of the small quantity of char gasified in the upper part of the reactor, as shown during the fuel reactor modeling [60].

Fig. 39D presents the analysis of the results obtained at the 100 kW_{th} unit at CUT, also with a circulating fluidized bed as the fuel reactor. In this case, ilmenite was the oxygen carrier and the fuel was wood char [121]. Temperature in the fuel reactor was 960 ºC in all the experiments and the solids circulation rate was varied. Using ilmenite as an oxygen carrier and bituminous coal as fuel, the combustion efficiency of gasification products was similar to that found in the 50 kW_{th} CLC unit at ICB-CSIC. Modeling results showed that the particle size of the fuel is highly relevant in the position where gasification mainly takes place [61, 286]. The fraction of char in the upper part of the circulating fluidized bed fuel reactor, i.e. the dilute region, decreases as the fuel size increases. Thus, gasification mainly occurs in the lower part of the reactor, i.e. the dense bed, where oxidation of gasification products is highly efficient, as was seen with a bubbling fluidized bed fuel reactor. However, combustion of volatile matter was less efficient.

5.2. Extrapolation of experimental results to optimum conditions for fuel conversion in the fuel reactor

Finally, once the values of $\eta_{comb,v}$ and $\eta_{comb,g}$ have been estimated for a specific configuration and under fixed experimental conditions, they can be used to further estimate the value for the oxygen demand with complete conversion of the fuel in the fuel reactor ($\Omega_{T,full}$) using Eq. (13), i.e. $x_{char,FR}$=1. This estimation of the oxygen demand for full fuel conversion, $\Omega_{T,full}$ can then be used to evaluate the expected fuel conversion in an optimized CLC unit from available experimental results in lab- or pilot CLC units.

In addition, the $\Omega_{T,full}$ value can be used to compare the performance of the CLC configurations already existing. Table 10 shows the values of $\Omega_{T,full}$ calculated for the CLC units evaluated in Fig. 39, again using "El Cerrejón" bituminous Colombian coal. According to these extrapolated values, similar oxygen demand values could be expected from both bubbling and circulating fluidized beds. However, the specific solids inventory needed is much lower in CFB, besides being more easily scalable.

It should be taken into account that the validity of the extrapolation method presented in this paper is limited to the assumptions already made to calculate $\eta_{comb,v}$ and $\eta_{comb,g.}$ For the same experimental setup, these values can be different for oxygen carriers with different reactivity. More reactive carriers would be expected to yield higher values of combustion efficiency.

6. Challenges for the future development of CLC with solid fuels

A review of experimental data obtained in currently operating *i*G-CLC continuous units burning solid fuels has been presented with the aim of facilitating comparison of the experimental results from different units and contributing to the optimization of CLC of solid fuels. There follows a brief discussion on the prospects of the CLC technology with solid fuels.

6.1. Scale-up of a CLC unit with solid fuels

The experience gained from operating these CLC units is very valuable for evaluating possible ways to optimize the design of a CLC unit, as well as to identify some milestones to achieve for the scale-up and future development of this technology.

In fact, results obtained in the 3 MW CLC unit by Alstom USA [43] replicated the high values of CO_2 capture usually obtained at low scale when an efficient char separation system was used. In addition, oxygen demands were also similar to those obtained at lower scales.

Nevertheless, special care should be taken in the CLC design to prevent a low performance, of which several examples can be found in the literature. In fact, low CO_2 capture efficiency was obtained in the 1 MW CLC unit at Darmstadt, due to the lack of a carbon stripper; or high oxygen demands as a consequence of an excessively low solid inventory in the unit [159, 287]. In addition, high oxygen demands were also obtained because of the non-optimized design for CLC operation in the 4 MW_{th} gasifier at Chalmers [166].

All these aspects lead us to define a range of valid conditions for operation on an industrial scale, such as temperatures of approximately 1000 ºC and solids inventories in the fuel reactor about 500 kg/MW. In addition, a good mixing between the solid fuel and the oxygen carrier is encouraged in order to improve the conversion of volatile matter and gasification products.

Nowadays, two different approaches are being developed to scale-up the combustion of solid fuels in a CLC unit. They differ in the configuration chosen for the fuel reactor. Thus, a circulating fluidized bed [4, 244] or a moving bed [53, 182] design is preferred to a bubbling fluidized bed [255].

6.1.1. CLC unit with a circulating fluidized bed as the fuel reactor

The fuel reactor can be designed as a circulating fluidized bed reactor, as in the case of the two largest CLC installations currently in operation, the 1 and 3 MW_{th} CLC units developed by Alstom [43]. With these, the gas velocity in the fuel reactor is high enough to allow the entrainment of solids, which also takes place in the air reactor. Thus, the CLC configuration including two circulating fluidized beds, one as fuel reactor and the other one as air reactor is preferred at present for the scale-up of CLC. This configuration is more flexible, scalable and easier to control than other configurations based on bubbling fluidized beds or moving beds. In addition, experience

gained during coal combustion in circulating fluidized bed boilers can be significant for the development of CLC technology with solid fuels [4]. Further considerations presented next mostly refer to this configuration.

The scale-up of the *i*G-CLC reactors has been done using the design for either the 1 MW_{th} (TUD) or 3 MW_{th} (Alstom) CLC units, mainly based on the presence, or otherwise, of a dedicated carbon stripper unit. Fig. 41A shows the design for a 100 MW_{th} unit based on the 1 MW_{th} CLC unit configuration, which includes the carbon stripper in the solids stream from the fuel reactor to the air reactor [244]. This option entrains the circulating solids from the fuel reactor and separates them from the gaseous stream in a cyclone. The exiting solids include the oxygen carrier and unconverted char particles. Thus, an external carbon separation system is required so that the unconverted char does not reach the air reactor. This design enables control of the operation of the carbon stripper to maximize the char separation efficiency [145]. The fuel reactor can be designed solely in terms of both the required amount of solids and the solids circulation rate. A map for the design of the fuel and air reactor was presented by Abad et al. [244] based only on fluid dynamics; see Fig. 42. They concluded that the cross sectional area of both fuel and air reactor would be around 0.25 m^2/MW_{th}. At stoichiometric conditions, the required solids flow in the reactors would be around 30 kg m^2 s^{-1}, while the pressure drop in the fuel and air reactor would be 30 and 20 kPa to operate with 750 and 500 kg/MW_{th} in the fuel and air reactors, respectively.

The alternative option for the scale-up to 1000 MW_{th} was described by Lyngfelt and Leckner [4], based on the existing 3 MW_{th} CLC unit by Alstom [43]. In this design, the bottom part of the fuel reactor is hydraulically connected to the air reactor, and therefore solids from the fuel reactor are extracted by the bottom part of the reactor; see Fig. 41B. Entrained solids are recirculated to the fuel reactor. In this option, an in-built carbon

stripper is included, so a section of the fuel reactor is below the coal feeding point, which functions as a carbon stripper, and operates under conditions that prevent carbon particles from following the descending stream of solids.

There have been several proposals for boosting the scale-up of CLC on a commercial scale [250]. The operation of CLC units on an intermediate scale without purification and storage of CO_2 can reduce the costs during an evaluation period of CLC technology. Also, retrofitting a circulating fluidized bed to CLC by adding a coupled reactor to the existing one, or constructing a dual fluidized bed system designed to operate at CLC conditions for a time, and then operate as a commercial fluidized bed combustor, have been suggested as the most promising ones.

6.1.2. CLC unit with a moving bed as the fuel reactor

CLC units at OSU are based on the use of moving bed as the fuel reactor, and with a thermal power of 2.5 and 25 kW_{th} [153]. In the moving bed configuration, the oxygen carrier is designed to flow counter-current to the gas and the coal is fed at an intermediate position in the reactor; see Fig. 43A. In the upper part (Section 1), volatile matter and gasification products are converted by gas-solid reaction with the oxygen carrier, while in the bottom part (Section 2) enough time is given for the char particles to be gasified. Since Fe_2O_3 can be reduced to Fe in a moving bed configuration (see section 3.1.7), the oxygen transport capacity of the material is maximized and the solids circulation rate can be relatively low, which facilitates the high solids residence time required. In addition, to ensure that no char enters the air reactor, the gas velocity at the bottom of the fuel reactor should be higher than the minimum fluidization velocity of the char [53].

The fuel reactor must also facilitate good distribution of coal over the whole of the cross section area. For this purpose, the design proposed by Schwebel et al. [182] is shown in

Fig. 43B. Coal is fed at mid-height, where the cross section narrows. Thus, the fuel is fed at a concentrated point with a relatively low cross section, which increases as the solids drop and coal is distributed over the whole of the cross section in the bottom part. However, the cross section of the fuel reactor must be wide enough to maintain the gas velocity below the minimum fluidization velocity, u_{mf}, of oxygen carrier particles. The scale-up of the moving bed requires a careful evaluation of the homogeneity of solids and temperature across the section of the reactor. In addition, coarse oxygen carrier particles are required, e.g. above 1 mm diameter, in order to increase u_{mf}.

The configuration of a fluidized bed connected to a riser is adopted for the air reactor [53, 151]; see Fig. 11. In this case, special care must be taken with the air reactor design during the scale-up of the CLC unit, which must allow re-oxidation of the oxygen carrier particles, while coarse particles are being entrained to elevate them to the fuel reactor inlet situated in the upper part. The fluidized bed provides a constant, homogeneous temperature during the exothermic oxidation reaction so that sintering and agglomeration problems are avoided. Next, the particles are entrained in the riser and pneumatically conveyed back to the fuel reactor. The cross section in the riser should be designed to guarantee sufficient particle transfer to the fuel reactor [53].

Moreover, the moving bed could be operated at high pressure, as there is wide experience in operating pressurized moving bed gasifiers [288]. In addition, the experience gained in the development of syngas chemical looping (SCL), where H_2 and electricity are produced using an iron ore as an oxygen carrier, could be useful [25].

6.2. Improvement in combustion efficiency of the CLC with solid fuels

In view of the results gathered, the main problem encountered in the operation of *i*G-CLC units is the existence of unburned compounds at the reactor outlets when interconnected fluidized bed reactors are used [52, 251]. It seems clear that the next step

in development and further scale-up of *iG*-CLC technology for solid fuels is to reduce the unburnt compounds generated. Specific modifications in the CLC unit can be made to improve the combustion of unburnt compounds, which could come from either unburnt volatiles or unburnt gasification products. Knowing the contribution of unconverted volatiles and gasification products to the oxygen demand will help to improve the performance of the CLC system and propose new designs that will minimize the oxygen demand; see section 5. Thus, several measures have already been undertaken or proposed to minimize the unburnt compounds, including options to improve gas-oxygen carrier contact or incorporate new design concepts into the current scheme of the *iG*-CLC system; see Fig. 44.

Vienna University of Technology (TUV) proposed a modification of the fuel reactor in dual fluidized bed systems, intended to maximize the residence time of solid particles and the contact efficiency between solid and gaseous phases. The geometry of the fuel reactor was modified to include wedged-ring-type internals that increased the total hold-up and homogenized the solids distribution in the reactor, as shown in option D-1A in Fig. 44 [289, 290]. Results obtained in a cold flow model demonstrated that incorporation of the internals increases particle concentration in the counter-current section of the fuel reactor, and that the residence time distribution of the particles was more symmetrical and had lower dispersion. Recently, the 50 kW_{th} unit at ICB-CSIC was modified to include this type of internals in the fuel reactor riser. In experiments performed after the modification, an improvement in the combustion of unburned gaseous compounds in the fuel reactor was observed, as better oxidation of methane and full conversion of hydrogen were recorded [146].

Another modification to the fuel reactor design has been suggested by Lyngfelt and Leckner [4], who proposed and patented a new design for the fuel feed to the fuel

reactor, aimed at avoiding the local plume of volatiles at the fuel injection point [291]. They called it a "volatile distributor", see option D-1B in Fig. 44. It was described as a box inserted at the bottom of the fuel reactor bed with the opening downward and holes in the sides. Design details are still uncertain and have to be optimized using a cold-flow model and fluid-dynamic models. Once the design is optimized, the impact on minimizing unburned compounds at the outlet of the fuel reactor should be evaluated under *iG*-CLC operating conditions.

Alternatively, various technological improvements for the *iG*-CLC configuration have recently been proposed by Gayán et al. [52]. As shown in Fig. 44, the alternatives included incorporating a secondary fuel reactor (D-2), the recirculation of exhaust gases to the fuel reactor (D-3A) or the carbon stripper (D-3B), the separation of CO_2 from unburnt compounds (D-4), or changing the coal feed to the carbon stripper instead of the fuel reactor (D-5).

An attempt to include a secondary fuel reactor has already been presented by Thon et al.; see Fig. 9 [148], who divided the fuel reactor bed into two bubbling fluidized beds. In the lower bubbling bed, char gasification took place while in the upper, volatiles and gasification products were further oxidized by a fresh oxygen carrier. However, the results did not show such significant improvements in the oxygen demand as were expected, probably due to the elutriation of unconverted char from the fluidized beds, which is gasified in the freeboard without coming into contact with the oxygen carrier particles. Another fact to take into account is that, by incorporating a secondary fuel reactor, a higher solids inventory is needed in the CLC system. This should not be an issue if a low-cost oxygen carrier is used, but a more complex operation would also be expected, since a new fluidized bed reactor must be connected to those already operating. Thus, problems with the stability of the solids flow have been reported,

2283 which should be overcome by improving the design and optimizing operating
2284 conditions [179, 189].
2285 The recirculation of exhaust gases to be further converted in the fuel reactor or the
2286 carbon stripper minimizes the need for steam generation in either the fuel reactor or the
2287 carbon stripper; see option D-3A and D-3B in Fig. 44. However, the lack of steam
2288 available in the reacting atmosphere could lead to a decrease in char gasification rate
2289 and, therefore, lower CO_2 capture efficiency [137, 147]. Similarly, Volker and Alfons
2290 [292] analyzed different configurations to remove unburned compounds from the fuel
2291 reactor in the tail gas from the gas processing unit (GPU) using a model; see option D-4
2292 in Fig. 44. They concluded that post-combustion of these gases after the fuel reactor
2293 with an additional injection of oxygen provided by an air separation unit (ASU) was the
2294 best option when compared to burning in the air reactor. However, they also indicated
2295 that it would be better to separate the unburned gases from the nitrogen in the tail gas of
2296 the GPU by a sorption or membrane process and recycle them back into the fuel reactor,
2297 to increase the overall CO_2 capture efficiency.
2298 Finally, if the coal is fed to the carbon stripper, this reactor would be treated as the
2299 primary fuel reactor, where a small amount of char gasification takes place, since char
2300 particles are separated from oxygen carrier particles and sent to the fuel reactor, which
2301 becomes a secondary fuel reactor where char gasification takes place and the coal gases
2302 released in the carbon stripper are oxidized; see option D-5 in Fig. 44.
2303 The expected improvement in the oxygen demand for each of the alternatives was
2304 evaluated by Gayán et al.[52], and are included in Fig. 45. According to the modeling
2305 predictions, the largest reduction in the oxygen demand was obtained if a secondary fuel
2306 reactor was used (option D-2).

Therefore, a new configuration for the reactors in the *i*G-CLC process was proposed; see option D-6 in Fig. 44. Coal is fed into the fuel reactor where volatile matter and gasification products are partially converted to CO_2 and H_2O, with CH_4, CO and H_2 also present as unburned compounds. Solids are then transported to the carbon stripper which, in turn, would be fluidized by hot gases coming from the fuel reactor. Thus, the carbon stripper would also act as a secondary fuel reactor. According to the modeling predictions, total oxygen demand as low as 0.9% would be achievable under this configuration. However, further investigation is needed to confirm predictions from the models experimentally.

It should be noted that, although these design modifications contribute to a significant improvement in the oxygen demand, in no case will full combustion ever be reached [52].

6.3. Oxygen carrier development and scale-up

Regarding the development of oxygen carriers for the *i*G-CLC process, the focus of research is still expected to be on low cost materials, especially Mn-based. The use of synthetic Fe-Mn based materials for *i*G-CLC could also be advantageous due to their magnetic properties. However, the development of synthetic materials should be competitive enough to outweigh the benefits of using low-cost materials that already perform well.

On the contrary, efforts in oxygen carrier development must be focused on synthetic materials with an oxygen uncoupling capability, due to the high combustion efficiency and CO_2 capture values obtained in CLOU mode. Therefore, focusing future research on CLOU combustion is an interesting option. However, there is a large gap in the degree of development of this process when compared to *i*G-CLC. Most of the CLOU results have been obtained from small units (up to 10 kW_{th}), while *i*G-CLC has been largely

demonstrated at MW_{th} scale. Therefore, CLOU should also be demonstrated with larger scale units, based on circulating fluidized beds. In order to reach this objective, it is essential to develop new CLOU oxygen carriers which maintain chemical properties and mechanical stability with the redox cycles. It must be remembered that those tested so far are mostly based on CuO, which is an expensive material, and none of them has demonstrated a long particle lifetime. This means that most of the cost of the CO_2 capture in CLOU combustion is attributed to the oxygen carrier. Moreover, the fact that some loss of oxygen carrier is also expected when draining the solid fuel ashes adds the need to develop CLOU oxygen carriers with properties that enable easy recovery.

Thus, an important development in CLOU oxygen carriers is expected in the near future. Some future research lines can already be outlined. Besides CuO-based materials, mixed oxides based on Mn with Cu, Fe, Mg, Si or Ti are being tested to be used as CLOU or CL*a*OU oxygen carriers. Cu-Fe and Fe-Mn materials have shown magnetic properties [79, 199] and it was recently found that adding Fe-Mn to Ti improved the reactivity and magnetism of the oxygen carriers produced [89]. The magnetic properties found for Fe-Mn-Ti materials could facilitate separation of the oxygen carrier from the ashes during solid fuel combustion. Furthermore, a Mn-Cu material has been identified as a promising oxygen carrier for CLOU [88]. In order to improve the reliability of the CLOU process, ton-scale oxygen carriers manufactured industrially should be developed and the use of the cheapest possible raw materials should also be encouraged.

6.4. Management of ash in the CLC process with solid fuels

Finally, ash generation during fuel combustion is another aspect to be considered in CLC of solid fuels. Two types of ash are generated in the CLC unit: bottom ashes from particles that remain mixed in the bed solids, and fly ashes, which are ash particles

escaping from the cyclone exiting the reactors with the exhaust gases. The bottom ashes remain in the CLC system and accumulate, leading to fluidization and operational problems and eventually stopping operation if the ash content in the fuel reactor exceeds a limit value [293]. Therefore, ash should be periodically drained, although a certain amount of oxygen carrier may be lost in the process. Thus, the lifetime of the oxygen carrier depends on the frequency of ash draining. An estimation of the lifetime of Fe-based oxygen carrier particles as a function of the fly ash content in the coal was recently presented, which would affect the cost of oxygen carrier composition [271]. Both solids in the draining stream and fines collected from a CLC system are a residue whose disposal should be evaluated [271]. If the oxygen carrier can be easily separated from ash, e.g. by rotating fluidized beds [284] or magnetic separation [240], it could be re-used in the CLC process. This fact is especially relevant for high-cost CLOU materials.

Moreover, ashes can interact with the oxygen carrier during solid fuel combustion. There has recently been research on the reactions that may take place. The effect of the interaction depends on several factors, such as the type of oxygen carrier, the nature of the ash (coal/biomass) and the ash content, as well as operating conditions in the CLC unit. Most studies in the literature on this aspect concern Cu-based [294] and especially Fe-based oxygen carriers [269, 295-298]. With coal ash, a low ash load seems to decrease the reactivity of Fe-based oxygen carriers [296]; however, if the ash load increases and the ashes have a high Fe_2O_3 or $CaSO_4$ content, an increase in the reactivity of the oxygen carrier is observed, as these components can act as an oxygen carrier [297]. Recently, experiments performed at TUHH with a coal with high-sodium content evaluated the sodium transfer routes in CLC with an iron ore as oxygen carrier. They concluded that most of the sodium in this type of coal would be released and converted

in the fuel reactor [269]. Preliminary studies on biomass ash indicate the influence of the type of biomass used as fuel. The presence of silica in the ashes can lead to formation of potassium silicates facilitating sintering of iron ore particles, while large amounts of K improves the reactivity of the oxygen carrier [298]. However, more research should be conducted in order to optimize ash handling in a CLC system.

7. Techno-economic evaluation

7.1. Thermal integration

The overall efficiency in the use of a fuel in a power plant is affected by the irreversibilities inherent to the combustion process. In this sense, CLC is an alternative combustion method to decrease this kind of irreversibility and increase the exergy of the process [299-301]. This effect is highlighted when the reaction in the fuel reactor is endothermic, thus having a higher temperature in the air reactor than in the fuel reactor. According to this fact, some redox systems have been identified from theoretical calculations in order to operate the air reactor at considerable higher temperature than the fuel reactor, e.g. see CdO, CoO, K_2O, Na_2O, PbO, SnO_2, WO_3 or ZnO in Table 11 [302]. However, the redox systems linked to these metal oxides suffer from either low melting point of the reduced or oxidized form, requirement for too low/high temperature in the fuel/air reactor, or low equilibrium constant for the oxidation of CO and H_2 to CO_2 and H_2O. Other metal oxides such as Co_3O_4 or NiO are not commonly used in CLC with solid fuels because their high cost and environmental impact. Both facts affect the drainage of the ashes generated during solid fuel combustion. The loss of oxygen carrier during this process would impact the economy of the process and, on the other hand, toxic elements would be present in the drained ashes.

Therefore, in practice, systems based on $CaSO_4$, Fe_2O_3 or Mn_3O_4 are mainly used. These systems also present the desired endothermic reaction in the fuel reactor to take

advantage of the possible exergy increase; see Table 11. However, the temperature in the fuel reactor should be as high as possible to improve the coal conversion and combustion efficiency, thus allowing CO_2 capture rates close to 100% [7] ; see section 4.2.2. At the same time, operating conditions must be carefully selected to avoid a high excess of temperature in the air reactor. Thus, a temperature about 1000 ºC with Fe_2O_3 or Mn_3O_4 is proposed for the fuel reactor temperature, while the temperature increase in the air reactor would be about 50-100 ºC. Some lower (950 ºC) is allowed for $CaSO_4$ to minimize losses of sulphur in gases; see Table 11. In addition, the temperature in both reactors must be precisely controlled for CLOU systems such as CuO/Cu_2O and Mn_2O_3/Mn_3O_4 due to thermodynamic considerations related to the oxidation reaction. In these cases, the global process in the fuel reactor is exothermic, which is beneficial in order to operate the fuel reactor at a higher temperature than the air reactor.

Although the CLC capability to increase the exergy in the energy generation is minimized for practical reasons related to the temperatures in air and fuel reactors, CLC has been identified as a combustion method with inherent CO_2 capture, which can be relevant in a future scenery with restricted CO_2 emissions to the atmosphere [303].

In any case, the thermal integration between the fuel and air reactors is a key issue in the design of a CLC unit, both in *i*G-CLC and CLOU modes. The usual endothermicity of the fuel reactor in *i*G-CLC forces the air reactor to operate at a higher temperature than the fuel reactor in order to supply the energy required in the fuel reactor as sensible heat in solids particles. However, the global process in the fuel reactor is usually exothermic in CLOU, which facilitates the energetic integration of the reactors [304]. In addition, it allows decreasing the temperature of the air reactor below the fuel reactor temperature which facilitates the oxidation of the oxygen carrier by thermodynamic considerations [112].

The thermal integration between fuel and air reactors can be evaluated by performing mass and enthalpy balances to the CLC unit. The optimum temperature in each reactor depends on the solids circulation rate and on the oxygen carrier used. The solids circulation rate affects the temperature difference between the fuel and air reactors in a similar way to the case of gaseous fuels [209], i.e. the difference temperature decreases as the solids circulation rate increases. This fact allows controlling the temperature in the air reactor if the fuel reactor temperature is fixed. Thus, optimum temperatures in the fuel and air reactors of ≈1000 ºC and ≈1045 ºC have been suggested for Fe-based oxygen carriers [244], while the optimum temperature when using a Ni-based oxygen carrier was about 900-950 ºC and 1050-1150 ºC, respectively [305]. In the CLOU process with Cu-based oxygen carriers the optimum temperature in fuel reactor would be about 900-950 ºC, while temperature in the air reactor would be in the 850-900 ºC interval [306, 307].

The heat released in a CLC unit must be used to produce steam, which can be used as a heating medium or to produce electricity using turbines in a steam cycle. Besides that generated inside the air reactor, heat is also available in the high temperature gaseous streams from the fuel and air reactors. A fraction of this enthalpy can be used to preheat the inlet streams to the CLC systems such as air, steam or CO_2. If steam is used to fluidize the fuel reactor in the *i*G-CLC process, Abad et al. [244]. concluded that the sensible heat in flue gases available for steam generation only represents about 45 % of the total thermal energy in the fuel. This value was calculated from Fig. 46a considering the enthalpies entering the system with the inlet streams. Another fraction (~32%) must be extracted from the solids, usually considered from oxidized oxygen carrier due to the high exothermicity of the oxidation reaction. Heat from oxidized solids could be extracted in an external heat exchanger, which would allow operating at a low gas

velocity in a non-corrosive environment for the cooling surfaces. Thus, the heat management is a crucial issue to maintain the desired temperature in the fuel and air reactors. In addition, a relevant fraction of the available heat (~23 %) is found as latent heat, which would be recovered during steam condensation at low temperature. The use of recirculated CO_2 as fluidizing gas can contribute to increase the enthalpy available as sensible heat in the gaseous streams up to ~65 %, while the required heat extracted from the air reactor and the latent heat in steam from the fuel reactor decreases to 29 and 6 %, respectively; see Fig. 46b.

In the CLOU process the thermal integration is influenced by the fact that both air and fuel reactors are exothermic. Thus lower temperatures are necessary and recirculated CO_2 can be used as fluidization agent in the fuel reactor instead of steam. Thus, the difference in temperature between fuel and air reactors can be varied by tuning the heat extracted from fuel and air reactors in the CLOU unit. The temperature in fuel and air reactors can be fixed to 950 and 850 ºC, respectively, by extracting most heat (58 %) from the air reactor [306, 307]; but these temperatures can be matched to 900 ºC if heat extracted from the air reactor was decreased to 31 % which requires that the fraction of fuel thermal power extracted from the fuel reactor was 22 %.

In addition, the steam to carbon ratio in the *i*G-CLC process and the air to fuel ratio, both in *i*G-CLC and CLOU, have been identified as a relevant parameter influencing the enthalpy balance in the system. On the one hand, the energy required in the fuel reactor increased with the steam to carbon ratio, which involves a higher circulation of solids to maintain the enthalpy balance in the system [305]. On the other hand, it must be considered that the heat extracted from the solids decreases as the air to fuel ratio increases [306].

7.2. Net energy efficiency

The enthalpy balance in a CLC unit is directly related to the achievable net efficiency. Both in *i*G-CLC and CLOU, the net electrical efficiency, including CO_2 compression and oxygen production for the oxygen polishing step when required, has been calculated to be 35-36 % for super critical steam cycle [191, 308] and 41-42 % considering ultra-super critical plants [309-313]. Recently, the net electric efficiency of a power plant based on CLOU has been estimated in the 46-48 % interval for coal, lignite and sawdust, while the CO_2 capture rate was above 99 % [314]. In this case the oxygen polishing step is not required. This result is higher than the reference value for a super-critical plant without CCS (43 %).

For comparison purposes, the above studies also present the net efficiency obtained by other CO_2 capture technologies. A compilation of these results is shown in Fig. 47. For ultra-super critical conditions, the net efficiency values for post-combustion with amines, pre-combustion or oxy-combustion technology are in the range of 34-35 %, 34-36 % and 34-37 %, respectively. The energy penalty for CLC technologies with coal compared to a conventional power plant without CO_2 capture is usually estimated in 2-3 percentage points with the capability to capture more than 95 % of the CO_2 avoided. But for other CO_2 capture technologies the energy penalty is estimated in the 7-9 percentage points interval. Note that in these cases the CO_2 avoided is lower than CLC, with values about 90 %.

The use of pressurized CLC units would represent an improvement in the net efficiency by using a combined cycle to produce electricity. In this case, coal can be used in two ways in CLC: (i) integrating the *ex-situ* pressurised gasification of coal with oxygen with a CLC unit (IGCC-CLC); and (ii) the *in-situ* conversion of fuel by a direct feeding of coal in the pressurised CLC unit, such as in the *i*G-CLC and CLOU processes. From

an energetic point of view, the coal direct CLC is preferred because the energy penalty for oxygen production is avoided. If a combined cycle is incorporated and the air reactor is operated at high temperature, the estimated net efficiency oscillates between 39-41 % and 45-50 % for IGCC-CLC and pressure *i*G-CLC, respectively [315, 316]. Compared to conventional IGCC power plants without CCS, no differences in the net efficiency were estimated for *i*G-CLC, while the energy penalty was in the 7-9 % interval for IGCC with CO_2 capture. [315]. Nevertheless, a high temperature in the turbine is required to take advantage of the combined cycle. For example, having the air reactor temperature at 1050 and 1200 ºC the net efficiency was estimated to be 46 % and 49.6 %, respectively [316, 317]. Note that the state of the art in the oxygen carrier development would allow temperatures about 1000-1100 ºC in the operation of an oxygen carrier for solid fuel combustion. However, CLOU materials cannot be oxidized at such high temperature, and the maximum temperature is limited to 900-1000 ºC. Therefore, pressurized CLC operation would involve a limited increase in the net efficiency of the power plant due to the limited temperature of the reactors which also affects to the efficiency of the gas turbine [312, 318].

In addition, some specific characteristics of a CLC unit with solid fuels can affect to the overall efficiency of the system such as the air excess ratio, the pressure drop in the reactors, the steam to carbon ratio and the necessity of an oxygen polishing step specifically for *i*G-CLC.

An increase in the air excess ratio of 10% would decrease the net electric efficiency in 0.05-0.13 percentage points, depending on the pressure drop in the air reactor [310, 319]. Thus, an increase in the pressure drop of 10 kPa in air reactor decreased the net electric efficiency by 0.3 [4] or 0.5 percentage points [319]. Similar increases in the fuel reactor pressure drop decreased the efficiency only by 0.05-0.1 percentage points [319].

In this sense, the better performance of the CLOU process compared to *i*G-CLC burning a solid fuel makes that a lower amount of solids where required for CLOU. Therefore, the energy required to fluidize particles in CLOU is lower than the corresponding energy spent in *i*G-CLC [112].

Regarding the steam to coal ratio, this factor is highly sensitive for *i*G-CLC; note that the CLOU process does not require steam as gasifying agent. Thus, the H_2O/C ratio has been identified as a relevant parameter affecting the net electric efficiency in *i*G-CLC. A decrease of 1.3 % when the steam to coal mass ratio was increased from 1 to 1.5, corresponding to values of steam to fixed carbon molar ratio of H_2O/C_{fix}=1.2-1.8 was reported [319]. Therefore, a low H_2O/C_{fix} ratio is preferred. Shen et al. [305] and Lyngfelt and Leckner [4] selected values of the H_2O/C_{fix} ratio in the 0.4-0.5 range. Note that in this process it is possible to fully gasify the coal with H_2O/C_{fix} molar ratios below 1 because H_2O is continuously formed during the combustion of gasification products by the oxygen carrier. Indeed, no significant effect was observed during coal combustion when the H_2O/C_{fix} ratio was experimentally decreased below 1 in a CLC unit [138]. Also, the efficiency would be increased if hot exhaust recycled gases were used as fluidizing media [310], which is not problematic for CLOU [199], although CO_2 capture could be affected for *i*G-CLC if less reactive CO_2 was used as fluidizing and gasifying agent [137, 138, 140]. The efficiency penalty has been estimated in 0.8 % when only steam is used for fluidization of the fuel reactor. This value could decrease to 0.2 % if "hot CO_2" was recirculated [4].

In addition, complete combustion in the fuel reactor is not found in *i*G-CLC mode, which requires the use of an oxygen polishing step. An increase in the oxygen demand of 5 % would only represent a decrease in the net electric efficiency of 0.2-0.3 % [4, 292]. In order to decrease the oxygen requirements for this oxygen polishing some

technological solutions have been evaluated, including the use of a secondary fuel reactor or the recirculation of flue gases, which would allow an increase in the net efficiency of the whole *i*G-CLC process [52].

In addition of the applicability of CLC to a power plant, CLC technology can be also considered for steam generation. In this case, the steam produced by CLOU is about 15 % higher than that produced by *i*G-CLC because the steam requirement for the fuel reactor is avoided [320].

Finally, it should be remarked that the lower energetic penalty of CLC compared to other CO_2 capture technologies has a direct impact on lower fuel requirements. This fact has been identified as a fundamental issue in order to identify the CLC with coal as a technology with a considerably lower environmental impact than other CO_2 capture technologies [321].

7.3. Cost of CO_2 capture by CLC

The relatively low energy penalty for the CLC process compared to other CO_2 capture technologies benefits the economy of CLC regarding the electricity and CO_2 costs. Thus, CLC was identified by the CCP (CO_2 Capture Project) among the best alternatives to reduce the economic cost of CO_2 capture [322]. Moreover, the IPCC in their special report on Carbon Dioxide Capture and Storage identified CLC as one of the cheapest technologies for CO_2 capture [323]. It is of high relevance the capability of CLC to achieve capture rates close to 100 % when solid fuels are considered, which are very difficult to reach by other CO_2 capture technologies [7, 35, 301].

Regarding the CO_2 capture cost there is a variability of data. The EU project "Enhanced Capture of CO_2" (ENCAP) also concluded that the incremental in the electricity cost was lower than the calculated for other technologies of CO_2 capture [191]. Taken as a reference a pulverised fuel fired power plant without CO_2 capture using bituminous coal

as fuel, the increase in the electricity generation cost for an *i*G-CLC plant was about 12-22 %. The estimated cost of the capture was 6-13 €/ton CO_2 avoided for CLC. The same study estimated 18-37 €/ton CO_2 avoided for a pre-combustion technology using IGCC, and 13-30 €/ton CO_2 avoided for an oxy-fuel process. In a recent work, the cost of the avoided CO_2 for CLOU was estimated in 24-27 €/ton, which is also lower than the CO_2 cost in reference power plant with solid fuels (35-60 €/ton) [312].

Lyngfelt and Leckner [4] evaluated the additional cost and efficiency penalty of a CLC unit with coal including CO_2 compression compared to the reference cost of coal combustion in a circulating fluidized bed boiler. They identified the cost associated to the oxygen carrier and the oxygen polishing step as the major contributors to the CO_2 capture cost in a *i*G-CLC process. Thus, the oxygen carrier would contribute with 1.3-4 €/tonne CO_2, while the oxygen polishing step will add a cost of 4-9 €/tonne CO_2. The total cost would be 16-26 €/tonne CO_2 avoided, including CO_2 compression.

The additional cost related to the oxygen carrier depends on the price of the oxygen carrier (materials, particles production, calcination, etc.), the lifetime of particles, solids inventory in the CLC unit and the ratio of the oxygen carrier being recovered [324]. But in the worst case scenario, i.e. low lifetime and relatively high cost of the oxygen carrier, the cost of the oxygen carrier is easily below 5 % of the assumed yearly operational cost. Then, the oxygen carrier cost would not be a showstopper for the development of the CLC technology, being highly competitive compared to other CO_2 capture technologies as, for example, the oxy-fuel case. For example, the cost of the oxygen carrier could add 3.3 € per ton CO_2 avoided considering a price of the oxygen carrier of 1500 €/ton, a solids inventory of 1500 kg/MW_{th}, a lifetime of 1250 h and a recovery factor of 50 % [324].

The levelized cost of electricity (LCOE) for the *i*G-CLC process in the USA market has been estimated in the range 105-120 $/MWh, which represents an increase of ~20 $/MWh compared to the LCOE for conventional power plants without CO_2 capture, and lower than the cost for the DOE base case for post-combustion CO_2 capture with amines (132.5 $/MWh) or oxy-combustion (158 $/MWh) [191, 308]. Thus, the CLC with coal complies by far with the DOE goal of 90 % capture with an increase of the electricity cost of 35 %. For CLOU with solid fuels in the EU market, the LCOE was estimated to be in the 84-92 €/MWh interval, which are lower than the cost for other CCS technologies (90-110 €/MWh) [312].

In addition, the electricity production by CLC with coal can become highly competitive if the CO_2 market fixes a relatively high price [325]. For example, in the German scenario with a CO_2 allowances of 50 €/ton, the electricity production cost can be 40-45 €/MWh for CLC, which can be compared to 50 €/MWh for the oxy-fuel case or 65 €/MWh for a reference case without CCS. This low price would boost the hours of peak load operation of power plant based on CLC technology.

8. Highlights on the future research of CLC with solid fuels

During the last decade, a firm base has been achieved in the development of CLC for solid fuels. Thus, the main concerns on fuel conversion and environmental issues have been analyzed in depth from experimental results in CLC units ranging from 0.5 kW_{th} to 4 MW_{th}. Research on coal combustion in CLC will be relevant in the coming years, as this fuel will play a significant part in the mix of energy production in the near future. In addition, there have been encouraging results on biomass-fueled CLC, which remains one of the BECCS technologies with a good chance of achieving negative CO_2 emissions.

The scale-up of the CLC process should include the experience gained to date on aspects such as design, operating conditions and oxygen carrier development.

Most of the experience has been gained in plants, including interconnected fluidized bed systems, but a moving bed used as fuel reactor also returned interesting results.

The combustion technology based on CFB at atmospheric pressure is already mature. Retrofitting a circulating fluidized bed to CLC by adding a coupled reactor to the existing one is seen as a promising option in the next stage of the scale-up process. For the energy generation sector, Pressurized Chemical Looping Combustion coupled with a Combined Cycle (PCLC-CC) has also attracted attention in the bid to increase the energy efficiency of CLC of solid fuels, although possible damage to the turbine caused by solid fines elutriated from the CFB should be taken into account.

The *i*G-CLC process mainly focuses on the use of low-cost materials, generally based on minerals or industrial residues containing Fe and Mn. Temperatures higher than 1000 ºC and a solids inventory up to 1000 kg/MW_{th} were desirable to reach high CO_2 capture efficiencies. In addition, the presence of a highly efficient carbon stripper was a decisive factor in obtaining CO_2 capture efficiency close to 100%. Nevertheless, unburned compounds have always been found at the outlet of the fuel reactor, which makes an oxygen polishing step necessary.

The use of more reactive oxygen carriers leads to a decrease in the oxygen demand, but the improvements were not sufficient to avoid oxygen polishing. Improved design, such as the use of a secondary fuel reactor, could lead to a significant reduction in oxygen demand requirements. However, complete combustion of solid fuel cannot be expected from these technological solutions alone. Alternatively, a moving bed fuel reactor would solve this problem, although other design challenges in the scale-up have to be overcome.

The development of synthetic materials with oxygen uncoupling (CLOU) capability is an alternative to the low-cost materials used in *i*G-CLC. Excellent results both in CO_2 capture and combustion efficiencies have been obtained with Cu-based materials. Mn-based materials (Fe-Mn or Ca-Mn) with some oxygen uncoupling capability (CL*a*OU) open up an opportunity to use lower cost materials. A key factor in the scale-up of synthetic oxygen carriers is their lifetime, thus, development of long-life oxygen carriers will be a subject of future research.

Moreover, the loss of oxygen carrier in the purge ash stream is important in any solid-fueled CLC, especially for coals with high ash content. A separation process, possibly based on various fluid dynamics or magnetic properties, is needed to recover the oxygen carrier from the ash mix, and developing oxygen carrier materials for the purpose, based on Fe-Mn oxides with magnetic properties, remains attractive.

To boost the scale-up of CLC at the commercial scale, confidence in the use of oxygen carrier materials with solid fuels must be guaranteed; therefore, experience gained in the use of oxygen carrier particles as bed material in a fluidized bed combustor working under OCAC conditions will be very valuable. Thus, determination of the lifetime of oxygen carrier under certain conditions and the ageing of the particles in the presence of ash components are relevant aspects useful for further development of solid-fueled CLC.

Considering the results obtained in CLC of solid fuels, its implementation on a commercial scale is a solid option in a CO_2 restricted scenario and has special advantages if using biomass. In addition to the energy generation sector, a market search identified paper, cement and other end-users requiring industrial boilers, as an interesting niche which could be early adopters of CLC.

Acknowledgments

This work was supported by the Spanish Ministry of Economy and Competitiveness (projects ENE 2013-45454-R, ENE2014-56857-R and ENE2016-77982-R), by the European Regional Development Fund (ERDF), by the CSIC (projects 2014-80E101 and 201780E035) and by the Government of Aragón (Spain, Ref. T06). T. Mendiara gives thanks for the Ramón y Cajal post-doctoral contract awarded by the Spanish Ministry of Economy and Competitiveness.

Nomenclature

$F_{C,AR,out}$	carbon flow at the air reactor outlet (mol/s)
$F_{C,FR,out}$	carbon flow at the fuel reactor outlet (mol/s)
$F_{C,char}$	carbon flow in the char (mol/s)
$F_{C,elut}$	carbon flow in the char elutriated (mol/s)
$F_{C,sf}$	carbon flow in the solid fuel (mol/s)
$F_{C,vol}$	carbon flow in the volatiles (mol/s)
$F_{CO2,AR}$	flow of CO_2 at the air reactor outlet (mol/s)
$F_{CO2,in}$	flow of CO_2 at the fuel reactor inlet (mol/s)
$F_{H2O,in}$	flow of H_2O at the fuel reactor inlet (mol/s)
$F_{i,FR,out}$	flow of *i* species at the fuel reactor outlet (mol/s)
$F_{O,comb,FR}$	oxygen demanded by solid fuel converted in the fuel reactor (mol O/s)
$F_{O,comb,sf}$	oxygen needed to burn solid fuel (mol O/s)
$F_{O,FR,in}$	flow of oxygen at the fuel reactor inlet (mol O/s)
$F_{O,FR,out}$	flow of oxygen at the fuel reactor outlet (mol O/s)
$F_{O,op}$	flow of oxygen needed in the oxygen polishing step (mol O/s)
$F_{O2,char}$	oxygen flow reacted with the char in the air reactor (mol O_2/s)
$F_{O2,OC}$	oxygen flow reacted with the oxygen carrier in the air reactor (mol O_2/s)
M_i	molecular/atomic weight of species *i* (g/mol)
$\dot{m}_{sf}$	mass flow of solid fuel (kg/s)
R_{OC}	oxygen transport capacity of the oxygen carrier (-)
X_{char}	conversion of char in the whole CLC unit (-). Usually defined in literature as $\eta_{char.}$
$X_{char,FR}$	conversion of char in the FR (-).
X_{sf}	conversion of solid fuel (-). Usually defined in literature as $\eta_{sf.}$

x_C	fraction of carbon in solid fuel (-)
$x_{char,FR}$	fraction of carbon in char converted in the fuel reactor (-)
x_{fc}	fraction of fixed carbon in solid fuel (-)
x_i	fraction of specie *i* in solid fuel (-)
$y_{CO2,AR}$	fraction of CO_2 at the air reactor outlet (-)
$y_{O2,AR}$	fraction of O_2 at the air reactor outlet (-)

Greek symbols

η_{CC}	CO_2 capture efficiency (%)
η_{CC}^{*}	estimated CO_2 capture efficiency (%)
$\eta_{comb,FR}$	combustion efficiency in the fuel reactor (%)
$\eta_{comb,g}$	combustion efficiency of the char gasification products (%)
$\eta_{comb,v}$	combustion efficiency of the volatiles (%)
χ_{oo}	oxide oxygen fraction (%). Usually defined in literature as $\eta_{OO.}$
Ω_{char}	oxygen demand of the char (kg O/kg solid fuel)
Ω_{FR}	oxygen demand in the fuel reactor (%). Usually defined in literature as $\Omega_{OD.}$
Ω_{sf}	oxygen demand of the solid fuel (kg O/kg solid fuel)
Ω_T	total oxygen demand (%)
$\Omega_{T,full}$	total oxygen demand for complete fuel conversion in the FR (%)
Ω_{vol}	oxygen demand of the volatiles (kg O/kg solid fuel)
ϕ	Oxygen carrier to fuel ratio (-)

Glossary:

AR	air reactor

ASU	air separation unit
BECCS	bioenergy and carbon capture and storage
BFB	bubbling fluidized bed
CCS	carbon capture and storage
CFB	circulating fluidized bed
CL*a*OU	chemical looping *assisted* by oxygen uncoupling
CLC	chemical looping combustion
CLOU	chemical looping with oxygen uncoupling
DFT	density functional theory
FR	fuel reactor
GPU	gas processing unit
*i*G-CLC	*in-situ* gasification chemical looping combustion
IPCC	intergovernmental panel on climate change
IGCC	integrated gasification combined cycle
LCL™	limestone-based chemical looping process
LCOE	levelized cost of electricity
OC	oxygen carrier
OCAC	oxygen carrier aided combustion
PCLC	pressurized chemical looping combustion
SCL	syngas chemical looping
SFB	spouted fluidized bed
SPA	solid phase adsorption

References

[1] United Nations Framework Convention for Climate Change. The Paris Agreement. http://unfccc.int/paris_agreement/items/9485.php. 2015.

[2] Fan LS, Zeng L, Wang W, Luo S. Chemical looping processes for CO_2 capture and carbonaceous fuel conversion - Prospect and opportunity. Energy Environ Sci. 2012;5:7254-80.

[3] Epple B, Ströhle J. Chemical Looping in power plants. In: Scherer DSaV, editor. Efficient carbon capture for coal power plants, First ed. Germany: Wiley-VCH Verlag GmbH & Co KGaA; 2011. p. 505-24.

[4] Lyngfelt A, Leckner B. A 1000 MW_{th} boiler for chemical-looping combustion of solid fuels - Discussion of design and costs. Appl Energ. 2015;157:475-87.

[5] Rubin ES, Davison JE, Herzog HJ. The cost of CO_2 capture and storage. Int J Greenh Gas Con. 2015;40:378-400.

[6] Rubin ES, Mantripragada H, Marks A, Versteeg P, Kitchin J. The outlook for improved carbon capture technology. Prog Energy Combust Sci. 2012;38:630-71.

[7] Adanez J, Abad A, Garcia-Labiano F, Gayan P, De Diego LF. Progress in chemical-looping combustion and reforming technologies. Prog Energy Combust Sci. 2012;38:215-82.

[8] Abanades JC, Arias B, Lyngfelt A, Mattisson T, Wiley DE, Li H, et al. Emerging CO_2 capture systems. Int J Greenh Gas Con. 2015;40:126-66.

[9] Fan LS. Chemical Looping Systems for Fossil Energy Conversion: John Wiley & Sons; 2010. AIChE. ISBN: 978-04708752-9.

[10] Hossain MM, de Lasa HI. Chemical-looping combustion (CLC) for inherent CO_2 separations-a review. Chem Eng Sci. 2008;63:4433-51.

[11] Lyngfelt A, Mattisson T. Chemical looping materials for CO_2 separation. In: Scherer DSaV, editor. Efficient carbon capture for coal power plants, First ed. Germany: Wiley-VCH Verlag GmbH & Co KGaA; 2011. p. 475-504.

[12] Lyngfelt A. Oxygen carriers for chemical looping combustion -4000 h of operational experience. Oil Gas Sci Technol. 2011;66:161-72.

[13] Fan LS, Li F. Chemical looping technology and its fossil energy conversion applications. Ind Eng Chem Res. 2010;49:10200-11.

[14] Mayer K, Penthor S, Pröll T, Hofbauer H. The different demands of oxygen carriers on the reactor system of a CLC plant - Results of oxygen carrier testing in a 120 kW_{th} pilot plant. Appl Energ. 2015;157:323-9.

[15] Sit SP, Reed A, Hohenwarter U, Horn V, Marx K, Proell T. Cenovus 10 MW CLC field pilot. Energy Procedia. 2013;37:671-6.

[16] Cabello A, Gayán P, García-Labiano F, De Diego LF, Abad A, Adánez J. On the attrition evaluation of oxygen carriers in Chemical Looping Combustion. Fuel Process Technol. 2016;148:188-97.

[17] Lambert A, Comte E, Marti D, Sozinho T, Bertholin S, Stainton H, et al. On the mechanism of oxygen carrier degradation during multiple CLC cycles. 6th High Temperature Solid Looping Network Meeting. Milano (Italy). 2015.

[18] Rydén M, Moldenhauer P, Lindqvist S, Mattisson T, Lyngfelt A. Measuring attrition resistance of oxygen carrier particles for chemical looping combustion with a customized jet cup. Powder Technol. 2014;256:75-86.

[19] Mattisson T, Adánez J, Mayer K, Snijkers F, Williams G, Wesker E, et al. Innovative oxygen carriers uplifting chemical-looping combustion. Energy Procedia. 2014;63:113-30.

[20] Wolf J, Anheden M, Yan J. Comparison of nickel- and iron-based oxygen carriers in chemical looping combustion for CO_2 capture in power generation. Fuel. 2005;84:993-1006.

[21] Naqvi R, Bolland O. Multi-stage chemical looping combustion (CLC) for combined cycles with CO_2 capture. Int J Greenh Gas Con. 2007;1:19-30.

[22] Noorman S, Van Sint Annaland M, Kuipers H. Packed bed reactor technology for chemical-looping combustion. Ind Eng Chem Res. 2007;46:4212-20.

[23] Pishahang M, Larring Y, McCann M, Bredesen R. $Ca_{0.9}Mn_{0.5}Ti_{0.5}O_{3-\delta}$: A suitable oxygen carrier material for fixed-bed chemical looping combustion under syngas conditions. Ind Eng Chem Res. 2014;53:10549-56.

[24] Nordness O, Han L, Zhou Z, Bollas GM. High-Pressure Chemical-Looping of Methane and Synthesis Gas with Ni and Cu Oxygen Carriers. Energy Fuels. 2016;30:504-14.

[25] Fan LS, Zeng L, Luo S. Chemical-looping technology platform. AlChE J. 2015;61:2-22.

[26] Ridha FN, Duchesne MA, Lu X, Lu DY, Filippou D, Hughes RW. Characterization of an ilmenite ore for pressurized chemical looping combustion. Appl Energ. 2016;163:323-33.

[27] Hoteit A, Forret A, Pelletant W, Roesler J, Gauthier T. Chemical looping combustion with different types of liquid fuels. Oil Gas Sci Technol. 2011;66:193-9.

[28] Cao Y, Li B, Zhao HY, Lin CW, Sit SP, Pan WP. Investigation of asphalt (Bitumen)-fuelled chemical looping combustion using durable copper-based oxygen carrier. Energy Procedia. 2011;4:457-64.

[29] Moldenhauer P, Rydén M, Mattisson T, Hoteit A, Jamal A, Lyngfelt A. Chemical-looping combustion with fuel oil in a 10 kW pilot plant. Energy Fuels. 2014;28:5978-87.

[30] de Diego LF, Serrano A, García-Labiano F, García-Díez E, Abad A, Gayán P, et al. Bioethanol combustion with CO_2 capture in a $1kW_{th}$ Chemical Looping Combustion prototype: Suitability of the oxygen carrier. Chem Eng J. 2016;283:1405-13.

[31] IPCC. Climate Change 2014: Synthesis Report. Contribution of Working Groups I, II and III to the Fifth Assessment Report of the Intergovernmental Panel on Climate Change. In: Core Writing Team RKPaLAM, editor. Geneva (Switzerland). 2014. p. 151.

[32] Gasser T, Guivarch C, Tachiiri K, Jones CD, Ciais P. Negative emissions physically needed to keep global warming below 2°C. Nature Communications. 2015;6.

[33] MIT. The Role of Coal in Energy Growth and CO_2 Emissions. The future of coal: Massachusetts Institute of Technology; 2007. ISBN:978-0-615-14092-6.

[34] IEA. Coal market outlook. World Energy Outlook 2013. Paris (France): International Energy Agency; 2013.

[35] Lyngfelt A. Chemical-looping combustion of solid fuels - Status of development. Appl Energ. 2014;113:1869-73.

[36] Berguerand N, Lyngfelt A. Design and operation of a 10 kW_{th} chemical-looping combustor for solid fuels - Testing with South African coal. Fuel. 2008;87:2713-26.

[37] Berguerand N, Lyngfelt A. The use of petroleum coke as fuel in a 10 kW_{th} chemical-looping combustor. Int J Greenh Gas Con. 2008;2:169-79.

[38] Shen L, Wu J, Xiao J. Experiments on chemical looping combustion of coal with a NiO based oxygen carrier. Combust Flame. 2009;156:721-8.

[39] Shen L, Wu J, Xiao J, Song Q, Xiao R. Chemical-looping combustion of biomass in a 10 kW_{th} reactor with iron oxide as an oxygen carrier. Energy Fuels. 2009;23:2498-505.

[40] Wang P, Means N, Shekhawat D, Berry D, Massoudi M. Chemical-looping combustion and gasification of coals and oxygen carrier development: A brief review. Energies. 2015;8:10605-35.

[41] Linderholm C, Lyngfelt A. Chemical Looping Combustion of solid fuels. In: Anthony PFaB, editor. Calcium and Chemical Looping Technology for Power Generation and Carbon Dioxide (CO_2) Capture, First ed. Germany: Wiley-VCH Verlag GmbH & Co KGaA; 2015. p. 505-24.

[42] Ströhle J, Orth M, Epple B. Design and operation of a 1 MW_{th} chemical looping plant. Appl Energ. 2014;113:1490-5.

[43] Abdulally I, Beal C, Herbert A, Epple B, Lyngfelt A, Lani B. Alstom´s Chemical Looping Prototypes, Program Update. 37th International Technical Conference on Clean Coal & Fuel Systems. Clearwater, FL, USA. 2012.

[44] Kluger F, Abdulally I, Andrus H, Levasseur A, Beal C, Marion J. Overview of ALSTOM´s Chemical Looping Programs. 5th Meeting of the IEAGHG International Oxyfuel Combustion Research Network. Wuhan (China). 2015.

[45] Siriwardane R, Tian H, Miller D, Richards G, Simonyi T, Poston J. Evaluation of reaction mechanism of coal-metal oxide interactions in chemical-looping combustion. Combust Flame. 2010;157:2198-208.

[46] Piekiel NW, Egan GC, Sullivan KT, Zachariah MR. Evidence for the predominance of condensed phase reaction in chemical looping reactions between carbon and oxygen carriers. J. Phys. Chem. C. 2012;116:24496-502.

[47] Mendiara T, García-Labiano F, Gayán P, Abad A, De Diego LF, Adánez J. Evaluation of the use of different coals in Chemical Looping Combustion using a bauxite waste as oxygen carrier. Fuel. 2013;106:814-26.

[48] Cao Y, Pan WP. Investigation of chemical looping combustion by solid fuels. 1. Process analysis. Energy Fuels. 2006;20:1836-44.

[49] Kramp M, Thon A, Hartge EU, Heinrich S, Werther J. Carbon Stripping - A Critical Process Step in Chemical Looping Combustion of Solid Fuels. Chem Eng Technol. 2012;35:497-507.

[50] Sun H, Cheng M, Chen D, Xu L, Li Z, Cai N. Experimental Study of a Carbon Stripper in Solid Fuel Chemical Looping Combustion. Ind Eng Chem Res. 2015;54:8743-53.

[51] Sun H, Cheng M, Li Z, Cai N. Riser-Based Carbon Stripper for Coal-Fueled Chemical Looping Combustion. Ind Eng Chem Res. 2016;55:2381-90.

[52] Gayán P, Abad A, de Diego LF, García-Labiano F, Adánez J. Assessment of technological solutions for improving chemical looping combustion of solid fuels with CO_2 capture. Chem Eng J. 2013;233:56-69.

[53] Kim HR, Wang D, Zeng L, Bayham S, Tong A, Chung E, et al. Coal direct chemical looping combustion process: Design and operation of a 25-kW_{th} sub-pilot unit. Fuel. 2013;108:370-84.

[54] Schmitz M, Linderholm C, Hallberg P, Sundqvist S, Lyngfelt A. Chemical-Looping Combustion of Solid Fuels Using Manganese Ores as Oxygen Carriers. Energy Fuels. 2016;30:1204-16.

[55] Adánez J, Gayán P, Adánez-Rubio I, Cuadrat A, Mendiara T, Abad A, et al. Use of Chemical-Looping processes for coal combustion with CO_2 capture. Energy Procedia. 2013;37:540-9.

[56] Mendiara T, Adánez-Rubio I, Gayán P, Abad A, de Diego LF, García-Labiano F, et al. Process Comparison for Biomass Combustion: *In Situ* Gasification-Chemical Looping Combustion (*i*G-CLC) versus Chemical Looping with Oxygen Uncoupling (CLOU) Energy Technol. 2016;4:1130-6.

[57] Schmitz M, Linderholm CJ. Performance of calcium manganate as oxygen carrier in chemical looping combustion of biochar in a 10 kW pilot. Appl Energ. 2016;169:729-37.

[58] Adánez-Rubio I, Abad A, Gayán P, de Diego LF, García-Labiano F, Adánez J. Performance of CLOU process in the combustion of different types of coal with CO_2 capture. Int J Greenh Gas Con. 2013;12:430-40.

[59] Mattisson T, Lyngfelt A, Leion H. Chemical-looping with oxygen uncoupling for combustion of solid fuels. Int J Greenh Gas Con. 2009;3:11-9.

[60] Abad A, Gayán P, de Diego LF, García-Labiano F, Adánez J. Fuel reactor modelling in chemical-looping combustion of coal: 1. model formulation. Chem Eng Sci. 2013;87:277-93.

[61] García-Labiano F, de Diego LF, Gayán P, Abad A, Adánez J. Fuel reactor modelling in chemical-looping combustion of coal: 2-simulation and optimization. Chem Eng Sci. 2013;87:173-82.

[62] Mattisson T. Materials for Chemical-Looping with Oxygen Uncoupling. ISRN Chemical Engineering. 2013:Article ID 526375.

[63] Imtiaz Q, Hosseini D, Müller CR. Review of Oxygen Carriers for Chemical Looping with Oxygen Uncoupling (CLOU): Thermodynamics, Material Development, and Synthesis. Energy Technol. 2013;1:633-47.

[64] Rydén M, Leion H, Mattisson T, Lyngfelt A. Combined oxides as oxygen-carrier material for chemical-looping with oxygen uncoupling. Appl Energ. 2014;113:1924-32.

[65] Arjmand M, Azad AM, Leion H, Lyngfelt A, Mattisson T. Prospects of Al_2O_3 and $MgAl_2O_4$-supported CuO oxygen carriers in chemical-looping combustion (CLC) and chemical-looping with oxygen uncoupling (CLOU). Energy Fuels. 2011;25:5493-502.

[66] Coppola A, Senneca O, Solimene R, Chirone R, Cortese L, Salatino P. Chemical looping combustion of char with a Cu-based carrier. International Conference on Coal Science and Technology (ICCS&T 2011). Oviedo (Spain). 2011.

[67] Gayán P, Adánez-Rubio I, Abad A, De Diego LF, García-Labiano F, Adánez J. Development of Cu-based oxygen carriers for Chemical-Looping with Oxygen Uncoupling (CLOU) process. Fuel. 2012;96:226-38.

[68] Adánez-Rubio I, Gayán P, Abad A, De Diego LF, García-Labiano F, Adánez J. Evaluation of a spray-dried $CuO/MgAl_2O_4$ oxygen carrier for the chemical looping with oxygen uncoupling process. Energy Fuels. 2012;26:3069-81.

[69] Peterson SB, Konya G, Clayton CK, Lewis RJ, Wilde BR, Eyring EM, et al. Characteristics and CLOU performance of a novel SiO_2-supported oxygen carrier prepared from CuO and β-SiC. Energy Fuels. 2013;27:6040-7.

[70] Xu L, Wang J, Li Z, Cai N. Experimental study of cement-supported CuO oxygen carriers in chemical looping with oxygen uncoupling (CLOU). Energy Fuels. 2013;27:1522-30.

[71] Imtiaz Q, Broda M, Müller CR. Structure-property relationship of co-precipitated Cu-rich, Al_2O_3- or $MgAl_2O_4$-stabilized oxygen carriers for chemical looping with oxygen uncoupling (CLOU). Appl Energ. 2014;119:557-65.

[72] Song Q, Liu W, Bohn CD, Harper RN, Sivaniah E, Scott SA, et al. A high performance oxygen storage material for chemical looping processes with CO_2 capture. Energy Environ Sci. 2013;6:288-98.

[73] Mei D, Abad A, Zhao H, Adánez J. Characterization of a sol-gel derived $CuO/CuAl_2O_4$ oxygen carrier for chemical looping combustion (CLC) of gaseous fuels: Relevance of gas-solid and oxygen uncoupling reactions. Fuel Process Technol. 2015;133:210-9.

[74] Shulman A, Cleverstam E, Mattisson T, Lyngfel A. Manganese/iron, manganese/nickel, and manganese/silicon oxides used in chemical-looping with oxygen uncoupling (CLOU) for combustion of methane. Energy Fuels. 2009;23:5269-75.

[75] Shulman A, Cleverstam E, Mattisson T, Lyngfelt A. Chemical - Looping with oxygen uncoupling using Mn/Mg-based oxygen carriers - Oxygen release and reactivity with methane. Fuel. 2011;90:941-50.

[76] Azimi G, Rydén M, Leion H, Mattisson T, Lyngfelt A. $(Mn_zFe_{1-z})_yO_x$ combined oxides as oxygen carrier for chemical-looping with oxygen uncoupling. AlChE J. 2013;59:582-8.

[77] Shafiefarhood A, Stewart A, Li F. Iron-containing mixed-oxide composites as oxygen carriers for Chemical Looping with Oxygen Uncoupling (CLOU). Fuel. 2015;139:1-10.

[78] Larring Y, Braley C, Pishahang M, Andreassen KA, Bredesen R. Evaluation of a mixed Fe-Mn oxide system for chemical looping combustion. Energy Fuels. 2015;29:3438-45.

[79] Pérez-Vega R, Abad A, Adánez J, De Diego LF, García-Labiano F, Gayán P. Development of a Mn-Fe-Ti based oxygen carrier in Chemical Looping Combustion of coal. 7th International Conference on Clean Coal Technologies. Kraków (Poland). 2015.

[80] Mattisson T, Jing D, Lyngfelt A, Rydén M. Experimental investigation of binary and ternary combined manganese oxides for chemical-looping with oxygen uncoupling (CLOU). Fuel. 2016;164:228-36.

[81] Leion H, Larring Y, Bakken E, Bredesen R, Mattisson T, Lyngfelt A. Use of $CaMn_{0.875}Ti_{0.125}O_3$ as oxygen carrier in chemical-looping with oxygen uncoupling. Energy Fuels. 2009;23:5276-83.

[82] Galinsky N, Mishra A, Zhang J, Li F. $Ca_{1-x}A_xMnO_3$ (A=Sr and Ba) perovskite based oxygen carriers for chemical looping with oxygen uncoupling (CLOU). Appl Energ. 2015;157:358-67.

[83] Azad A-M, Hedayati A, Rydén M, Leion H, Mattisson T. Examining the Cu-Mn-O Spinel System as an Oxygen Carrier in Chemical Looping Combustion. Energy Technol. 2013;1:59-69.

[84] Mungse P, Saravanan G, Uchiyama T, Nishibori M, Teraoka Y, Rayalu S, et al. Copper-manganese mixed oxides: CO_2-selectivity, stable, and cyclic performance for chemical looping combustion of methane. Phys Chem Chem Phys. 2014;16:19634-42.

[85] Hosseini D, Imtiaz Q, Abdala PM, Yoon S, Kierzkowska AM, Weidenkaff A, et al. CuO promoted Mn_2O_3-based materials for solid fuel combustion with inherent CO_2 capture. J Mater Chem A. 2015;3:10545-50.

[86] Fan Y, Siriwardane R, Tian H. Trimetallic Oxygen Carriers $CuFeMnO_4$, $CuFeMn_2O_4$, and $CuFe_{0.5}Mn_{1.5}O_4$ for Chemical Looping Combustion. Energy Fuels. 2015;29:6616-24.

[87] Adánez-Rubio I, Abad A, Gayán P, Adánez I, de Diego LF, García-Labiano F, et al. Use of Hopcalite-Derived Cu-Mn Mixed Oxide as Oxygen Carrier for Chemical-Looping with Oxygen Uncoupling Process. Energy Fuels. 2016.

[88] Adánez-Rubio I, Abad A, Gayán P, García-Labiano F, de Diego LF, Adánez J. Cu-Mn mixed oxide as oxygen carrier for CLOU process. 4th International Conference on Chemical Looping. Nanjing (China). 2016.

[89] Pérez-Vega R. Captura de CO_2 en la combustión de carbón con transportadores sólidos de oxígeno: Universidad de Zaragoza; 2016. Ph.D. Thesis.

[90] Wen YY, Li ZS, Xu L, Cai NS. Experimental study of natural Cu ore particles as oxygen carriers in chemical looping with oxygen uncoupling (CLOU). Energy Fuels. 2012;26:3919-27.

[91] Zhao H, Wang K, Fang Y, Ma J, Mei D, Zheng C. Characterization of natural copper ore as oxygen carrier in chemical-looping with oxygen uncoupling of anthracite. Int J Greenh Gas Con. 2014;22:154-64.

[92] Fossdal A, Bakken E, Øye BA, Schøning C, Kaus I, Mokkelbost T, et al. Study of inexpensive oxygen carriers for chemical looping combustion. Int J Greenh Gas Con. 2011;5:483-8.

[93] Sundqvist S, Arjmand M, Mattisson T, Rydén M, Lyngfelt A. Screening of different manganese ores for chemical-looping combustion (CLC) and chemical-looping with oxygen uncoupling (CLOU). Int J Greenh Gas Con. 2015;43:179-88.

[94] Haider SK, Azimi G, Duan L, Anthony EJ, Patchigolla K, Oakey JE, et al. Enhancing properties of iron and manganese ores as oxygen carriers for chemical looping processes by dry impregnation. Appl Energ. 2016;163:41-50.

[95] Knutsson P, Linderholm C. Characterization of ilmenite used as oxygen carrier in a 100 kW chemical-looping combustor for solid fuels. Appl Energ. 2015;157:368-73.

[96] Adánez J, Cuadrat A, Abad A, Gayán P, de Diego LF, García-Labiano F. Ilmenite activation during consecutive redox cycles in chemical-looping combustion. Energy Fuels. 2010;24:1402-13.

[97] Cuadrat A, Abad A, Adánez J, de Diego LF, García-Labiano F, Gayán P. Behavior of ilmenite as oxygen carrier in chemical-looping combustion. Fuel Process Technol. 2012;94:101-12.

[98] Mendiara T, Pérez R, Abad A, de Diego LF, García-Labiano F, Gayán P, et al. Low-cost Fe-based oxygen carrier materials for the *i*G-CLC process with coal. 1. Ind Eng Chem Res. 2012;51:16216-29.

[99] Abad A, Gayán P, Mendiara T, de Diego LF, García-Labiano F, Adánez J. Kinetics of oxygen carriers. ACCLAIM project (RFCP-CT-2012-00006) Deliverable D6.3. 2014.

[100] Linderholm C, Schmitz M. Chemical-looping combustion of solid fuels in a 100 kW dual circulating fluidized bed system using iron ore as oxygen carrier. J Environ Chem Eng. 2016;4:1029-39.

[101] Mendiara T, De Diego LF, García-Labiano F, Gayán P, Abad A, Adánez J. On the use of a highly reactive iron ore in Chemical Looping Combustion of different coals. Fuel. 2014;126:239-49.

[102] Mei D, Mendiara T, Abad A, De Diego LF, García-Labiano F, Gayán P, et al. Evaluation of Manganese Minerals for Chemical Looping Combustion. Energy Fuels. 2015;29:6605-15.

[103] Mei D, Mendiara T, Abad A, De Diego LF, García-Labiano F, Gayán P, et al. Manganese Minerals as Oxygen Carriers for Chemical Looping Combustion of Coal. Ind Eng Chem Res. 2016;55:6539-46.

[104] Larring Y, Pishahang M, Sunding MF, Tsakalakis K. Fe-Mn based minerals with remarkable redox characteristics for chemical looping combustion. Fuel. 2015;159:169-78.

[105] Arjmand M, Leion H, Mattisson T, Lyngfelt A. Investigation of different manganese ores as oxygen carriers in chemical-looping combustion (CLC) for solid fuels. Appl Energ. 2014;113:1883-94.

[106] Xiao R, Song Q. Characterization and kinetics of reduction of $CaSO_4$ with carbon monoxide for chemical-looping combustion. Combust Flame. 2011;158:2524-39.

[107] Zheng M, Shen L, Feng X, Xiao J. Kinetic model for parallel reactions of $CaSO_4$ with CO in chemical-looping combustion. Ind Eng Chem Res. 2011;50:5414-27.

[108] Tian H, Guo Q, Chang J. Investigation into decomposition behavior of $CaSO_4$ in chemical-looping combustion. Energy Fuels. 2008;22:3915-21.

[109] Tian H, Guo Q. Investigation into the behavior of reductive decomposition of calcium sulfate by carbon monoxide in chemical-looping combustion. Ind Eng Chem Res. 2009;48:5624-32.

[110] Liu Y, Guo Q, Cheng Y, Ryu HJ. Reaction mechanism of coal chemical looping process for syngas production with $CaSO_4$ oxygen carrier in the CO_2 atmosphere. Ind Eng Chem Res. 2012;51:10364-73.

[111] Abad A, de Las Obras-Loscertales M, García-Labiano F, de Diego LF, Gayán P, Adánez J. *In situ* gasification Chemical-Looping Combustion of coal using limestone as oxygen carrier precursor and sulphur sorbent. Chem Eng J. 2017;310:226-39.

[112] Adánez-Rubio I, Gayán P, Abad A, García-Labiano F, de Diego LF, Adánez J. Kinetic analysis of a Cu-based oxygen carrier: Relevance of temperature and oxygen partial pressure on reduction and oxidation reactions rates in Chemical Looping with Oxygen Uncoupling (CLOU). Chem Eng J. 2014;256:69-84.

[113] Cabello A, Abad A, Gayán P, de Diego LF, García-Labiano F, Adánez J. Effect of operating conditions and H_2S presence on the performance of $CaMg_{0.1}Mn_{0.9}O_{3-\delta}$ perovskite material in chemical looping combustion (CLC). Energy Fuels. 2014;28:1262-74.

[114] Cuadrat A, Linderholm C, Abad A, Lyngfelt A, Adánez J. Influence of limestone addition in a 10 kW_{th} chemical-looping combustion unit operated with petcoke. Energy Fuels. 2011;25:4818-28.

[115] Linderholm C, Lyngfelt A, Cuadrat A, Jerndal E. Chemical-looping combustion of solid fuels - Operation in a 10 kW unit with two fuels, above-bed and in-bed fuel feed and two oxygen carriers, manganese ore and ilmenite. Fuel. 2012;102:808-22.

[116] Linderholm C, Lyngfelt A, Dueso C. Chemical-looping combustion of solid fuels in a 10 kW reactor system using natural minerals as oxygen carrier. Energy Procedia. 2013;37:598-607.

[117] Schmitz M, Linderholm C, Lyngfelt A. Chemical Looping combustion of sulphurous solid fuels using spray-dried calcium manganate particles as oxygen carrier. Energy Procedia. 2014;63:140-52.

[118] Berguerand N, Lyngfelt A. Chemical-looping combustion of petroleum coke using ilmenite in a 10 kW_{th} unit-high-temperature operation. Energy Fuels. 2009;23:5257-68.

[119] Berguerand N, Lyngfelt A. Operation in a 10 kW_{th} chemical-looping combustor for solid fuel-Testing with a Mexican petroleum coke. Energy Procedia. 2009;1:407-14.

[120] Abad A, Adánez J, de Diego LF, Gayán P, García-Labiano F, Lyngfelt A. Fuel reactor model validation: Assessment of the key parameters affecting the chemical-looping combustion of coal. Int J Greenh Gas Con. 2013;19:541-51.

[121] Linderholm C, Schmitz M, Knutsson P, Källén M, Lyngfelt A. Use of low-volatile solid fuels in a 100 kW chemical-looping combustor. Energy Fuels. 2014;28:5942-52.

[122] Linderholm C, Schmitz M, Knutsson P, Lyngfelt A. Chemical-looping combustion in a 100-kW unit using a mixture of ilmenite and manganese ore as oxygen carrier. Fuel. 2016;166:533-42.

[123] Markström P, Linderholm C, Lyngfelt A. Chemical-looping combustion of solid fuels - Design and operation of a 100kW unit with bituminous coal. Int J Greenh Gas Con. 2013;15:150-62.

[124] Markström P, Linderholm C, Lyngfelt A. Operation of a 100kW chemical-looping combustor with Mexican petroleum coke and Cerrejón coal. Appl Energ. 2014;113:1830-5.

[125] Shen L, Wu J, Gao Z, Xiao J. Reactivity deterioration of NiO/Al_2O_3 oxygen carrier for chemical looping combustion of coal in a 10 kW_{th} reactor. Combust Flame. 2009;156:1377-85.

[126] Shen L, Wu J, Gao Z, Xiao J. Characterization of chemical looping combustion of coal in a 1 kW_{th} reactor with a nickel-based oxygen carrier. Combust Flame. 2010;157:934-42.

[127] Gu H, Shen L, Xiao J, Zhang S, Song T. Chemical looping combustion of biomass/coal with natural iron ore as oxygen carrier in a continuous reactor. Energy Fuels. 2011;25:446-55.

[128] Song T, Shen L, Zhang H, Gu H, Zhang S, Xiao J. Chemical looping combustion of two bituminous coal/char with natural hematite as oxygen carrier in 1 kW_{th} reactor. 2nd International Conference on Chemical Looping. Darmstadt (Germany). 2012.

[129] Song T, Shen T, Shen L, Xiao J, Gu H, Zhang S. Evaluation of hematite oxygen carrier in chemical-looping combustion of coal. Fuel. 2013;104:244-52.

[130] Gu H, Shen L, Zhong Z, Niu X, Ge H, Zhou Y, et al. Potassium-modified iron ore as oxygen carrier for coal chemical looping combustion: Continuous test in 1 kW reactor. Ind Eng Chem Res. 2014;53:13006-15.

[131] Niu X, Shen L, Gu H, Song T. Performance of chemical looping combustion of sewage sludge and phosphorus migration based on hematite oxygen carrier in a 1 kW_{th} reactor. 3rd International Conference on Chemical Looping. Göteborg (Sweden). 2014.

[132] Niu X, Shen L, Gu H, Jiang S, Xiao J. Characteristics of hematite and fly ash during chemical looping combustion of sewage sludge. Chem Eng J. 2015;268:236-44.

[133] Ge H, Shen L, Gu H, Song T, Jiang S. Combustion performance and sodium transformation of high-sodium ZhunDong coal during chemical looping combustion with hematite as oxygen carrier. Fuel. 2015;159:107-17.

[134] Jiang S, Shen L, Niu X, Ge H, Gu H. Chemical Looping Co-combustion of Sewage Sludge and Zhundong Coal with Natural Hematite as the Oxygen Carrier. Energy Fuels. 2016;30:1720-9.

[135] Xiao R, Chen L, Saha C, Zhang S, Bhattacharya S. Pressurized chemical-looping combustion of coal using an iron ore as oxygen carrier in a pilot-scale unit. Int J Greenh Gas Con. 2012;10:363-73.

[136] Cuadrat A, Abad A, García-Labiano F, Gayán P, de Diego LF, Adánez J. The use of ilmenite as oxygen-carrier in a 500 W_{th} chemical-looping coal combustion unit. Int J Greenh Gas Con. 2011;5:1630-42.

[137] Cuadrat A, Abad A, García-Labiano F, Gayán P, de Diego LF, Adánez J. Relevance of the coal rank on the performance of the *in situ* gasification chemical-looping combustion. Chem Eng J. 2012;195-196:91-102.

[138] Cuadrat A, Abad A, García-Labiano F, Gayán P, de Diego LF, Adánez J. Effect of operating conditions in Chemical-Looping Combustion of coal in a 500 W_{th} unit. Int J Greenh Gas Con. 2012;6:153-63.

[139] Mendiara T, Abad A, de Diego LF, García-Labiano F, Gayán P, Adánez J. Biomass combustion in a CLC system using an iron ore as an oxygen carrier. Int J Greenh Gas Con. 2013;19:322-30.

[140] Mendiara T, de Diego LF, García-Labiano F, Gayán P, Abad A, Adánez J. Behaviour of a bauxite waste material as oxygen carrier in a 500 W_{th} CLC unit with coal. Int J Greenh Gas Con. 2013;17:170-82.

[141] Mendiara T, Izquierdo MT, Pérez-Astray A, Abad A, de Diego LF, García-Labiano F, et al. Biomass with CO_2 capture using CLC: results in a 500 W_{th} unit. 4^{th} International Conference on Chemical Looping. Nanjing (China). 2016.

[142] Abad A, Adánez-Rubio I, Gayán P, García-Labiano F, de Diego LF, Adánez J. Demonstration of chemical-looping with oxygen uncoupling (CLOU) process in a 1.5 kW_{th} continuously operating unit using a Cu-based oxygen-carrier. Int J Greenh Gas Con. 2012;6:189-200.

[143] Adánez-Rubio I, Abad A, Gayán P, De Diego LF, García-Labiano F, Adánez J. Biomass combustion with CO_2 capture by chemical looping with oxygen uncoupling (CLOU). Fuel Process Technol. 2014;124:104-14.

[144] Abad A, Pérez-Vega R, de Diego LF, García-Labiano F, Gayán P, Adánez J. Design and operation of a 50 kW_{th} Chemical Looping Combustion (CLC) unit for solid fuels. Appl Energ. 2015;157:295-303.

[145] Pérez-Vega R, Abad A, García-Labiano F, Gayán P, de Diego LF, Adánez J. Coal combustion in a 50 kW_{th} Chemical Looping Combustion unit: Seeking operating conditions to maximize CO_2 capture and combustion efficiency. Int J Greenh Gas Con. 2016;50:80-92.

[146] Abad A, Bueno JA, Pérez-Vega R, García-Labiano F, Gayán P, de Diego LF, et al. Implementation of design improvements into a 50 kW_{th} CLC pilot plant wiht coal. 4^{th} International Conference on Chemical Looping. Nanjing (China). 2016.

[147] Sozinho T, Pelletant W, Stainton H, Guillou F, Gauthier T. Main results of the 10 kW_{th} pilot plant operation. 2^{nd} International Conference on Chemical Looping. Darmstadt (Germany). 2012.

[148] Thon A, Kramp M, Hartge EU, Heinrich S, Werther J. Operational experience with a system of coupled fluidized beds for chemical looping combustion of solid fuels using ilmenite as oxygen carrier. Appl Energ. 2014;118:309-17.

[149] Haus J, Lyu K, Hartge EU, Heinrich S, Werther J. Analysis of a two-stage fuel reactor system for the chemical-looping combustion of lignite and bituminous coal. Energy Technol. 2016;4:1263-73.

[150] Cao Y, Sit SP, Pan WP. The development of 10-kW Chemical Looping Combustion Technology in ICSET, WKU. 2nd International Conference on Chemical Looping. Darmstadt (Germany). 2012.

[151] Tong A, Bayham S, Kathe MV, Zeng L, Luo S, Fan LS. Iron-based syngas chemical looping process and coal-direct chemical looping process development at Ohio State University. Appl Energ. 2014;113:1836-45.

[152] Bayham SC, Kim HR, Wang D, Tong A, Zeng L, McGiveron O, et al. Iron-based coal direct chemical looping combustion process: 200-h continuous operation of a 25-kW_{th} subpilot unit. Energy Fuels. 2013;27:1347-56.

[153] Bayham S, McGiveron O, Tong A, Chung E, Kathe M, Wang D, et al. Parametric and dynamic studies of an iron-based 25-kWth coal direct chemical looping unit using sub-bituminous coal. Appl Energ. 2015;145:354-63.

[154] Huseyin S, Wei GQ, Li HB, He F, Huang Z. Chemical-looping gasification of biomass in a 10 kW_{th} interconnected fluidized bed reactor using Fe_2O_3/Al_2O_3 oxygen carrier. Ranliao Huaxue Xuebao/Journal of Fuel Chemistry and Technology. 2014;42:922-31.

[155] Wei G, He F, Huang Z, Zheng A, Zhao K, Li H. Continuous operation of a 10 kW_{th} chemical looping integrated fluidized bed reactor for gasifying biomass using an iron-based oxygen carrier. Energy Fuels. 2015;29:233-41.

[156] Ma J, Zhao H, Tian X, Wei Y, Rajendran S, Zhang Y, et al. Chemical looping combustion of coal in a 5 kW_{th} interconnected fluidized bed reactor using hematite as oxygen carrier. Appl Energ. 2015;157:304-13.

[157] Ma J, Zhao H, Niu P, Chen X, Tian X, Zheng C. Design and Operation of a 50 kW_{th} Chemical Looping Combustion (CLC) Reactor Using Coal as Fuel. 4^{th} International Conference on Chemical Looping. Nanjing (China). 2016.

[158] Pikkarainen T, Hiltunen I, Teir S. Piloting of bio-CLC for BECCS. 4^{th} International Conference on Chemical Looping. Nanjing (China).2016.

[159] Ströhle J, Orth M, Epple B. Chemical looping combustion of hard coal in a 1 MW_{th} pilot plant using ilmenite as oxygen carrier. Appl Energ. 2015;157:288-94.

[160] Ohlemuller P, Busch JP, Reitz M, Strohle J, Epple B. Chemical-Looping Combustion of Hard Coal: Autothermal Operation of a 1 MW_{th} Pilot Plant. J Energy Res Technol, Transactions of the ASME. 2016;138:Article number 042203.

[161] Ströhle J, Ohlemüller P, Epple B. Chemical looping combustion of coal and biomass in a 1 MW_{th} pilot plant using ilmenite and iron ore as oxygen carrier. 6^{th} High Temperature Solid Looping Network Meeting. Milano (Italy). 2015.

[162] Abdulally I, Edberg C, Andrus HE, Chiu J, Thibeault P, Lani B. ALSTOM´s Chemical Looping Combustion Prototype for CO_2 Capture from Existing Pulverized

3224 Coal Fired Power Plants. NETL CO_2 Capture Technology Meeting. Pittsburgh
3225 (Pennsylvania, USA). 2011.

3226 [163] Abdulally I, Andrus HE, Edberg C, Chiu J, Thibeault P, Lani B. ALSTOM´s
3227 Chemical Looping Combustion Prototype for CO_2 Capture from Existing Pulverized
3228 Coal Fired Power Plants. NETL CO_2 Capture Technology Meeting. Pittsburgh
3229 (Pennsylvania, USA). 2012.

3230 [164] Chiu J, Andrus HE. Alstom's Chemical Looping Technology Program Update.
3231 NETL CO_2 Capture Technology Meeting. Pittsburgh (Pennsylvania, USA). 2014.

3232 [165] Berdugo Vilches T, Thunman H. Experimental Investigation of Volatiles-Bed
3233 Contact in a 2-4 MW_{th} Bubbling Bed Reactor of a Dual Fluidized Bed Gasifier. Energy
3234 Fuels. 2015;29:6456-64.

3235 [166] Berdugo Vilches T, Lind F, Rydén M, Thunman H. Experience of more than
3236 1000 h of operation with oxygen carriers and solid biomass at large scale. Appl Energ.
3237 2017;190:1174-83.

3238 [167] Lin S-Y, Saito T. Development of Three-Tower (reactors) Technology for
3239 Chemical Looping Coal Combustion. 4^{th} International Conference on Chemical
3240 Looping. Nanjing (China). 2016.

3241 [168] Lighty J, Whitty K, Smith P, Eyring T. Chemical Looping with Oxygen
3242 Uncoupling with Coal. NETL CO_2 Capture Technology Meeting 2012.

3243 [169] Lighty J, Whitty K, Sahir A, Clayton C. Chemical Looping Combustion Research
3244 at the University of Utah. 5^{th} High Temperature Solid Looping Network Meeting.
3245 Cambridge (UK). 2013.

[170] Velázquez-Vargas LG. Atmospheric Iron-Based Coal Direct Chemical Looping Process for Power Production. NETL CO2 Capture Technology Meeting. Pittsburgh (USA). 2015.

[171] De Diego LF, Abad A, Cabello A, Gayán P, García-Labiano F, Adánez J. Reduction and oxidation kinetics of a $CaMn_{0.9}Mg_{0.1}O_{3-\delta}$ oxygen carrier for chemical-looping combustion. Ind Eng Chem Res. 2014;53:87-103.

[172] Abad A, Gayán P, de Diego LF, García-Labiano F, Adánez J, Mayer K, et al. Modelling a CLC process improved by CLOU and validation in a 120 kW unit. CFB-11: Proceedings of the 11th International Conference on Fluidized Bed Technology 2014. p. 861-7.

[173] Berguerand N, Lyngfelt A, Mattisson T, Markström P. Chemical looping combustion of solid fuels in a 10 kW_{th} unit. Oil Gas Sci Technol. 2011;66:181-91.

[174] Linderholm C, Schmitz M, Källén M, Lyngfelt A. Use of iron ore as oxygen carrier in a 100 kW chemical-looping combustor for solid fuels. 22nd International Conference on Fluidized Bed Conversion. Turku, (Finland). 2015.

[175] García-Labiano F, de Diego LF, Gayán P, Adánez J, Abad A, Dueso C. Effect of fuel gas composition in chemical-looping combustion with ni-based oxygen carriers. 1. fate of sulfur. Ind Eng Chem Res. 2009;48:2499-508.

[176] Dueso C, Izquierdo MT, García-Labiano F, de Diego LF, Abad A, Gayán P, et al. Effect of H_2S on the behaviour of an impregnated NiO-based oxygen-carrier for chemical-looping combustion (CLC). Appl Catal B: Environ. 2012;126:186-99.

[177] Cuadrat A, Abad A, de Diego LF, García-Labiano F, Gayán P, Adánez J. Prompt considerations on the design of Chemical-Looping Combustion of coal from experimental tests. Fuel. 2012;97:219-32.

[178] Abad A, Cuadrat A, Mendiara T, García-Labiano F, Gayán P, de Diego LF, et al. Low-cost Fe-based oxygen carrier materials for the *i*G-CLC process with coal. 2. Ind Eng Chem Res. 2012;51:16230-41.

[179] Hartge EU, Haus J, Heinrich S, Werther J. Instabilities in the solids cycle of a CLC pilot plant - A CFD (MP-PIC) simulation study. 22nd Int Conf Fluidized Bed Conversion. Turku (Finland). 2015.

[180] Cao Y, Sit SP, Pan WP. Biomass-Fueled Chemical Looping Combustion. 3rd International Conference on Chemical Looping. Göteborg (Sweden). 2014.

[181] Jerndal E, Mattisson T, Lyngfelt A. Thermal analysis of chemical-looping combustion. Chem Eng Res Des. 2006;84:795-806.

[182] Schwebel GL, Gipperich A, Krumm W. Design considerations of Chemical-Looping systems incorporating a moving bed fuel reactor (MBFR). 2nd International Conference on Chemical Looping. Darmstadt (Germany). 2012.

[183] Wei G, He F, Zhao Z, Huang Z, Zheng A, Zhao K, et al. Performance of Fe-Ni bimetallic oxygen carriers for chemical looping gasification of biomass in a 10 kW_{th} interconnected circulating fluidized bed reactor. Int J Hydrogen Energy. 2015;40:16021-32.

[184] Abad A. Chemical looping for hydrogen production. In: Anthony PFaB, editor. Calcium and Chemical Looping Technology for Power Generation and Carbon Dioxide (CO_2) Capture. Cambridge (UK): Woodhead Publishing; 2015. p. 327-74.

[185] Charitos A, Hawthorne C, Bidwe AR, Sivalingam S, Schuster A, Spliethoff H, et al. Parametric investigation of the calcium looping process for CO_2 capture in a 10 kW_{th} dual fluidized bed. Int J Greenh Gas Con. 2010;4:776-84.

[186] Bidwe AR, Mayer F, Hawthorne C, Charitos A, Schuster A, Scheffknecht G. Use of ilmenite as an oxygen carrier in chemical looping combustion-batch and continuous dual fluidized bed investigation. Energy Procedia. 2011;4:433-40.

[187] Mayer F, Bidwe AR, Schopf A, Taheri K, Zieba M, Scheffknecht G. Comparison of a new micaceous iron oxide and ilmenite with respect to syngas conversion in a BFB reactor and adaptation of a 10 kW_{th} DFB system for CLC to solid fuels. 2nd International Conference on Chemical Looping. Darmstadt (Germany). 2012.

[188] Proell T, Hofbauer H. A dual fluidized bed system for chemical looping combustion of solid fuels. 10AIChE - 2010 AIChE Annual Meeting, Conference Proceedings. Salt Lake City, Utah, (USA). 2010.

[189] Shen L. Reactor for Chemical-Looping Combustion of Solid Fuels - Development and Discussion. 4th International Conference on Chemical Looping. Nanjing (China). 2016.

[190] Lighty J, Smith P, Whitty K, Eyring T, Sarofim A. Chemical Looping with Oxygen Uncoupling (CLOU). presented at US DOE NETL 2012 CO_2 Capture Technology Meeting, July 2012. Invited Talk/Keynote, Presented, 07/2012.

[191] Velázquez-Vargas LG, Devault DJ, Flynn TJ, Siengchum T, Zeng K, Tong A, et al. Techno-economic Analysis of a 550 MWe Atmospheric Iron-Based Coal-Direct Chemical Looping Process. 3rd International Conference on Chemical Looping. Göteborg (Sweden). 2014.

[192] Chiu JH, Andrus HE, Liljedahl GN, Thibeault PR. Patent Title: System for hot solids combustion and gasification. C10J 3/02 (2006.01) 2010. International Patent Number WO 2010/014938 A9.

[193] Beal C, Epple B, Lyngfelt A, Adanez J, Larring Y, Joumani Y, et al. Development of Metal Oxides Chemical Looping Process for Coal-Fired Power Plants. 2nd International Conference on Chemical Looping. Darmstadt (Germany). 2012.

[194] Ströhle J, Orth M, Epple B. Chemical Looping Combustion of Hard Coal in a 1 MW_{th} Pilot Plant Using Ilmenite as Oxygen Carrier. 3rd International Conference on Chemical Looping. Göteborg (Sweden), 2014.

[195] Basu P. Combustion of coal in circulating fluidized-bed boilers: A review. Chem Eng Sci. 1999;54:5547-57.

[196] Linderholm C, Knutsson P, Schmitz M, Markström P, Lyngfelt A. Material balances of carbon, sulfur, nitrogen and ilmenite in a 100 kW CLC reactor system. Int J Greenh Gas Con. 2014;27:188-202.

[197] Mendiara T, Gayán P, Abad A, de Diego LF, García-Labiano F, Adánez J. Performance of a bauxite waste as oxygen-carrier for chemical-looping combustion using coal as fuel. Fuel Process Technol. 2013;109:57-69.

[198] Mendiara T, Izquierdo MT, Abad A, Gayán P, García-Labiano F, De Diego LF, et al. Mercury release and speciation in chemical looping combustion of coal. Energy Fuels. 2014;28:2786-94.

[199] Pérez-Vega R, Adánez-Rubio I, Gayán P, Izquierdo MT, Abad A, García-Labiano F, et al. Sulphur, nitrogen and mercury emissions from coal combustion with CO_2 capture in chemical looping with oxygen uncoupling (CLOU). Int J Greenh Gas Con. 2016;46:28-38.

[200] Linderholm C, Cuadrat A, Lyngfelt A. Chemical-looping combustion of solid fuels in a 10 kW_{th} pilot- Batch tests with five fuels. Energy Procedia. 2011;4:385-92.

[201] Ge H, Shen L, Gu H, Song T, Jiang S. Combustion performance and sodium absorption of ZhunDong coal in a CLC process with hematite oxygen carrier. Appl Therm Eng. 2016;94:40-9.

[202] Song T, Shen L, Xiao J, Chen D, Gu H, Zhang S. Nitrogen transfer of fuel-N in chemical looping combustion. Combust Flame. 2012;159:1286-95.

[203] Bazhenova E, Honkala K. Screening the bulk properties and reducibility of Fe-doped Mn_2O_3 from first principles calculations. Catal Today. 2017. DOI:dx.doi.org/10.1016/j.cattod.2017.02.004.

[204] Qin W, Lin CF, Long DT, Wang JY, Dong CQ. Activity of Fe2O3 with a high index facet for bituminous coal chemical looping combustion: A theoretical and experimental study. RSC Advances. 2016;6:85551-8.

[205] Liu YC, Nachimuthu S, Chuang YC, Ku Y, Jiang JC. Reduction mechanism of iron titanium based oxygen carriers with H2 for chemical looping applications-a combined experimental and theoretical study. RSC Advances. 2016;6:106340-6.

[206] Liu F, Liu J, Dai J, Yang Y, Zhang Z, Wang M. Periodic density functional study of the interaction mechanism of CO with spinel-type $MnFe_2O_4$ surface in chemical-looping combustion. 4th International Conference on Chemical Looping. Nanjing (China). 2016.

[207] Cheng Z, Qin L, Guo M, Xu M, Fan JA, Fan LS. Oxygen vacancy promoted methane partial oxidation over iron oxide oxygen carriers in the chemical looping process. Phys Chem Chem Phys. 2016;18:32418-28.

[208] Strickland-Constable RF. Some comments on the work of key on the reactions between coke and carbon dioxide and between coke and steam. J Chim Phys. 1950;47:356-60.

[209] Abad A, Adánez J, García-Labiano F, de Diego LF, Gayán P, Celaya J. Mapping of the range of operational conditions for Cu-, Fe-, and Ni-based oxygen carriers in chemical-looping combustion. Chem Eng Sci. 2007;62:533-49.

[210] Leion H, Lyngfelt A, Johansson M, Jerndal E, Mattisson T. The use of ilmenite as an oxygen carrier in chemical-looping combustion. Chem Eng Res Des. 2008;86:1017-26.

[211] Abad A, Adánez J, Cuadrat A, García-Labiano F, Gayán P, de Diego LF. Kinetics of redox reactions of ilmenite for chemical-looping combustion. Chem Eng Sci. 2011;66:689-702.

[212] Mendiara T, Abad A, De Diego LF, García-Labiano F, Gayán P, Adánez J. Use of an Fe-based residue from alumina production as an oxygen carrier in chemical-looping combustion. Energy Fuels. 2012;26:1420-31.

[213] Abad A, García-Labiano F, de Diego LF, Gayán P, Adánez J. Reduction kinetics of Cu-, Ni-, and Fe-based oxygen carriers using syngas (CO + H_2) for chemical-looping combustion. Energy Fuels. 2007;21:1843-53.

[214] Zhang S, Xiao R. Performance of iron ore oxygen carrier modified by biomass ashes in coal-fueled chemical looping combustion. Greenhouse Gases Sci Technol. 2016;6(5):695-709.

[215] Wang J, Zhao H. Evaluation of CaO-decorated Fe_2O_3/Al_2O_3 as an oxygen carrier for in-situ gasification chemical looping combustion of plastic wastes. Fuel. 2016;165:235-43.

[216] Yu Z, Li C, Jing X, Zhang Q, Wang Z, Fang Y, et al. Catalytic chemical looping combustion of carbon with an iron-based oxygen carrier modified by K_2CO_3: Catalytic mechanism and multicycle tests. Fuel Process Technol. 2015;135:119-24.

[217] Gu H, Shen L, Zhong Z, Niu X, Liu W, Ge H, et al. Cement/CaO-modified iron ore as oxygen carrier for chemical looping combustion of coal. Appl Energ. 2015;157:314-22.

[218] Ge H, Shen L, Gu H, Jiang S. Effect of co-precipitation and impregnation on K-decorated Fe_2O_3/Al_2O_3 oxygen carrier in Chemical Looping Combustion of bituminous coal. Chem Eng J. 2015;262:1065-76.

[219] Siriwardane R, Tian H, Miller D, Richards G. Fluidized bed testing of commercially prepared MgO-promoted hematite and CuO-Fe_2O_3 mixed metal oxide oxygen carriers for methane and coal chemical looping combustion. Appl Energ. 2015;157:348-57.

[220] Chen L, Liu F, S NH, Fan Z, Liu K. Coal char-fueled chemical looping combustion use different iron based oxygen carriers. Energy Procedia. 2014;63:73-9.

[221] Yu Z, Li C, Jing X, Zhang Q, Fang Y, Zhao J, et al. Effects of CO_2 atmosphere and K_2CO_3 addition on the reduction reactivity, oxygen transport capacity, and sintering of CuO and Fe_2O_3 oxygen carriers in coal direct chemical looping combustion. Energy Fuels. 2013;27:2703-11.

[222] Gu H, Shen L, Xiao J, Zhang S, Song T, Chen D. Iron ore as oxygen carrier improved with potassium for chemical looping combustion of anthracite coal. Combust Flame. 2012;159:2480-90.

[223] Arjmand M, Leion H, Lyngfelt A, Mattisson T. Use of manganese ore in chemical-looping combustion (CLC)-Effect on steam gasification. Int J Greenh Gas Con. 2012;8:56-60.

[224] Keller M, Leion H, Mattisson T. Mechanisms of Solid Fuel Conversion by Chemical-Looping Combustion (CLC) using Manganese Ore: Catalytic Gasification by Potassium Compounds. Energy Technol. 2013;1:273-82.

[225] Frohn P, Arjmand M, Azimi G, Leion H, Mattisson T, Lyngfelt A. On the high-gasification rate of Brazilian manganese ore in chemical-looping combustion (CLC) for solid fuels. AlChE J. 2013;59:4346-54.

[226] Linderholm C, Lyngfelt A. Use of Manganese Ores as Oxygen Carriers in Chemical-Looping Combustors for Solid Fuels. 4th International Conference on Chemical Looping. Nanjing (China). 2016.

[227] Shen L, Zheng M, Xiao J, Xiao R. A mechanistic investigation of a calcium-based oxygen carrier for chemical looping combustion. Combust Flame. 2008;154:489-506.

[228] Wang J, Anthony EJ. Clean combustion of solid fuels. Appl Energ. 2008;85:73-9.

[229] Song Q, Xiao R, Deng Z, Shen L, Xiao J, Zhang M. Effect of temperature on reduction of $CaSO_4$ oxygen carrier in chemical-looping combustion of simulated coal gas in a fluidized bed reactor. Ind Eng Chem Res. 2008;47:8148-59.

[230] Song Q, Xiao R, Deng Z, Zheng W, Shen L, Xiao J. Multicycle study on chemical-looping combustion of simulated coal gas with a $CaSO_4$ oxygen carrier in a fluidized bed reactor. Energy Fuels. 2008;22:3661-72.

[231] Tian H, Guo Q, Yue X, Liu Y. Investigation into sulfur release in reductive decomposition of calcium sulfate oxygen carrier by hydrogen and carbon monoxide. Fuel Process Technol. 2010;91:1640-9.

[232] Tian H, Hu X, Chang J, Han M, Sun G, Guo Q. Simulation of a new chemical-looping combustion process without sulfur evolution based on ca-based oxygen carrier. Int J Chem Reactor Eng. 2014;12.

[233] Song T, Zheng M, Shen L, Zhang T, Niu X, Xiao J. Mechanism investigation of enhancing reaction performance with $CaSO_4/Fe_2O_3$ oxygen carrier in chemical-looping combustion of coal. Ind Eng Chem Res. 2013;52:4059-71.

[234] Zhang S, Xiao R, Liu J, Bhattacharya S. Performance of $Fe_2O_3/CaSO_4$ composite oxygen carrier on inhibition of sulfur release in calcium-based chemical looping combustion. Int J Greenh Gas Con. 2013;17:1-12.

[235] Zheng M, Shen L, Feng X. *In situ* gasification chemical looping combustion of a coal using the binary oxygen carrier natural anhydrite ore and natural iron ore. Energy Convers Manage. 2014;83:270-83.

[236] Zheng M, Shen L. In Situ Gasification Chemical Looping Combustion of Coal Using the Mixed Oxygen Carrier of Natural Anhydrite Ore and Calcined Limestone. Int J Chem Reactor Eng. 2016;14:637-52.

[237] Ding N, Zhang C, Luo C, Zheng Y, Liu Z. Effect of hematite addition to $CaSO_4$ oxygen carrier in chemical looping combustion of coal char. RSC Advances. 2015;5:56362-76.

[238] Zhang S, Xiao R, Yang Y, Chen L. CO_2 Capture and Desulfurization in Chemical Looping Combustion of Coal with a $CaSO_4$ Oxygen Carrier. Chem Eng Technol. 2013;36:1469-78.

[239] Schmitz M, Linderholm C, Lyngfelt A. Chemical Looping Combustion of four different solid fuels using a manganese-silicon-titanium oxygen carrier. 4th International Conference on Chemical Looping. Nanjing (China). 2016.

[240] Abián M, Abad A, Izquierdo MT, Gayán P, de Diego LF, García-Labiano F, et al. Titanium Substituted Manganese-Ferrite as an Oxygen Carrier with Permanent Magnetic Properties for Chemical Looping Combustion of Solid Fuels. Fuel. 2017;195:38-48.

[241] Luo S, Bayham S, Zeng L, McGiveron O, Chung E, Majumder A, et al. Conversion of metallurgical coke and coal using a Coal Direct Chemical Looping (CDCL) moving bed reactor. Appl Energ. 2014;118:300-8.

[242] Adánez J, Gayán P, Celaya J, De Diego LF, García-Labiano F, Abad A. Chemical looping combustion in a 10 kW_{th} prototype using a CuO/Al_2O_3 oxygen carrier: Effect of operating conditions on methane combustion. Ind Eng Chem Res. 2006;45:6075-80.

[243] Adánez J, Dueso C, Diego LFD, García-Labiano F, Gayán P, Abad A. Methane combustion in a 500 W_{th} chemical-looping combustion system using an impregnated ni-based oxygen carrier. Energy Fuels. 2009;23:130-42.

[244] Abad A, Adánez J, Gayán P, de Diego LF, García-Labiano F, Sprachmann G. Conceptual design of a 100 MW_{th} CLC unit for solid fuel combustion. Appl Energ. 2015;157:462-74.

[245] Cuadrat A, Abad A, Gayán P, De Diego LF, García-Labiano F, Adánez J. Theoretical approach on the CLC performance with solid fuels: Optimizing the solids inventory. Fuel. 2012;97:536-51.

[246] Xiao R, Song Q, Zhang S, Zheng W, Yang Y. Pressurized chemical-looping combustion of chinese bituminous coal: Cyclic performance and characterization of iron ore-based oxygen carrier. Energy Fuels. 2010;24:1449-63.

[247] Xiao R, Song Q, Song M, Lu Z, Zhang S, Shen L. Pressurized chemical-looping combustion of coal with an iron ore-based oxygen carrier. Combust Flame. 2010;157:1140-53.

[248] Markström P, Lyngfelt A. Designing and operating a cold-flow model of a 100kW chemical-looping combustor. Powder Technol. 2012;222:182-92.

[249] Cheng M, Sun H, Li Z, Cai N. Annular Carbon Stripper for Chemical-looping Combustion of coal. Ind Eng Chem Res. 2017;56:1580-93.

[250] Lyngfelt A, Mattisson T, Linderholm C, Rydén M. Chemical-Looping Combustion of Solid Fuels – What is Needed to Reach Full-Scale? 4th International Conference on Chemical Looping. Nanjing (China). 2016.

[251] Abad A, Mendiara T, Gayan P, Garcia-Labiano F, De Diego LF, Bueno JA, et al. Comparative Evaluation of the Performance of Coal Combustion in 0.5 and 50 kW_{th} Chemical Looping Combustion units with ilmenite, redmud or iron ore as oxygen carrier. Energy Procedia. 2017. (in press)

[252] Adánez-Rubio I, Abad A, Gayán P, García-Labiano F, De Diego LF, Adánez J. The fate of sulphur in the Cu-based Chemical Looping with Oxygen Uncoupling (CLOU) Process. Appl Energ. 2014;113:1855-62.

[253] Källén M, Rydén M, Dueso C, Mattisson T, Lyngfelt A. $CaMn_{0.9}Mg_{0.1}O_{3-\delta}$ as oxygen carrier in a gas-fired 10 kW_{th} chemical-looping combustion unit. Ind Eng Chem Res. 2013;52:6923-32.

[254] Adánez-Rubio I, Abad A, Gayán P, De Diego LF, García-Labiano F, Adánez J. Identification of operational regions in the Chemical-Looping with Oxygen Uncoupling (CLOU) process with a Cu-based oxygen carrier. Fuel. 2012;102:634-45.

[255] Hamilton MA, Whitty KJ, Lighty JAS. Numerical simulation comparison of two reactor configurations for chemical looping combustion and chemical looping with

oxygen uncoupling. J Energy Res Technol, Transactions of the ASME. 2016;138:Article number 042213.

[256] Fuss S, Canadell JG, Peters GP, Tavoni M, Andrew RM, Ciais P, et al. Betting on negative emissions. Nature Climate Change. 2014;4:850-3.

[257] Kemper J. Biomass and carbon dioxide capture and storage: A review. Int J Greenh Gas Con. 2015;40:401-30.

[258] Tokimatsu K, Yasuoka R, Nishio M. Global zero emissions scenarios: The role of biomass energy with carbon capture and storage by forested land use. Appl Energ. 2017;185:1899-906.

[259] Sanchez DL, Callaway DS. Optimal scale of carbon-negative energy facilities. Appl Energ. 2016;170:437-44.

[260] Creutzig F, Ravindranath NH, Berndes G, Bolwig S, Bright R, Cherubini F, et al. Bioenergy and climate change mitigation: An assessment. GCB Bioenergy. 2015;7:916-44.

[261] Salimben A, Beal C. Biomass chemical looping combustion: Advanced combustion technology for low cost CO_2 storage and NO_x free bioenergy generation. 23rd European Biomass Conference and Exhibition 2015. p. 1802-8.

[262] Luo S, Majumder A, Chung E, Xu D, Bayham S, Sun Z, et al. Conversion of woody biomass materials by chemical looping process - Kinetics, light tar cracking, and moving bed reactor behavior. Ind Eng Chem Res. 2013;52:14116-24.

[263] Rydén M, Hanning M, Corcoran A, Lind F. Oxygen Carrier Aided Combustion (OCAC) of Wood Chips in a Semi-Commercial Circulating Fluidized Bed Boiler Using Manganese Ore as Bed Material. Applied Science 2016;6:347.

[264] Thunman H, Lind F, Breitholtz C, Berguerand N, Seemann M. Using an oxygen-carrier as bed material for combustion of biomass in a 12-MW_{th} circulating fluidized-bed boiler. Fuel. 2013;113:300-9.

[265] Zhao D, Schwebel G, Pour NM, Leion H, Lind F, Thunman H. Laboratory fluidized bed testing of ilmenite as bed material for oxygen carrier aided combustion (OCAC). CFB-11: Proceedings of the 11th International Conference on Fluidized Bed Technology 2014. p. 721-6.

[266] Källén M, Rydén M, Lind F. Improved Performance in Fluidised Bed Combustion by the Use of Manganese Ore as Active Bed Material. 22nd Int Conf Fluidized Bed Conversion. Turku (Finland). 2015.

[267] Anderson BÅ, Lind F, Corcoran A, Thunman H. 4000 Hours of Operation with Oxygen-Carriers in Industrial Relevant Scale (75 MW_{th}). 4th International Conference on Chemical Looping. Nanjing (China). 2016.

[268] Corcoran A, Marinkovic J, Lind F, Thunman H, Knutsson P, Seemann M. Ash properties of ilmenite used as bed material for combustion of biomass in a circulating fluidized bed boiler. Energy Fuels. 2014;28:7672-9.

[269] Song T, Hartge EU, Heinrich S, Shen L, Werther J. Chemical looping combustion of high sodium lignite in the fluidized bed: combustion performance and sodium transfer. 4th International Conference on Chemical Looping. Nanjing (China). 2016.

[270] de Visser E, Hendriks C, Barrio M, Mølnvik MJ, de Koeijer G, Liljemark S, et al. Dynamis CO_2 quality recommendations. Int J Greenh Gas Con. 2008;2:478-84.

[271] Mendiara T, Gayán P, Abad A, García-Labiano F, de Diego LF, Adánez J. Characterization for disposal of Fe-based oxygen carriers from a CLC unit burning coal. Fuel Process Technol. 2015;138:750-7.

[272] Mendiara T, Izquierdo MT, Abad A, de Diego LF, García-Labiano F, Gayán P, et al. Release of pollutant components in CLC of lignite. Int J Greenh Gas Con. 2014;22:15-24.

[273] Gu H, Shen L, Zhong Z, Niu X, Ge H, Zhou Y, et al. NO release during chemical looping combustion with iron ore as an oxygen carrier. Chem Eng J. 2015;264:211-20.

[274] Cabello A, Dueso C, García-Labiano F, Gayán P, Abad A, De Diego LF, et al. Performance of a highly reactive impregnated Fe_2O_3/Al_2O_3 oxygen carrier with CH_4 and H_2S in a 500 W_{th} CLC unit. Fuel. 2014;121:117-25.

[275] de Diego LF, García-Labiano F, Gayán P, Abad A, Cabello A, Adánez J, et al. Performance of Cu- and Fe-based oxygen carriers in a 500 W_{th} CLC unit for sour gas combustion with high H_2S content. Int J Greenh Gas Con. 2014;28:168-79.

[276] García-Labiano F, de Diego LF, Gayán P, Abad A, Cabello A, Adánez J, et al. Energy exploitation of acid gas with high H_2S content by means of a chemical looping combustion system. Appl Energ. 2014;136:242-9.

[277] Forero CR, Gayán P, García-Labiano F, de Diego LF, Abad A, Adánez J. Effect of gas composition in Chemical-Looping Combustion with copper-based oxygen carriers: Fate of sulphur. Int J Greenh Gas Con. 2010;4:762-70.

[278] Ishida M, Jin H. A novel chemical-looping combustor without NO_x formation. Ind Eng Chem Res. 1996;35:2469-72.

[279] Simell P, Ståhlberg P, Kurkela E, Albrecht J, Deutsch S, Sjöström K. Provisional protocol for the sampling and anlaysis of tar and particulates in the gas from large-scale biomass gasifiers. Version 1998. Biomass Bioenergy. 2000;18:19-38.

[280] Brage C, Yu Q, Chen G, Sjöström K. Use of amino phase adsorbent for biomass tar sampling and separation. Fuel. 1997;76:137-42.

[281] Mendiara T, Pérez-Astray A, Izquierdo MT, Abad A, De Diego LF, García-Labiano F, et al. Chemical Looping Combustion of different types of biomass in a 0.5 kW_{th} unit. Fuel. 2017 (submitted)

[282] Reed TB, Levie B, Graboski MS. Tar conversion. Fundamentals, Development and Scaleup of the Air-Oxygen Stratified Downdraft Gasifier: Solar EnergyResearch Institute, SERI/PR-234-2571; 1987.

[283] DIRECTIVE 2010/75/EU of the European Parliament and of the Council on industrial emissions (integrated pollution prevention and control). 2010.

[284] Weber JM, Stehle RC, Breault RW, De Wilde J. Experimental study of the application of rotating fluidized beds to particle separation. Powder Technol. 2016. (in press)

[285] Abad A, Gayán P, Mendiara T, de Diego LF, García-Labiano F, Adánez J. Operational results obtained with selected design solutions in continuous unit. ACCLAIM project (RFCP-CT-2012-00006) Deliverable D7.2. 2015.

[286] Schöny G, Pallarés D, Leion H, Wolf J. Assessment of the scale-up and operational design of the fuel reactor in chemical looping combustion. 36th Int Techn Conf Clean Coal & Fuel Systems. Clearwater (Florida, USA). 2011.

[287] Ohlemüller P, Busch JP, Ströhle J, Epple B. Autothermal operation of a 1 MW_{th} Chemical Looping plant. 22nd International Conference on Fluidized Bed Conversion. Turku, Finland 2015.

[288] Elliot MA. Chemistry of coal utilization. New York: John Wiley & Sons, Inc.; 1981.

[289] Guío-Pérez DC, Pröll T, Hofbauer H. Influence of ring-type internals on the solids residence time distribution in the fuel reactor of a dual circulating fluidized bed system for chemical looping combustion. Chem Eng Res Des. 2014;92:1107-18.

[290] Guío-Pérez DC, Pröll T, Penthor S, Hofbauer H. Optimization of the loop seal in the counter-current reactor of the dual circulating fluidized bed system for chemical looping processes. Ind Eng Chem Res. 2014;53:16374-83.

[291] Lyngfelt A, Pallarès D, Linderholm C, Rydén M, Mattisson T. Patent title: Distributor of volatile gases in the bottom part of a fluidized bed. 2014. Swedish Patent Application No. 1400085.5.

[292] Volker K, Alfons K. Chemical Looping Combustion: Comparative Analysis of two Different Overall Process Configurations for Removing Unburnt Gaseous Components. 2nd International Conference on Chemical Looping. Darmstadt (Germany). 2012.

[293] Adánez J. Chemical looping combustion of fossil fuels: recent developments. 8th Mediterranean Combustion Symposium. Çesme (Turkey). 2013.

[294] Saha C, Zhang S, Xiao R, Bhattacharya S. Chemical Looping Combustion (CLC) of two Victorian brown coals - Part 2: Assessment of interaction between CuO and minerals inherent in coals during multi cycle experiments. Fuel. 2012;96:335-47.

[295] Keller M, Arjmand M, Leion H, Mattisson T. Interaction of mineral matter of coal with oxygen carriers in chemical-looping combustion (CLC). Chem Eng Res Des. 2014;92:1753-70.

[296] Azis MM, Leion H, Jerndal E, Steenari BM, Mattisson T, Lyngfelt A. The Effect of Bituminous and Lignite Ash on the Performance of Ilmenite as Oxygen Carrier in Chemical-Looping Combustion. Chem Eng Technol. 2013;36:1460-8.

[297] Bao J, Li Z, Cai N. Interaction between iron-based oxygen carrier and four coal ashes during chemical looping combustion. Appl Energ. 2014;115:549-58.

[298] Gu H, Shen L, Zhong Z, Zhou Y, Liu W, Niu X, et al. Interaction between biomass ash and iron ore oxygen carrier during chemical looping combustion. Chem Eng J. 2015;277:70-8.

[299] Richter HJ, Knoche KF. Reversibility of combustion process. In: Gaggioli RA, editor. Efficiency and costing, second law analysis of process,ACS Symposium Series. Washington DC: American Chemical Society1983. p. 71-85.

[300] Ishida M, Zheng D, Akehata T. Evaluation of a chemical-looping-combustion power-generation system by graphic exergy analysis. Energy. 1987;12:147-54.

[301] Anheden M, Svedberg G. Exergy analysis of chemical-looping combustion systems. Energy Convers Manage. 1998;39:1967-80.

[302] McGlashan NR. Chemical-looping combustion - a thermodynamic study. Proceedings of the Institution of Mechanical Engineers, Part C: Journal of Mechanical Engineering Science. 2008;222:1005-19.

[303] Lyngfelt A, Leckner B, Mattisson T. A fluidized-bed combustion process with inherent CO2 separation; Application of chemical-looping combustion. Chem Eng Sci. 2001;56:3101-13.

[304] Sahir AH, Dansie JK, Cadore AL, Lighty JS. A comparative process study of chemical-looping combustion (CLC) and chemical-looping with oxygen uncoupling (CLOU) for solid fuels. Int J Greenh Gas Con. 2014;22:237-43.

[305] Shen L, Zheng M, Xiao J, Zhang H, Xiao R. Chemical looping combustion of coal in interconnected fluidized beds. Science in China, Series E: Technological Sciences. 2007;50:230-40.

[306] Peltola P, Tynjälä T, Ritvanen J, Hyppänen T. Mass, energy, and exergy balance analysis of chemical looping with oxygen uncoupling (CLOU) process. Energy Convers Manage. 2014;87:483-94.

[307] Eyring EM, Konya G, Lighty JS, Sahir AH, Sarofim AF, Whitty K. Chemical looping with copper oxide as carrier and coal as fuel. Oil and Gas Science and Technology. 2011;66:209-21.

[308] Levasseur A. Limestone-based Chemical Looping Development for Advanced Gasification. 2015. DOE Workshop: Gasification Systems and Coal&Biomass to Liquids: Morgantown. WV. USA.

[309] Ekström C, Schwendig F, Biede O, Franco F, Haupt G, de Koeijer G, et al. Techno-Economic Evaluations and Benchmarking of Pre-combustion CO_2 Capture and Oxy-fuel Processes Developed in the European ENCAP Project. Energy Procedia. 2009;1:4233-40.

[310] Fillman B, Anheden M, Wolf J. Parameter study in order to reveal critical design issues in the design for a CLC power plant using solid carbon as fuel. 1st International Conference on Chemical Looping. Lyon (France) 2010.

[311] Authier O, Le Moullec Y. Coal chemical-looping combustion for electricity generation: Investigation for a 250 MWe power plant. Energy Procedia 2013;37:588-97.

[312] Villani M, Spinelli M, Bischi A, Romano MC. Process integration of chemical looping combustion with oxygen uncoupling. 3rd International Conference on Chemical Looping. Göteborg (Sweden). 2014.

[313] Spinelli M, Peltola P, Bischi A, Ritvanen J, Hyppänen T, Romano MC. Process integration of chemical looping combustion with oxygen uncoupling in a coal-fired power plant. Energy. 2016;103:646-59.

[314] Cormos CC. Chemical Looping with Oxygen Uncoupling (CLOU) concepts for high energy efficient power generation with near total fuel decarbonisation. Appl Therm Eng. 2017;112:924-31.

[315] Mukherjee S, Kumar P, Yang A, Fennell P. Energy and exergy analysis of chemical looping combustion technology and comparison with pre-combustion and oxy-fuel combustion technologies for CO_2 capture. J Environ Chem Eng. 2015;3:2104-14.

[316] Luo M, Wang S, Zhu J, Wang L, Lv M. Capture of CO2 from coal using chemical-looping combustion: Process simulation. Korean J Chem Eng. 2015;32:373-82.

[317] Fan J, Zhu L, Hong H, Jiang Q, Jin H. A thermodynamic and environmental performance of in-situ gasification of chemical looping combustion for power generation using ilmenite with different coals and comparison with other coal-driven power technologies for CO2 capture. Energy. 2017;119:1171-80.

[318] Fan Z, Chen L, Liu F, Bao J, Nikolic H, Liu K. Coal Based Pressurized Chemical Looping Combustion Combined Cycle Process development and Analysis. 4th International Conference on Chemical Looping. Nanjing (China)2016.

[319] Volker K, Alfons K. Thermodynamic analysis of a coal fired chemical looping combustion power plant. 5th International Conference on Clean Coal Technologies. Zaragoza (Spain). 2011.

[320] Dansie JK, Sahir AH, Hamilton MA, Lighty JS. An investigation of steam production in chemical-looping combustion (CLC) and chemical-looping with oxygen uncoupling (CLOU) for solid fuels. Chem Eng Res Des. 2015;94:12-7.

[321] Petrakopoulou F, Tsatsaronis G. Can carbon dioxide capture and storage from power plants reduce the environmental impact of electricity generation? Energy Fuels. 2014;28:5327-38.

[322] Kerr HR. Capture and separation technology gaps and priority research needs. In: Thomas DC, Benson SM, editors. Carbon dioxide capture for storage in deep geologic formationse results from the CO_2 capture project,1. Oxford, UK: Elsevier; 2005.

[323] IPCC. IPCC special report on carbon dioxide capture and storage. Cambridge, UK2005.

[324] Tähtinen M, Tsupari E, Kärki J. Feasibility and sensitivity of solid fuel CLC plant investment with oxygen carrier recovery. 3rd International Conference on Chemical Looping. Göteborg (Sweden). 2014.

[325] Tsupari E, Tähtinen M, Kärki J. Feasibility of solid fuel CLC plant investment in the future energy systems including high share of solar and wind. Energy Procedia 2014;63:7508-16.

List of Figure captions

Fig. 1. Scheme of the CLC process for solid fuels.

Fig. 2. Scheme of the *i*G-CLC and CLOU processes for solid fuel combustion.

Fig.3. CLC units burning solid fuels distributed by thermal power and operation date. Empty symbols indicate upcoming prototypes not yet in operation.

Fig. 4. CLC units burning solid fuels at Chalmers University of Technology (CUT). (A) 10 kW_{th}. Reprinted from Ref. [57] with permission of Elsevier, (B) 100 kW_{th}. Reprinted from Ref. [174].

Fig. 5. CLC units burning solid fuels at Southeast University (SU). (A) 1 kW_{th}. Reprinted from Ref. [130] with permission of ACS, (B) 10 kW_{th}. Reprinted from Ref. [38] with permission of Elsevier.

Fig. 6. 50 kW_{th} Pressurized CLC unit at Southeast University (SU). Reprinted from Ref. [135] with permission of Elsevier.

Fig.7. CLC units burning solid fuels at Instituto de Carboquímica (ICB-CSIC) (A) 0.5 kW_{th}. Adapted from Ref. [136], (B) 50 kW_{th}. Adapted from Ref. [144].

Fig. 8. 10 kW_{th} unit at IFP Energies Nouvelles (IFPEN). Reprinted from Ref. [147]. (A) Overview the unit, (B) Adaptation of a carbon stripper to the existing fuel reactor.

Fig. 9. 25 kW_{th} unit at Hamburg University of Technology (TUHH). Reprinted from Ref. [148] with permission of Elsevier.

Fig. 10. 10 kW_{th} unit at Institute for Combustion Science and Environmental Technology (ICSET) of Western Kentucky University (WKU). Reprinted from Ref. [180].

Fig. 11. 25 kW_{th} unit at Ohio State University (OSU). Reprinted from Ref. [152] with permission of ACS.

Fig. 12. 10 kW_{th} CLC unit at CAS Key Laboratory of Renewable Energy at Guangzhou Institute of Energy Conversion in Guangzhou (GIEC). Reprinted from Ref. [155] with permission of ACS.

Fig. 13. CLC units burning solid fuels at State Key Laboratory of Coal Combustion at Huazhong University of Science and Technology (HUST). (A) 5 $kW_{th.}$ Reprinted from Ref. [156] with permission of Elsevier, (B) 50 kW_{th}. Reprinted from Ref. [157].

Fig. 14. 10-50 kW_{th} unit at VTT Technical Research Centre (VTT). Reprinted from Ref. [158].

Fig. 15. Dual fluidized bed 10 kW_{th} facility for CLC of solid fuels at the Institute of Combustion and Power Plant Technology (IFK-University of Stuttgart). Reprinted from Ref. [187].

Fig.16. Three tower concept for CLC of coal by Japan Coal Energy Center (JCOAL). Reprinted from Ref. [167].

Fig. 17. 225 kW_{th} CLOU unit at the University of Utah. Reprinted from Ref. [168].

Fig. 18. 250 kW_{th} unit designed by B&W. Reprinted from Ref. [170].

Fig. 19. 1 MW_{th} CLC pilot plant at Technische Universität Darmstadt (TUD). Reprinted from Ref. [194].

Fig. 20. 3 MW_{th} CLC pilot plant from Alstom Power based on the LCL^{TM} process. Reprinted from Ref. [43].

Fig. 21. 4 MW_{th} unit at Chalmers University of Technology (CUT). Reprinted from Ref. [166] with permission of Elsevier.

Fig. 22. Flow chart including the variables employed to estimate the solid fuel conversion, CO_2 capture efficiency and combustion efficiency in a CLC system with solid fuels.

Fig. 23. Flow chart including the carbon flows necessary to determine the solid fuel conversion and carbon capture efficiency in a CLC system with solid fuels.

Fig. 24. Flow chart including the oxygen flows necessary to determine the combustion efficiency in a CLC system with solid fuels.

Fig. 25. Scheme of the main variables influencing the CO_2 capture efficiency and oxygen demand.

Fig. 26. Carbon capture efficiency and oxygen demand at different fuel reactor temperatures. S**ymbols:** Empty=with CS, Filled=without CS. **References:** Ilmenite [115, 124, 136, 137, 145, 146, 148, 159, 200]; Fe_2O_3-based [39, 101, 127, 129, 132, 140, 201]; NiO-based [38, 126, 202]; CuO-based [149]; $CaSO_4$ [163]. Interactive plots available in the web version of the paper.

- *This figure includes 4 interactive plots in the web version of the paper. (*Fig 26A_1.csv, Fig 26A_2.csv, Fig 26B_1.csv, Fig 26B_2.csv).

Fig. 27. Carbon capture efficiency and oxygen demand at different oxygen carrier to fuel ratios**.**. S**ymbols:** Empty=with CS, Filled=without CS. **References:** Ilmenite [36, 115, 118, 122, 123, 138, 146] Fe_2O_3-based [140] Mn_3O_4-based [115]. Interactive plots available in the web version of the paper

- *This figure includes 2 interactive plots in the web version of the paper. (*Fig 27A.csv, Fig 27B.csv).

Fig. 28. Carbon capture efficiency and oxygen demand as a function of the solids inventory in the fuel reactor**. Symbols**: Empty=with CS; Filled=without CS.

References: Ilmenite [119, 122, 123, 146]; Fe_2O_3-based [100, 140]. Interactive plots available in the web version of the paper.

- *This figure includes 2 interactive plots in the web version of the paper. (*Fig 28A.csv, Fig 28B.csv).

Fig. 29. Effect of the composition of the gasifying agent on (A) the CO_2 capture efficiency (η_{CC}) and (B) the combustion efficiency in the fuel reactor ($\eta_{comb,FR}$) and the oxygen demand (Ω_T). Adapted from Ref. [137].

Fig. 30. Different designs for the carbon stripper. (A) Adapted from Ref. [57], (B) Reprinted from Ref. [43] (C) Adapted from Ref. [144] (D) Reprinted from Ref. [123] with permission of Elsevier, (E) Reprinted from Ref. [249] with permission of Elsevier, (F) Reprinted from Ref. [51] with permission of ACS, (G) Adapted from Ref. [43].

Fig. 31. Carbon capture as a function of the temperature and the mean residence time of solids in the fuel reactor. (A) 0.5 and 50 kW_{th} at ICB-CSIC, and (B) 10 and 100 kW_{th} at CUT. Selected data from Table 4.

Fig. 32. Total oxygen demand as a function of the specific solids inventory and the oxygen carrier to fuel ratio. (A) 0.5 and 50 kW_{th} at ICB-CSIC, and (B) 10 and 100 kW_{th} at CUT. Selected data from Table 4.

Fig. 33. Carbon capture efficiency at different fuel reactor temperatures for CLOU**.** **Symbols:** Empty=with CS, Filled=without CS. **References:** [57, 58, 88, 117, 142, 143, 252]. Interactive plots available in the web version of the paper.

- *This figure includes an interactive plot in the web version of the paper. (*Fig 33.csv).

Fig. 34. Oxygen concentration at gas-solid equilibrium for different redox pairs used in the CLOU process. Adapted from Ref. [59].

Fig. 35. Performance of CLC units burning biomass under *i*G-CLC or CLOU mode. Reprinted from Ref. [56] with permission of Wiley.

Fig. 36. Scheme of pollutant formation in the CLC process with solid fuels.

Fig. 37. Tar composition for different biomasses. T= 980 ºC. Adapted from Ref. [141].

Fig. 38. Ω_{FR} and Ω_T for different values of the carbon fraction in char gasified in the fuel reactor. Dashed line represents the oxygen demand level considering complete conversion of the solid fuel. Colombian bituminous coal is considered as fuel in all the Figures [136].

Fig. 39. Determination of combustion efficiency of the volatiles released ($\eta_{comb,v}$) and char gasification products ($\eta_{comb,g}$) following Eq.(17) and using data from different CLC units:

[1] = ilmenite and bituminous coal (125-200 μm) [136]
[2] = bauxite waste and bituminous coal (200-300 μm) [140]
[3] = ilmenite and bituminous coal [115]
[4] = ilmenite and petcoke [115, 119]
[5] = ilmenite and petcoke In-bed feeding [115]
[6] = ilmenite and bituminous coal (200-300 μm) [285]
[7] = ilmenite and wood char [121]
[8] = ilmenite and wood char [121]
[9] = ilmenite and bituminous coal [120]

Fig. 40. Determination of combustion efficiency of the volatiles released ($\eta_{comb,v}$) and char gasification products ($\eta_{comb,g}$) following Eq. (17) and using data for combustion experiments of bituminous coals in the ICB-CSIC 0.5 kW_{th} unit (bubbling bed fuel reactor) and CUT 100 kW_{th} unit (high velocity fuel reactor).

Fig. 41. Scheme of the design of a CLC unit based on a CFB fuel reactor. (A) 100 MW_{th}. Reprinted from Ref. [244] with permission of Elsevier, and (B) 1000 MW_{th}. Reprinted from Ref. [4] with permission of Elsevier.

Fig. 42. Map of the design of CFB-based fuel and air reactors. Reprinted from Ref. [244] with permission of Elsevier.

Fig. 43. Scheme of the design of a CLC unit based on a moving bed fuel reactor. (A) Two-stage counter-current moving bed reducer. Reprinted from Ref. [53] with permission of Elsevier, and (B) Shape of the moving bed fuel reactor. Reprinted from Ref. [182].

Fig. 44. Diagrams of the different configurations for the improvement of the *i*G-CLC process implementing different technological solutions. Adapted from Ref. [52] and Ref. [4].

Fig. 45. Coefficient of variation, CV, for the oxygen demand predicted for different *iG*-CLC configurations. Adapted from Ref. [52].

Fig. 46. Simplified Sankey diagrams with enthalpy flows to and from the iG-CLC system with the fluidization agent (A) H_2O or (B) CO_2. Reprinted from [244] with permission of Elsevier.

Fig. 47. Net power efficiency (LHV) in electricity generation by different coal-feed power technologies. Adapted from [317].

Figures

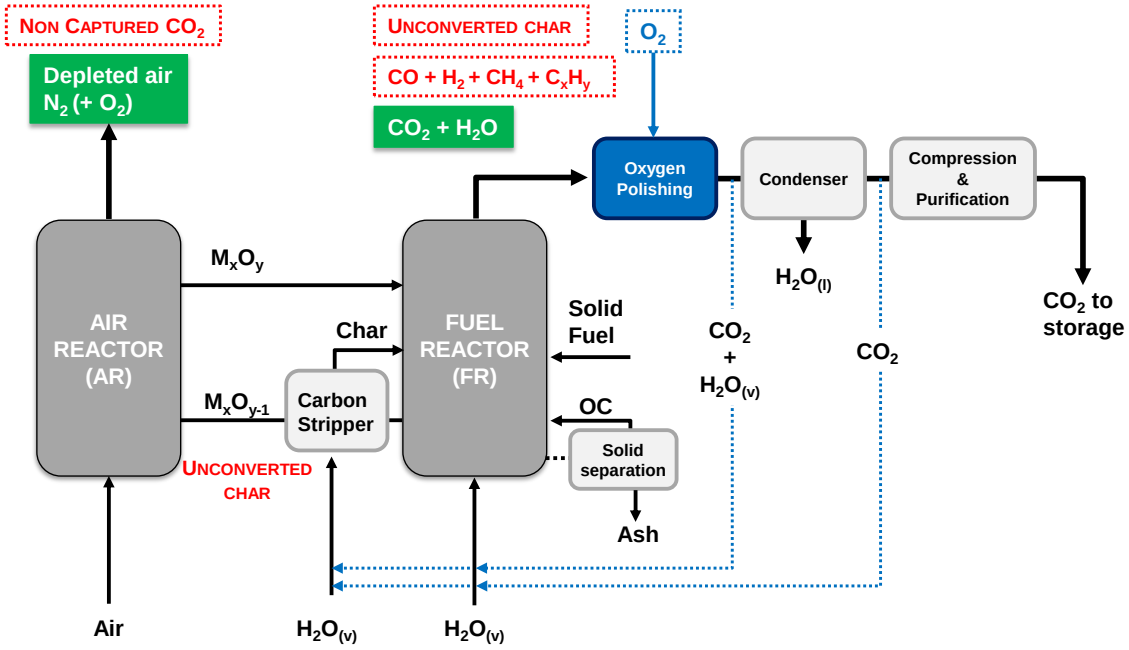

Fig. 1. Scheme of the CLC process for solid fuels.

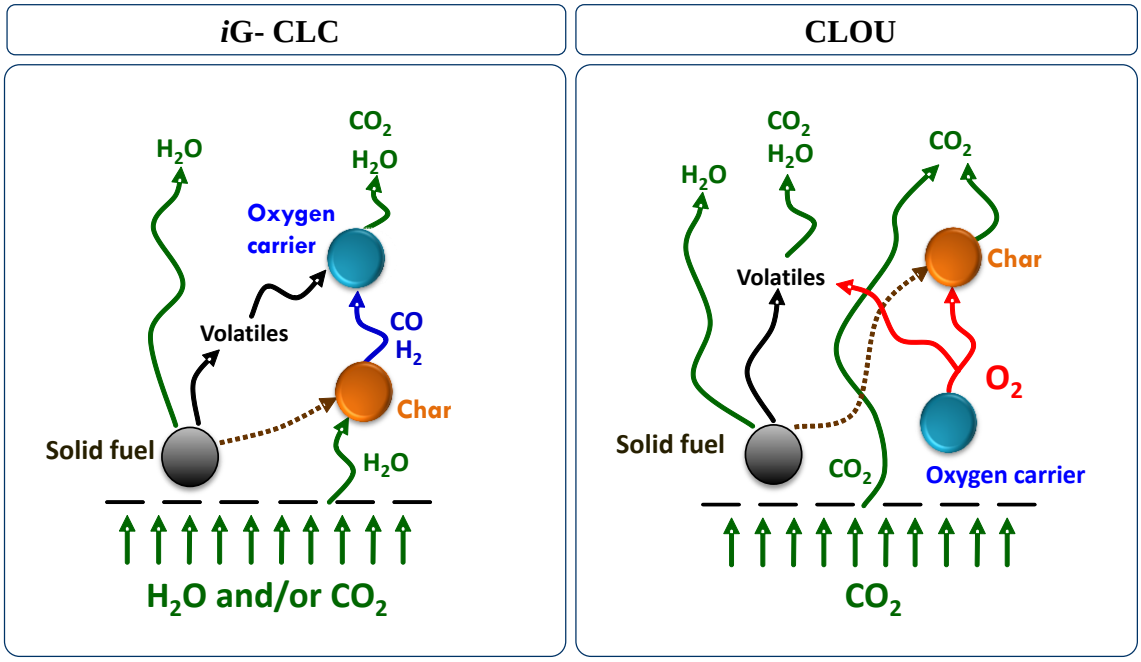

Fig. 2. Scheme of the *i*G-CLC and CLOU processes for solid fuel combustion.

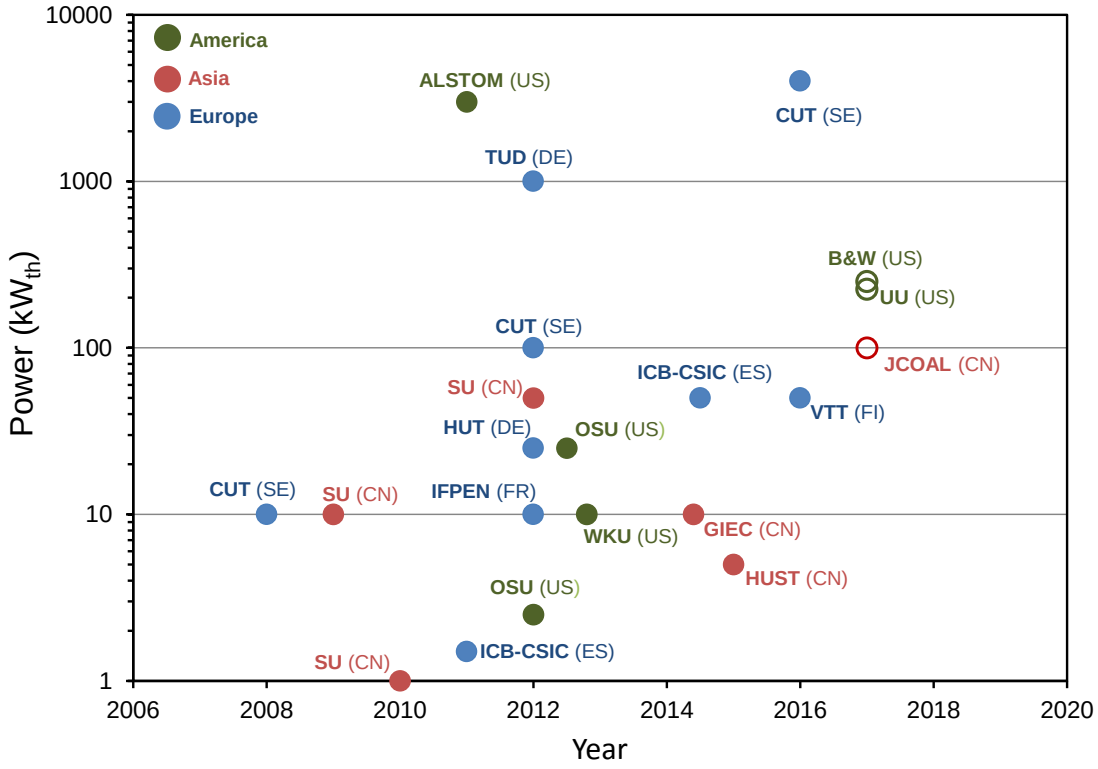

Fig.3. CLC units burning solid fuels distributed by thermal power and operation date. Empty symbols indicate upcoming prototypes not yet in operation.

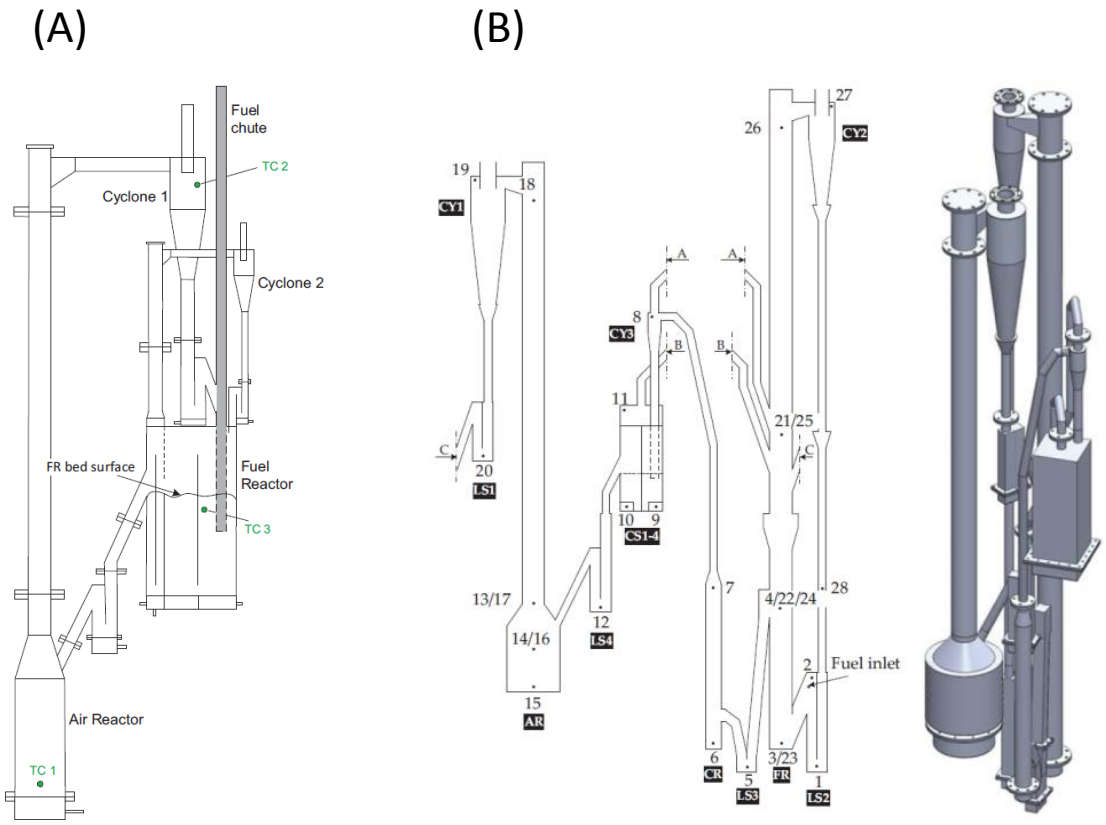

Fig. 4. CLC units burning solid fuels at Chalmers University of Technology (CUT). (A) 10 kW_{th}. Reprinted from Ref. [57] with permission of Elsevier, (B) 100 kW_{th}. Reprinted from Ref. [174].

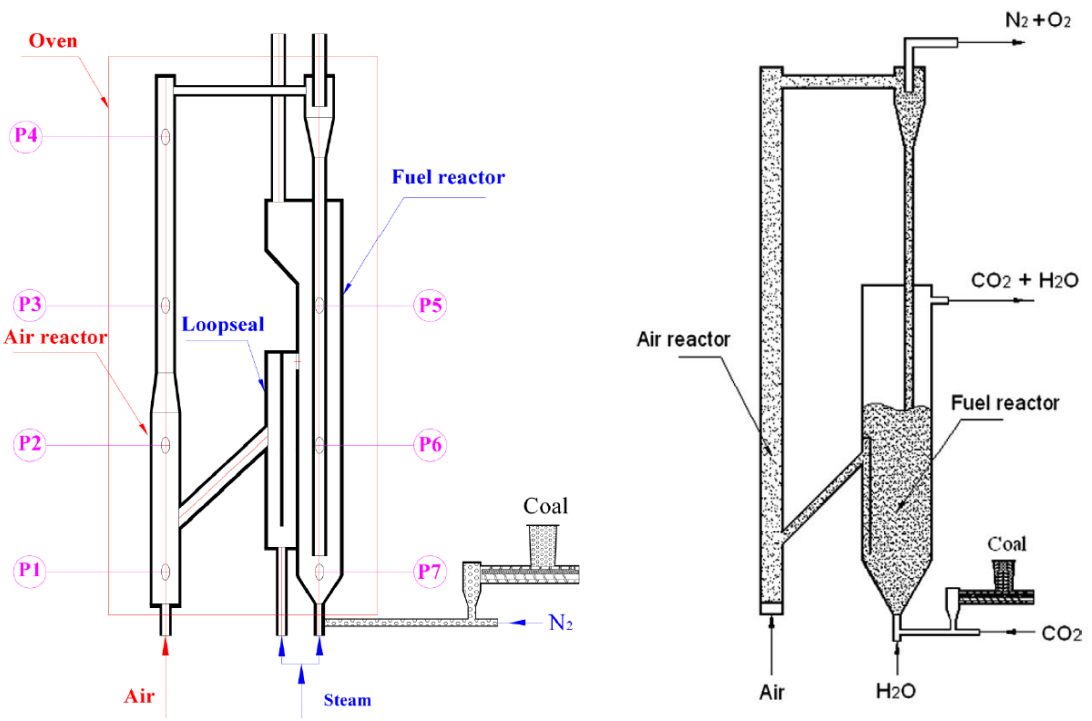

Fig. 5. CLC units burning solid fuels at Southeast University (SU). (A) 1 kW_{th}. Reprinted from Ref. [130] with permission of ACS, (B) 10 kW_{th}. Reprinted from Ref. [38] with permission of Elsevier.

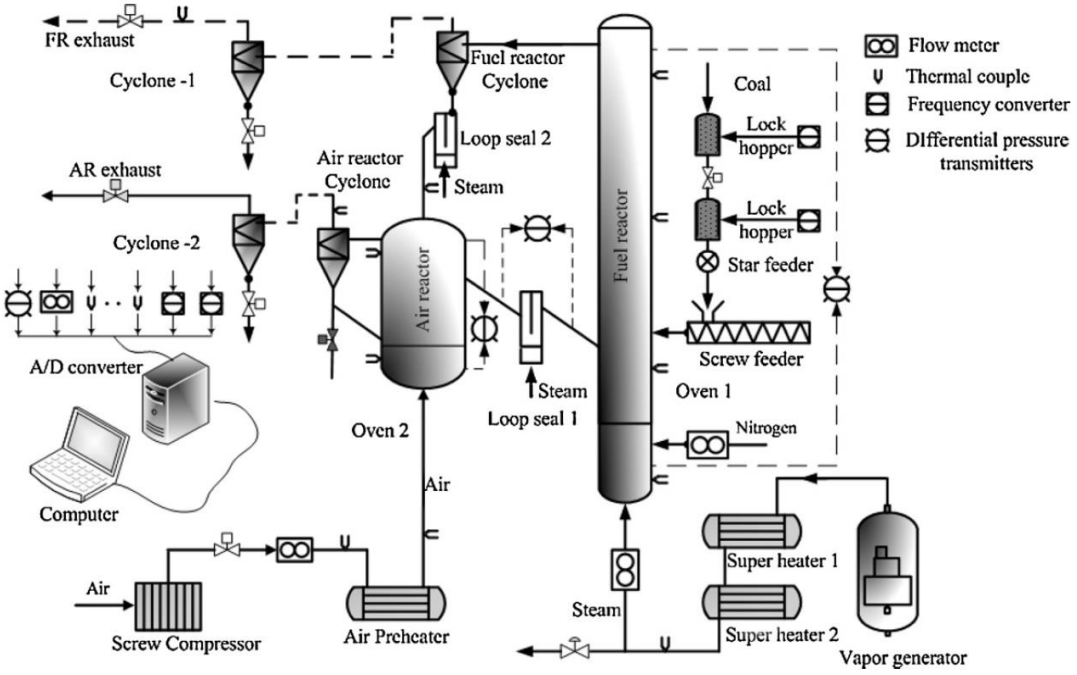

Fig. 6. 50 kW_{th} Pressurized CLC unit at Southeast University (SU). Reprinted from Ref. [135] with permission of Elsevier.

3908

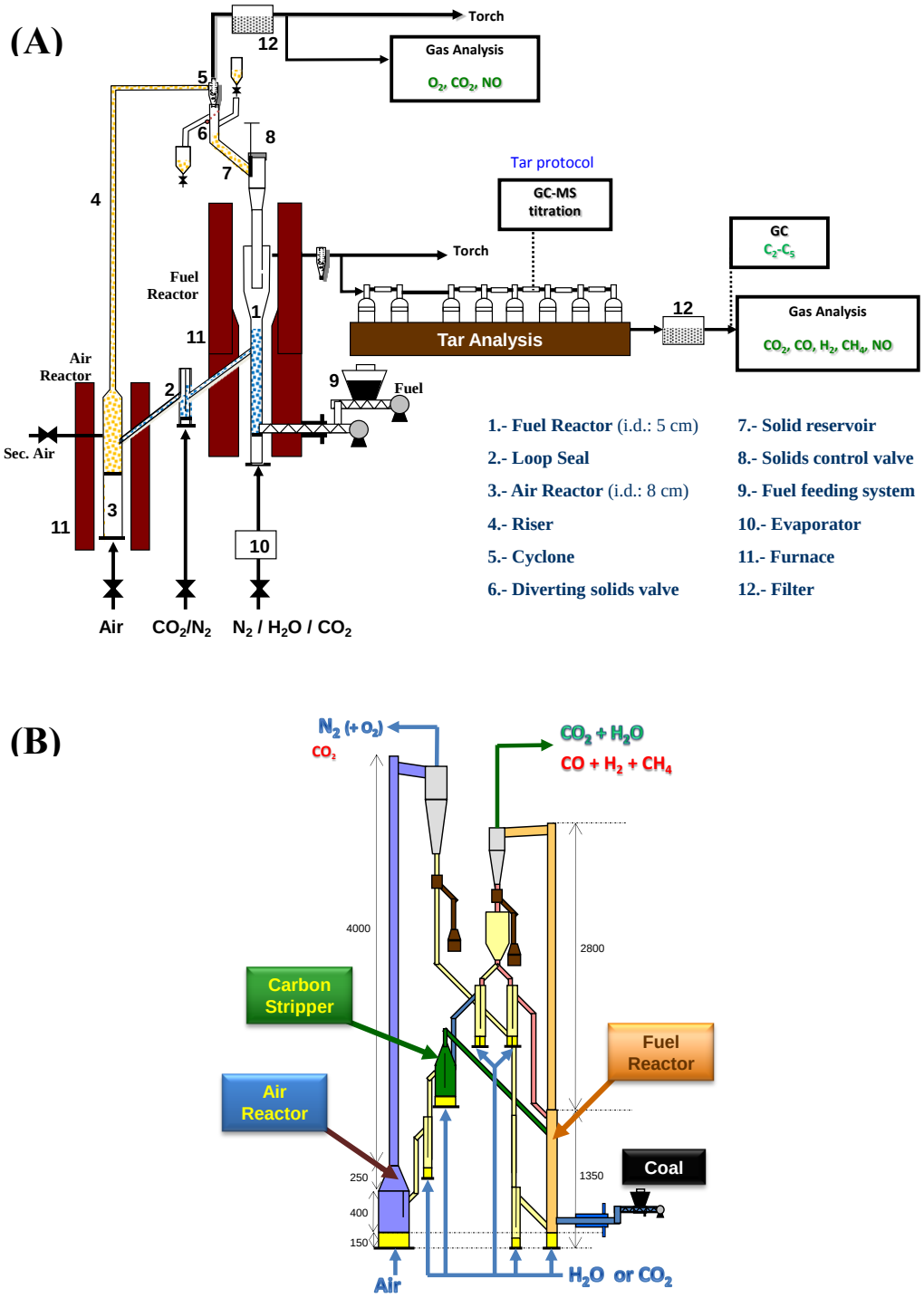

3909 **Fig.7.** CLC units burning solid fuels at Instituto de Carboquímica (ICB-CSIC) (A) 0.5

3910 kW_{th}. Adapted from Ref. [136], (B) 50 kW_{th}. Adapted from Ref. [144].

3911

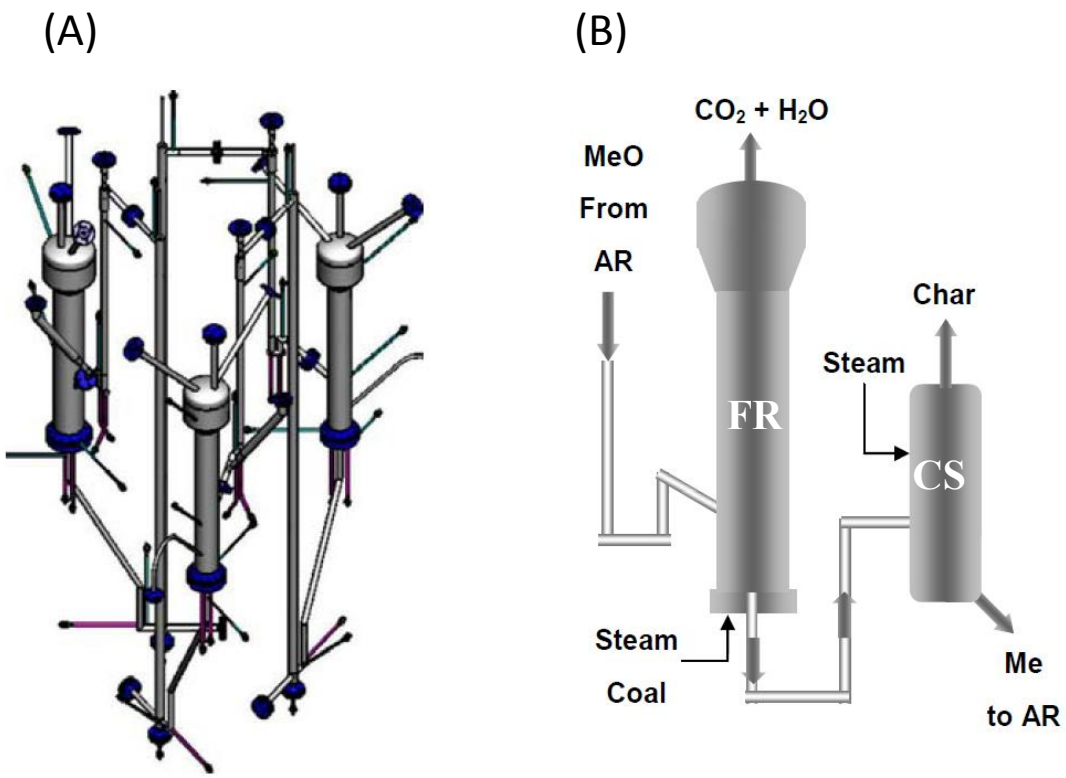

Fig. 8. 10 kW_{th} unit at IFP Energies Nouvelles (IFPEN). Reprinted from Ref. [147]. (A) Overview the unit, (B) Adaptation of a carbon stripper to the existing fuel reactor.

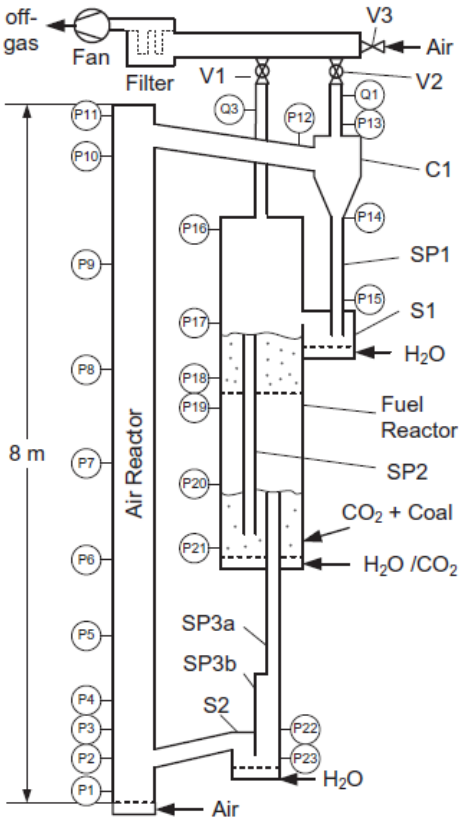

Fig. 9. 25 kW_{th} unit at Hamburg University of Technology (TUHH). Reprinted from Ref. [148] with permission of Elsevier.

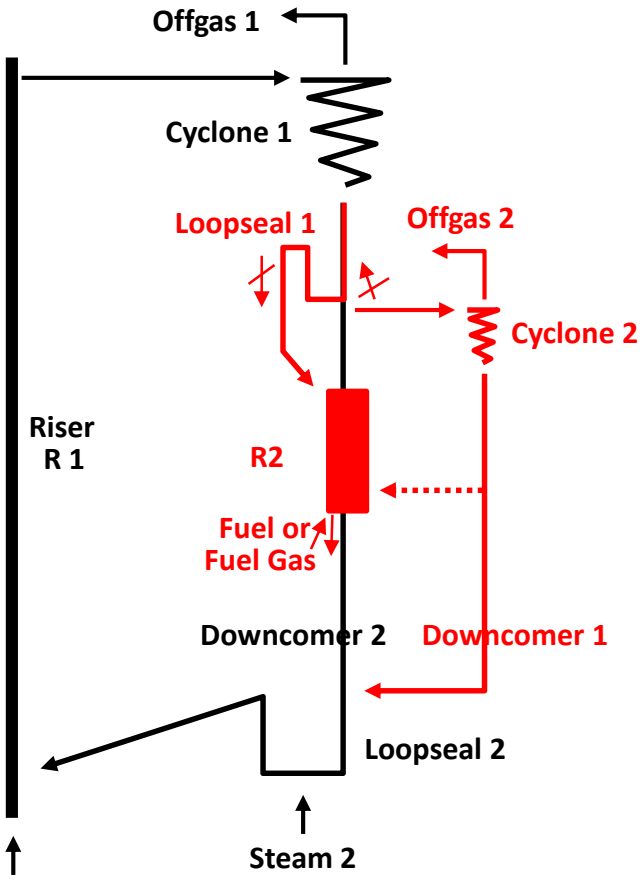

Fig. 10. 10 kW_{th} unit at Institute for Combustion Science and Environmental Technology (ICSET) of Western Kentucky University (WKU). Reprinted from Ref. [180].

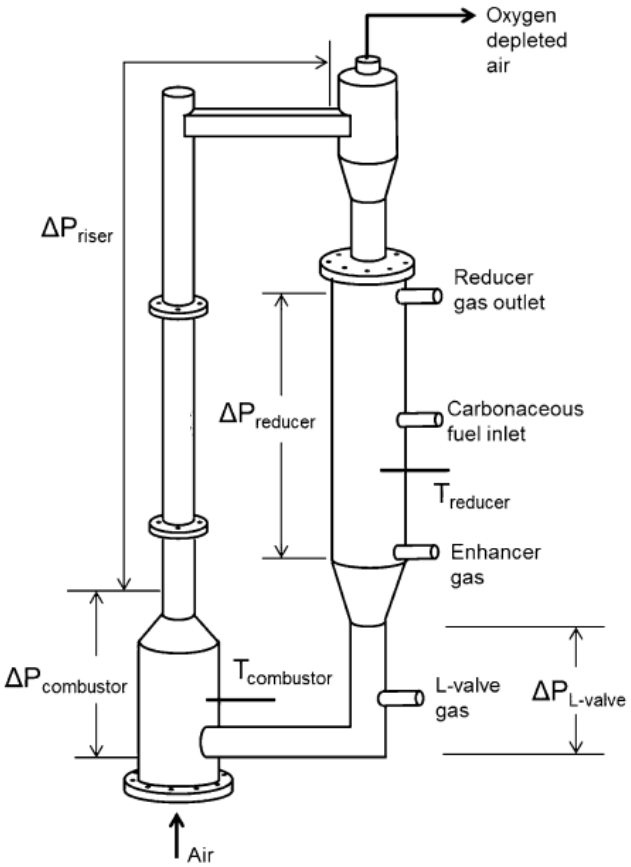

Fig. 11. 25 kW_{th} unit at Ohio State University (OSU). Reprinted from Ref. [152] with permission of ACS.

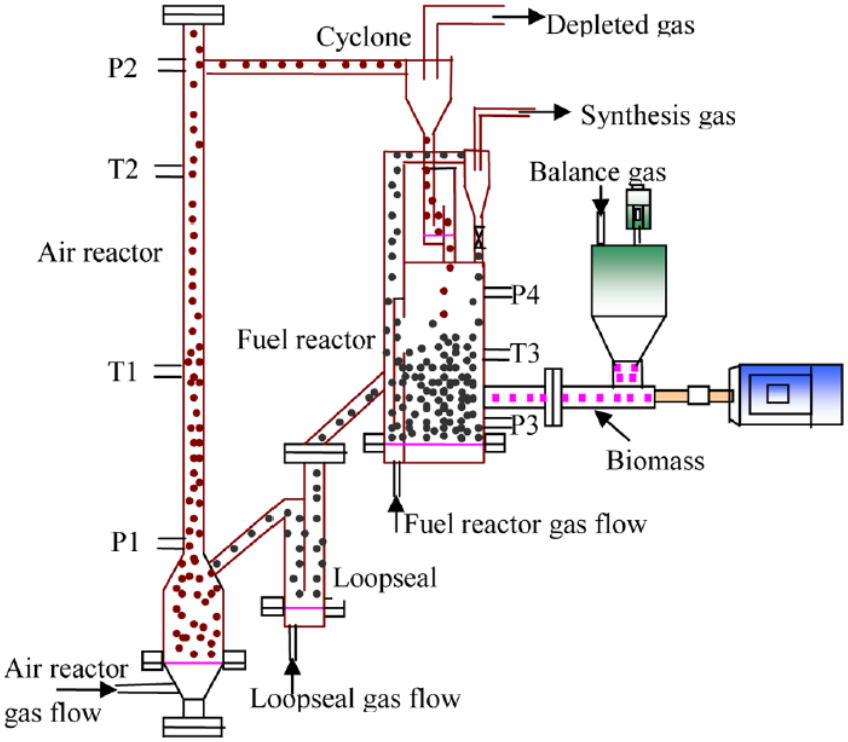

Fig. 12. 10 kW_{th} CLC unit at CAS Key Laboratory of Renewable Energy at Guangzhou Institute of Energy Conversion in Guangzhou (GIEC). Reprinted from Ref. [155] with permission of ACS.

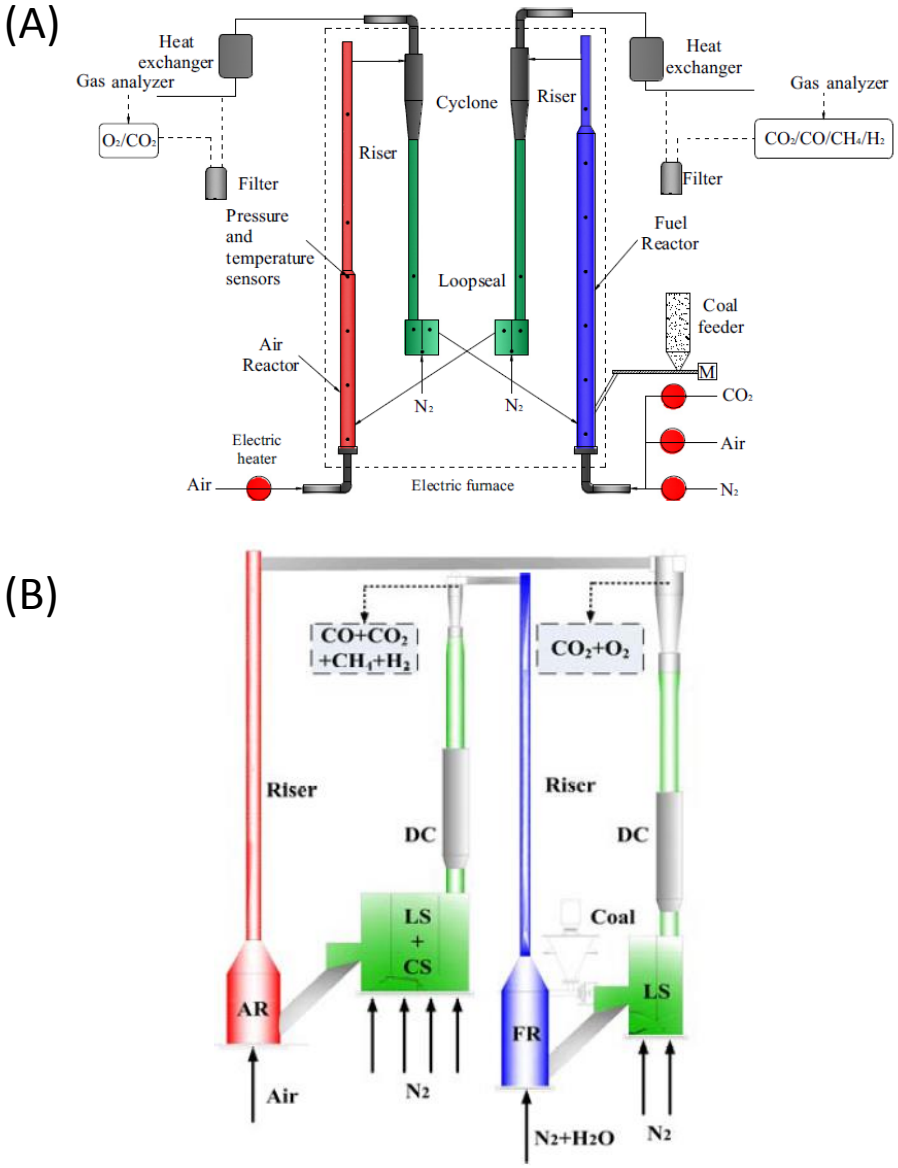

Fig. 13. CLC units burning solid fuels at State Key Laboratory of Coal Combustion at Huazhong University of Science and Technology (HUST). (A) 5 $kW_{th.}$ Reprinted from Ref. [156] with permission of Elsevier, (B) 50 kW_{th}. Reprinted from Ref. [157].

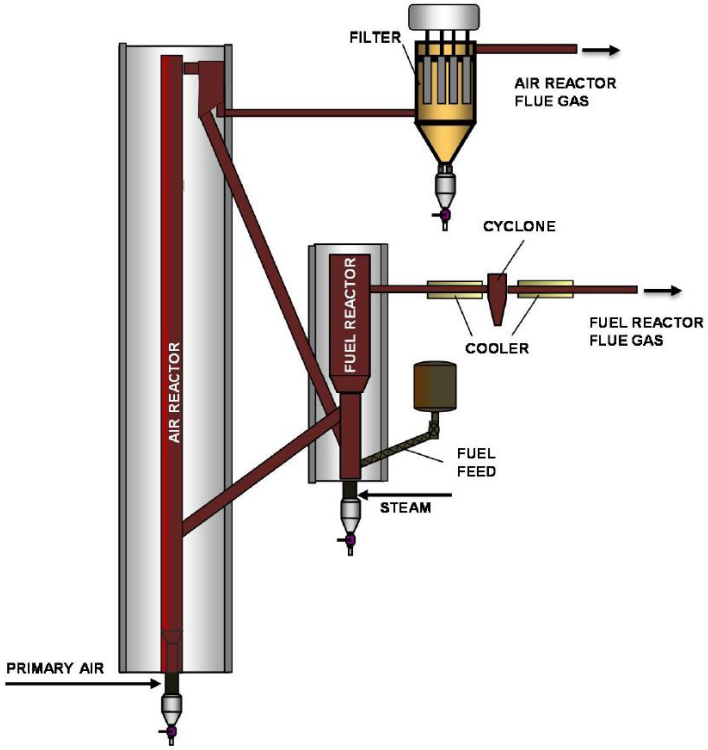

Fig. 14. 10-50 kW_{th} unit at VTT Technical Research Centre (VTT). Reprinted from Ref. [158].

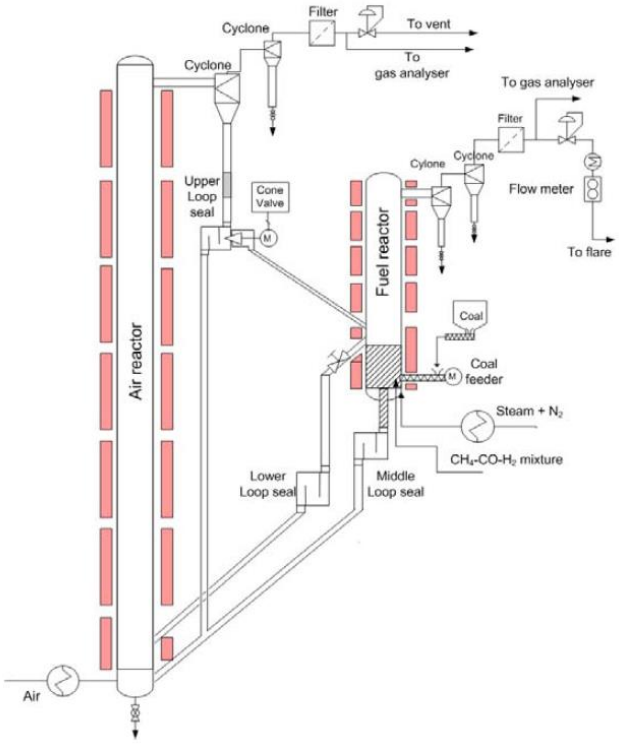

Fig. 15. Dual fluidized bed 10 kW_{th} facility for CLC of solid fuels at the Institute of Combustion and Power Plant Technology (IFK-University of Stuttgart). Reprinted from Ref. [187].

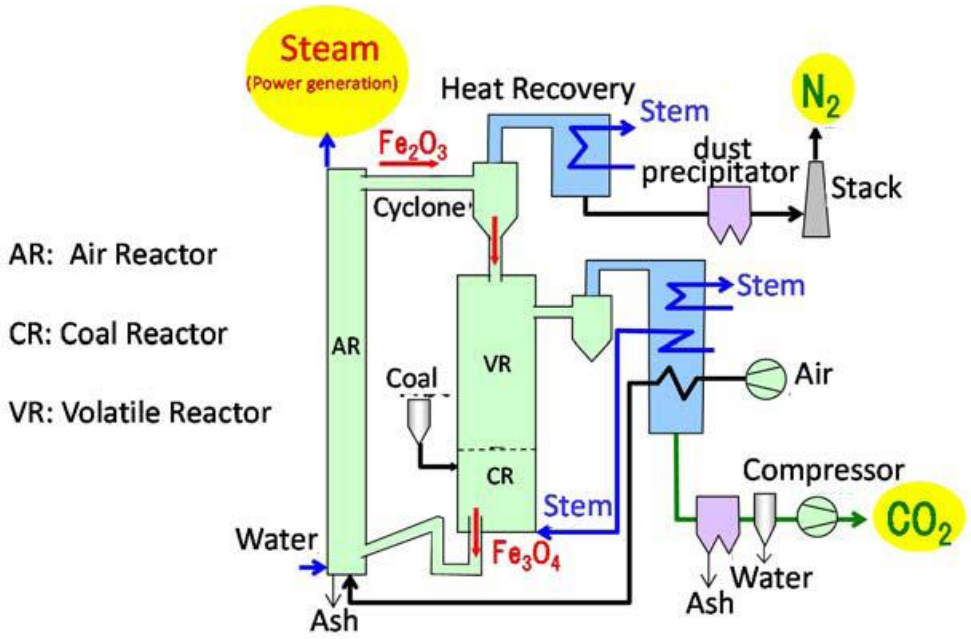

Fig.16. Three tower concept for CLC of coal by Japan Coal Energy Center (JCOAL). Reprinted from Ref. [167].

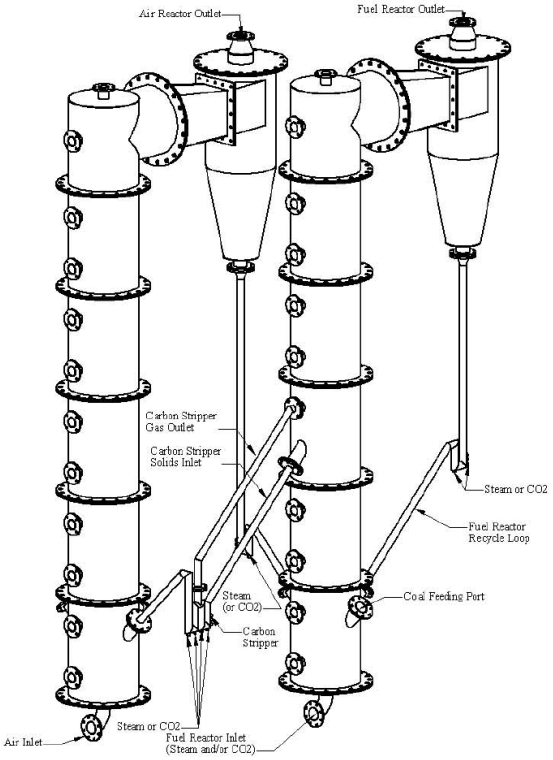

Fig. 17. 225 kW_{th} CLOU unit at the University of Utah. Reprinted from Ref. [168].

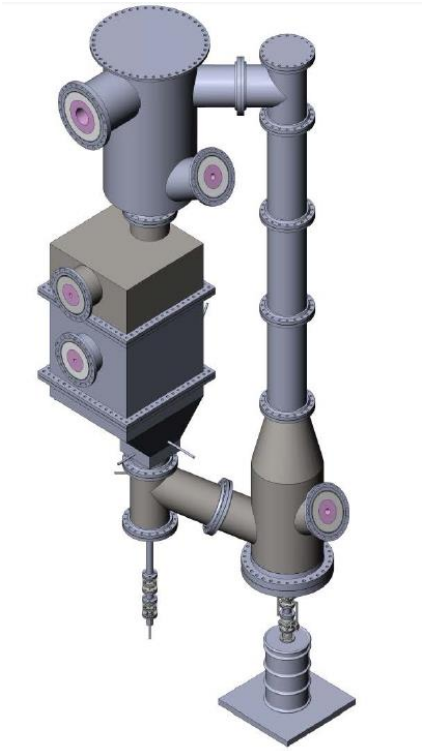

Fig. 18. 250 kW_{th} unit designed by B&W. Reprinted from Ref. [170].

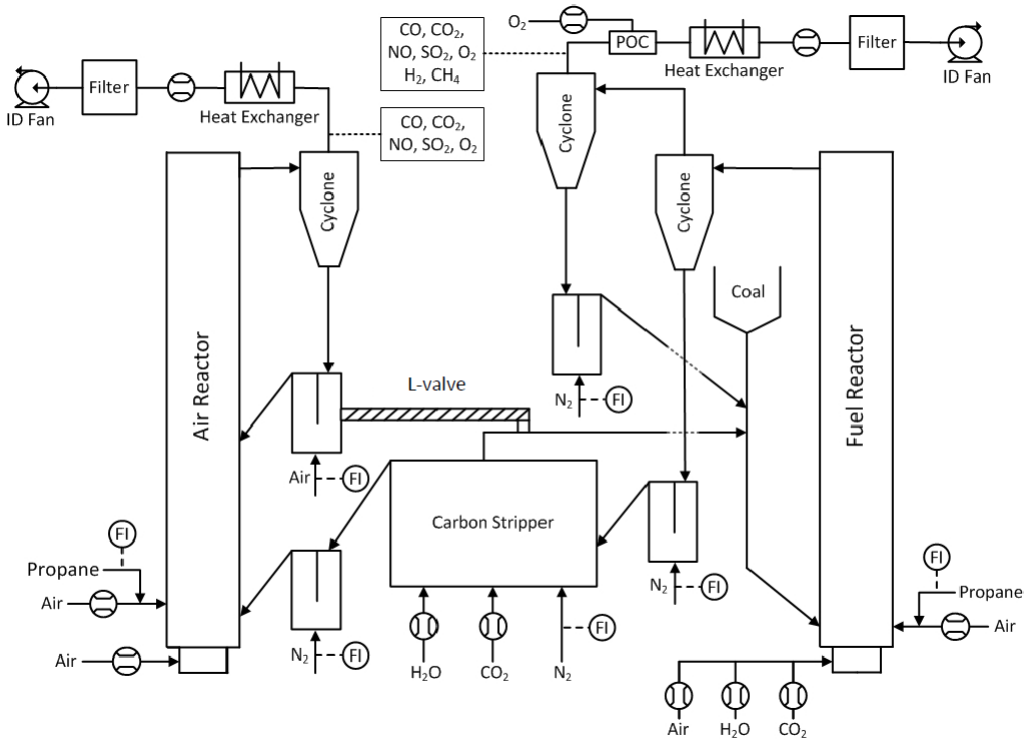

Fig. 19. 1 MW_{th} CLC pilot plant at Technische Universität Darmstadt (TUD). Reprinted from Ref. [194].

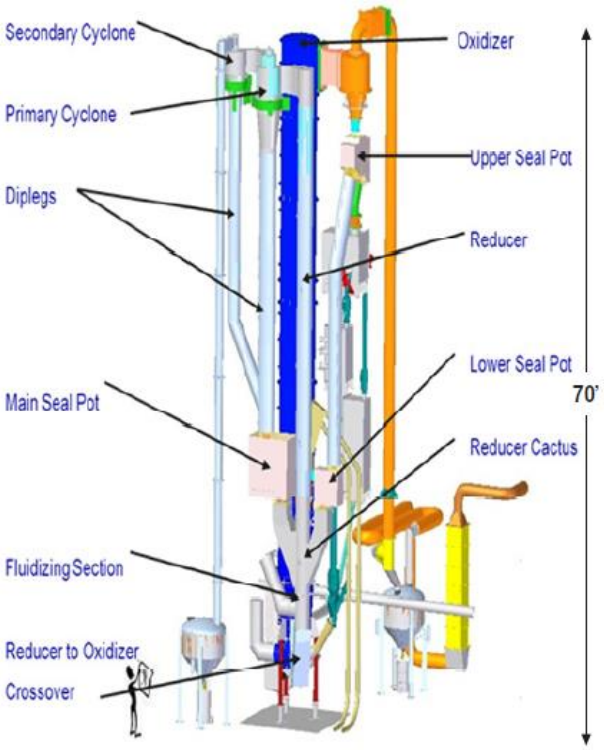

Fig. 20. 3 MW_{th} CLC pilot plant from Alstom Power based on the LCL^{TM} process. Reprinted from Ref. [43].

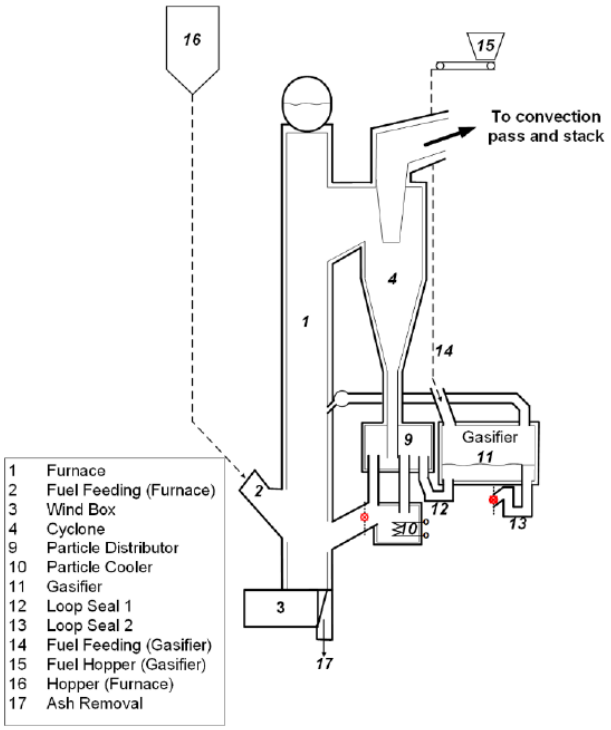

Fig. 21. 4 MW_{th} unit at Chalmers University of Technology (CUT). Reprinted from Ref. [166] with permission of Elsevier.

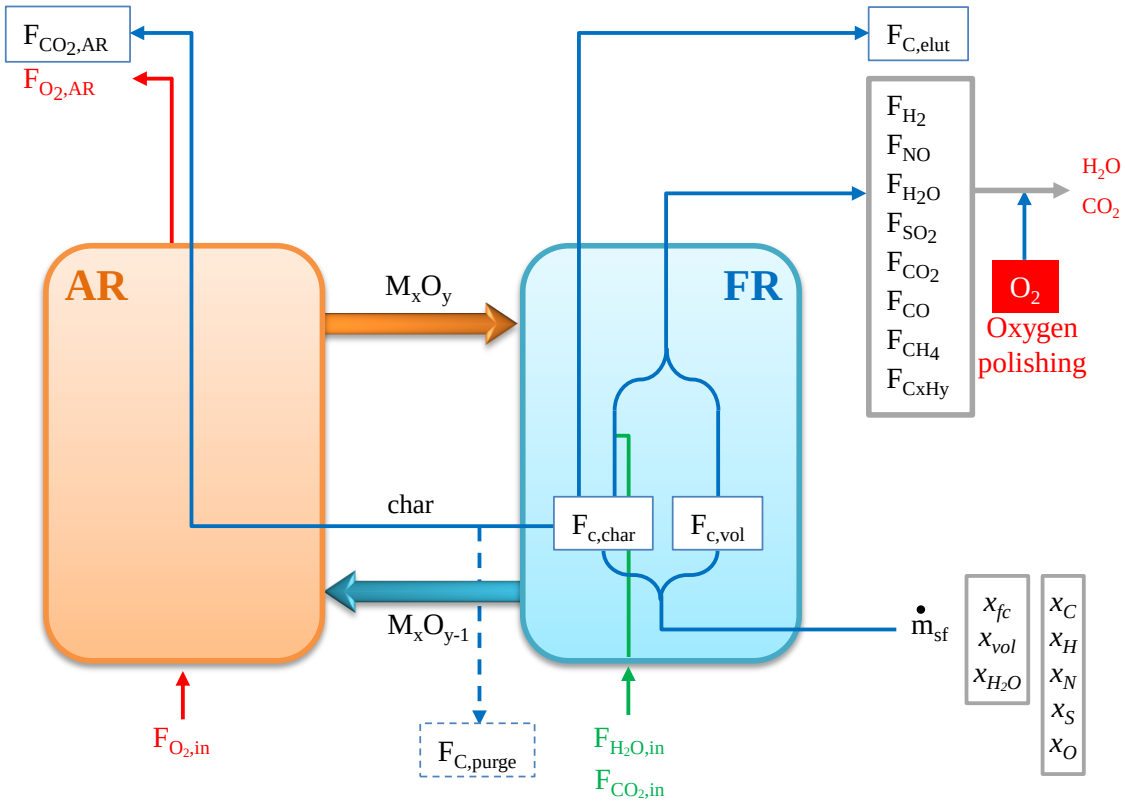
F_CO2,AR
F_O2,AR
F_C,elut
F_H2
F_NO
F_H2O
F_SO2
F_CO2
F_CO
F_CH4
F_CxHy
H2O
CO2
O2
Oxygen polishing
AR
M_xO_y
FR
char
F_c,char
F_c,vol
M_xO_y-1
ṁ_sf
x_fc
x_vol
x_H2O
x_C
x_H
x_N
x_S
x_O
F_O2,in
F_C,purge
F_H2O,in
F_CO2,in

Carbon in gases from FR (only coming from solid fuel conversion)	$F_{C,FR,out} - F_{CO_2,in}$
Carbon in gases from FR and AR (only coming from solid fuel conversion)	$(F_{C,FR,out} - F_{CO_2,in}) + F_{C,AR,out}$
Carbon in solid fuel	$F_{C,sf} = \frac{1000}{12} \dot{m}_{sf}\ x_C$
Fixed carbon in solid fuel	$F_{C,char} = \frac{1000}{12} \dot{m}_{sf}\ x_{fc}$
Carbon in elutriated char	$F_{C,elut}$
Fixed carbon converted in FR and AR	$(F_{C,FR,out} - F_{CO_2,in}) + F_{C,AR,out} - F_{C,vol} = F_{C,char} - F_{C,elut}$
Fixed carbon gasified in FR	$(F_{C,FR,out} - F_{CO_{2,in}}) - F_{C,vol}$
Oxygen reacted with the OC in AR	$F_{O_2,oc}$
Total oxygen reacted in AR (OC+char)	$F_{O_2,oc} + F_{O_2,char}$
Oxygen needed to burn unconverted gases	$F_{O,op} = F_{CO} + F_{H_2} + 4F_{CH_4} + (2x + y/2)F_{C_xH_y}$
Oxygen needed to burn solid fuel	$F_{O,comb,sf} = \frac{1000}{16} \dot{m}_{sf}\ \Omega_{sf}$
Oxygen transferred in FR	$F_{O,FR,out} - F_{O,FR,in}$
Oxygen demanded by solid fuel converted in FR	$F_{O,comb,FR} = \frac{1000}{16} \dot{m}_{sf}\ \Omega_{sf} - 2F_{CO_2,AR} - 2F_{C,elut}$

4059

$$F_{C,AR,out} = F_{CO_2,AR}$$

$$F_{C,FR,out} = \left[F_{CO_2} + F_{CO} + F_{CH_4} + xF_{C_xH_y} \right]_{FR,out}$$

$$F_{C,elut} = \frac{1000}{12} \dot{m}_{sf} x_C + F_{CO_2,in} - (F_{C,FR,out} + F_{C,AR,out})$$

$$F_{C,vol} = \frac{1000}{12} \dot{m}_{sf} (x_C - x_{fc})$$

$$\Omega_{sf} = 2\frac{16}{12} x_C + \frac{1}{2} 16 x_H + \frac{1}{14} 16 x_N + 2\frac{16}{32} x_S - x_O$$

$$F_{O,FR,in} = F_{H_2O,in} + 2F_{CO_2,in} + \frac{1000}{18} \dot{m}_{sf} x_{H_2O} + \frac{1000}{16} \dot{m}_{sf} x_O$$

$$F_{O,FR,out} = \left[F_{NO} + F_{H_2O} + 2F_{SO_2} + 2F_{CO_2} + F_{CO} \right]_{FR,out}$$

4060

4061 **Fig. 22.** Flow chart indicating the variables employed to estimate the solid fuel
4062 conversion, CO_2 capture efficiency and combustion efficiency in a CLC system with
4063 solid fuels.

4064

4065

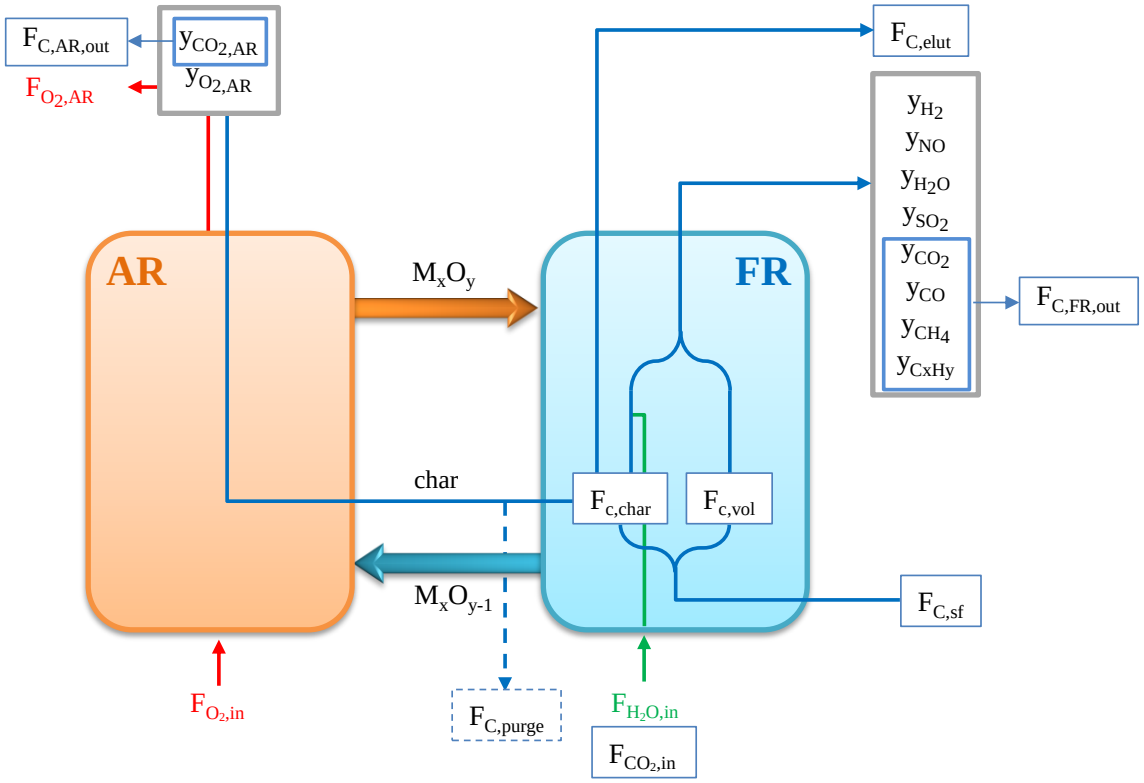

4066

4067

4068

	Parameter value equal to 1 means that:
Solid fuel conversion	
$X_{sf} = \frac{(F_{C,FR,out} - F_{CO_2,in}) + F_{C,AR,out}}{F_{C,sf}}$	- All carbon is converted in the CLC - No elutriation exists - No distinction between carbon captured (FR) or not captured (AR)
Char conversion in the CLC unit	
$X_{char} = \frac{(F_{C,FR,out} - F_{CO_2,in}) + F_{C,AR,out} - F_{C,vol}}{F_{C,char}} = \frac{F_{C,char} - F_{C,elut}}{F_{C,char}}$	- All char is converted in the CLC - No elutriation exists - No distinction between carbon captured (FR) or not captured (AR)
Carbon capture efficiency	
$\eta_{CC} = \frac{(F_{C,FR,out} - F_{CO2,in})}{(F_{C,FR,out} - F_{CO_2,in}) + F_{C,AR,out}}$	- No carbon from FR to AR - Elutriation is not evaluated
Char conversion in the fuel reactor	
$X_{char,FR} = \frac{(F_{C,FR,out} - F_{CO_2,in}) - F_{C,vol}}{F_{C,char} - F_{C,elut}}$	- No char from FR to AR - Elutriation is not evaluated
Fraction of char converted in the fuel reactor	
$x_{char,FR} = X_{char} X_{char,FR} = \frac{(F_{C,FR,out} - F_{CO_2,in}) - F_{C,vol}}{F_{C,char}}$	- All char is converted in FR - No elutriation exists - Carbon capture is complete

Fig. 23. Flow chart including the carbon flows necessary to determine the solid fuel conversion and carbon capture efficiency in a CLC system with solid fuels.

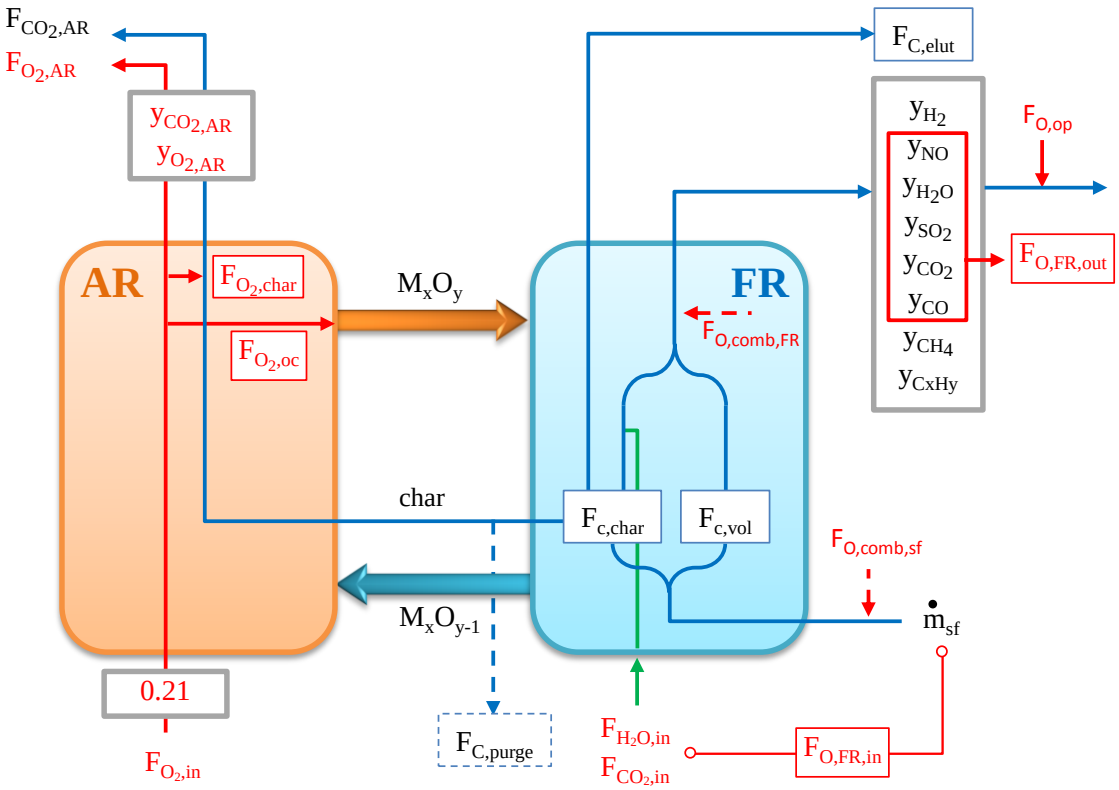
$F_{CO_2,AR}$
$F_{O_2,AR}$
$y_{CO_2,AR}$
$y_{O_2,AR}$
AR
$F_{O_2,char}$
$F_{O_2,oc}$
M_xO_y
M_xO_{y-1}
char
FR
$F_{O,comb,FR}$
$F_{C,elut}$
y_{H_2}
y_{NO}
y_{H_2O}
y_{SO_2}
y_{CO_2}
y_{CO}
y_{CH_4}
y_{CxHy}
$F_{O,op}$
$F_{O,FR,out}$
$F_{c,char}$
$F_{c,vol}$
$F_{O,comb,sf}$
$\dot{m}_{sf}$
0.21
$F_{O_2,in}$
$F_{C,purge}$
$F_{H_2O,in}$
$F_{CO_2,in}$
$F_{O,FR,in}$

4079

Oxide oxygen fraction

$$\chi_{OO} = \frac{F_{O_2,oc}}{F_{O_2,oc} + F_{O_2,char}}$$

$$\chi_{OO} = \frac{0.21 - y_{O_2,AR} - y_{CO_2,AR}}{0.21 - y_{O_2,AR} - 0.21 y_{CO_2,AR}}$$

If $\chi_{OO} = 1$
- No char from FR to AR
- Elutriation is not evaluated

Total oxygen demand

$$\Omega_T = \frac{F_{O,op}}{F_{O,comb,sf}}$$

If $\Omega_T = 0$
- No unburnt products in FR

If $\Omega_T \neq 0$
- Oxygen needed in oxygen polishing step with respect to the required to burn the solid fuel
- Fraction of oxygen required in an oxyfuel process

Combustion efficiency in fuel reactor

$$\eta_{comb,FR} = \frac{F_{O,FR,out} - F_{O,FR,in}}{F_{O,comb,FR}}$$

Same information as Ω_{FR}

Oxygen demand in the FR

$$\Omega_{FR} = \frac{F_{O,op}}{F_{O,comb,FR}} = 1 - \eta_{comb,FR}$$

If $\Omega_{FR} = 0$
- No unburnt products in FR

If $\Omega_{FR} \neq 0$
- Oxygen needed in oxygen polishing step with respect to the required to burn the solid fuel converted in the fuel reactor
- Depends on elutriation and on carbon capture efficiency

4080

4081 **Fig. 24.** Flow chart including the oxygen flows necessary to determine the combustion

4082 efficiency in a CLC system with solid fuels.

4083

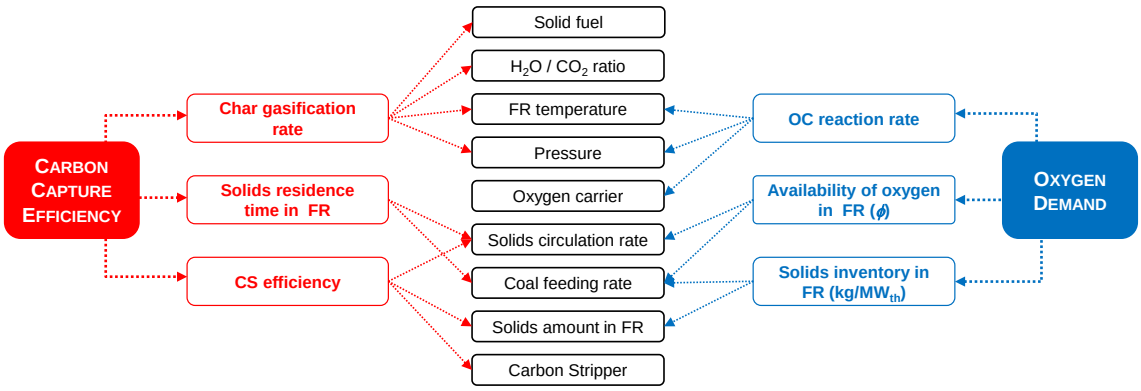

Fig. 25. Scheme of the main variables influencing the CO_2 capture efficiency and oxygen demand.

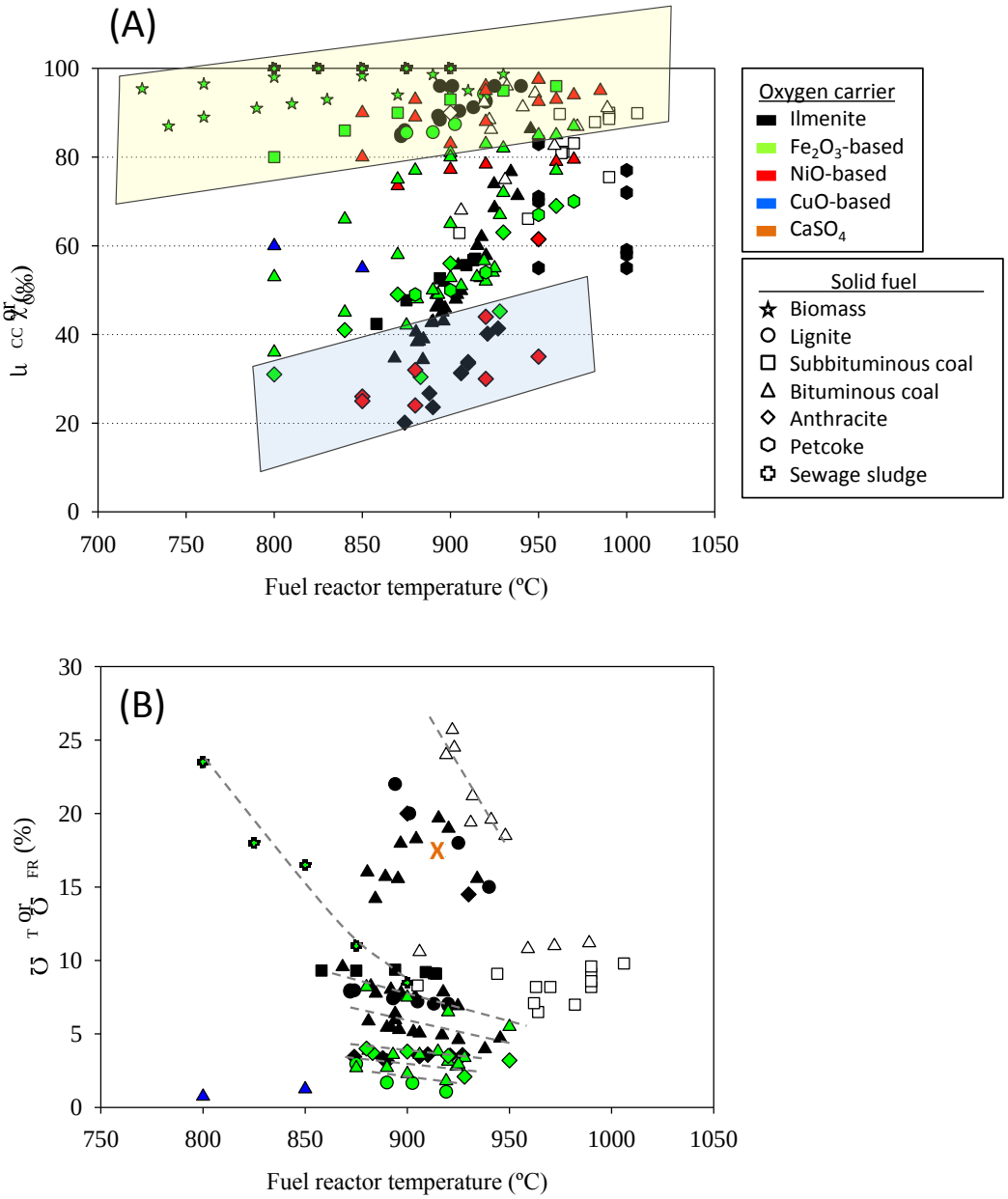

4096

4097 **Fig. 26.** Carbon capture efficiency and oxygen demand at different fuel reactor

4098 temperatures. S**ymbols:** Empty=with CS, Filled=without CS. **References:** Ilmenite

4099 [115, 124, 136, 137, 145, 146, 148, 159, 200]; Fe_2O_3-based [39, 101, 127, 129, 132,

4100 140, 201]; NiO-based [38, 126, 202]; CuO-based [149]; $CaSO_4$ [163]. Interactive plots

4101 available in the web version of the paper.

4102 • *This figure includes 4 interactive plots in the web version of the paper. (*Fig
4103 26A_1.csv, Fig 26A_2.csv, Fig 26B_1.csv, Fig 26B_2.csv).
4104

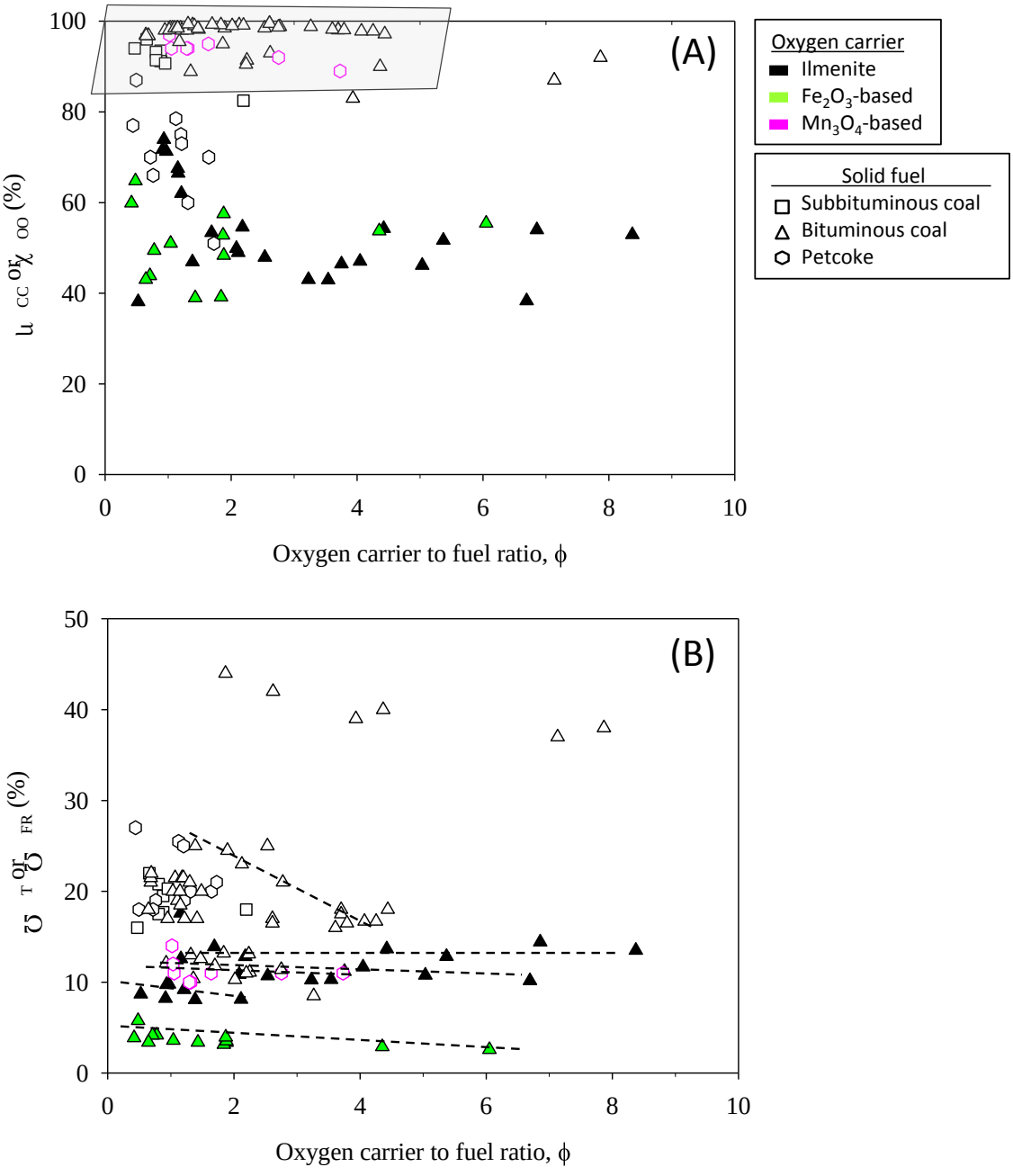

Fig. 27. Carbon capture efficiency and oxygen demand at different oxygen carrier to fuel ratios.. S**ymbols:** Empty=with CS, Filled=without CS. **References:** Ilmenite [36, 115, 118, 122, 123, 138, 146] Fe_2O_3-based [140] Mn_3O_4-based [115]. Interactive plots available in the web version of the paper.

- *This figure includes 2 interactive plots in the web version of the paper.* (Fig 27A.csv, Fig 27B.csv).

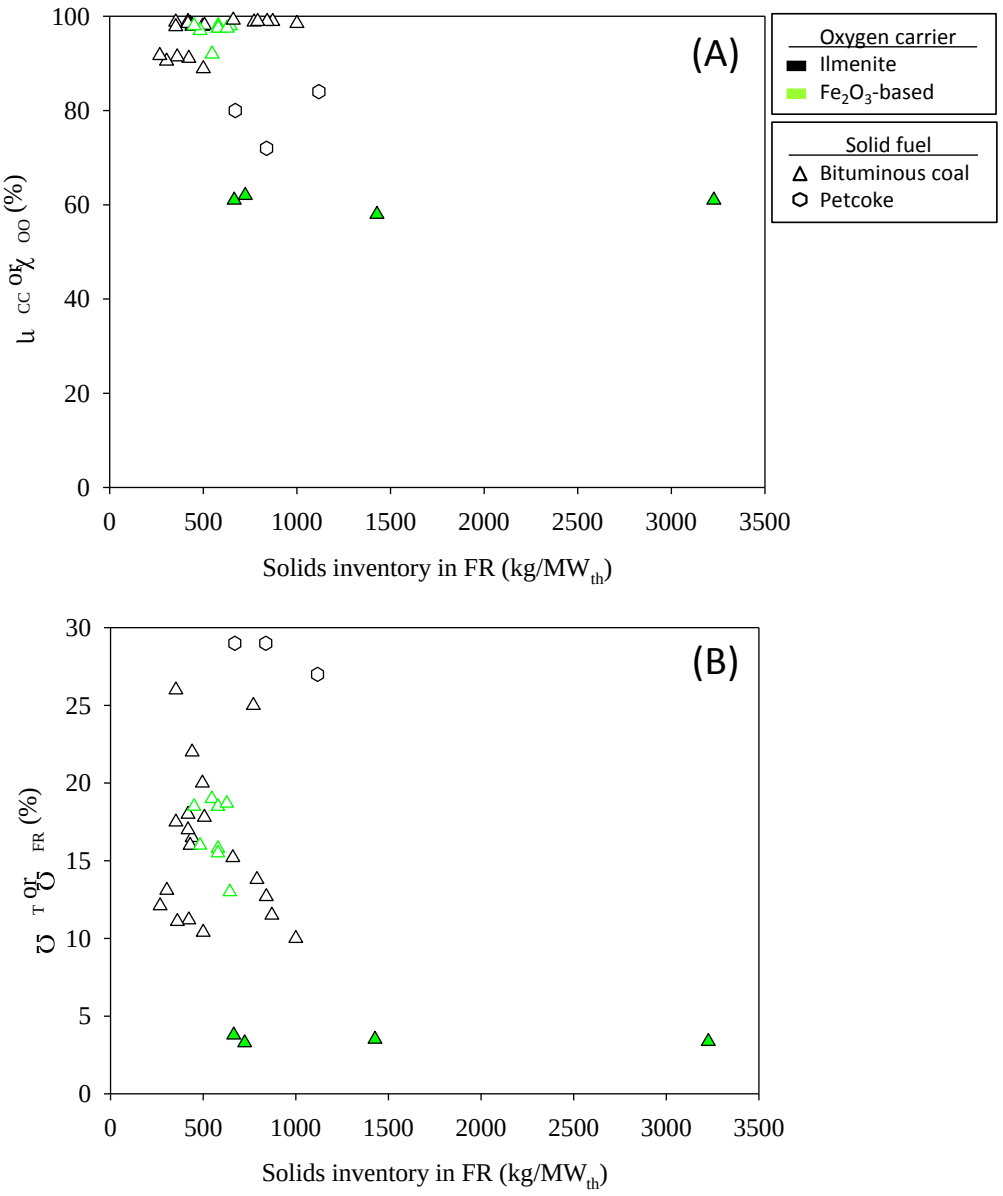

Fig. 28. Carbon capture efficiency and oxygen demand as a function of the solids inventory in the fuel reactor**. Symbols**: Empty=with CS; Filled=without CS. **References:** Ilmenite [119, 122, 123, 146]; Fe_2O_3-based [100, 140]. Interactive plots available in the web version of the paper.

*This figure includes 2 interactive plots in the web version of the paper. (*Fig 28A.csv, Fig 28B.csv).

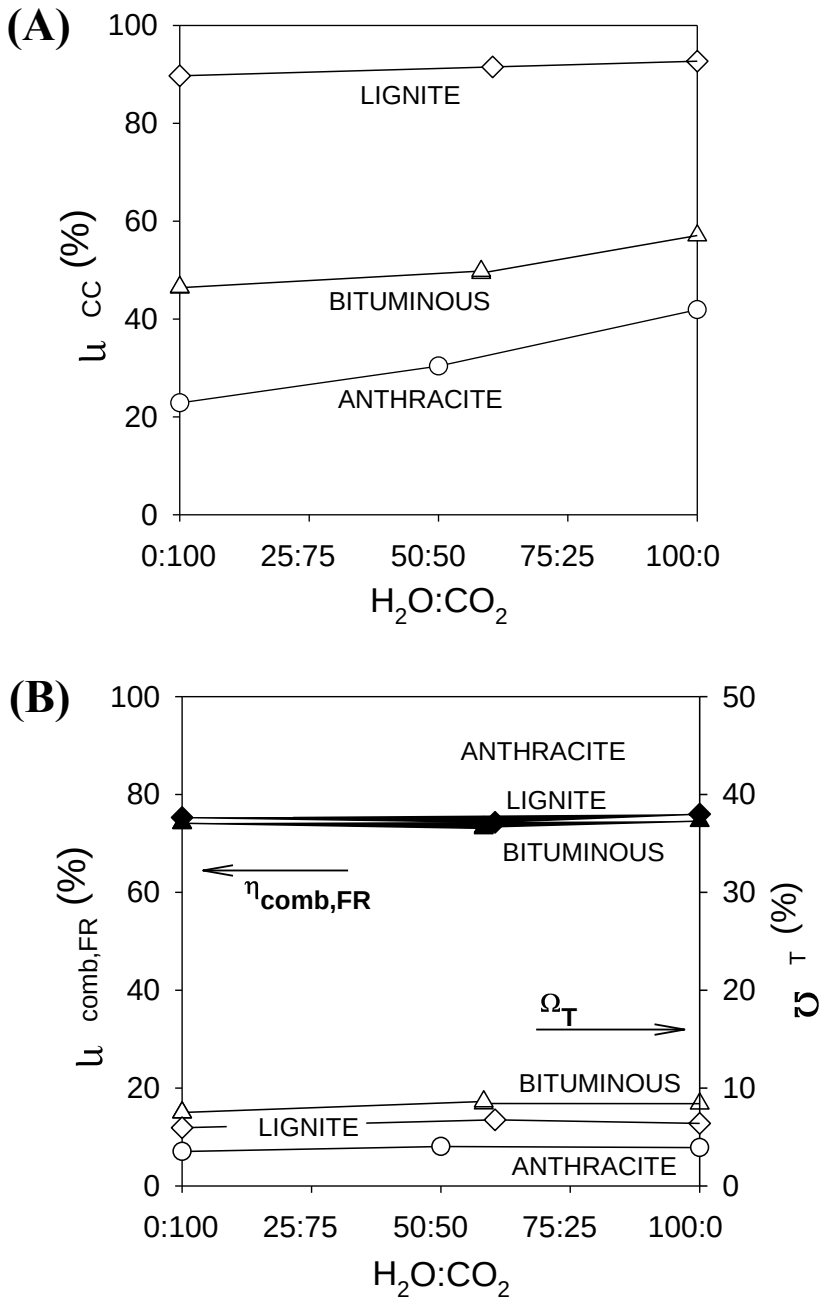

Fig. 29. Effect of the composition of the gasifying agent on (A) the CO_2 capture efficiency (η_{CC}) and (B) the combustion efficiency in the fuel reactor ($\eta_{comb,FR}$) and the oxygen demand (Ω_T). Adapted from Ref. [137].

4129

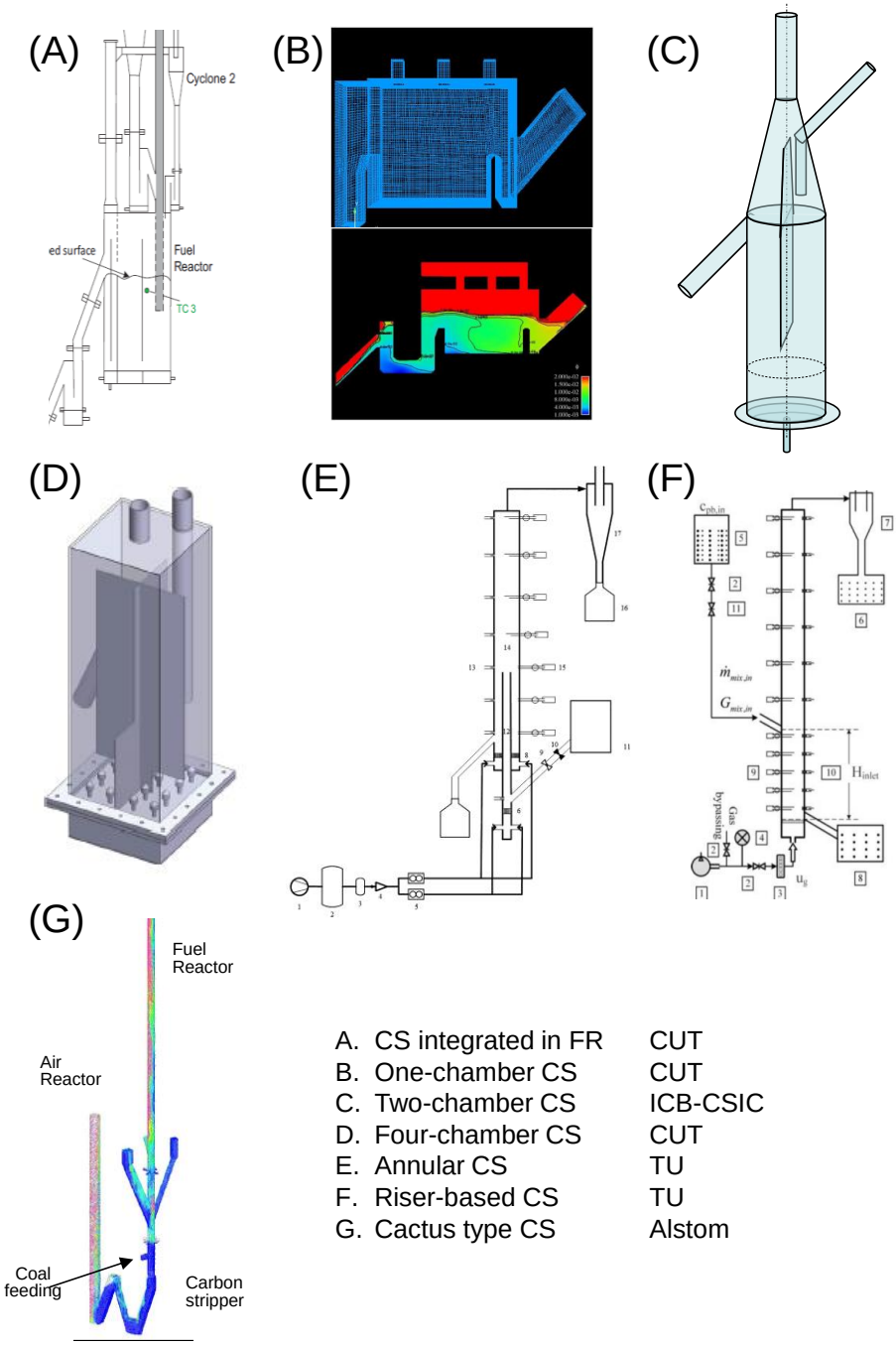

A.	CS integrated in FR	CUT
B.	One-chamber CS	CUT
C.	Two-chamber CS	ICB-CSIC
D.	Four-chamber CS	CUT
E.	Annular CS	TU
F.	Riser-based CS	TU
G.	Cactus type CS	Alstom

4130

4131 **Fig. 30.** Different designs for the carbon stripper. (A) Adapted from Ref. [57], (B)
4132 Reprinted from Ref. [43] (C) Adapted from Ref. [144] (D) Reprinted from Ref. [123]
4133 with permission of Elsevier, (E) Reprinted from Ref. [249] with permission of ACS, (F)
4134 Reprinted from Ref. [51] with permission of ACS, (G) Adapted from Ref. [43].

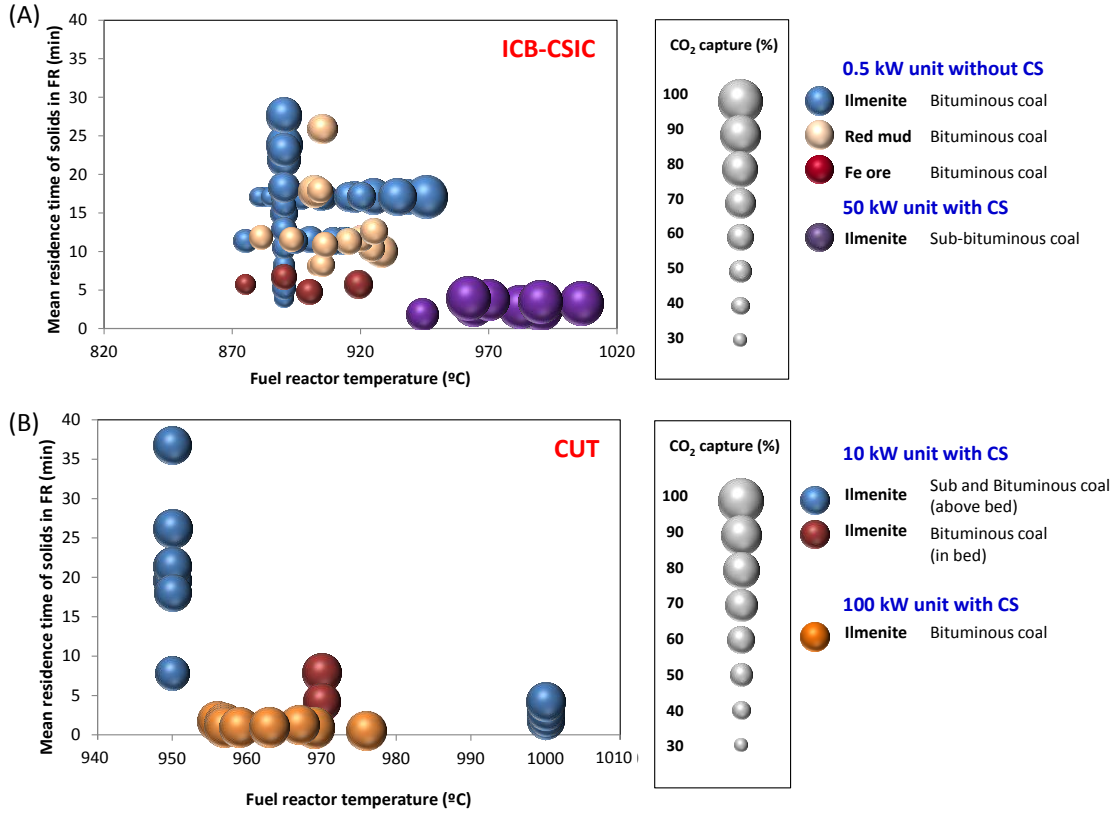

Fig. 31. Carbon capture as a function of the temperature and the mean residence time of solids in the fuel reactor. (A) 0.5 and 50 kW_{th} at ICB-CSIC, and (B) 10 and 100 kW_{th} at CUT. Selected data from Table 4.

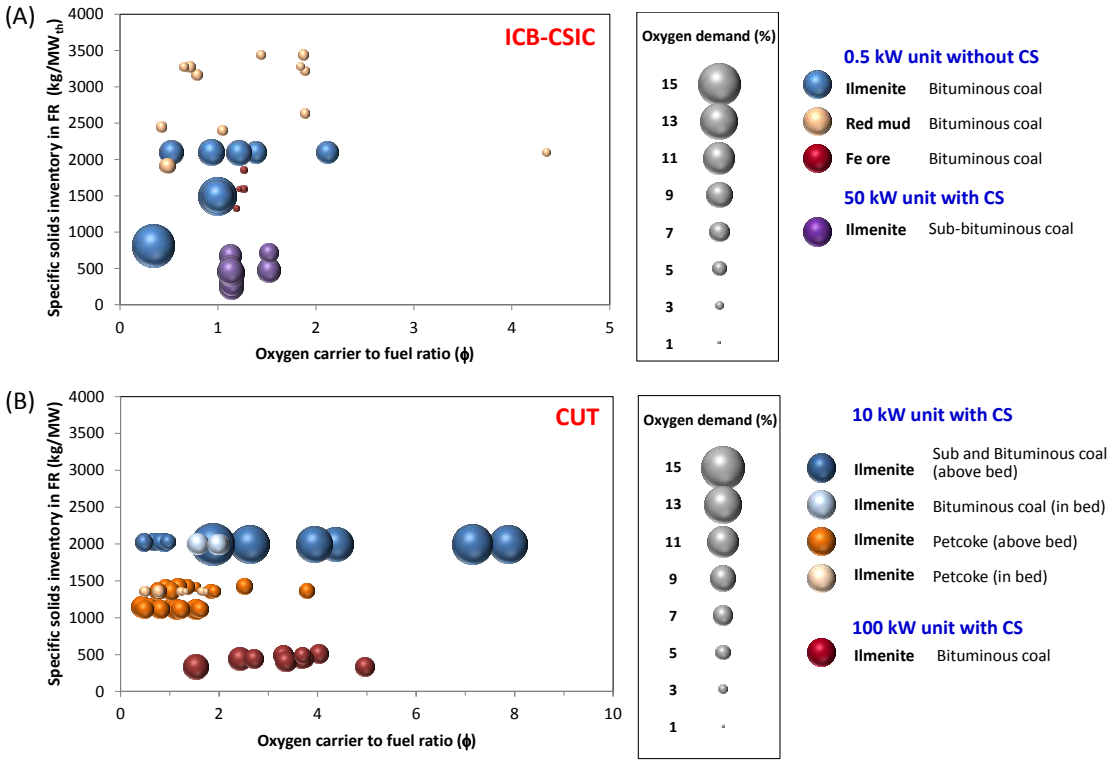

Fig. 32. Total oxygen demand as a function of the specific solids inventory and the oxygen carrier to fuel ratio. (A) 0.5 and 50 kW_{th} at ICB-CSIC, and (B) 10 and 100 kW_{th} at CUT. Selected data from Table 4.

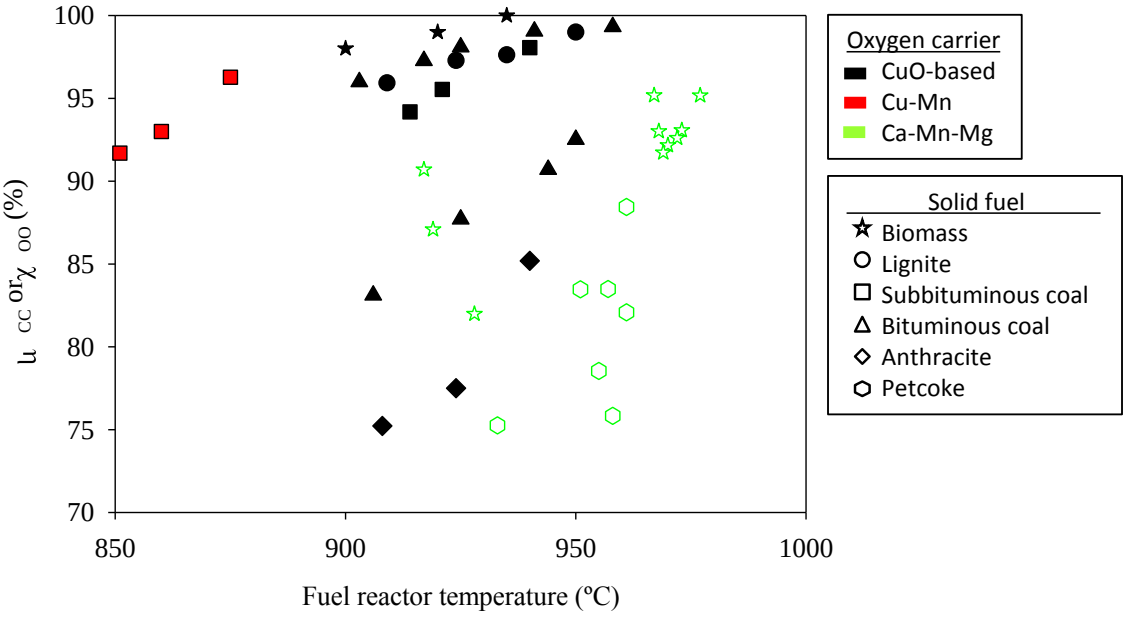

Fig. 33. Carbon capture efficiency at different fuel reactor temperatures for CLOU**.** **Symbols:** Empty=with CS, Filled=without CS. **References:** [57, 58, 88, 117, 142, 143, 252].

- *This figure includes an interactive plot in the web version of the paper. (*Fig 33.csv).

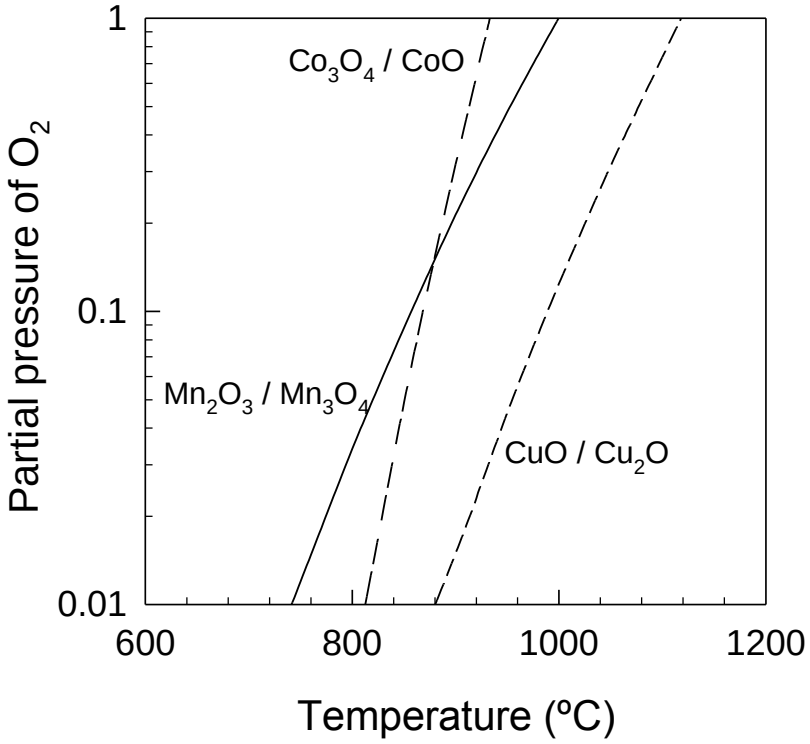

Fig. 34. Oxygen concentration at gas-solid equilibrium for different redox pairs used in the CLOU process. Adapted from Ref. [59].

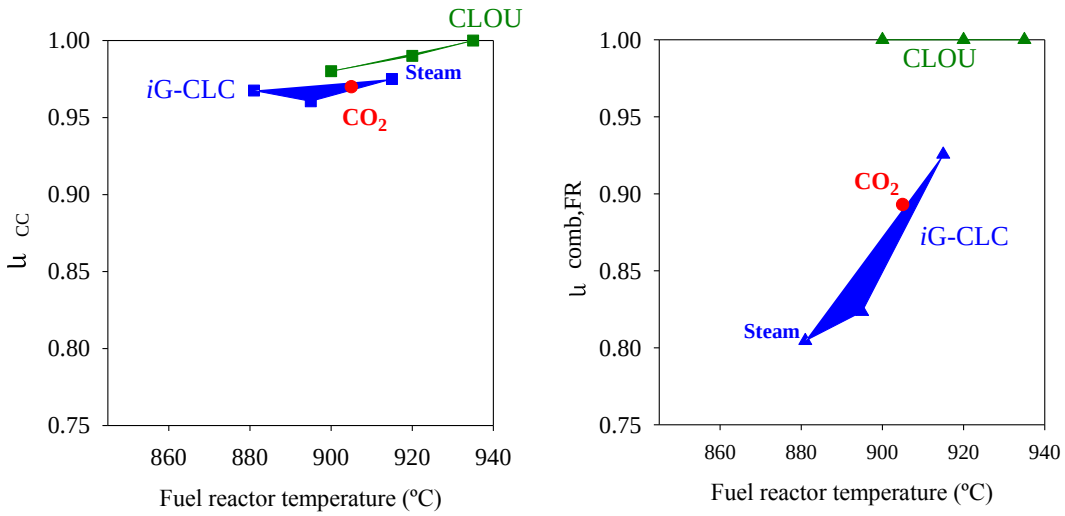

Fig. 35. Performance of CLC units burning biomass under *i*G-CLC or CLOU mode. Reprinted from Ref. [56] with permission of Wiley.

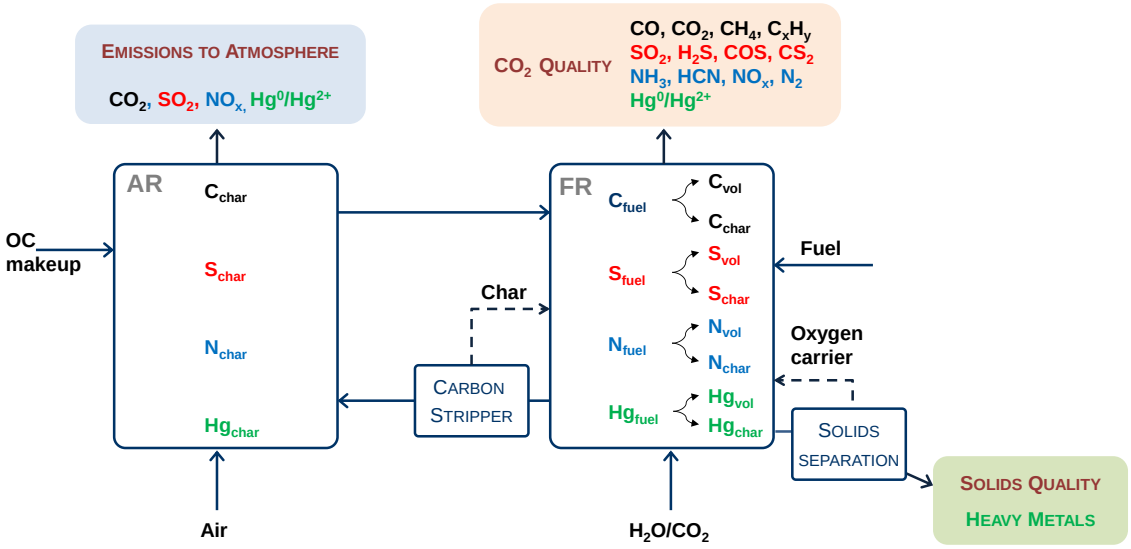

Fig. 36. Scheme of pollutant formation in the CLC process with solid fuels.

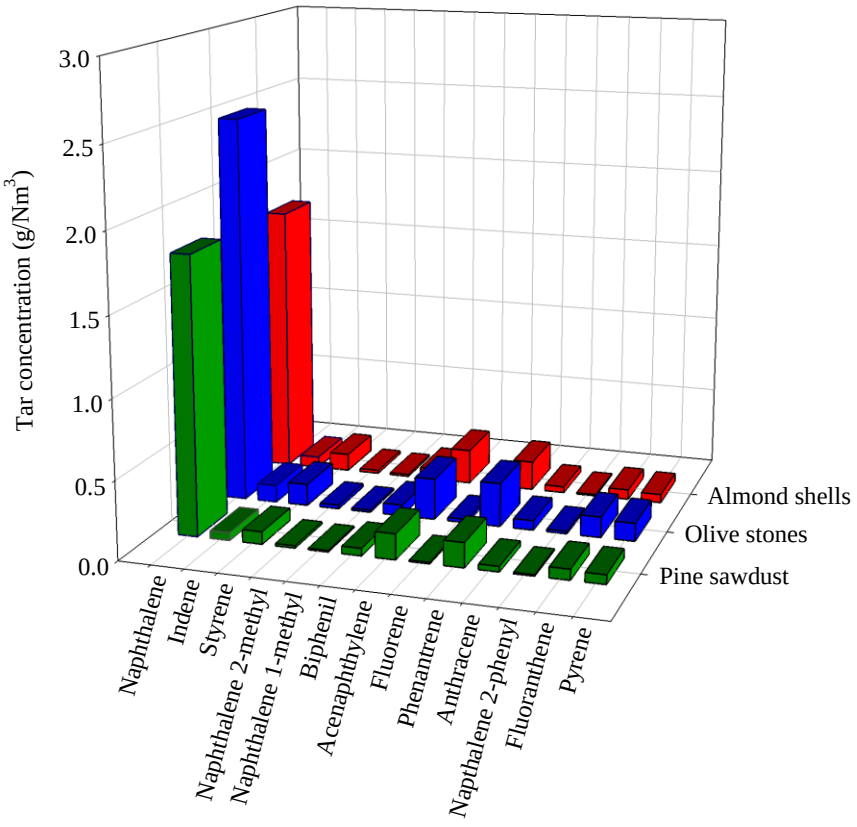

Fig. 37. Tar composition for different biomasses. T= 980 ºC. Adapted from Ref. [141].

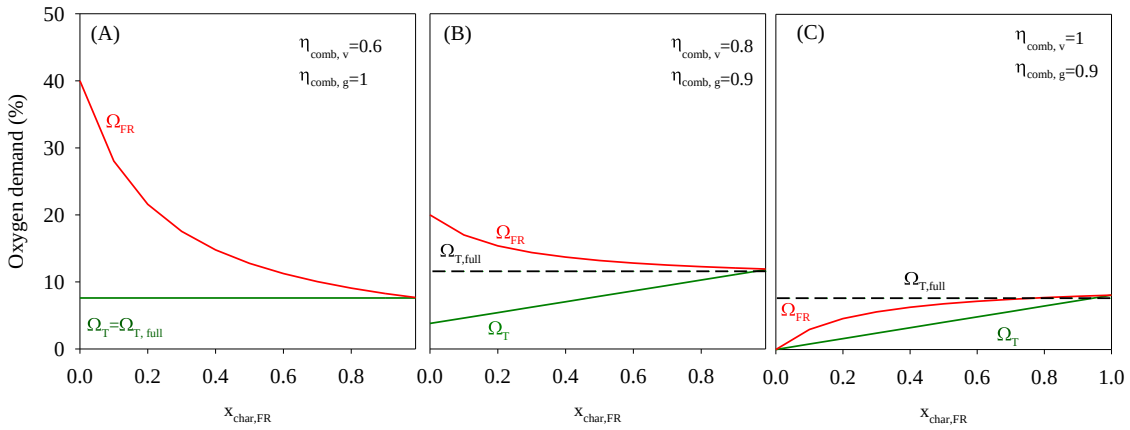

Fig. 38. Ω_{FR} and Ω_T for different values of the carbon fraction in char gasified in the fuel reactor. Dashed line represents the oxygen demand level considering complete conversion of the solid fuel. Colombian bituminous coal is considered as fuel in all the Figure; see Table 9.

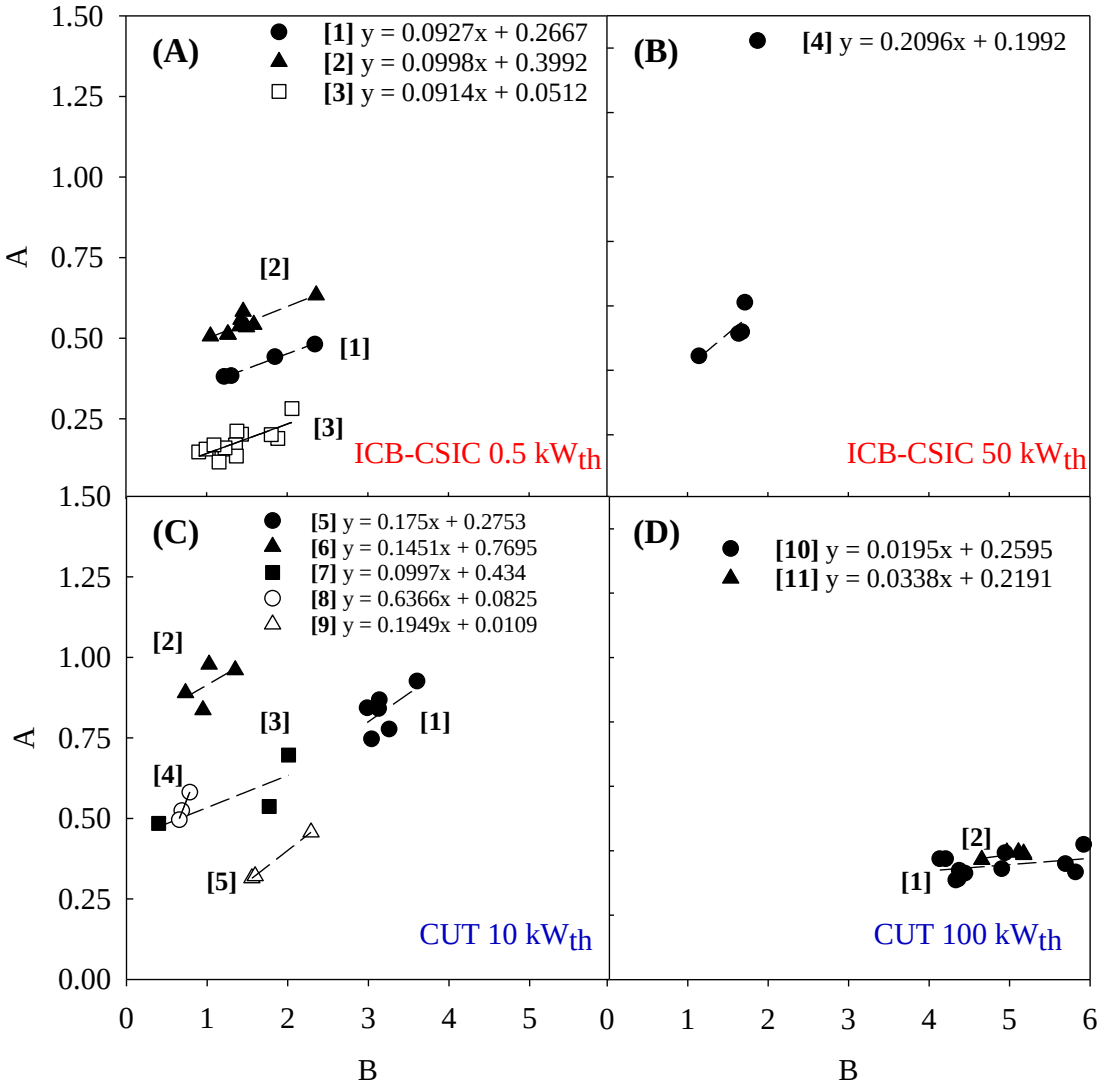

Fig. 39. Determination of combustion efficiency of the volatiles released ($\eta_{comb,v}$) and char gasification products ($\eta_{comb,g}$) following Eq.(17) and using data from different CLC units:

[1] = ilmenite and bituminous coal (125-200 μm) [136]
[2] = bauxite waste and bituminous coal (200-300 μm) [140]
[3] = ilmenite and bituminous coal [115]
[4] = ilmenite and petcoke [115, 119]
[5] = ilmenite and petcoke In-bed feeding [115]
[6] = ilmenite and bituminous coal (200-300 μm) [285]
[7] = ilmenite and wood char [121]
[8] = ilmenite and wood char [121]
[9] = ilmenite and bituminous coal [120]

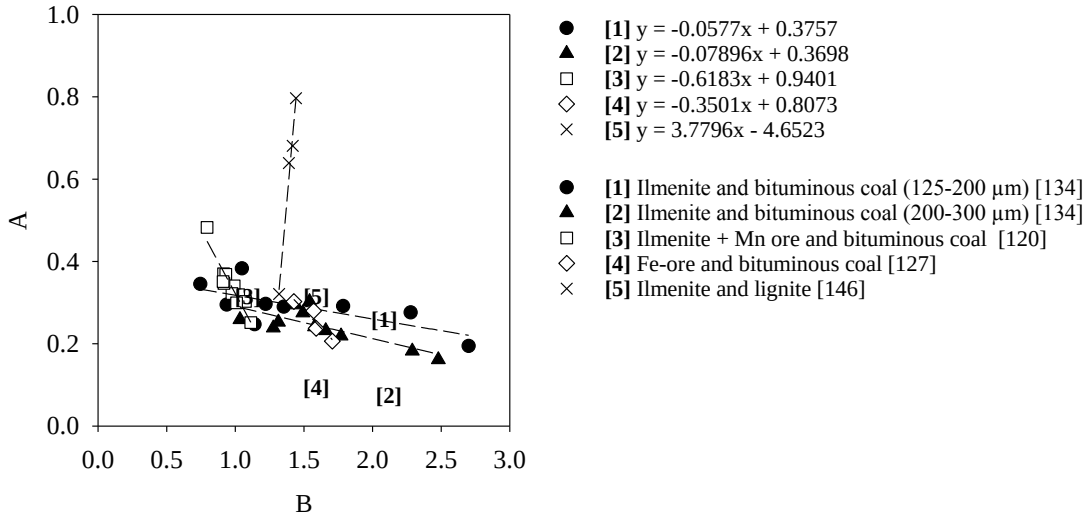

Fig. 40. Determination of combustion efficiency of the volatiles released ($\eta_{comb,v}$) and char gasification products ($\eta_{comb,g}$) following Eq. (17) and using data for combustion experiments of bituminous coals in the ICB-CSIC 0.5 kW_{th} unit (bubbling bed fuel reactor) and CUT 100 kW_{th} unit (high velocity fuel reactor).

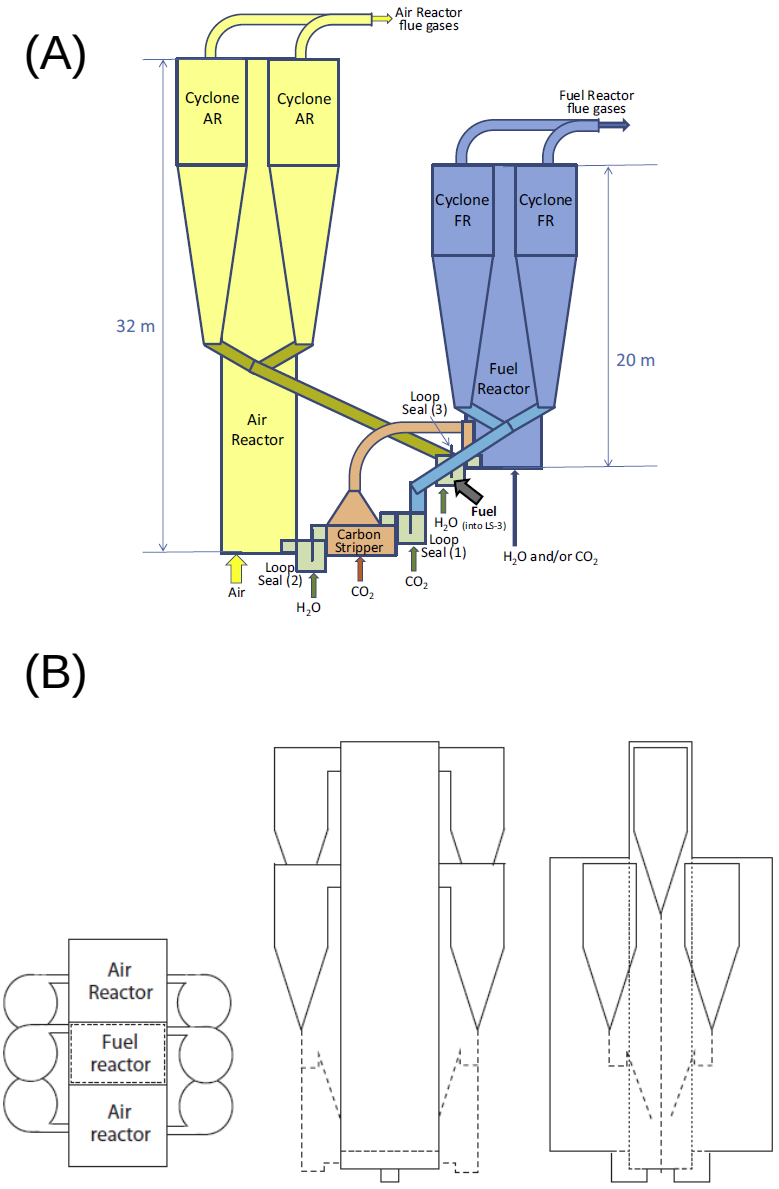

Fig. 41. Scheme of the design of a CLC unit based on a CFB fuel reactor. (A) 100 MW_{th}. Reprinted from Ref. [244] with permission of Elsevier, and (B) 1000 MW_{th}. Reprinted from Ref. [4] with permission of Elsevier.

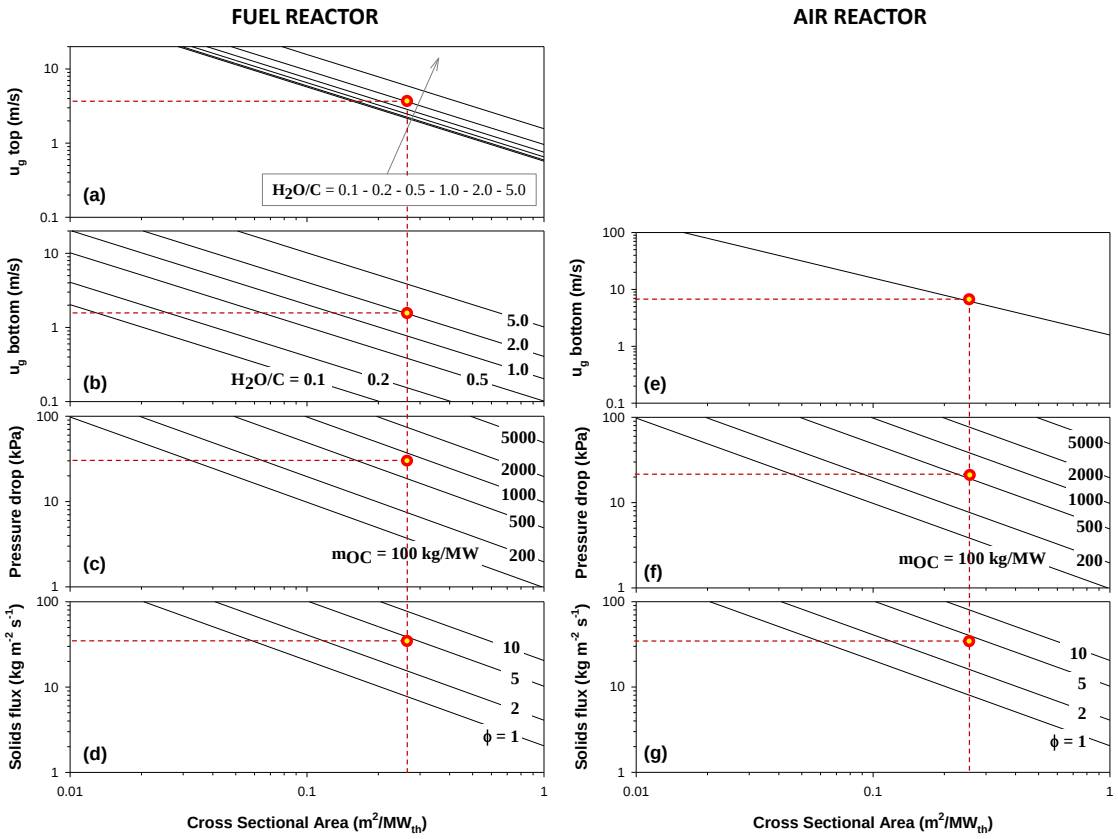

Fig. 42. Map of the design of CFB-based fuel and air reactors. Reprinted from Ref. [244] with permission of Elsevier.

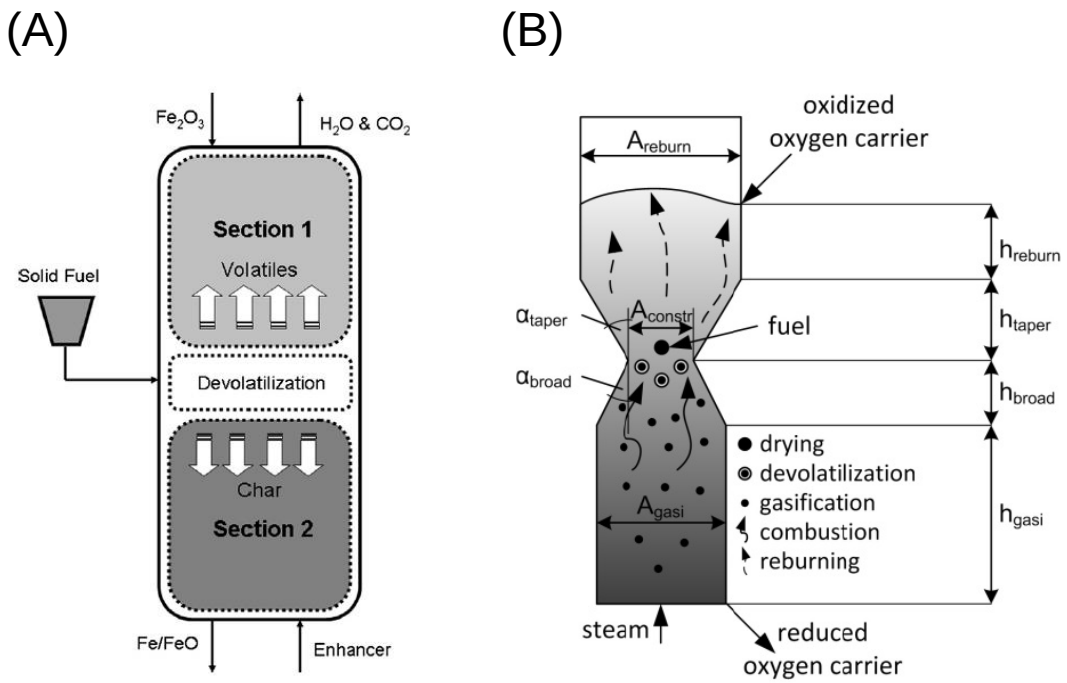

Fig. 43. Scheme of the design of a CLC unit based on a moving bed fuel reactor. (A) Two-stage counter-current moving bed reducer. Reprinted from Ref. [53] with permission of Elsevier, and (B) Shape of the moving bed fuel reactor. Reprinted from Ref. [182].

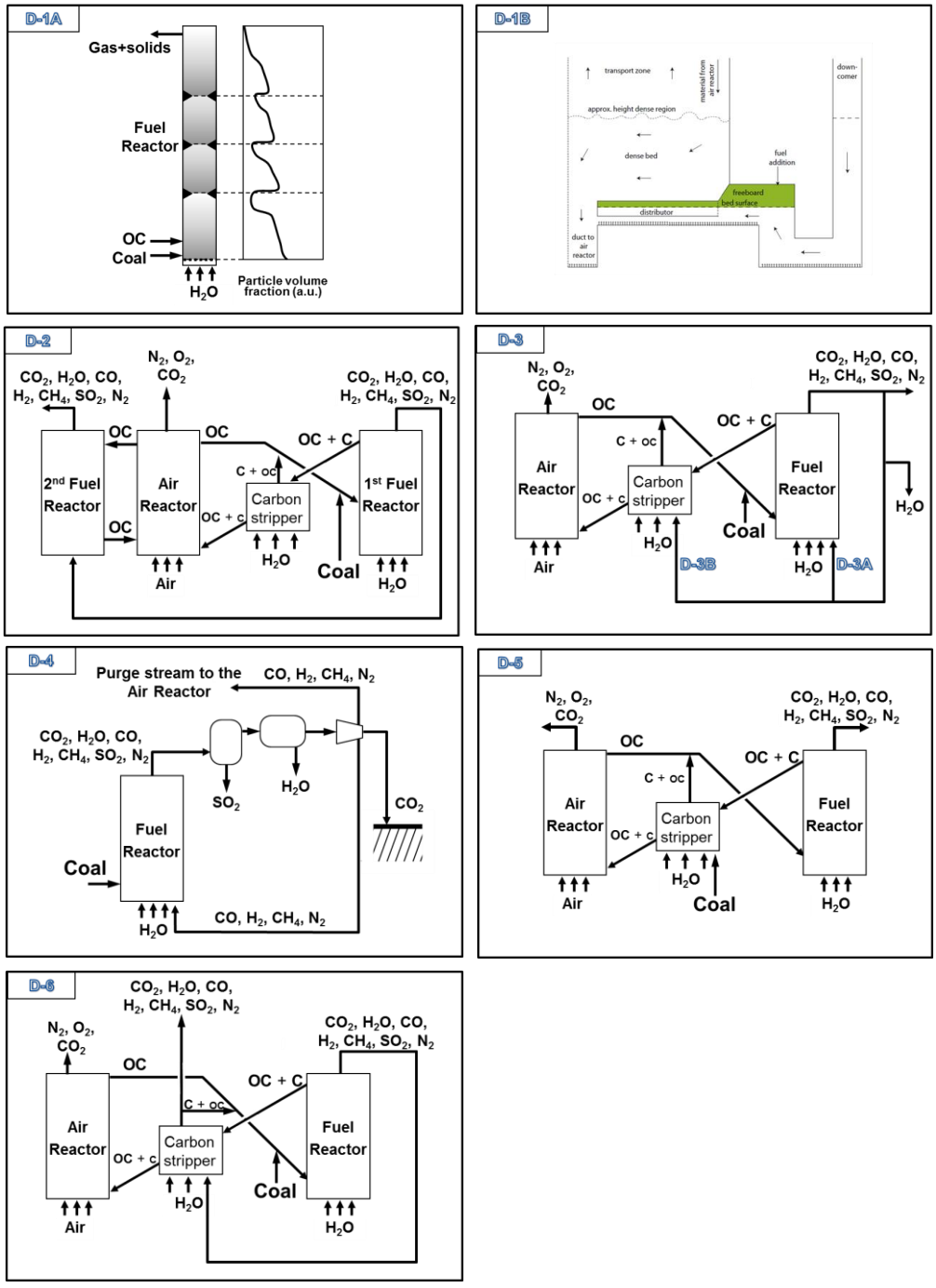

Fig. 44. Diagrams of the different configurations for the improvement of the *i*G-CLC process implementing different technological solutions. Adapted from Ref. [52] and Ref. [4].

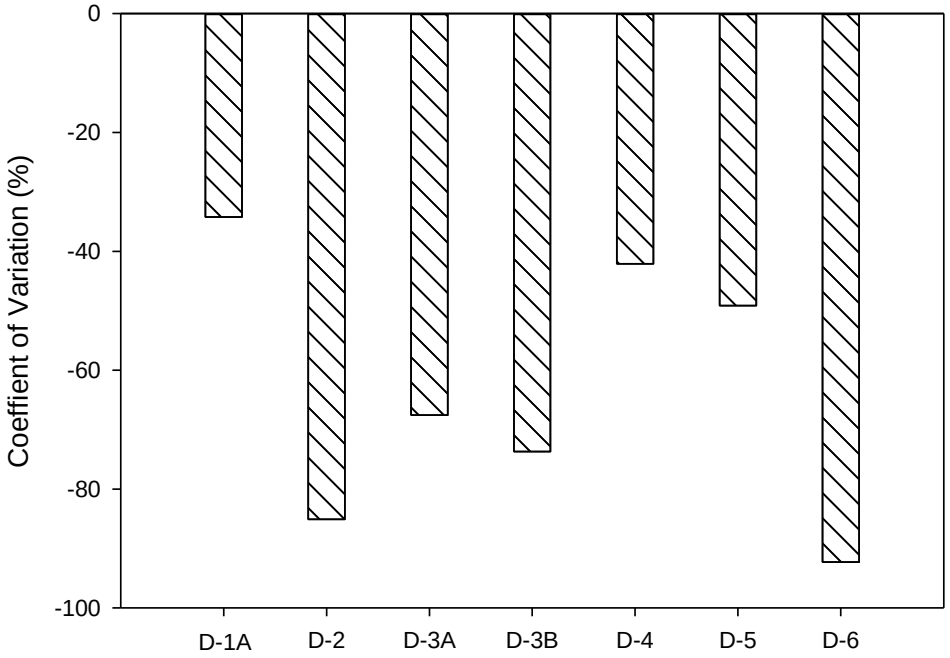

Fig. 45. Coefficient of variation, CV, for the oxygen demand predicted for different *iG*-CLC configurations. Adapted from Ref. [52].

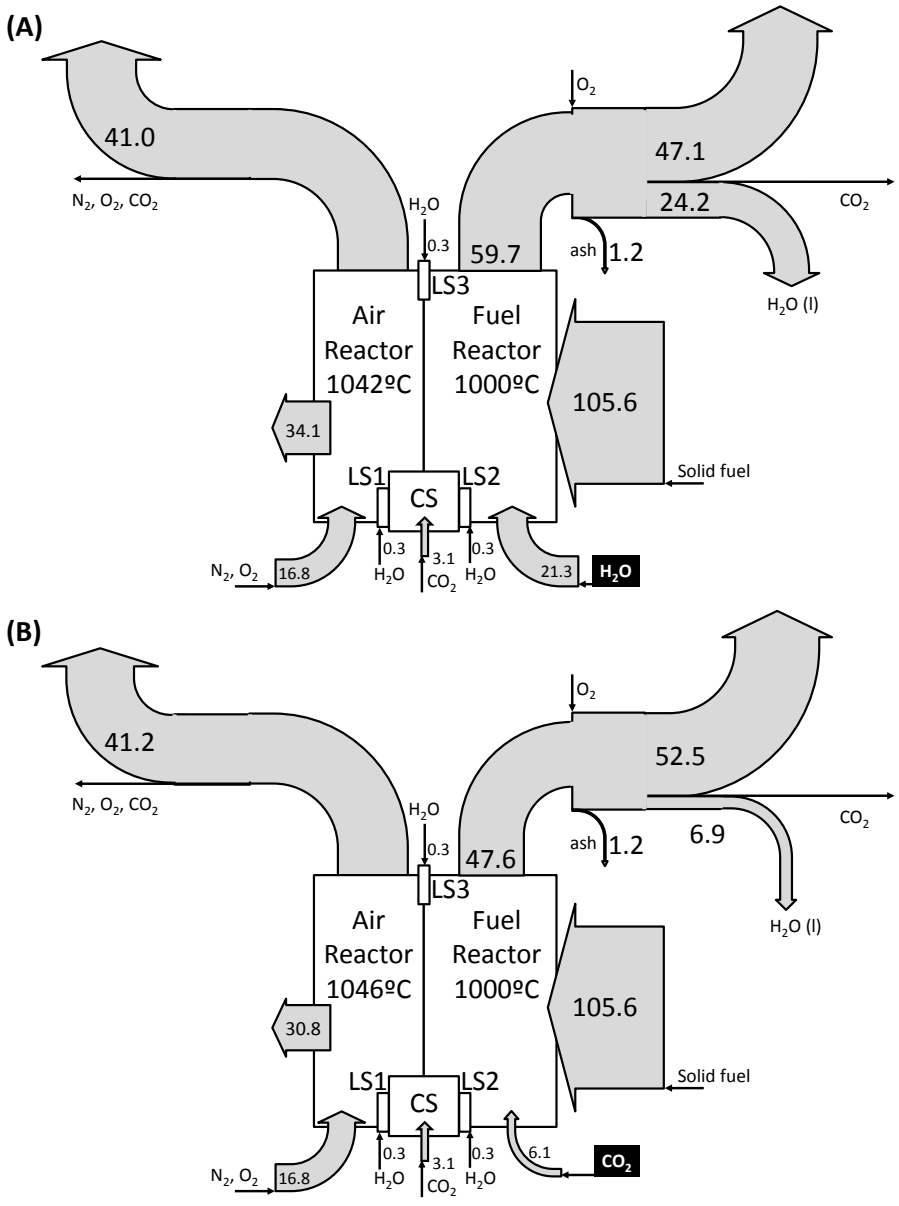

Fig. 46. Simplified Sankey diagrams with enthalpy flows to and from the iG-CLC system with the fluidization agent (A) H_2O or (B) CO_2. Reprinted from [244] with permission of Elsevier.

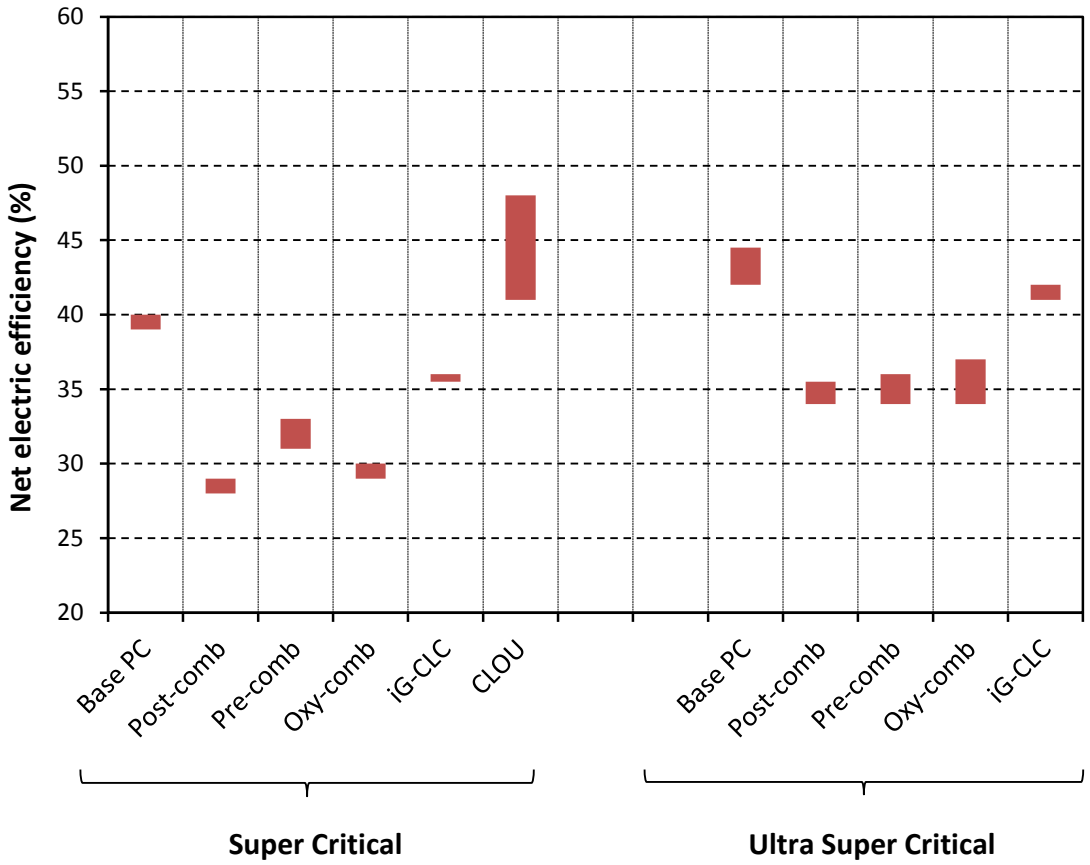

Fig. 47. Net power efficiency (LHV) in electricity generation by different coal-feed power technologies. Adapted from [317].

List of Tables

Table 1. Summary of the chemical reactions for the oxygen carriers in solid fuel CLC.

Process	Oxygen carrier	Redox pair	FR reactions	AR reaction
***i*G-CLC**	Ilmenite	$FeTiO_3/Fe_2TiO_5$	$Fe_2TiO_5 + TiO_2 + H_2 \rightarrow 2\ FeTiO_3 + H_2O$ $Fe_2TiO_5 + TiO_2 + CO \rightarrow 2\ FeTiO_3 + CO_2$ $4\ Fe_2TiO_5 + 4\ TiO_2 + CH_4 \rightarrow 8\ FeTiO_3 + CO_2 + 2H_2O$	$4\ FeTiO_3 + O_2 \rightarrow 2\ Fe_2TiO_5 + 2\ TiO$
	Iron ore	Fe_2O_3/Fe_3O_4	$3\ Fe_2O_3 + H_2 \rightarrow 2\ Fe_3O_4 + H_2O$ $3\ Fe_2O_3 + CO \rightarrow 2\ Fe_3O_4 + CO_2$ $12\ Fe_2O_3 + CH_4 \rightarrow 8\ Fe_3O_4 + CO_2 + 2H_2O$	$4\ Fe_3O_4 + O_2 \rightarrow 6\ Fe_2O_3$
	Manganese ore	Mn_2O_3/MnO	$3\ Mn_3O_4 + H_2 \rightarrow 2\ MnO + H_2O$ $3\ Mn_3O_4 + CO \rightarrow 2\ MnO + CO_2$ $4\ Mn_3O_4 + CH_4 \rightarrow 12\ MnO + CO_2 + 2\ H_2O$	$3\ MnO + ½\ O_2 \rightarrow Mn_3O_4$
	$CaSO_4$	$CaSO_4/CaS$	$CaSO_4 + 4\ H_2 \rightarrow CaS + 4\ H_2O$ $CaSO_4 + 4\ CO \rightarrow CaS + 4\ CO_2$ $CaSO_4 + CH_4 \rightarrow CaS + CO_2 + 2\ H_2O$	$CaS + 2\ O_2 \rightarrow CaSO_4$
CLOU	Copper oxide	CuO/Cu	$4\ CuO \rightarrow 2\ Cu_2O + O_2$ $Char + O_2 \rightarrow CO_2$ $Gaseous\ fuels\ (H_2, CO, CH_4) + O_2 \rightarrow CO_2 + H_2O$	$2\ Cu_2O + O_2 \rightarrow 4\ CuO$
	Manganese oxide	Mn_2O_3/Mn_3O_4	$6\ Mn_2O_3\ (s) \rightarrow 4\ Mn_3O_4\ (s) + O_2\ (g)$	$2\ Mn_3O_4 + ½\ O_2 \rightarrow 3\ Mn_2O_3$
	Mn-Cu mixed oxide	$Cu_{1.5}Mn_{1.5}O_4/CuMnO_2$	$2\ Cu_{1.5}Mn_{1.5}O_4 \rightarrow 3\ CuMnO_2 + O_2\ (g)$	$3\ CuMnO_2 + O_2 \rightarrow 2\ Cu_{1.5}Mn_{1.5}O_4$
	Ca-Mn mixed oxide	$CaMn_{0.9}Mg_{0.1}O_{3-\delta}/CaMn_{0.9}Mg_{0.1}O_{3-\gamma}$	$CaMn_{0.9}Mg_{0.1}O_{3-\delta} \leftrightarrow CaMn_{0.9}Mg_{0.1}O_{3-\gamma} + \frac{\gamma-\delta}{2} O_2$ $(\gamma\text{-}\delta)\ H_2 + CaMn_{0.9}Mg_{0.1}O_{3-\delta} \rightarrow CaMn_{0.9}Mg_{0.1}O_{3-\gamma} + (\gamma\text{-}\delta)\ H_2O$ $(\gamma\text{-}\delta)\ CO + CaMn_{0.9}Mg_{0.1}O_{3-\delta} \rightarrow CaMn_{0.9}Mg_{0.1}O_{3-\gamma} + (\gamma\text{-}\delta)\ CO_2$ $(\gamma\text{-}\delta)CH_4 + 4CaMn_{0.9}Mg_{0.1}O_{3-\delta} \rightarrow 4\ CaMn_{0.9}Mg_{0.1}O_{3-\gamma} + (\gamma\text{-}\delta)\ CO_2 + (\gamma\text{-}\delta)\ H_2O$	$CaMn_{0.9}Mg_{0.1}O_{3-\gamma} + \frac{\gamma-\delta}{2} O_2 \leftrightarrow CaMn_{0.9}Mg_{0.1}O_{3-\delta}$
CL*a*OU	Fe-Mn mixed oxide	$(Mn_xFe_{1-x})_2O_3/(Mn_xFe_{1-x})_3O_4$	$6\ (Mn_xFe_{1-x})_2O_3 \leftrightarrow 4\ (Mn_xFe_{1-x})_3O_4 + O_2\ (g)$	$4\ (Mn_xFe_{1-x})_3O_4 + O_2 \leftrightarrow 6\ (Mn_xFe_{1-x})_2O_3$
		$(Mn_xFe_{1-x})_3O_4/Mn_xFe_{1-x}O$	$(Mn_xFe_{1-x})_3O_4 + H_2 \rightarrow 3\ Mn_xFe_{1-x}O + H_2O$ $(Mn_xFe_{1-x})_3O_4 + CO \rightarrow 3\ Mn_xFe_{1-x}O + CO_2$ $4\ (Mn_xFe_{1-x})_3O_4 + CH_4 \rightarrow 12\ Mn_xFe_{1-x}O + CO_2 + 2\ H_2O$	$6\ Mn_xFe_{1-x}O + O_2 \rightarrow 2\ (Mn_xFe_{1-x})_3O_4$

Table 2. Summary of the main properties for the oxygen carriers used in solid fuel CLC.

Process	Oxygen carrier	Oxygen transport capacity, R_{OC}	Mechanical strength	Lifetime	Rate Index[a]				Kinetics	Activation with redox cycles	Refs.
					H_2	CO	CH_4	O_2			
		(%)	(N)	(h)	(%/min)						
*i*G-CLC	Ilmenite	2.1-4	1.0-2.2	700-1300	7.9	2.5	5.0	9.7	Yes	Yes	[95-97]
	Iron ore	2.5	5.8	280-1000	12.4	3.4	3.3	5.5	Yes	Yes	[98-101]
	Manganese ore	1.25-5.8	1-4.6	150-1600	1.3-26.4	5.1-9	0.9-12.7	8.4-11.3	Yes	No	[92, 102-105]
	$CaSO_4$	16.7	-	-	-	-	-	-	Yes	Yes	[106-111]
CLOU	Copper oxide	6	2.4	-	-	-	-	-	Yes	No	[68, 112]
	Mn-Cu mixed oxide	4	1.9	-	-	-	-	-	No	-	[88]
	Ca-Mn mixed oxide	9.4	1.2	1100	-	-	-	-	Yes	No	[16, 113]
CL*a*OU	Fe-Mn mixed oxide	9.6	2.7	400	12.2	3.3	2.5	8.4	No	No	[89]

[a] Normalized reaction rate at gas concentration of 15% and T =950 ºC.

353

354 **Table 3.** Summary of chemical-looping units for solid fuels in operation and upcoming.

	Center / Company	Initial	Location	Operation year	Configuration	Power (kW_{th})	Fuel	Oxygen carrier	Operation time (h)	References
1	Chalmers University of Technology	CUT	Goteborg (Sweden)	2008	CFB-BFB	10	Coal, petcoke, biochar	Ilmenite, Mn ore, perovskites	253	[36, 37, 54, 114-119]
2				2012	CFB-CFB	100	Ilmenite, Iron ore	Coal, petcoke, biochar	116	[100, 120-124]
3	Southeast University	SU	Nanjing (China)	2009	CFB-spouted bed	10	Coal, biomass	NiO, Fe_2O_3	130	[38, 39, 125]
4				2010	CFB-spouted bed	1	Coal, biomass, sewage sludge	Hematite	260	[126-134]
5				2012	CFB-CFB	50	Coal	Iron ore	19	[135]
6	Instituto de Carboquímica	ICB-CSIC	Zaragoza (Spain)	2011	BFB-BFB	1.5	Coal, biomass	Ilmenite, bauxite waste, iron ore, Fe-Mn oxides, CuO and Cu-Mn oxide	450	[55, 58, 79, 101, 136-143]
7				2014	CFB-CFB	50	Coal	Ilmenite	50	[144-146]
8	IFP Energies Nouvelles	IFPEN	Solaize (France)	2012	BFB-BFB-BFB	10	Coal	Natural ore (BMP)	52	[147]
9	Hamburg University of Technology	TUHH	Hamburg (Germany)	2012	CFB-BFB	25	Coal	Ilmenite, CuO	80	[148, 149]
10	Western Kentucky University	WKU	Bowling Green (USA)	2012	CFB-BFB	10	Biomass	CuO	240	[150]
11	Ohio State University	OSU	Columbus (USA)	2012	Moving-bed-Entrained bed	25	Coal, metallurgical coke, biomass	Fe_2O_3	> 680	[53, 151-153]
12				2012	Moving-bed-Entrained bed	2.5	Coal	Fe_2O_3	300	[53, 151]
13	CAS Key Laboratory of Renewable Energy (Guangzhou Institute of Energy Conversion)	GIEC	Guangzhou (China)	2014	CFB-BFB	10	Biomass	Fe_2O_3, Fe-Ni oxides	>60	[154, 155]
14	State Key Laboratory of Coal Combustion (Huazhong	HUST	Wuhan (China)	2015	CFB-CFB	5	Coal	Hematite	6	[156]

	University of Science and Technology)									
15				2016	CFB-BFB	50	Coal	Iron ore	-	[157]
16	VTT Technical Research Centre	VTT	Espoo (Finland)	2015-2016	CFB-BFB	10-50	Biomass	Ilmenite	16	[158]
17	Darmstadt University of Technology	TUD	Darmstadt (Germany)	2012	CFB-CFB	1000	Coal, biomass	Ilmenite, iron ore	>100	[42, 159-161]
18	Alstom		Bloomfield (USA)	2011	CFB-CFB	3000	Coal	Limestone	> 500	[43, 44, 162-164]
19	Chalmers University of Technology	CUT	Goteborg (Sweden)	2016	CFB	4000	Biomass	Ilmenite, manganese ore	1000	[165, 166]
20	Japan Coal Energy Center	JCOAL	Tokyo (Japan)	2017	CFB-CFB	100	-	-	-	[167]
21	University of Utah	UU	Salt Lake City (USA)	2017	CFB-CFB	225	-	-	-	[168, 169]
22	Babcock & Wilcox	B&W	-	2017	Moving bed – Entrained bed	250	-	-	-	[170]

Table 4. Experimental conditions for CO_2 capture efficiency and oxygen demand from different *i*G-CLC continuous units.

No.	Name	Nominal power (kW)	OC	Fuel	FR design	T (ºC)	ϕ	m_{OC} (kg/MW_{th})	X_{sf} (%)	Carbon capture η_{CC} (%)	Carbon capture χ_{OO} (%)	Oxygen demand Ω_{FR} (%)	Oxygen demand Ω_T (%)	Ref.
1	CUT	10	Ilmenite	Bit. Coal	Bubbling	950	0.5-2.2	1850-2940	50-80	82.5-96	83-93	16-22	*n.a.*	[36]
2	CUT	10	Ilmenite	Petcoke	Bubbling	950	0.4-1	1030	66-78	60-75	*n.a.*	~ 25	*n.a.*	[37]
3	CUT	10	Ilmenite	Petcoke	Bubbling	950-1000	0.5-1.5	1117	55-75	68-87	*n.a.*	27-36	*n.a.*	[118]
4	CUT	10	Ilmenite + $CaCO_3$	Petcoke	Bubbling	950-1000	0.7-2.5	1430	41-81	58-86	64-81	24-33	*n.a.*	[114]
5	CUT	10[a]	Ilmenite	Bit. Coal	Bubbling	970	1.5-8	2000	54-56	90-95	88-92	23	*n.a.*	[115]
6	CUT	10[a]	Ilmenite	Petcoke	Bubbling	970-1000	0.5-3.8	1364	45-65	51-87	61-83	18-21	*n.a.*	[115]
7	CUT	10[a]	Mn ore	Petcoke	Bubbling	970	1-3.7	1500	60-69	89-98	91-97	11-14	*n.a*	[115]
8	CUT	100	Ilmenite	Bit. Coal	High vel.	940-980	1-5	200-770	52-67	*n.a.*	96-99.5	16-25	*n.a.*	[120, 123]
9	CUT	100	Ilmenite	Wood char	High vel.	929-973	1-6	300-850	54-89	*n.a.*	91-97	4.7-15.5	*n.a.*	[121]
10	CUT	100	Ilmenite + Mn ore	Bit. Coal	High vel.	935-971	0.5-3	370-1300	54-77	*n.a*	98-99	8.5-18.5	*n.a*	[122]
11	CUT	100	Iron ore	Bit. Coal	High vel.	945	1.5	480-650	*n.a.*	*n.a.*	92-98	13-19	*n.a.*	[100]
12	SU	1	Iron ore	Biomass	Spouted	720-930	*n.a.*	*n.a.*	*n.a.*	95.5-98.5	~ 98	*n.a.*	*n.a.*	[127]
13	SU	1	Iron ore	Bit. Coal	Spouted	880-970	*n.a*	970	92	77-87	*n.a.*	5.5-8.2	*n.a.*	[129]
14	SU	1	Iron ore	Anthracite	Spouted	880-970	*n.a*	750	66-82	49-70	*n.a.*	3.2-4	*n.a.*	[129]
15	SU	1	Iron ore + K_2CO_3	Anthracite	Spouted	900-975	*n.a.*	2130	*n.a.*	35-92.5	*n.a.*	*n.a.*	*n.a.*	[130]
16	SU	1	Hematite	Sewage s.	Spouted	800-900	*n.a.*	7200	82-91	~ 100	*n.a.*	*n.a.*	8.5-23.5.	[132]
17	SU	1	Hematite	Bit. coals	Spouted	800-960	*n.a.*	900-1000.	56-91	36-96	*n.a.*	*n.a.*	*n.a.*	[133]
18	SU	50	Fe_2O_3	Bit. Coal	High vel.	950	0.24	50-100	>85	83-87	*n.a.*	2-6.5	*n.a.*	[135]
19	ICB-CSIC	0.5	Ilmenite	Bit. Coal	Bubbling	870-950	1.1	3140	95	35-86	*n.a.*	5-15	5-10	[136]
20	ICB-CSIC	0.5	Ilmenite	Bit. Coal	Bubbling	890	0.5-8.4	1500-3900	80-95	38-74	*n.a*	14-36	8-15	[138]
21	ICB-CSIC	0.5	Ilmenite	Bit. Coal	Bubbling	850-920	1.0	1380	77	41-55	*n.a.*	~ 25	~ 9.5	[137]
22	ICB-CSIC	0.5	Ilmenite	Lignite	Bubbling	870-920	1.2	1770	89	82-93	*n.a.*	29-31	7-8	[137]
23	ICB-CSIC	0.5	Ilmenite	Anthracite	Bubbling	870-930	1.0	1400	87	20-40	*n.a.*	~ 16	~ 3.5	[137]

24	ICB-CSIC	0.5	Fe-ESF	Bit. Coal	Bubbling	880-930	1-6	2850-3500	89	44.5-67	*n.a.*	6.8-13.5	3.2-6.7	[140]
25	ICB-CSIC	0.5	Fe-ESF	Anthracite	Bubbling	875-930	1.0	2070	88	8-20	*n.a.*	5.7-21.2	1-1.5	[198]
26	ICB-CSIC	0.5	Iron ore	Bit. Coal	Bubbling	875-920	1.2	1463	87	40-55	*n.a.*	5.9-10.4	1.8-2.7	[101]
27	ICB-CSIC	0.5	Iron ore	Lignite	Bubbling	875-920	1.0	2023	87	85.5-94	*n.a.*	10.7-15	1.1-2.9	[101]
28	ICB-CSIC	0.5	Iron ore	Anthracite	Bubbling	880-930	1.0	2847	70	31-45	*n.a.*	7-17	2.1-3.7	[101]
29	ICB-CSIC	0.5	Iron ore	Biomass	Bubbling	880-980	1-4	600-1550	85-90	90-100	*n.a.*	7-34.6	3.4-29.9	[139, 141]
30	ICB-CSIC	0.5	Fe-Mn	Bit.-Sub-Bit	Bubbling	900	1-1.5	1275-1750	97	74-95.5	*n.a.*	2.9-3.8	2.8-4.4	[79, 89]
31	ICB-CSIC	50	Ilmenite	Bit. Coal	High vel.	905-1006	1.1-1.5	253-680	80-94	61-90	*n.a.*	8-14	6.5-9.8	[144, 145]
32	TUHH	25	Ilmenite	Lignite	2 reactors	900-940	16-55	4505[c].	92	96-98	*n.a.*	11-25	10-24	[148]
33	TUHH	25	CuO	Bit. Coal	2 reactors	800-850	*n.a.*	*n.a*	92-99	35-63	45-64	0.25-1.25	*n.a.*	[149]
34	OSU	25	Fe_2O_3	Sub-Bit.	Moving	900-1000	*n.a.*	*n.a.*	*n.a.*	94-95	94-96	0.1-1.3	*n.a.*	[153]
35	HUST	5	Hematite	Bit. Coal	Bubbling	900-1000	*n.a.*	417-1250	*n.a.*	40-85	*n.a.*	3.7-26.5	*n.a.*	[156]
36	Alstom	3000	$CaSO_4$	Coal+$CaCO_3$	High vel.	900-930	*n.a.*	*n.a.*	*n.a.*	*n.a.*	*n.a.*	15-20	*n.a.*	[163]
37	TUD	1000	Ilmenite	Bit. Coal	High vel.	930	1	156	*n.a.*	*n.a.*	*n.a.*	12-17[b]	*n.a.*	[42]
38	TUD	1000	Ilmenite	Anthracite	High vel.	900	1.6	100	50	90	*n.a.*	20	*n.a.*	[159]

[a]: In-bed coal feeding

[b]: Fuel reactor was fluidized with a mixture of air and steam

[c]: Solids inventory per fuel reactor stage

Table 5. Experimental conditions for CO_2 capture efficiency and oxygen demand from different CLOU and CL*a*OU continuous units.

No.	Process	Name	Nominal power	OC	Fuel	FR	T	ϕ	m_{OC}	X_{sf}	Carbon capture		Oxygen demand		Ref.
			(kW)				(ºC)		(kg/MW_{th})	(%)	η_{CC} (%)	χ_{OO} (%)	Ω_{FR} (%)	Ω_T (%)	
1	CLOU	ICB-CSIC	1.5	$CuO/MgAl_2O_4$	Bit. Coal	Bubbling	900-960	1.1-4.3	235-1150	*n.a.*	94.7-99.3	*n.a.*	0	0	[142]
2		ICB-CSIC	1.5	$CuO/MgAl_2O_4$	Anthracite	Bubbling	900-950	1.1	894	*n.a.*	75-83	*n.a.*	0	0	[58]
3		ICB-CSIC	1.5	$CuO/MgAl_2O_4$	Lignite	Bubbling	900-950	1.2	845	*n.a.*	95-99.3	*n.a.*	0	0	[58]
4		ICB-CSIC	1.5	$CuO/MgAl_2O_4$	Biomass	Bubbling	900-935	1.2	565	95	98-100	*n.a.*	0	0	[143]
5		ICB-CSIC	1.5	$CuO\text{-}Fe_2O_3/MgAl_2O_4$	Lignite	Bubbling	900-945	1.1	950	96	96-98.4	*n.a.*	0	0	[199]
6		ICB-CSIC	1.5	$Cu_{1.5}Mn_{1.5}O_4$	Bit. Coal	Bubbling						*n.a.*			[88]
7	CL*a*OU	ICB-CSIC	1.5	$Mn_{0.66}Fe_{0.33}TiO_2$	Bit.-Sub-Bit.	Bubbling	900	1-7	840-1450	82-99.6	48-97	*n.a*	1.1-12.2	0.6-7.5	[79, 89]
8	CLOU	CUT	10	$CaMn_{0.9}Mg_{0.1}O_{3-\delta}$	Petcoke	Bubbling	930-960	*n.a.*	770-1660	*n.a.*	*n.a.*	75.2-88.4	7.7-11.2	*n.a.*	[117]
9		CUT	10	$CaMn_{0.9}Mg_{0.1}O_{3-\delta}$	Biochar	Bubbling	917-970	*n.a,*	1875	*n.a.*	*n.a.*	82-95.2	2.1-4.9	*n.a.*	[57]

369

370 **Table 6.** Summary of the characteristics of the main operating CLC unit. Adapted from [250].

CLC unit		**CUT**				**SU**		**ICB-CSIC**		**HUT**	**OSU**	**TUD**		**Alstom**
Data		**1**	**2**	**3**	**4**	**5**	**6**	**7**	**8**	**9**	**10**	**11**	**12**	**13**
Nominal Power	**kWth**	**10**	**100**			**1**	**50[a]**	**0.5**	**50**	**25**	**25**	**1000**		**3000**
Fuel		IC	PC	PC	IC	LC	LC	IC	IC	PC	PC	PC	LC	na
Oxygen carrier		ilmenite	ilmenite	Ilmenite + Mn ore 1	Mn ore 2	iron ore	iron ore	ilmenite, iron ore	ilmenite	ilmenite	iron ore	ilmenite	ilmenite	$CaSO_4$
Carbon capture	(%)	50-96	98-99	99	99	35-90	83-87	35-94	90	96-98	94-95	80	44-52	96
Carbon loss by elutriation	(%)	20-50	35	(26-46)	8-12	8-34	15	5-35	7	8	-	50	5	0.5
Oxygen demand	(%)	16-36	17-25	8.5-18	11-17	3-8	2-6.5	1-10	7-10	10-24	0.1-1.3	20[b] (26-38)	22-28	-
Pressure drop fuel reactor	(kPa)	-	14-25			-	10	2.9	9	8	4.3		7.5	-
solids inventory in FR	(kg/MW_{th})	1000-2900	300-500			970-2100	50-100	1400-3900	450-720	4500	-	156	105	-
T_{FR}	(ºC)	950-1000	965-980	960-974	970-980	880-975	950	870-950	~1000	900	920-950	900	920-950	-

371

372 [a] at pressure

373 [b]Not isothermal. Propane and air added to fuel reactor to keep up temperature.

374 PC = pulverized coal: a majority below 90 μm; IC = intermediate sized coal: a majority in the size range 90-300 μm; LC = larger coal, <8 mm.

375

1. [36, 37, 115, 118, 200] 2. [196] 3. [122] 4. [250] 5. [127, 129, 133]	6. [135] 7. [101, 136-138, 140, 198] 8. [145] 9. [148] 10. [153]	11. [159] 12. [160] 13. [163]

376

377

378

379
380

4381

4382

4383 **Table 7.** Comparison between variables affecting *i*G-CLC and CLOU performance.

	***i*G-CLC**	**CLOU**
Oxygen carrier requirements	- High reactivity with gaseous products (H_2, CO, CH_4)	- Availability to release gaseous oxygen
Coal conversion rate	- Gasification - High temperature	- Combustion
FR temperature	- As high as possible. Usually 1000 ºC to maximize char gasification rate	- Determined by the MeO thermodynamic in oxygen carrier
Solids residence time	- High - Requirements of high efficient CS to increase time for char	- Efficiency of CS not as high as in *i*G-CLC
Solids inventory	400-700 kg/MW	- As low as 200 kg/MW_{th} would be possible with highly reactive oxygen carriers
OC recovery from ash	- Low relevance if low cost materials are used	- Highly relevant with synthetic materials. Easy separation with magnetic materials.
Fluidizing agent preferred	- Steam	- Recirculated CO_2
CO_2 capture efficiency	20 - 98	75 - 100
Oxygen demand	6 - 9	0
FR design	- CFB: better volatile combustion - Moving bed (counter-current): Better volatile combustion	- BFB: posible if no limitations in the solids circulation rate - CFB - Moving bed (countercurrent): more careful design

4384

4385

Table 8. Values for SO_2 and NO_x in [199, 272] compared to those set as adequate (fuel reactor) [270] and set by legislation (air reactor) [283].

	Depleted Air		CO_2 stream	
Origin	Air reactor		Fuel reactor	
Destination	Atmosphere		Compression, transport and sequestration	
	Measured*	Legislation*	Measured	DYNAMIS
Units	mg/Nm^3	mg/Nm^3	mg/Nm^3	mg/Nm^3
SO_2 (*i*G-CLC)	450	200	28103	286
SO_2 (CLOU)	1000		18500	
NO_x(*i*G-CLC)	74	200	47	125
NO_x (CLOU)	100		625	

* for the air reactor, normalized to 6 vol% O_2

Table 9. Main characteristics of "El Cerrejón" coal and char [136].

		Coal	Char[b]
Moisture	wt%	2.3	-
Ash	wt%	8.8	-
Volatile matter	wt%	33.0	-
Fixed carbon	wt%	55.9	-
C	wt%	65.8	79.8
H[c]	wt%	3.3	0.7
N	wt%	1.6	1.3
S	wt%	0.6	0.6
O[a]	wt%	17.6	4.0
LHV	kJ/kg	21900	
Ω_{sf}	kg O/kg coal	1.84	
Ω_{vol}	kg O/kg coal	0.35	
Ω_{char}	kg O/kg coal	1.49	

[a] By difference

[b] Obtained by pyrolysis at 900 ºC in nitrogen atmosphere using a heating rate of 20 ºC /min

[c] H from moisture not considered

Table 10. Experimental averaged values of $\eta_{comb,v}$ and $\eta_{comb,g}$ obtained in the evaluation of data in Table 4 according to Eq. (17) and estimation of the oxygen demand expected according to these values when $x_{char,FR} = 1$ ($\Omega_{T,full}$).

	Nominal power		**OC**	**Solid fuel**	**m_{OC}**	**Ref.**	$\eta_{comb,v}$	$\eta_{comb,g}$	$\Omega_{T,full}$
	(kW)				(kg/MW_{th})		(%)	(%)	(%)
ICB-CSIC	0.5		Ilmenite	Bit.Coal	3131	[136, 140]	73	91	12.6
			Fe-ESF	Bit.Coal	2850		95	91	8.4
ICB-CSIC	50		Ilmenite	Bit.Coal	500	[285]	72	86	16.9
CUT	10	AB	Ilmenite	Bit.Coal	2000	[115, 119]	17	89	25.1
			Ilmenite	Petcoke	1200		61	86	15.8
		IB	Ilmenite	Petcoke	1364	[115]	99	81	18.0
CUT	100		Ilmenite	Wood char	700	[120, 121]	76	97	7.3
			Ilmenite	Bit.Coal	450		39	88	21.2

AB= Above-bed feeding; IB= In-bed feeding

Table 11. Thermochemical data for different redox systems proposed for active material in the oxygen carrier. Data includes the melting point for the reduced and oxidized form, proposed temperature for the fuel and air reactors, enthalpy of reaction with oxygen and carbon at standard (ΔH_r^0) and reactor ($\Delta H_r^{T_{react}}$) conditions, and equilibrium constant for reduction with H_2 and CO ($K_{eq,H_2}^{T_{FR}}$ and $K_{eq,CO}^{T_{FR}}$) at the proposed fuel reactor temperature.

	Melting point (ºC)	Proposed temperature (ºC)		ΔH_r^0 (kJ/mol C or O_2)		$\Delta H_r^{T_{react}}$ (kJ/mol C or O_2)		$K_{eq,H_2}^{T_{FR}} = \frac{P_{H_2O}}{P_{H_2}}$	$K_{eq,CO}^{T_{FR}} = \frac{P_{CO_2}}{P_{CO}}$
	Ox / Red	Air reactor	Fuel reactor	O_2	C	O_2	C		
Common redox systems in CLC with solid fuels									
iG-CLC									
$CaSO_4$/CaS	1460 / 2525	~1000	~950	-482.2	88.7	-471.9	76.7	$1.1 \cdot 10^2$	$7.7 \cdot 10^1$
Fe_2O_3/Fe_3O_4	1565 / 1597	~1050	~1000	-476.0	82.5	-490.4	95.2	$7.7 \cdot 10^4$	$4.6 \cdot 10^4$
Fe_3O_4/FeO	1597 / 1377	~1050	~1000	627.4	233.9	585.2	190.0	$4.3 \cdot 10^0$	$2.6 \cdot 10^0$
FeO/Fe	1377 / 1538	~1050	~1000	534.5	141.0	531.6	136.4	$4.0 \cdot 10^{-1}$	$6.7 \cdot 10^{-1}$
Fe_2TiO_5/$FeTiO_3$	1395 / 1050	~1050	~1000	-454.4	60.9	-443.5	48.3	$4.4 \cdot 10^3$	$2.6 \cdot 10^3$
Mn_3O_4/MnO	1562 / 1842	~1050	~1000	-464.3	70.8	-449.4	54.2	$1.9 \cdot 10^4$	$1.2 \cdot 10^4$
CLOU									
CuO/Cu_2O	1446 / 1235	~900	~950	-282.0	-111.5	-262.1	-134.0	$1.0 \cdot 10^7$	$6.9 \cdot 10^6$
Mn_2O_3/Mn_3O_4	1347 / 1562	~800	~850	-202.8	-190.7	-194.7	-201.0	$1.3 \cdot 10^8$	$1.2 \cdot 10^8$
Non-common redox systems in CLC with solid fuels [302]									
CaO/Ca	2899 / 842	3494	2465	-1269.8	876.3	-1083.9	883.6	--	--
CdO/Cd	~900 / 321	1523	562	-518.0	124.5	-508.4	130.3	$4.7 \cdot 10^1$	$1.5 \cdot 10^2$
Co_3O_4/CoO	895 / 1830	~850	~850	-392.4	-1.1	-408.2	13.4	$9.2 \cdot 10^7$	$8.2 \cdot 10^7$
CoO/Co	1830 / 1495	2641	233	-475.9	82.4	-383.4	77.2	$1.2 \cdot 10^2$	$1.6 \cdot 10^4$
K_2O/K	978 / 63	1443	814	-726.4	332.9	-636.6	252.2	$6.6 \cdot 10^{-1}$	$6.7 \cdot 10^{-1}$
Na_2O/Na	1132 / 98	1573	949	-830.2	436.7	-670.7	419.1	$1.2 \cdot 10^{-1}$	$8.0 \cdot 10^{-2}$
NiO/Ni	1955 / 1455	~1000	~1000	-479.4	85.9	-468.5	73.3	$1.3 \cdot 10^2$	$7.7 \cdot 10^1$
PbO/Pb	887 / 328	1782	-28	-436.1	42.6	-348.6	43.1	$7.6 \cdot 10^7$	$2.9 \cdot 10^{14}$
SnO_2/Sn	1630 / 232	2369	579	-580.8	187.3	-519.0	187.5	$8.2 \cdot 10^{-1}$	$2.4 \cdot 10^0$
WO_3/W	1472 / 3407	2916	667	-561.9	168.4	-457.2	160.0	$5.9 \cdot 10^{-1}$	$1.1 \cdot 10^0$
ZnO/Zn	1975 / 420	1566	808	-701.0	307.5	-701.9	316.4	$3.6 \cdot 10^{-2}$	$3.7 \cdot 10^{-2}$

4418